PETROCHEMISTRY, RELATED MINERALIZATION AND GENESIS OF THE AMBALAVAYAL GRANITE AND ASSOCIATED PEGMATITES, WYNAD DISTRICT, KERALA

Thesis submitted to the University of Cochin
for the degree of

DOCTOR OF PHILOSOPHY

in

GEOLOGY

By

M. SANTOSH, M. Sc.

CENTRE FOR EARTH SCIENCE STUDIES
P. B. 2235, TRIVANDRUM, INDIA

SEPTEMBER 1985

CERTIFICATE

This is to certify that this thesis is an authentic record of research carried out by Sri. M. Santosh, M. Sc., under my supervision and guidance in the Centre for Earth Science Studies, Trivandrum, for the Ph. D. Degree of the University of Cochin and no part of it has previously formed the basis for the award of any other degree in any University.

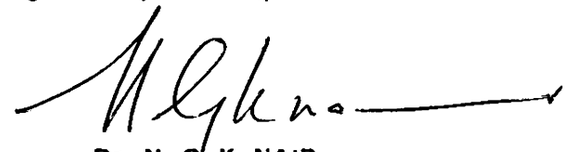

Dr. N. G. K. NAIR
(Supervising Teacher)
Head, Geosciences Division,
Centre for Earth Science Studies,
Trivandrum.

Trivandrum,
30th September 1985.

ABSTRACT

The Kerala region which forms a significant segment of the south-western Indian shield, dominantly comprises charnockites, khondalites and migmatitic gneisses of Precambrian age. Recent investigations have revealed the occurrences of a number of younger granite and syenite plutons in this region, spatially related to regional fault-lineaments. The granite of Ambalavayal in Wynad district of northern Kerala is a typical member of this suite of intrusives. The thesis is based on a comprehensive study in terms of geology, petrology, geochemistry and petrogenesis of the Ambalavayal granite, basement gneisses, associated pegmatites, quartz veins and related mineralization that together cover an area of about 90 sq km in Wynad district of northern Kerala.

The dominant rock types of northern Kerala are charnockites and migmatitic gneisses. The granite pluton of Ambalavayal is emplaced within Precambrian biotite gneisses and is spatially related to the intersection of two regional fault-lineaments, namely, the Moyar and Calicut lineaments. The granite is pink, medium to coarse grained, and consists of interlocking quartz and feldspar with hornblende and biotite as the major mafic constituents. The related pegmatites show a coarse assemblage of pink feldspar, quartz and hornblende with subordinate biotite. The granite, pegmatites and

related quartz veins show disseminated molybdenite mineralization. Molybdenite flakes and flaky aggregates measuring upto 20 cm have been recovered from the Ayiramkolly quarry.

Under the microscope, the granite shows a hypidiomorphic granular texture with quartz and alkali feldspar as the major minerals. Alkali feldspars show stringers and braids of perthitic phase and the megacrysts show microcline cross-hatching. Greenish pleochroic hornblende is the major mafic mineral. Accessories include biotite, riebeckite, zircon, apatite, sphene, epidote, monazite and calcite. The molybdenite flakes are seen as leafy aggregates adhering to the silicate minerals and more commonly show preferential distribution along grain boundaries of quartz and feldspar.

Major element geochemistry of seventeen feldspar samples from the granite and pegmatites are presented. The data show that the alkali feldspar in the granite varies in composition from $Or_{57.58}Ab_{42.42}$ to $Or_{62.06}Ab_{37.94}$. Plagioclase is dominantly albitic with a range in composition from $Ab_{90.15}An_{9.85}$ to $Ab_{86.30}An_{13.70}$. Feldspar geothermometry based on mol per cent Ab content in coexisting alkali feldspar and plagioclase indicates a temperature of equilibration of 722-740°C for the granite. The temperature estimates for feldspars from the pegmatites is 525-580°C.

Major and trace element analyses of coexisting biotites and

hornblendes from the Ambalavayal granite are also presented. The hornblendes correspond to edenitic composition, whereas the biotites correspond to annite. The hornblendes typically show high Al_2O_3 contents (9.69-11.89) comparable with those from anorogenic granites. The biotites are characteristically low Mg-type, similar to those reported from alkaline rocks. Based on the dsitribution of Al^{iv}-Ti-Fe^{3+} in the biotite, it is shown that the silica and alumina activities increase towards the felsic end. The biotite-hornblende tie lines in the compositional triangle, Fe^{3+}-Fe^{2+}-Mg lie parallel to those of buffered biotites, indicating crystallization in an environment closed to that of oxygen and well above the Ni-NiO buffer.

X-ray study of molybdenite indicates that it belongs to the hexagonal $2H_1$ polytype. Chemical analyses show an average Mo content of 58.4% with traces of Fe, Ni, Ti, Cu and Pb.

Rubidium and strontium determinations of seven whole rock samples of the granite are presented. Based on this data, a Rb-Sr isochron, corresponding to an age of 595 $\pm$ 20 Ma and an initial Sr-isotope ratio of 0.7171 $\pm$ 0.0022, is defined. This corresponds to a Late Precambrian-Early Paleozoic magmatism in the region, supplemented by a K-Ar mineral age (560 $\pm$ 30 Ma) determined from biotite separate of the granite. The acid magmatism of Ambalavayal is envisaged to be part of

a widespread anorogenic magmatism in this part of the Indian shield.

Major and trace element analyses of twenty four representative samples of the granite are presented. SiO_2 values of the granite show a range of 68.73 to 75.27 and Al_2O_3 range from 11.73 to 14.27. K_2O values are rather high, showing a range of 3.64 to 7.24. SiO_2 vs. $Log_{10}K_2O/MgO$ plots fall in the field of alkali granite. Na_2O values show a range of 2.05 to 5.58 and are consistently lower than K_2O, with K_2O/Na_2O values less than 1. The K_2O vs. Na_2O plots of the granite fall in the field of adamellite. The ranges of other oxides are: Fe_2O_3: 0.30-2.86, TiO_2: 0.05-0.29, MgO: 0.32-0.64, CaO: 0.46-2.69 and P_2O_5: 0.02-0.22. The A-F-M plots show an alkali enrichment trend and the K-Na-Ca plots indicate a dominant K-enrichment. In Harker variation diagrams, the oxide weight percentages show overall smooth trends against SiO_2. Thus, Al_2O_3 and Na_2O show slight increase whereas all the other elements show depletion towards higher SiO_2 levels.

Among trace elements, the ranges (in ppm) are: Ba: 9-309, Bi: 10-126, Ce: 54-540, Co: 9-22, Cr: 36-184, Cu: 4-40, La: 24-253, Li: 5-64, Mo: 6-28, Nb: 11-146, Ni: 16-152, Pb:8-51 Rb: 43-131, Sr: 3-62, Th: 5-40, U: 2-24, Y: 15-215, Zn: 48-254 and Zr: 115-528. The notable features are the general

low content of Rb and Sr, higher levels of Ni and Cr and extremely high values of LREE (La and Ce). Most of the elements show overall correlation with SiO_2. The behaviour of individual elements and element ratios implies that the granite was derived by in situ fractionation of a partial melt derived from a K-enriched, Rb-depleted deep crustal or upper mantle source.

The general mineralogic and geochemical features of the granite are comparable with those for granite-molybdenite systems. The $K_2O/K_2O + Na_2O$ contours show a high at the middle part of the study area, defining a NW-SE anomaly in the granite. There is a close agreement of this anomaly with that of the Mo content in the granite.

Major and trace element geochemistry of twenty four representative samples of the biotite gneisses, three samples of mafic-rich 'enclaves' (restites) and 2 samples of fuchsite quartzites are also presented. In normative Q-Ab-Or triangle, the plots of the gneisses fall mostly in the field of trondhjemites. The A-F-M and K-Na-Ca variations also suggest a trondhjemitic differentiation trend. The higher contents of Ba and Rb with lower K/Ba and K/Rb values and the lower contents of LREE (La and Ce) of the gneisses are in contrast to that of the granite. The major and trace elements show smooth correlation with SiO_2. Petrogenetic evaluation suggests an igneous parentage and derivation from a lithophile-rich

trondhjemitic magma which underwent subsequent crystal fractionation.

Detailed fluid inclusion studies in quartz associated with the granites, pegmatites and quartz veins are presented. Heating-freezing studies show that the quartz in the granite entrapped high density (0.90-0.95 g/cm^3) CO_2-rich fluids. Coexisting CO_2 and CO_2-H_2O inclusions in pegmatites yield a P-T estimate of 2.2 Kb and 500^{o}C for simultaneous entrapment. Fluid inclusions in the mineralised quartz veins show that the ore-forming fluids were heterogenous and the molybdenite precipitation was triggered by 'boiling' due to adiabatic decompression at temperatures of 340-360^{o}C and vapor pressures of 110-150 bars. The cooling curve of the granite constructed from combined P-V-T data shows T-convex path, implying isothermal upward movement of the granite magma, brought about by extensional tectonics.

I am grateful to Prof. S.Varadarajan, Department of Geology, University of Delhi, for kindly permitting me to use XRD facilities. Earlier, Dr. P.K.Joy, TTP, Trivandrum, had arranged a few XRD analyses.

I owe my sincere thanks to Dr. Subhash Jaireth, Department of Earth Sciences, University of Roorkee, for initiating my interest in fluid inclusion studies when I was a student at Roorkee. He also extended laboratory facilities whenever I visited Roorkee. In addition, I thank Dr.S.Balagopal, PDIL, Sindri, and Dr.P.S.Ranawat, Department of Geology, Udaipur (University of Rajasthan) for fluid inclusion laboratory facilities. Dr. Jana Durisova, UUG, Czechoslovakia encouraged my studies. She was so kind as to extend freezing facilities and assist me in freezing runs during my stay at Prague. My doubts on the interpretation of P-V-T data on fluid inclusions were cleared by Dr. Jens Konnerup-Madsen, Institute for Petrology, Copenhagen.

The matter contained in many of the chapters of this thesis have been communicated to various scientific journals as separate research papers. The comments and suggestions from the journals' reviewers have been incorporated while preparing this thesis. In this connection, I express my thanks to the anonymous reviewers.

Several others, including my colleagues, helped me directly or indirectly both in field and in the laboratory, for which

I am thankful. I wish to record the name of Sri. Shekhar Srivastava, ONGC, Assam, my class-mate at Roorkee, who encouraged me during the initial phase. Ms. K.G.Thara, TKM College, Quilon and Sri.G.Sankar, CESS were always helpful. The chemists of the Chemical Laboratory, CESS, helped me in analyses. The administrative staff of CESS patiently saw to all the official matters concerning my thesis work, ever since I registered for Ph.D. as a CSIR Research Fellow and continued my part-time research after I joined CESS as Scientist.

The Cochin University officials are also remembered with gratitude for encouragement by speedy execution of administrative matters concerned with my work.

The diagrams were drafted by Sri. Sivarajan, CESS. The typing work was carried out by Sri.C.N.Gopalakrishnan and Smt. R. Padmavathy Amma, CESS. Help rendered by Sri. Devdas and Sri. Mukundan, CESS is also acknowledged.

Finally, I must mention my obligations to my family members for their constant encouragement and for bearing with me, as I have always excused myself from family responsibilities in the name of research. The one who inspired me most and was constantly concerned about the progress of my work was my mother. She died young- recently- without seeing the fulfilment of my efforts. I dedicate this work to her memory.

M.SANTOSH

CONTENTS

Abstract		...	i
Acknowledgements		...	vii
Chapter 1	Introduction	...	1
1.1	Importance of granites in crustal evolution	...	1
1.2	Metallogeny related to granites	...	4
1.3	Regional geology	...	6
	1.3.1 Lithounits	...	6
	1.3.2 Structure	...	9
	1.3.3 Metamorphism	...	10
	1.3.4 Acid magmatism	...	11
	1.3.5 Geochronology	...	11
	1.3.6 Mineralization	...	12
1.4	Geology of Wynad region	...	12
1.5	Previous studies	...	14
Chapter 2	Geology of Ambalavayal area	...	16
2.1	Granite, pegmatites and quartz veins	...	16
2.2	Mineralization	...	17
2.3	Basement rocks	...	18
2.4	Petrography	...	19
	2.4.1 Granite	...	19
	2.4.2 Gneisses	...	26

Chapter	3	Geochronology	...	29
3.1		Rb-Sr geochronology	...	29
3.2		K-Ar geochronology	...	31
3.3		Discussion	...	32
Chapter	4	Mineral chemistry	...	33
4.1		Feldspars	...	33
4.2		Hornblende and biotite	...	43
		4.2.1 Geochemistry of biotite	...	43
		4.2.2 Geochemistry of hornblende	...	47
		4.2.3 Distribution of major and trace elements	...	50
		4.2.4 Intensive parameters	...	57
4.3		Molybdenite	...	59
Chapter	5	Geochemistry of granite	...	64
5.1		Major elements	...	64
5.2		Trace elements	...	74
5.3		Discussion	...	85
5.4		Petrogenesis	...	92
5.5		Geochemical signatures of ore potential	...	98
5.6		Taphrogenic affiliation	...	100
Chapter	6	Geochemistry of basement rocks	...	102
6.1		Major elements	...	107
6.2		Trace elements	...	120
6.3		Petrogenesis	...	121

Chapter 7	Fluid inclusion studies	...	125
7.1	Sample preparation	...	126
7.2	Fluid inclusion petrography	...	127
7.3	Heating-freezing techniques	...	130
7.4	Fluid inclusions in granite	...	130
7.5	Fluid inclusions in pegmatites	...	133
7.6	Fluid inclusions in quartz veins	...	135
7.7	Cooling history of Ambalavayal granite	...	136
7.8	Fluid evolution characteristics	...	138
7.9	Transport and deposition of molybdenum	...	139
Conclusions		...	144
References		...	152
Appendix		...	176

LIST OF TABLES

Table No.	
1	Modal composition of Ambalavayal granite
2	Modal analysis data of Ambalavayal gneisses
3	Rb-Sr analytical data for the Ambalavayal granite
4	Major element analyses of coexisting alkali feldspar and plagioclase from Ambalavayal granite and alkali feldspar from pegmatites
5	Structural formulae of feldspars from Ambalavayal
6	Chemical analyses and structural formulae of biotite from Ambalavayal.
7	Chemical analyses and structural formulae of hornblende from Ambalavayal.
8	Atomic ratio of elements to the sum of major elements occupying the respective sties in hornblende and biotite from Ambalavayal.
9	Distribution coefficients for coexisting hornblende and biotite from Ambalavayal.
10	Trace element analyses of hornblende and biotite from Ambalavayal.
11	Distribution coefficients of trace elements between coexisting biotite and hornblende from Ambalavayal
12	'2 θ' and 'd' values of molybdenites from Ambalavayal compared with that from Kondappalli.
13	Analyses of molybdenite fractions from Ambalavayal.
14	Major element analyses of Ambalavayal granite.
15	Normative composition of Ambalavayal granite

16 Trace element analyses of Ambalavayal granite

17 Comparison of selected major and trace elements in Ambalavayal granite with those of other alkali granites.

18 Major element analyses of gneisses, restites and fuchsite quartzite from Ambalavayal.

19 Trace element analyses of gneisses, restites and fuchsite quartzite from Ambalavayal.

20 Normative composition of trondhjemitic gneisses around Ambalavayal.

21 Major element data of Ambalavayal gneisses compared with other gneisses

A-1 Trace element data of U.S.G.S. standards analysed alongwith samples of present study.

A-2 Data of repetitive analyses, mean and standard deviation.

LIST OF FIGURES

Fig.No.

1 Generalised geological map of the Kerala region (after Rao, 1978) showing location of the study area. The inset shows Archaean high grade-low grade boundary in south India.

2. Generalised structural features of the northern Kerala region (after Rao, 1978).

3 Geological map of the northern Kerala region (after Rao, 1978).

4 Field photographs showing the features of granite, gneiss and their interrelationship around Ambalavayal.

5 Geological map of the Ambalavayal area showing the zone of molybdenite mineralization and sample locations of present study.

6 Ross diagram depicting the joint pattern data of Ambalavayal granite.

7 Lineament map of northern Kerala region showing the location of Ambalavayal granite.

8 Field and handspecimen photographs of pegmatites in A mbalavayal.

9 Photographs of flaky aggregates of molybdenite from Ambalavayal.

10 Equal area (lower hemisphere) plots of the foliation data of gneisses around Ambalavayal.

11 Photomicrographs showing the mineralogy of Ambalavayal granite. Bar scales represent 2mm.

12 Photomicrographs of polished sections showing the opaque minerals. Bar scales represent 2 mm.

Fig.No.

13 Q-A-P plots of modal data of Ambalavayal gneisses. The classification boundaries are after Streckeisen (1976).

14 Rb-Sr isochron plot of the Ambalavayal granite.

15 Ternary Ab-Or-An plots of coexisting feldspars from Ambalavayal, connected by tie-lines.

16 Plots of albite content in coexisting alkali feldspar and plagioclase pairs from the Ambalavayal granite in Whitney and Stormer's (1977) diagram (A) and Brown Parsons (1981) diagram (B).

17 Plots of alkali feldspars from pegmatites of Ambalavayal in the strain-free solvus of the Or-Ab system (after Ribbe, 1975).

18 Composition of Ambalavayal biotites in terms of Fe/Fe+Mg vs. Al atoms/22 oxygens. The broken lines represent the field of biotites as given by Anderson (1980).

19 Composition of Ambalavayal biotites compared with those from elsewhere. Note, the low Mg-content (a) and lower Ti with moderate Al and $Fe^{3}+$ (b).

20 Composition of hornblendes from Ambalavayal in terms of Si + Na + K vs. Al^{iv} + Ca relations.

21 Variations of K_D values of major elements between coexisting biotite and hornblende from Ambalavayal.

22 Variations of trace element K_D values between coexisting hornblende and biotite from Ambalavayal.

23 $Fe^{3} \pm Fe^{2} \pm Mg$ plots of coexisting biotite (circles) and hornblende (triangles) from Ambalavayal. The buffer limits are after Wones and Eugster (1965).

Fig. No.

24 Log fO_2 vs. temperature diagram with buffer limits after Wones and Eugster (1965), showing the stability of biotites from Ambalavayal. The solidus temperature has been estimated from the feldspar geothermometer.

25 Variations of major element oxides in the Ambalavayal granite with respect to SiO_2.

26 A-F-M and K-Na-Ca triangular variation diagrams of the Ambalavayal granite.

27 Na_2O vs. K_2O plots of the Ambalavayal granite. The field boundaries are after Harpum (1963).

28 SiO_2 vs. $Log_{10}K_2O/MgO$ plots of the granite. The fields of calc.alkaline and alkali granites are after Rogers and Greenberg (1981).

29 Trace element variations in the Ambalavayal granite.

30 Radioelement variations in the Ambalavayal granite.

31 Variations of La, Ce and Zr against P_2O_5 in the granite.

32 Variations of La, Ce and Zr against TiO_2 in the granite.

33 La/Y and Ce/Y vs. Y plots of the granite.

34 Projection of cotectic lines and isotherms on cotectic surface of the system Q-Ab-Or-An at PH_2O = 5Kb (after Winkler, 1976) showing the plots of the Ambalavayal granite.

35 Log Rb vs. Log Sr plots of the granite. The boundary lines are from Condie (1973).

36 SiO_2-Al_2O_3-Na_2O+K_2O (mol %) ternary plots of Ambalavayal granite. The classification boundaries are after Greenberg (1981).

Fig. No

37 Mol % $Na_2O + K_2O$ vs. Al_2O_3 plots of the granite. The field boundaries are after Westra and Keith (1981).

38 Contour diagram of whole rock molybdenum levels in the Ambalavayal granite, showing the anomalous zone.

39 Contour diagram of whole rock $K_2O/K_2O + Na_2O$ levels in the granite, showing the anomalous zones.

40 Normative An-Ab-Or plots of the gneisses from the Ambalavayal area. The classification boundaries are after O'Conner (1965).

41 Harker variation diagrams of major elements in the gneisses.

42 Trace element variations in the gneisses against SiO_2.

43 Inter-element variations in the gneisses.

44 Variations of element ratios in the gneisses.

45 Normative Q-Ab-Or plots of the gneisses (after Winkler, 1976).

46 A-F-M and K-Na-Ca ternary variations of the Ambalavayal gneisses.

47 Q-Ab-Or plots of the gneisses. The field of Uivak gneisses is after Collerson and Bridgwater (1979) and the trend lines are after Barker and Arth (1976).

48 Pattern of distribution and various phase-types of fluid inclusions in quartz from the granite, pegmatites and quartz veins of the Ambalavayal area.

FigNo.

49 Percentage of fluid inclusion phase-types in various localities of the granite pluton. The dotted line separates the biotite-rich zone (west) from the hornblende-rich zone (east).

50 Photomicrographs of various types of fluid inclusions in quartz from the Ambalavayal area. Bar scales represent 50 milli microns.

51 Temperatures of melting (A) and CO_2 homogenization (B) of monophase inclusions in quartz from the Ambalavayal granite.

52 Thermodynamics of CO_2-CH_4 system. See text for details.

53 Thermometric data of inclusions in pegmatitic quartz. (a) CO_2 homogenization temperatures in monophase inclusions, (b) CO_2 homogenization temperatures in CO_2-H_2O inclusions, (c) homogenization temperatures of aqueous bi-phase inclusions.

54 P-T data from coexisting CO_2 and CO_2-H_2O inclusions in pegmatitic quartz. The inset shows immiscibility data on the CO_2-H_2O system. See text for discussion.

55 (a) Homogenization temperatures of liquid-rich and vapour-rich inclusions and (b) ice melting temperatures of liquid-rich inclusions in quartz from the mineralised veins.

56 Boiling point curves for various NaCl-H_2O fluids (after Haas, 1971) showing the region of fluid inclusion data from Ambalavayal.

57 Homogenization (a) and ice-melting (b) temperatures of pseudosecondary liquid-rich inclusions in vein-quartz.

Fig.No.

58 Combined P-T diagram showing the isochores for carbonic inclusions in granite and pegmatites. The temperature estimates obtained from feldspar thermometry are superimposed.

59 Cooling curve of the granite computed from fluid inclusion data. The region of various fluids are also shown.

60 Evolutionary path of ore fluids in Ambalavayal as computed from fluid inclusion data. The thin lines denote H_2O densities.

CHAPTER - 1

INTRODUCTION

1.1. Importance of granites in crustal evolution

As the major component of continental crust and the second most abundant component of the surface of the earth after basalts, granitoids have ever been of geologic interest. Since Rosenbush (1876) coined the term granite, the petrology of this rock type and the criteria adopted for classification were highly debated (cf. Marmo, 1971). Johannsen (1941) defined granite as a rock 'characterised by quartz forming more than 5% and less than 50% of quarfeloids and by feldspar ratio such that K-feldspar forms from 50-95% of the total feldspar contents. The plagioclase is Ca-Na feldspar, and the mafites form more than 5% and less than 50% of the total constituents'. Since compositions of granitoids in various geologic settings deviate from this classical definition, Tuttle and Bowen (1958) adopted another criterion. According to this whenever the texture and environment may require, those rocks which contain 80% or more of the normative constituents, albite+orthoclase+quartz and those which occupy the central part of the Ab-Or-Q triangle are defined as granites. Recently, many advances have been made in the scheme of classification and characterisation of granitic rocks, based on mineralogical and geochemical characters. A few examples include those based on K_2O:Na_2O values (Harpum, 1963), normative Q-Ab-Or proportions (O'Conner, 1965), type of feldspar assemblage (Tuttle

and Bowen, 1958), nature of source rock (Chappell and White, 1974; White and Chappell, 1977), dominant type of iron oxide component (Ishihara, 1977) and the widely accepted classification which takes into account the modal Q-A-P proportions (Streckeisen 1976). Classifications based on the tectonic position have also been proposed (Eskola, 1932, Marmo, 1971).

Like granite petrology, the genesis of granites has also remained a topic of great debate and controversey of this century. In the 1930's geologists were eagerly disputing the question as to whether granite was magmatic, metamorphic or metasomatic in origin. This controversey had its inception in the days of the Neptunists. Thus, while Bowen (1928), Tuttle and Bowen (1958) and Winkler (1967) among others, were in favour of origin by fractional crystallization from a magma or remelting of metamorphic rocks exotic hypotheses like solid state diffusion or metasomatic transformation were advocated by workers like Perrin and Roubault (1939), Ramberg (1944) and Orville (1962). Treatises like that of Read's (1948) 'granites and granites' highlight varying views on granite genesis.

Recently, with the advances made in the field of trace element, rare earth element and isotope geochemistry, a more realistic and quantitative approach has evolved in understanding the petrogenesis of granitic rocks (cf. Anderson et al., 1980; Saha 1979).

Among the various granitoid types, the alkali granites form an important group and are characterised by unique geochemical and mineralogical characters. Their occurrence in anorogenic continental regions and their relationship with regions of crustal swelling and **rifting** are also significant (Murthy and Venkataraman, 1964; Sorensen, 1970; Le Bas, 1971; Anderson et al., 1980; Greenberg, 1981). Alkali granites are also economically significant for their rare earth and rare metal mineralization.

Granite rocks occur in a wide range of geological environments and play a significant role in tectonic and crustal evolution processes. They are the main components of continental shields. They also occur as huge batholiths in geosynclinal belts.

The first category occurs as batholiths in orogenic belts of folded, and in some instances, regionally metamorphosed terrains. In these regions, it is possible to identify syn-tectonic, late-tectonic and post-tectonic intrusives. In regions of major folding and regional metamorphism, syn-tectonic emplacement of granitic plutons commonly occur during the culmination of orogeny. In such instances, granite intrusion appears mostly where the metamorphic grade is the highest. In addition to this, anatectic melts of granitic composition are found in migmatitic terranes.

In many regions emplacement of granitic plutons is associated with synchronous eruption of chemically similar, presumably

co-genetic volcanic rocks. Peralkaline granites and quartz syenites of Oslo graben province is an example. Anorogenic granites, related to regions of crustal distension form a sub-group in this category.

1.2. Metallogeny related to granites.

Mineral deposits associated with granitoid rocks form a spectrum ranging from strictly chalcophile elements that form covalent bonds to strictly lithophile elements that form ionic bonds (Taylor, 1965; Stemprok et al., 1978; Drysdall et al, 1984). Economic concentrations of the chalcophile group in granitoid rocks typically occur as porphyry deposits formed by hydrothermal processes during sub-solidus cooling of high-level sub-volcanic dominantly calc-alkaline plutons (Sillitoe, 1972). Granitoid economic deposits of the lithophile group occur as veins and pegmatites formed during the magmatic stage of cooling of leucogranite bodies at intermediate depths. A major spectrum of lithochalcophile elements (Pb, Zn, As, Sb, Bi, Ag) span these two extremes and typically form vein-type deposits (Evans, 1982; Eugster, 1985).

Two main variables, namely, ionic radius and ionic potential, control the geochemical behaviour of elements that form different types of granitoid mineral deposits (Taylor, 1965; Strong, 1981). Thus, the strongly lithophile group tend to form tetrahedral complexes eg: $(SnO_4)^{4-}$ $(MoO_4)^{2-}$ etc. and is strongly

concentrated in differentiated silicic magmas formed either by crystal fractionation or as initial partial melts. The strongly chalcophile elements like Cu can either enter silicate lattices or form sulfides and thus tend to be randomly distributed during cooling of a magma or partial melting. The other lithochalcophile elements have strongly covalent bonds with oxygen which exclude them from silicate lattices. They would thus be concentrated in differentiated liquids. However, the behaviour of all these elements is critically influenced by fluid-melt partition coefficients when an aqueous fluid coexists with silicate melts (cf. Burnham, 1979).

Molybdenum is a chalcophile element and has a strong affinity for sulfur. It is found in metallogenic groups associated with sulfur and oxygen and covers a full range from magmatic to hydrothermal deposits. Due its peculiar crystallo-chemical nature, molybdenum even manages to behave as a lithophile element (in its chemical valence of 6) and also as a siderophile element. Molybdenum is quite scaree in the earth's crust, since the average crustal content is around 1.5 ppm. Various schemes of classification of molybdenite deposits have been proposed which include the recent one by Westra and Keith (1981). It has been noted that molybdenite mineralization associated with calc-alkaline and alkaline intrusives are usually related to deep crustal structures and both the magma and molybdenum have an origin in the deep crust or upper mantle (Schonwandt and Peterson, 1983).

Molybdenite bearing portions of the associated granites are typically enriched in potassium, with K_2O/Na_2O ratios generally greater than unity. Potassic alteration, mainly of biotite and potash feldspar is closely related in time and space to molybdenum (Marmo, 1971; Sutherland and Brown, 1976; Westra and Keith, 1981).

1.3. Regional geology.

1.3.1. Lithounits.

The Precambrian of south India comprises a granulite facies terrane in the south and an amphibilite facies terrain in the north, separated by a narrow transitional zone that passes through Mangalore, Bangalore and Madras (Fig.1, inset). The Kerala region forms part of the granulite facies terrane and occupies a significant portion of the south-western Indian shield and the western continental margin of India. The region is dominantly composed of Precambrian crystalline rocks including charnockites, khondalites and migmatitic gneisses. Intrusive plutons of granitic and syenitic composition occur in a number of localities (Fig.1). Mafic dykes of gabbro and dolerite cut across the various lithounits. Sedimentary formations of Tertiary age unconformably overlie the Precambrian basement rocks. They comprise a series of variegated clays and sandstones, underlain by more compact sands and clays and thin beds of limestone (Rao, 1978; Nair et al., 1975; Raha et al., 1983).

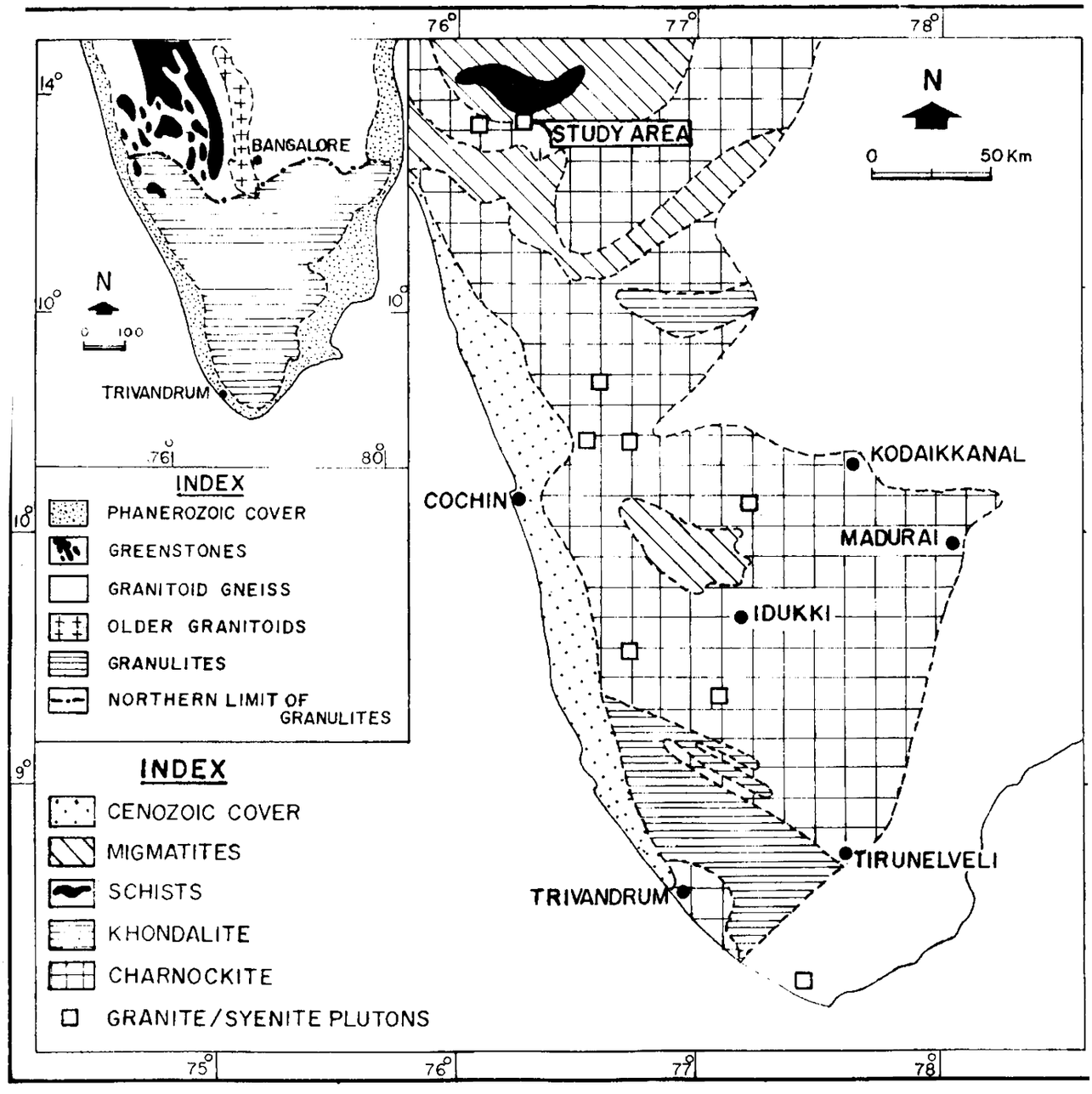

Fig. 1 Generalised geological map of the Kerala region (after Rao, 1978). The inset shows Archaean high-grade low-grade boundary in south India.

The various lithological units of the Precambrian crystalline rocks are as follows:

(1) The khondalite group: composed of garnetiferous biotite gneisses with or without sillimanite and graphite; quartzo-feldspathic gneisses and calc-granulites, (2) The charnockite group: made up of hypersthene and/or diopside bearing granulites and gneisses, their retrograded products and hornblende granulites, (3) The Sargur Group: represented by greenstone sequence comprising high grade schists being southward extension of the corresponding rocks in southern Karnataka. The Sargurs are represented by bands of quartz-mica schists with kyanite, quartz-sericite schists, quartz-magnetite, quartzite and meta-ultramafics, (4) The Dharwar Group: The younger Dharwar schists consist of oligomictic conglomerates, current bedded quartzites, quartz-mica schists and biotite-quartzites, forming an interlayered sequence, (5) Basic and ultrabasic rocks: represented by dykes of gabbro, dolerite, anorthosite, peridotite and pyroxenite, (6) Granites and related rocks: represented by minor intrusives of pink and grey granites, syenites and related pegmatites.

The following stratigraphic succession may be drawn from the available geologic data:

Cenozoic sediments

-----Unconformity-----

Gabbro/dolerite dykes

Acid and basic intrusives

Dharwar Group

-----Unconformity-----

Sargur Group

Migmatitic gneisses

Charnockite Group

Khondalite Group

Earlier, the granitic intrusives known in some localities in Kerala were correlated with the Precambrian granitic rocks of adjacent terranes. In the light of recent studies, as will be discussed presently, it is now understood that they form an younger group.

The migmatitic gneisses form two major zones, one in northern Kerala and the other in central Kerala. The major khondalite exposures occur in southern Kerala, where they extend to the Tamil Nadu region. Patches of khondalites are also exposed near Palghat and Kasaragod. The charnockite group of rocks form two broad zones. The northern zone extends from the coastal region towards SE into the Wynad plateau and Nilgiri plateau and from there it turns NE to the Mysore plateau. The second zone

occupies nearly half of the area of the state, extending eastwards into theKodaikanal-Madurai hills and the plains of Tirunelveli district of Tamil Nadu. Along the zone of charnockite-khondalite contact in central Kerala, elongated and lensoidal bodies of cordierite-bearing gneisses occur. The schistose rocks are restricted to northern Kerala where they occur as minor belts elongated in the E-W and NW-SE directions.

1.3.2. Structure

The Precambrian units exhibit polyphased deformation (Sinha Roy 1983). Primary stratification is not seen in any of the rock types. The most prevalent trend of foliation is from NNW-SSE to NW-SE. Towards south east and east, this trend swerves to E-W and ENE-WSW. Structural studies indicate that the various Precambrian rock units were folded on a NNW trending axis. Minor folds and broad warps with axes trending NNW-SSE are also seen. Towards the west, the NNW-SSE trend swerves E-W and WSW-ESE, strongly suggesting a complementary NNW-SSE fold axes. Structural analysis (Rao, 1978) indicates that the east-west trending folds (f_1) were refolded by younger NNW-SSE (f_2) folds (Fig.2). A minor third set (f_3) is also seen, interfering with f_1.

A number of shears, faults and fractures are also recognised in the region. They have been divided into 5 sets based on their general trend, namely, E-W, NE-SW, NW-SE, N-S and NNW-SSE.

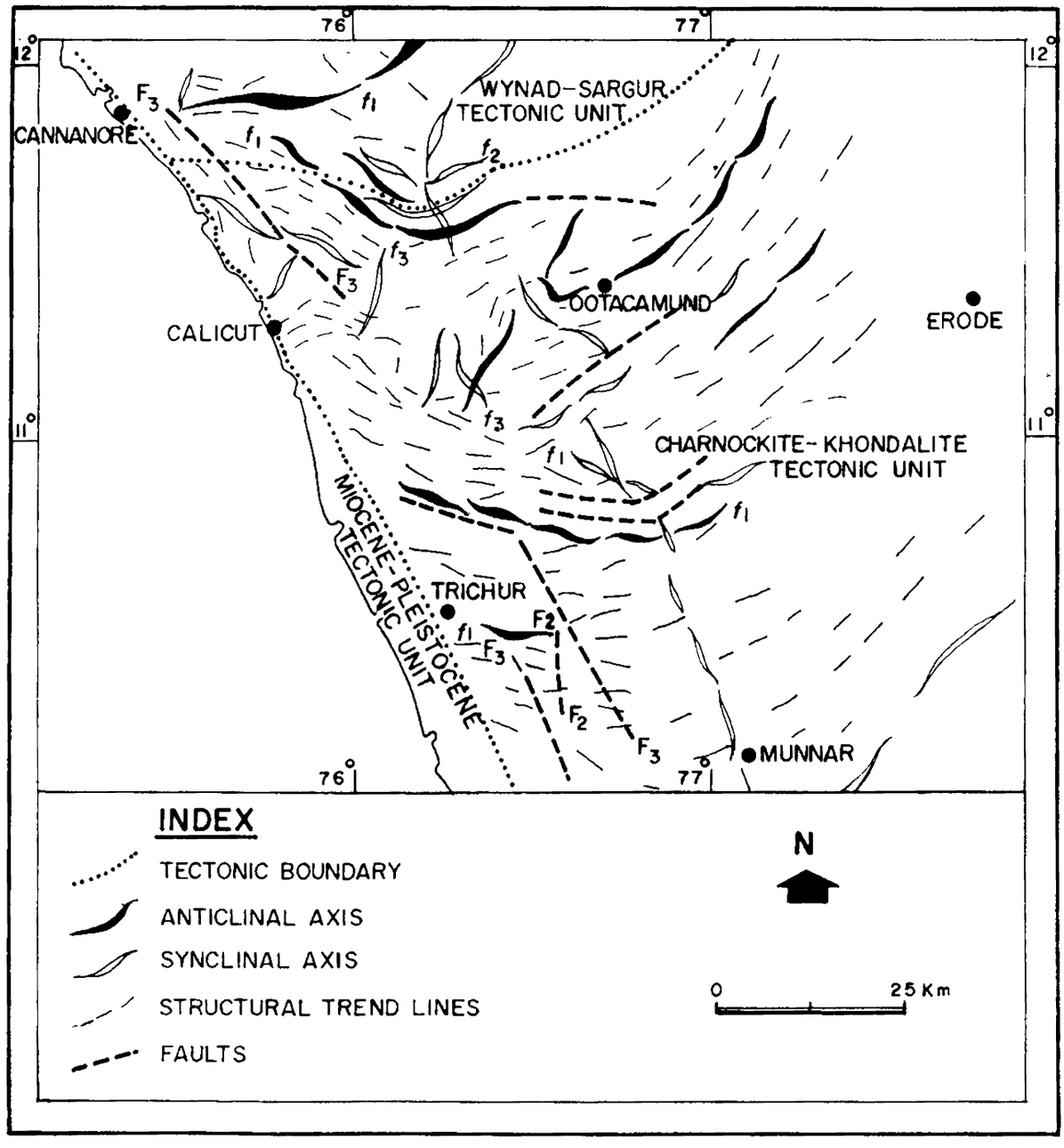

Fig. 2 Generalised structural features of the northern Kerala region (after Rao, 1978).

Out of these, the NNW-SSE, E-W, NW-SE and NE-SW trends are the major ones. Drury and Holt (1980), and Drury et al (1984) consider the major shear-zones to be of Proterozoic age.

1.3.3. Metamorphism

The charnockite and khondalite groups are products of granulite facies metamorphism. A younger metamorphic event which led to a retrogression of the granulites under the conditions of amphibolite facies, mainly along regional shear zones, is also recognised. The physical conditions of metamorphism has recently been studied by applying methods of mineral thermobarometry (Harris et al., 1982; Raith et al., 1982; Sinha Roy et al., 1984). P-T estimates for the peak granulites facies metamorphism range from 650-800°C and 6-9.5 Kb pressure. The high pressure granulites place a minimum constraint of ca. 30 km on the maximum thickness of the late Archaean crust in this region (Harris et al., 1982).

Fluid inclusion studies show that chemically distinct fluids were involved in the charnockite metamorphism. The pressure-temperature conditions recorded by fluid inclusions define a piezothermic array that is characterised by higher convexity towards the temperature axis than the array obtained by the locus of metamorphic geotherms from mineral assemblages (Santosh, 1985a). The carbonic metamorphism of charnockites was achieved under high P_{CO_2} conditions by the transfer of juvenile CO_2 from the upper mantle.

1.3.4. Acid magmatism

Till recently, it was believed that the region is more or less entirely composed of Precambrian crystallines and only little was known about acid magmatism of younger age. The known granitic intrusives were correlated with a Precambrian event. Intensive field and laboratory work undertaken recently have revealed the occurrences of a number of granitic and syenitic plutons in the region, spatially related to major fault-lineaments and showing unique petrochemical characters. Intrusives of granitic composition occur at Chengannoor (Santosh and Nair, 1983a), Pariyaram (Santosh et al., 1983), Munnar (Nair et al., 1983a), Ambalavayal (Nair et al., 1982, Santosh and Nair, 1983b), Kalpatta (Nair et al., 1983b), Peralimala (Nair and Santosh, 1984), Mercara, Thaluru, Puthur, Vellingiri and Wadakkancheri. The granites and granophyres of Ezhimala also belong to this group (Nair and Santosh 1983). Syenite plutons occur around Sholayar (Nair et al., 1984), Puttetti (Nair and Santosh, 1985), Mannapra (Santosh and Thara, 1985), Angadimogar (Santosh and Nair, 1985) and Kizhakkanchery.

1.3.5. Geochronology

The available geochronologic data attribute an age of 2.6 b.y. (Crawford, 1969) for the granulite facies event, which is considered to have been responsible for the stabilisation of the Archaean crust of south India (Harris et al., 1982; Raith et al.

1982). The younger magmatism which gave rise to the granite and syenite intrusives, of dominantly alkaline character, is now known to represent a Late Precambrian-Early Paleozoic episode (Odom, 1982; Nair and Vidyadharan, 1982; Nair et al, 1985). Eventhough older mafic and ultramafic intrusives of Precambrian age occur in some localities, the basic magmatism, largely represented by dolerite dykes, belong to Tertiary age, correlated with the Deccan trap activity (Sinha Roy and Furnes, 1982, Radhakrishna et al., 1985).

1.3.6. Mineralization

The economic and sub-economic minerals in the region associated with the Precambrian rocks include gold, graphite, scheelite, talc-steatite, muscovite, phlogopite, magnetite and crystalline limestones. The Miocene sedimentaries contain rich deposits of clay and the Quaternary sands contain ilmenite, monazite, rutile, zircon, garnet sillimanite and glass sands. Gemstones of chrysoberyl variety are associated with Early Paleozoic pegmatites of southern Kerala (Soman and Nair, 1983). Molybdenite mineralization has been reported earlier from adjacent terranes (Subramanian, 1979). However, the one associated with Ambalavayal granite was noted only recently (GSI News, 1981).

1.4. Geology of Wynad region

The lithounits around the region surrounding Ambalavayal in Wynad district of northern Kerala comprise charnockites, migma-

titic gneisses, schists, granites and dolerite dykes (Fig.3). The charnockites are of acid to intermediate variety with a mineral assemblage, quartz-K-feldspar, plagioclase, orthopyroxene, with or without garnet having accessory hornblende and biotite. The schistose group is represented by amphibolites, mica schists, fuchsite quartzite and talc-tremolite-actinolite schists. Two granitic plutons occur in the region, one near Kalpatta and the other near Ambalavayal. The Kalpatta granite occurs as an elliptical stock. It is a medium to coarse grained grey biotite granite, principally constituted of K-feldspar, plagioclase and quartz with biotite and hornblende as the major mafic minerals. The petrochemistry of this granite, invoking formation from a partial melt generated at deeper crustal levels, is given in Nair et al. (1983b). The granite of Ambalavayal is emplaced within Precambrian gneisses. The regional gravity survey data (Quereshy et al. 1969) shows a prominent gravity low around the Ambalavayal area, indicating subsurface extension of the pluton.

1.5. Previous studies

Only very little information is presently available on the geology of the Ambalavayal area which include a note on the occurrence of molybdenite in Ambalavayal (GSI News, 1981) based on unpublished GSI Technical Reports and preliminary reports on the petrochemical characters of the granite (Nair et al. 1982; Santosh and Nair 1983b).

1.6. Scope of present study

As already mentioned, recent investigations have shown a dominant acid magmatic event in the region, represented by a number of intrusives. The Ambalavayal granite is a typical member of this suite and has been chosen for comprehensive studies in order to decipher the characteristics and significance of this magmatic event and related metallogeny.

90 sq km area around Ambalavayal was demarcated for this study. Intensive field work involving mapping of the lithologic contacts the relationship of granite and basement rocks, delineation of the zone of mineralization and collection of representative samples was carried out by the author through three field seasons during 1982-1984. Laboratory work involving preparation of thin and polished sections, preparation of doubly polished plates for fluid inclusion studies, separation of monomineralic fractions for X-ray and geochemical analyses and isotope dating and chipping and pulverzing of representative samples for whole rock geochemistry was done. A total of 86 samples were chemically analysed which include 24 granites (major and trace) 24 gneisses (major and trace) 2 enclaves (major and trace) 2 fuchsite quartzites (major and trace), 17 feldspars (major elements), 6 hornblends (major and trace), 6 biotites (major and trace) and 5 molybdenites (Mo and trace).

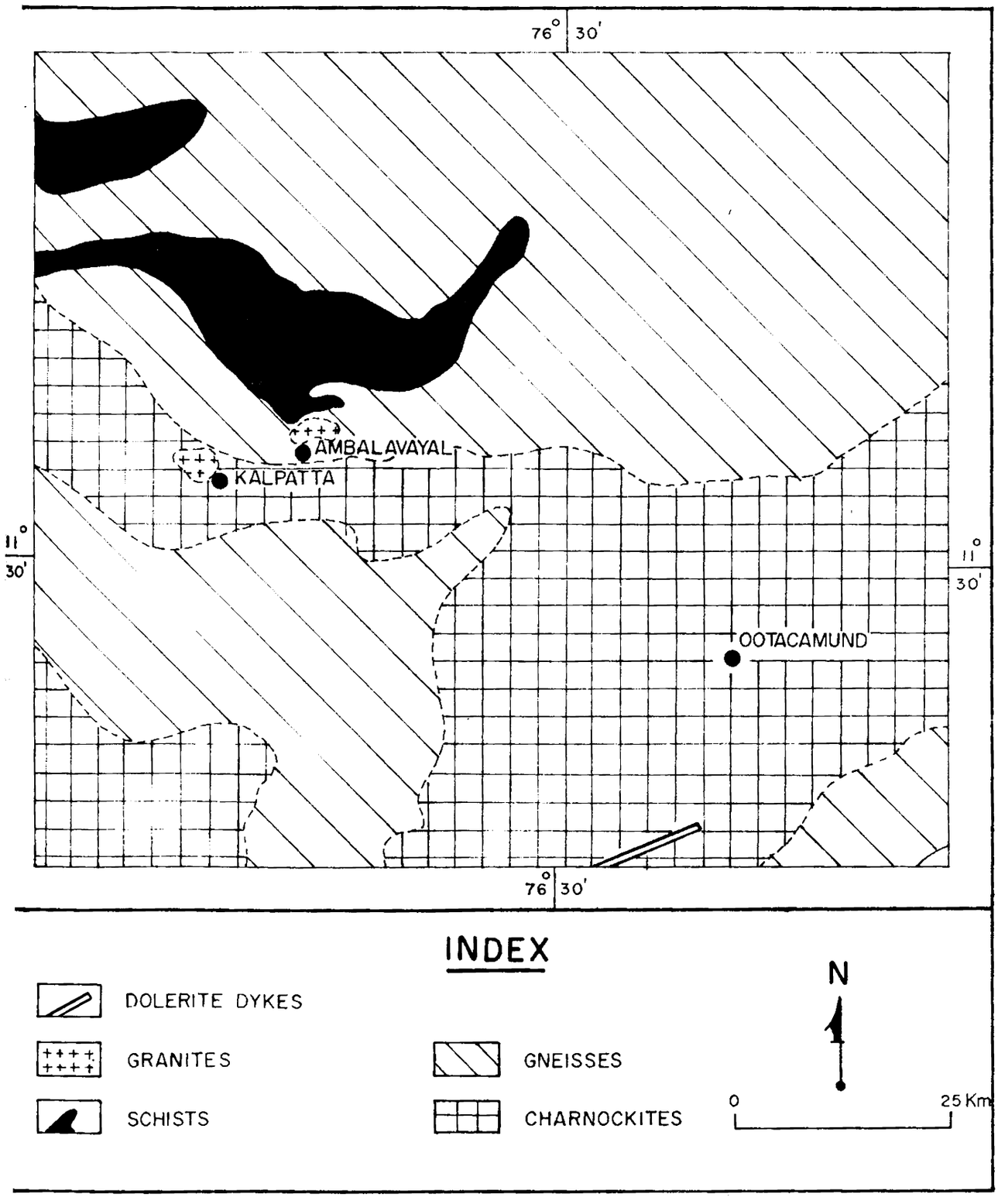

Fig. 3 Geological map of the northern Kerala region (after Rao, 1978).

The present work envisages the following objectives:

1) to prepare a lithologic map of the Ambalavayal area on 1:25,000 scale, to demarcate the granite boundary;
2) to understand the textural and mineralogic features of the granite and basement rocks through petrographic studies;
3) to understand the composition, structural state and intensive parameters of equilibration of various minerals in the granite through mineral-chemical and X-ray studies;
4) to know the age of magmatism through whole-rock isotope dating and to assess the last thermal event in the region through mineral dating;
5) to classify and characterise the granite and basement rock and to evaluate in detail their petrogenetic aspects through whole rock analyses of major and trace elements;
6) to reconstruct the nature of fluid evolution and to assess the composition and P-T parameters of fluids associated with the magmatism and mineralization through detailed optical and heating-freezing studies of fluid inclusions associated with the granite, pegmatites and quarts veins, and
7) to evaluate the tectonic significance of magmatism and metallogeny.

CHAPTER - 2

GEOLOGY OF THE AMBALAVAYAL AREA

2.1. Granite, pegmatites and quartz veins.

The granite pluton marks a conspicuous physiographic high, forming rocky hills with steep ridges around the Ambalavayal area (Fig.4). A number of working quarries around Ambalavayal expose fresh vertical sections of the granite, some of them upto 30m high. The granite maintains rather sharp contact with the gneisses, whereever the contacts are discernible. A faint foliation marked by the preferential alignment of mafic minerals is noted, especially towards the exposed peripheral portion of the pluton. These foliations trend parallel to the peripheries with steep outward dips, characteristic of intrusive granite plutons. Thegranite body outcrops as an E-W elongated elliptical pluton, covering an area of 20 sq km (Fig.5). It is generally pink, massive, medium to coarse grained, composed of interlocking feldspar and quartz, with hornblende and biotite constituting the major mafic phases. Towards the eastern and western margins of the pluton, joint planes are developed that trend mainly E-W, NW-SE and NE-SW. The trend of joint planes have been plotted in a Ross diagram (Fig.6). On a regional scale, the pluton is emplaced at the intersection point of the E-W trending Moyar and the NE-SW trending Calicut fault-lineaments (Fig.7). The region also falls in the zone of extension of the NE-SW trending Bavali lineament. It is presumed that the joint plane pattern has a probable relationship with the reactivisation of these fault-lineaments.

Fig. 4 Field photographs showing the features of granite, gneiss and their relationship around Ambalavayal

(a) The Ambalavayal granite forming rocky mounds

(b) An active granite quarry

(c) Sharp contact between the granite and the basement gneisses

(d) Minor folds in the granite towards its western periphery.

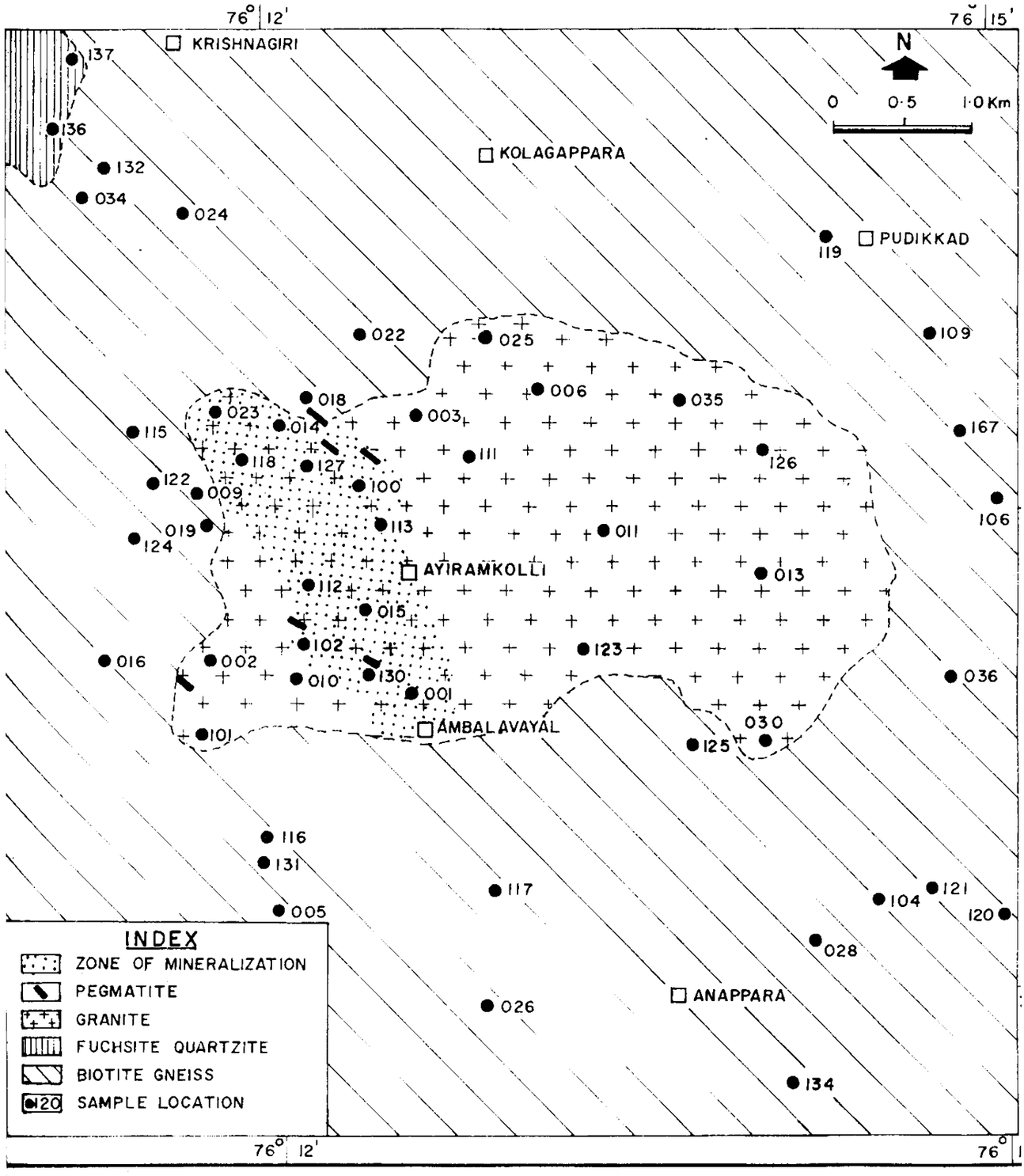

Fig. 5 Geological map of the Ambalavayal area showing the zone of molybdenite mineralisation and sample locations of present study.

AMBALAVAYAL

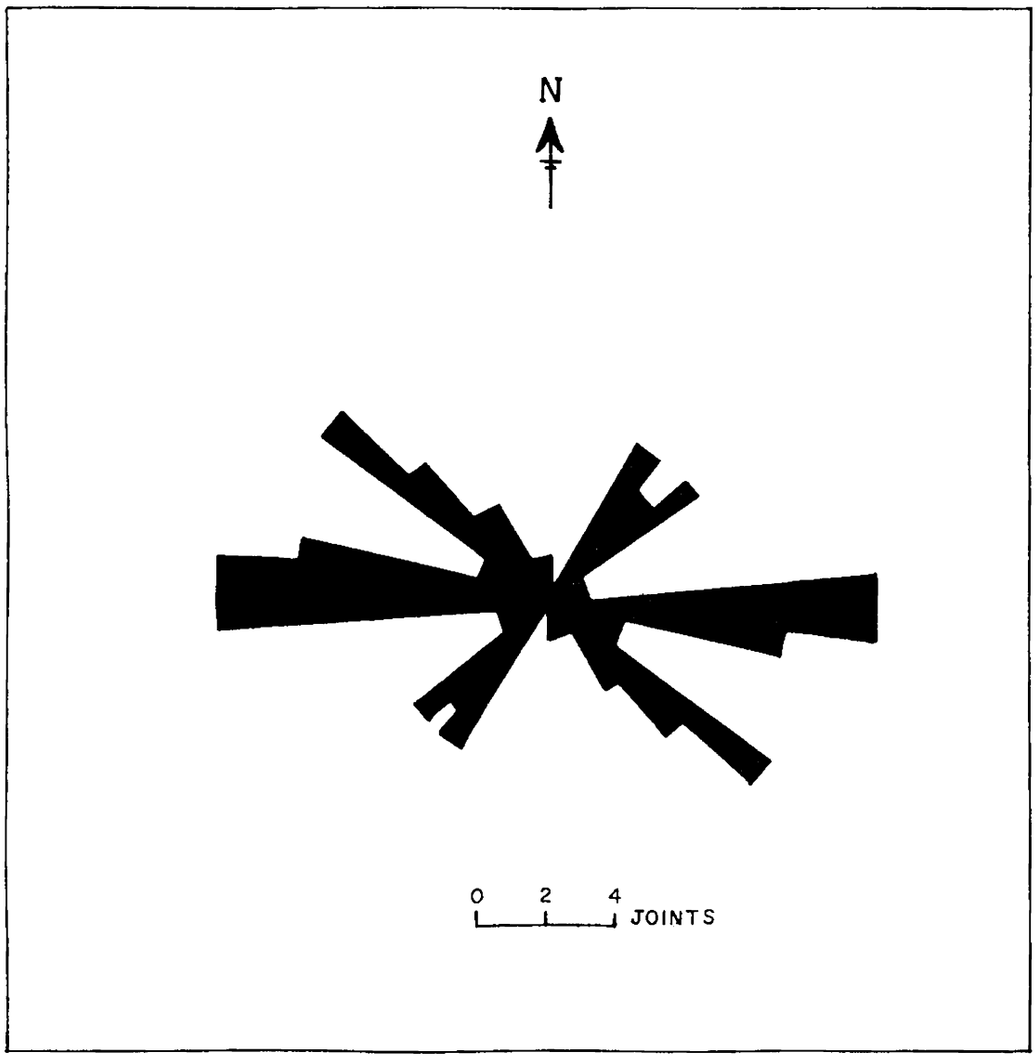

Fig. 6 Ross diagram depicting the joint pattern data of Ambalavayal granite.

Pegmatites in Ambalavayal are mainly found in the western region of the pluton, where they show general trends varying from E-W to NW-SE, with steep dips. The pegmatite bodies range in width from less than a metre upto 3m. They show a mineral assemblage of quartz, pink K-feldspar and hornblende. In some of them, biotite and calcite are also found. K-feldspar forms large crystals (Fig.8) measuring upto 20cm in some cases. Similarly, a unique feature is the occurrence of large hornblende crystals, sometimes measuring upto 15cm. A number of quartz veins ranging in width from a few cm upto 1m cut across the granite, mainly in the western part. Aplite veins of 40-60cm width are observed in a quarry behind the Ambalavayal hospital.

2.2. Mineralization

Molybdenite occurs as small flakes and flaky aggregates. It is found as disseminations within an 800m width zone trending NW-SE in the granite. Disseminated flakes of molybdenite also occur associated with minerals like hornblende, K-feldspar and quartz in pegmatites. Molybdenite forms flaky aggregates measuring usually 5-10 cm (Fig.9), in quartz veins. Large flaky aggregates measuring upto 20cm were recovered from the vein quartz in Ayiramkolli quarry.

In comparison to large mineral deposits, no profound wall-rock alteration features are noted in Ambalavayal. This is probably because a slow cooling system of large hydrothermal reservoir

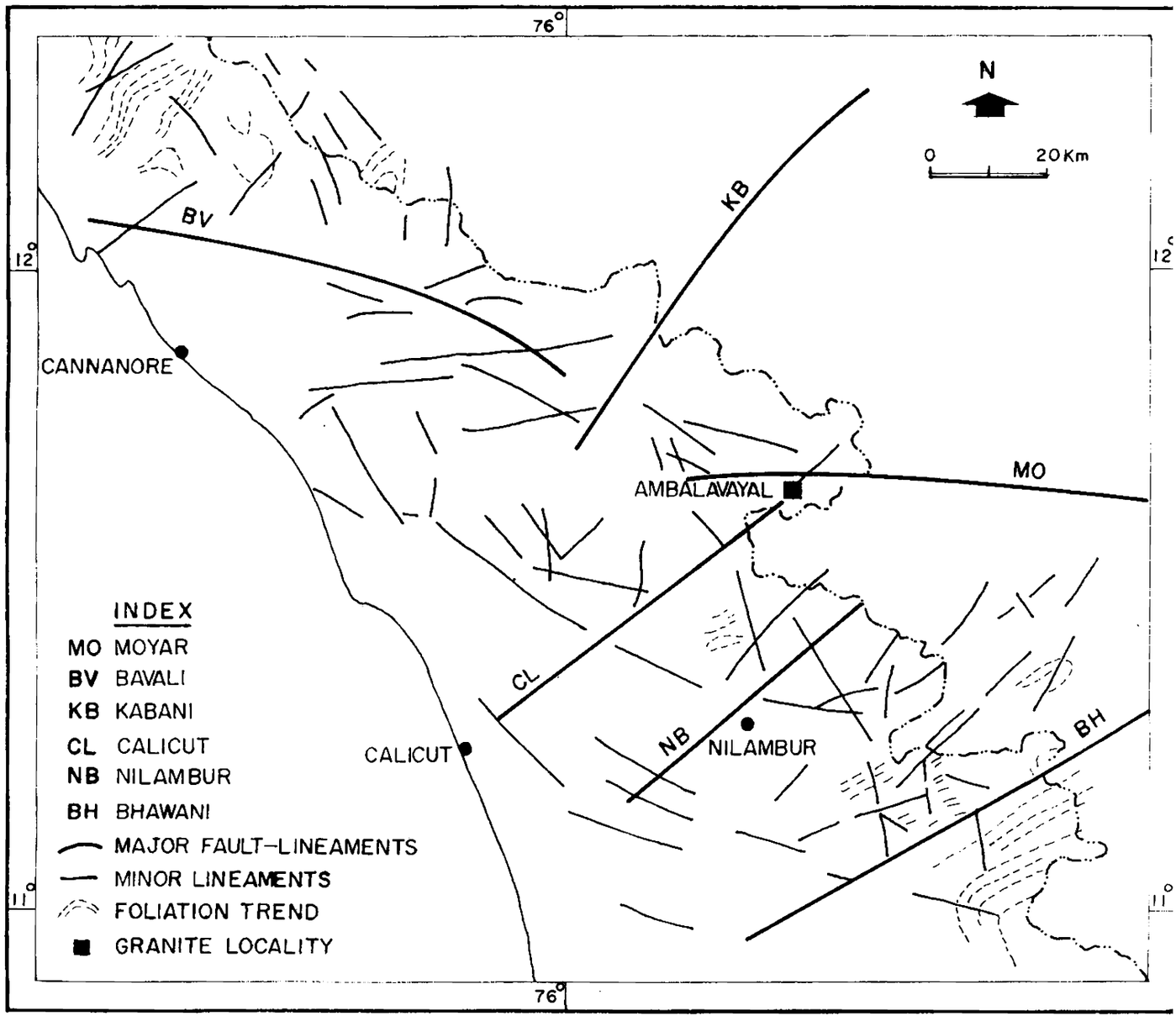

Fig. 7 Lineament map of northern Kerala region showing location of Ambalavayal.

Fig. 8 Field and hand specimen photographs of pegmatites in Ambalavayal

(a) Pegmatite cutting the granite, showing hornblende crystals as clots.

(b) K-feldspar megacrysts associated with hornblende

(c) Large hornblende crystals in association with K-feldspar.

Fig. 9 Photographs of flaky aggregates of molybdenite from Ambalavayal

(a) Molybdenite flakes associated with quartz vein

(b) Large flaky aggregates of molybdenite recovered from the Ayiramkolli quarry near Ambalavayal.

was never involved in the mineralization history of Ambalavayal as will be shown later, and is reflected in the fact that the disseminated mineralization is probably not of considerable economic significance. Nevertheless, the large pink K-feldspar megacrysts, their higher structural ordering (see section on mineralogy), occurrence of interstitial non perthitic microcline and common occurrence of biotite in the ore zone suggest a wall-rock alteration of potassic type.

2.3. Basement rocks.

The dominant country rock in the Ambalavayal area is a light grey, medium to coarse grained gneiss, which shows prominent mineralogical banding. Enclaves of biotite and biotite-hornblende rich assemblages are found in some localities. Towards the NW-part of the study area, a minor band of fuchsite quartzite is exposed in a nearby paddy field.

The earliest recognisable planar structure (S_1) of the rocks is a secondary compositional banding. S_1 in the gneisses is defined by alternating quartzo-feldspathic layers and mafic (biotite-rich and biotite+hornblende-rich) layers. The strike of secondary compositional banding is generally WNW-ESE to NW-SE. The dip of S_1 varies from 50 to 80°. S_1 planes of quartzo-feldspathic gneisses show mesoscopic fold patterns. From structural chronology, it appears that this fold structure belongs to the second generation. The axial plane cleavage (S_2) is poorly developed, extending in WNW-ESE direction.

The pole orientations of S_1 planes are plotted in the lower hemispheric projection on equal area net (Fig.10). The pole orientations show a regional spread of S_1 planes indicating folded structure. The S_1 planes define a girdle whose axis plunges 60° towards 240°, correlatable well with the regional structure. The interference of folds of subsequent generation probably contributed to the minor contour that falls outside the great circle, towards the southern part of the diagram.

2.4. Petrography

2.4.1. Granite

The granite generally exhibits a hypidiomorphic granular texture with quartz, perthitic K-feldspar and plagioclase as the dominant minerals (Fig.11). In some sections K-feldspar also forms megacrysts where small laths of albite occur at the grain border or as patches along the perthitic lamellae. The perthitic K-feldspar+plagioclase assemblage in the granite exemplifies a transition from transolvus to subsolvus texture (Martin and Bonin, 1976). This texture implies an early crystallization under 'dry' conditions and subsequent introduction of H_2O rich fluids. During this range, the temperatures were below the 'dry' solidus, but were still above the 'wet' solidus (Martin and Bonin, 1976).

Modal analyses were carried out in representative samples of the granite using an Electrical Integrator. The modal

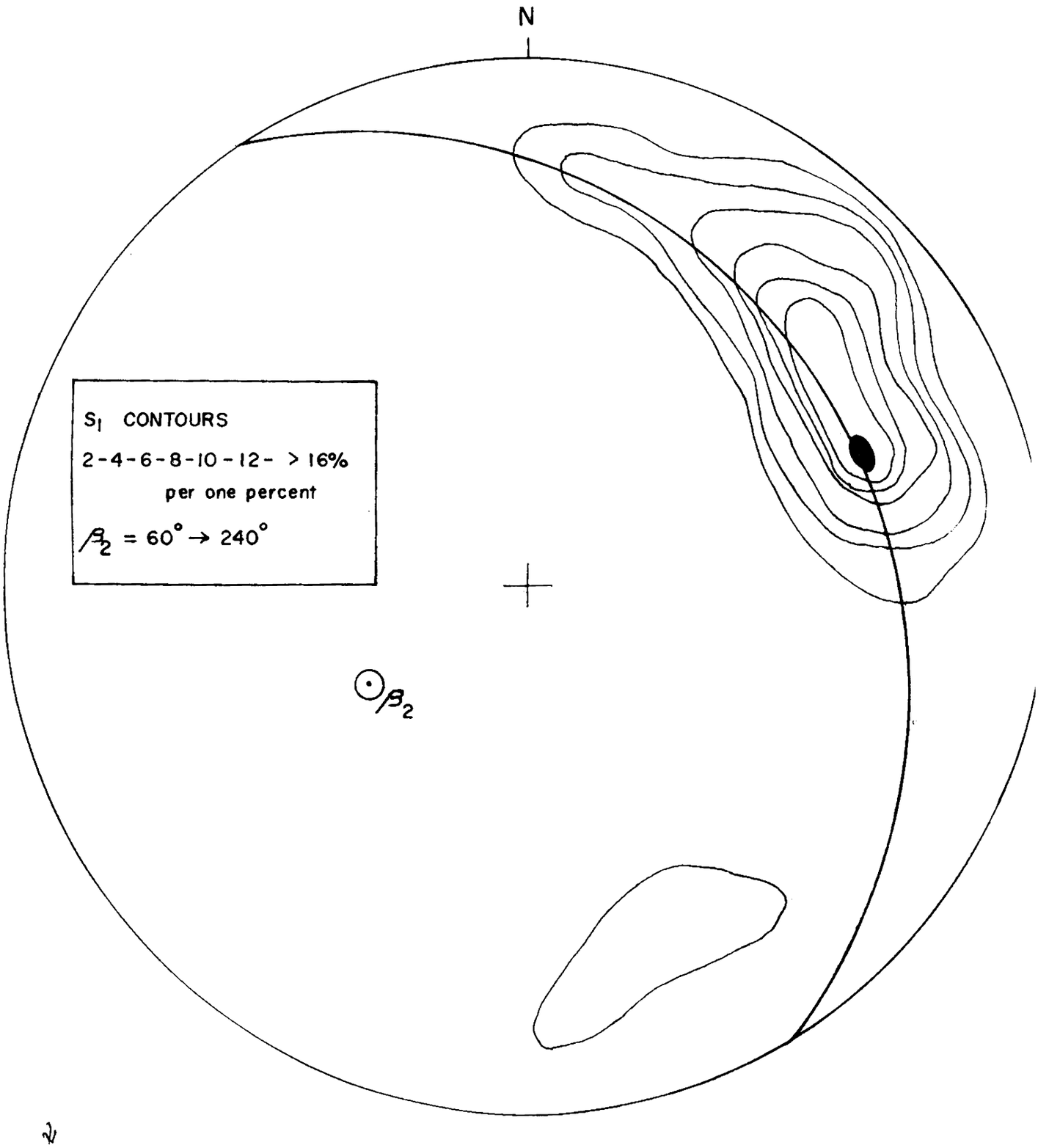

Fig. 10 Equal area (lower hemisphere) plots of the foliation data of gneisses around Ambalavayal.

abundances, presented in Table 1, show the following ranges (in per cent): quartz: 22.3-37.1; K-feldspar:24.2-48.3; plagioclase: 22.3-37.5; hornblende: 0.5-3.6; biotite: 0.7-4.1; riebeckite: 0.2-2.5; sphene+monazite: 0.2-3.2; opaques: 0.2-1.5; calcite + apatite: 0.2-1.3 and the rest comprising alteration products like epdidote and sericite.

The Q-A-P plots of the rock fall in the field of granite (Streckeisen, 1976). However, since the composition of plagioclase is mainly albitic, the feldspar components in the Q-A-P scheme can be coupled, whereby the plots fall in the field of quartz alkali feldspar granite.

K-feldspar: Anhedral to subhedral K-feldspar grains (3-7mm) usually show microperthitic lamellae (10-50 microns in width). The perthitic phase occurs as thin strngers but a local variation to coarser braids, blebs and patches is also seen, especially in the western part of the pluton. The variation in perthitic texture from fine to coarse is indicative of increasing pH_2O with increasing degree of fractionation (Parsons 1978). The host K-feldspar shows triclinic symmetry (Δ = 0.2955) and an increase in the degree of structural ordering towards late stages of crystallization (see section on mineral chemistry), which is also indicative of the dominance of a hydrous regime in the residual stage. The host K-feldspar exhibits microcline cross-hatching. Interstitial K-feldspar is usually rare but

Table: 1 Modal composition of Ambalavayal granite

Mineral	001	002	003	006	010	013	014
Quartz	31.1	32.9	31.6	26.8	28.4	30.7	33.6
K-feldspar (including perthite)	34.5	35.8	31.1	40.5	38.4	24.2	35.8
Plagioclase	28.4	23.7	29.4	22.3	26.1	36.3	22.4
Hornblende	1.7	1.9	3.6	2.8	1.2	2.1	1.2
Biotite	2.6	2.0	1.5	1.4	1.6	2.4	2.8
Riebeckite	0.2	1.5	0.2	2.5	0.2	1.2	-
Sphene + monazite	0.5	1.0	0.5	1.6	0.8	1.4	0.5
Calcite + apatite + zircon	0.3	0.2	0.4	0.3	1.2	0.4	0.6
Opaques	0.4	0.6	1.2	1.4	1.5	0.8	0.6
Others	0.3	0.4	0.5	0.4	0.6	0.5	2.5

Table: 1 (Contd.)

Mineral	015	023	030	100	112	123
Quartz	35.7	31.8	27.0	22.3	24.6	25.4
K-feldspar (including perthite)	29.7	30.5	35.4	48.3	42.4	28.7
Plagioclase	27.3	25.5	28.7	24.8	30.9	37.5
Hornblende	1.3	1.6	1.2	1.2	0.5	2.1
Biotite	1.7	4.1	2.6	1.5	0.7	1.8
Riebeckite	2.4	1.2	0.3	-	-	0.8
Sphene + monazite	0.7	3.2	0.8	0.5	0.2	2.2
Calcite + apatite + Zircon	0.3	0.6	1.3	0.8	0.3	0.4
Opaques	0.4	1.1	1.2	0.2	0.2	0.5
Others	0.5	0.4	1.5	0.4	0.2	0.6

Table : 1 (Contd.)

Mineral	126	127	Mean
Quartz	37.1	35.0	30.27
K-feldspar (including perthite)	27.6	29.8	34.18
Plagioclase	30.5	28.7	28.17
Hornblende	2.4	1.6	1.76
Biotite	1.2	1.4	1.94
Riebeckite	-	1.3	1.07
Sphene + monazite	0.3	0.8	1.01
Calcite + apatite + zircon	-	0.2	0.53
Opaques	0.4	0.6	0.74
Others	0.5	0.6	0.66

non-perthitic microcline with intense cross-hatching is locally found as minor grains at the grain borders of quartz and feldspars indicative of crystallization under low temperature water rich conditions (Marmo, 1971).

Plagioclase: Plagioclase laths are euhedral to subhedral, ranging in size from 2-4mm. They are seldom zoned but invariably show lamellar twinning. The composition is dominantly albitic as inferred from extinction angle measurements and geochemical data. Small laths of albite also occur along the grain margins of K-feldspar megacrysts.

Hornblende: Discrete euhedral laths of hornblende (edenite) with strong pleochroism as: X= greenish yellow, Y= yellowish green and Z= deep green and $Z \wedge c = 13°$ constitute the major mafic mineral in the granite. It is texturally associated with biotite. In some sections, large subhedral laths (upto 8mm) show partial resorption along grain margins with associated iron oxides and chlorite.

Riebeckite: Riebeckite occurs as euhedral crystals (0.5-3mm) showing deep blue colour, anomalous extinction and $Z \wedge c$ ranging from 3-9°. It is usually associated with hornblende.

Biotite: Biotite forms small to large flakes (0.2-4mm) which are seldom bent or deformed. Although occasional streaks of chloritic alteration is observed, the flakes are usually fresh.

Fig. 11 Photomicrographs showing the mineralogy of Ambalavayal granite. Bar scales represent 2 mm.

(a) Perthite-plagioclase-quartz assemblage

(b) Stringers and blebs of exsolved Na-phase in host K-feldspar

(c) Plagioclase lath showing lamellar twinning

(d) Interstitial microcline

(e) & (f) Mafic mineral assemblages of the granite comprising hornblende, riebeckite and biotite. Accessory sphene is also seen.

(g) Sphene occurring as a rim around opaque (magnetite).

(h) Biotite flakes fringing magnetite grain.

(a), (b), (c) and (d) in crossed nicols; rest in parallel nicols.

It shows brownish yellow to dark reddish brown pleochrodism, with a composition close to that of annite (see section on mineral chemistry). Small biotite laths fringing magnetite grains reflect the build up of an H_2O rich fluid phase towards later stages of crystallization (Parsons, 1980; Santosh and Thara, 1985).

Sphene: Euhedral crystals of sphene are ubiquitously found as an accessory phase. Typical wedge shaped crystals (upto 2mm) and twinned crystals are common.

Trace Phases: Eudedral grains of monazite, zircon and apatite occur both as discrete grains and as inclusions within biotite, hornblende and plagioclase. Calcite occurs as an interstitial phase at the grain boundaries of feldspars and is apparently not an alteration product. Similar primary interstitial calcite has been described from other alkali granites of the region (Nair and Santosh, 1984).

The opaques are mainly represented by magnetite which occur as early crystallized euhedral grains. Magnetite grains sometimes show replacement by hematite along grain boundaries. Molybdenite flakes occur along the grain boundaries of quartz and feldspars (Fig.12) showing high reflectivity, strong bireflectance and ink blue anisotropism. Molybdenite also occurs as thin stringers along cleavage traces and microfractures of feldspars and hornblende. Other sulfide phases present in minor amounts are pyrite and chalcopyrite.

Fig. 12 Photomicrographs of polished sections showing the opaque minerals. Bar scales represent 2mm.

(a) Molybdenite flake

(b) Molybdenite showing preferred occurrence along the grain margin of silicates

(c) Magnetite grain showing hematite replacement along grain margins

(d) Inclusions of chalcopyrite in pyrite.

Alteration products of ferromagnesium minerals include chlorite sericite and epidote.

The paragenetic sequence of various minerals in the granite can be summarised as below:

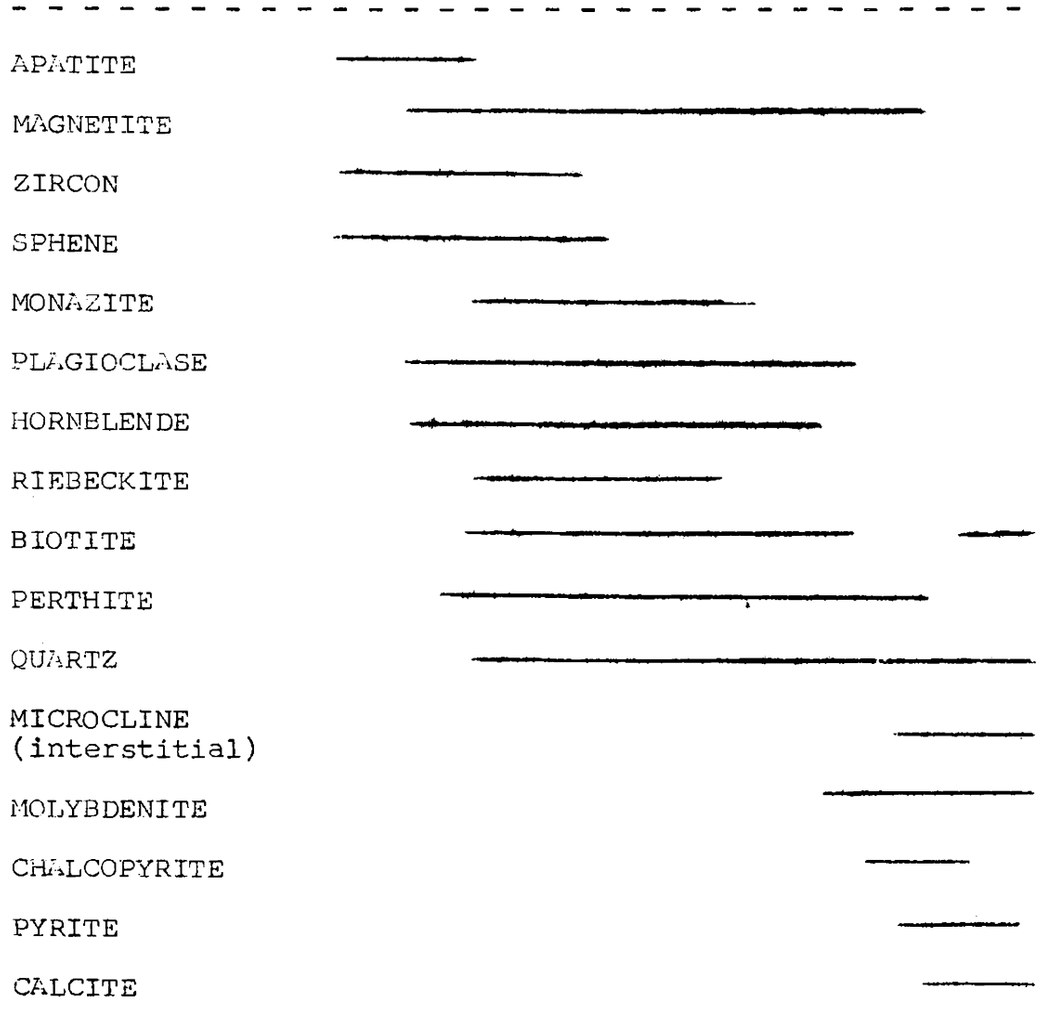

2.4.2. Gneisses

The general mineral assemblage of the gneisses comprises quartz,

K-feldspar and plagioclase with biotite as the dominant mafic mineral. Hornblende occurs in subordinate amount. Quartz forms anhedral grains. K-feldspar is usually microperthitic, sometimes forming megacrysts. Interstitial, non-perthitic K-feldspar (microcline) is also found. Subhedral laths of plagioclase showing lamellar twinning range in composition from Ab_5An_{95} to $Ab_{20}An_{80}$, as inferred from their extinction angle. At the plagioclase-K-feldspar interfaces, worm-like myrmekitic intergrowths are locally developed. Biotite and hornblende sometimes show irregular interfaces. Part of the biotite in the gneisses appears to be the product of homoaxial replacement of hornblende. In some sections, partially to completely resorbed grains of hypersthene is also found, with intimate association of fresh pleochroic hornblende. Epidote, iron-oxides and calcite are seen associated with the replacement. The accessories include Fe-Ti oxides, apatite, zircon and sphene.

Modal data (Table 2) show the following ranges (in per cent): quartz: 21.4-31.1; K-feldspar: 13.5-19.6; plagioclase: 44.2 - 56.2; biotite: 2.1-5.2; hornblende: 0.7-2.3; opaques: 0.3-1.2 and accessories: 0.9-5.5. In a Q-A-P diagram, the plots fall in the granodiorite field (Fig.13).

The 'restites' are mostly composed of biotite and hornblende. Sometimes, plagioclase laths of oligoclase composition are also associated. Relict grains of hypersthene are found in some sections. Fe-Ti oxides, apatite, zircon and sphene occur commonly.

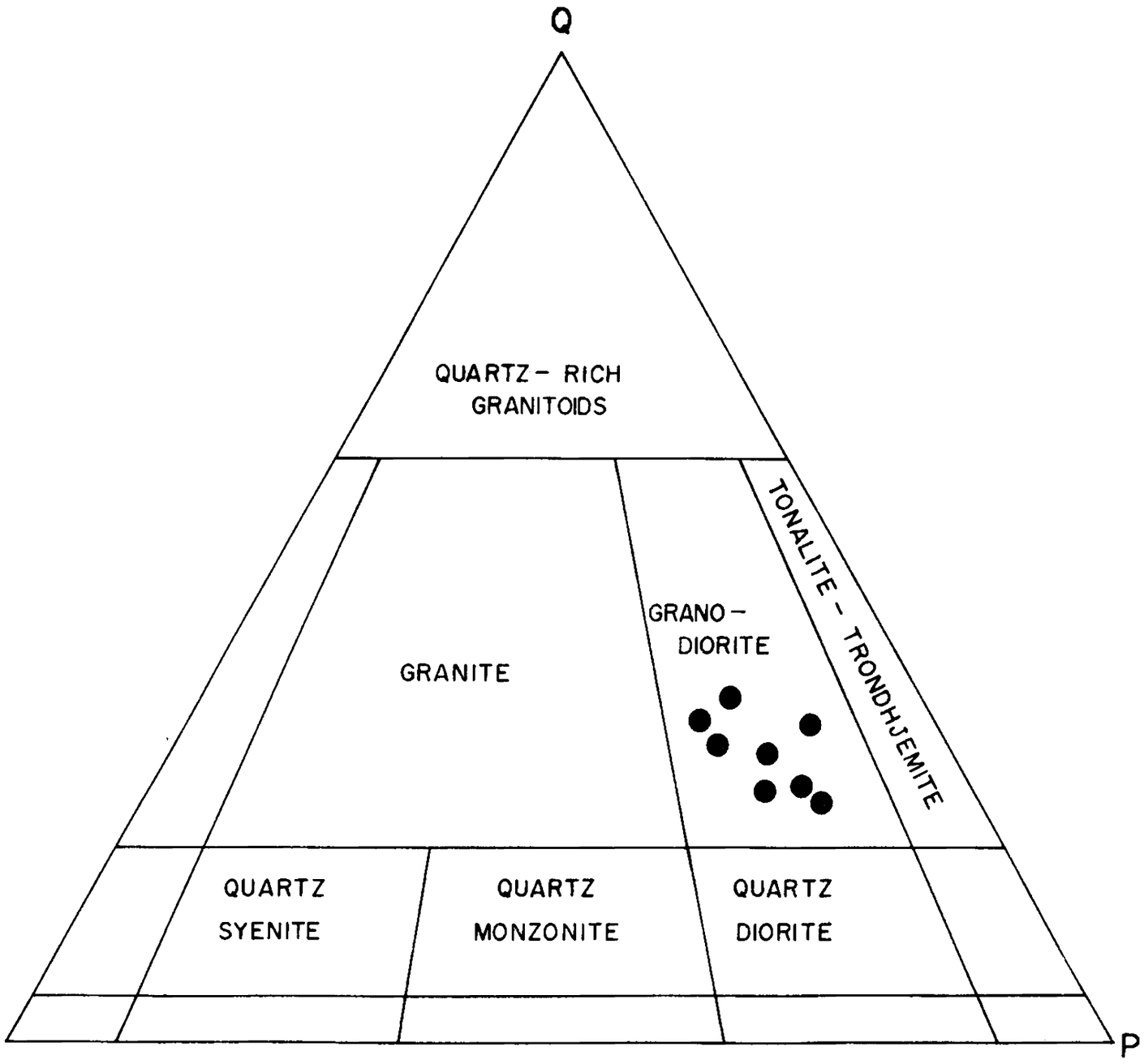

Fig. 13 Q-A-P plots of modal data of Ambalavayal gneisses. The classification boundaries are after Streckeisen (1976).

Table [illegible] Modal analysis data of Ambalavayal gneisses

	AS 005	AS 018	AS 024	AS 036	AS 116	AS 120	AS 125	AS 134
Quartz	25.4	22.7	27.8	29.6	21.4	31.1	28.5	32.7
K - feldspar	14.6	13.5	16.2	15.4	16.5	19.6	19.4	16.7
Plagioclase	54.4	56.?	50.6	47.7	47.9	44.2	46.1	44.4
Biotite	2.4	?.6	2.8	2.6	5.2	2.2	3.2	2.1
Hornblende	1.2	1.7	1.4	1.4	2.3	0.8	1.3	0.7
Opaques	0.4	0.8	0.3	0.5	1.2	0.4	0.5	0.5
Accessories	1.6	2.5	0.9	2.8	5.5	1.7	1.0	2.9
Recalculated								
Q	26.91	24.57	29.39	31.93	24.94	32.77	30.32	34.86
A	15.47	14.61	17.12	16.61	19.23	20.65	20.64	17.80
P	64.42	60.82	53.49	51.46	51.46	46.58	49.04	47.34

CHAPTER - 3

GEOCHRONOLOGY

Both Rb-Sr dating of the whole rock (granite) and K-Ar dating of mineral fraction (biotite from granite) have been carried out in connection with the present work.

3.1. Rb-Sr Geochronology

Seven whole rock samples of the granite were collected from active quarries that expose fresh, unaltered rocks. Sample preparation and dating were done at the Physical Research Laboratory, Ahmedabad. The sample preparation, analytical techniques, precision and accuracy are same as those given in Sarkar et al. (1981).

The Rb-Sr ratios and the isotopic composition of strontium for the Ambalavayal granite samples are presented in Table 3. Plots of $^{87}Sr/^{86}Sr$ versus $^{87}Rb/^{86}Rb$ are shown in Fig. 14. The vertical component of the error lines is the standard deviation for contiguous sets of 10-15 $^{87}Sr/^{86}Sr$ ratios, while the horizontal bar represents the $\pm$ 2 per cent uncertainty in the measured $^{87}Rb/^{86}Rb$ ratio. Except for the slight deviation of one sample, all the other six conform closely to a single straight line within experimental error, the straight line shown being the least squares fit of the data based on the two-error weighted regression method of York (1966). The slope of the line corresponds to an age of 595 $\pm$ 20 Ma, the error being the

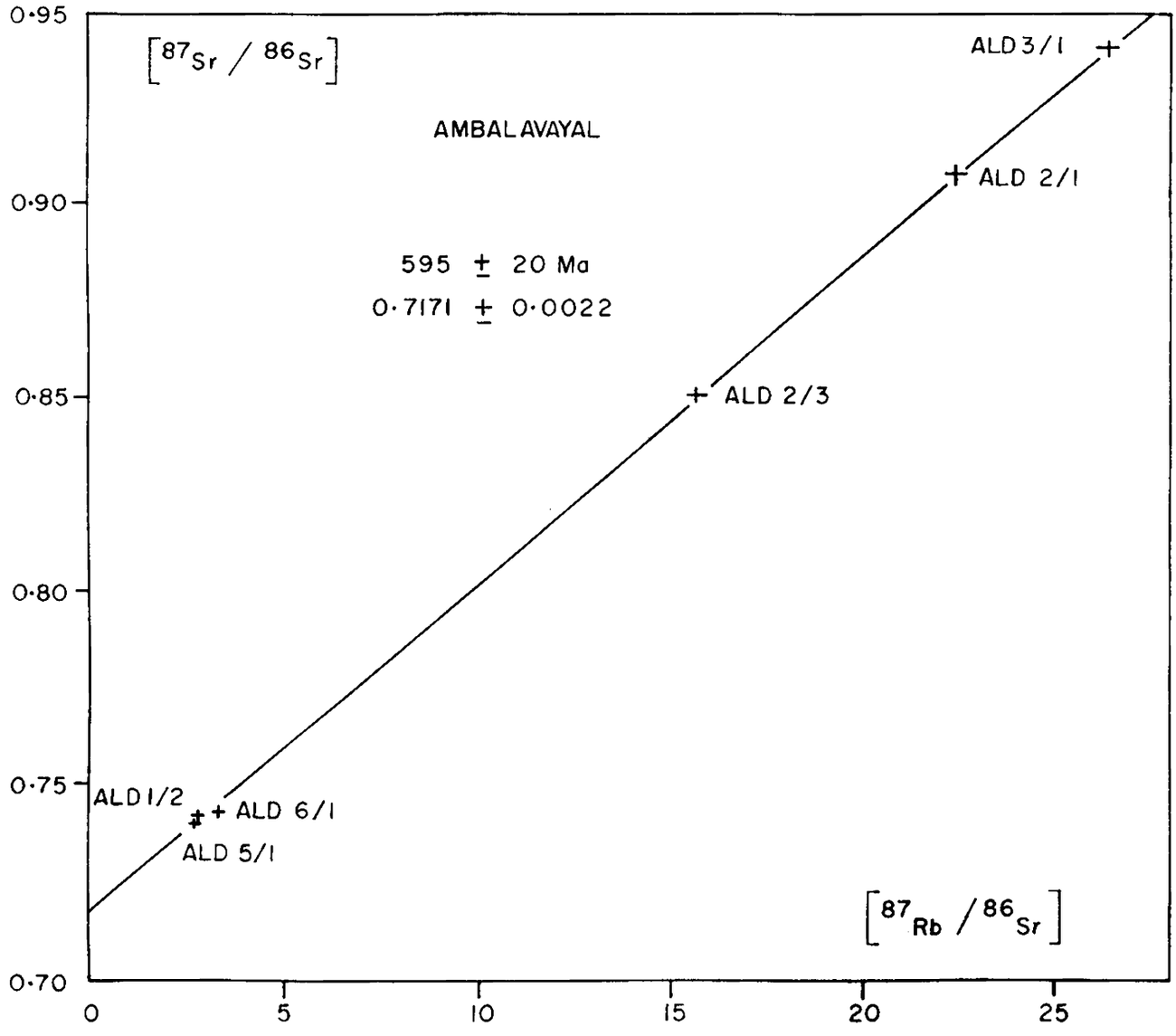

Fig. 14 Rb-Sr isochron plot of the Ambalavayal granite.

Table 3 Rb-Sr analytical data for the Ambalavayal granite.

Sample No	^{87}Rb (ppm)	^{86}Sr (ppm)	$^{87}Rb/^{86}Sr$ atomic	$^{87}Sr/^{86}Sr$ atomic
ALD 1/1	17.82	3.89	4.53	0.7402 ± 0.0016
ALD 1/2	11.83	4.23	2.80	0.7420 ± 0.0020
ALD 2/1	22.22	0.97	22.55	0.9076 ± 0.0029
ALD 2/3	11.26	0.71	15.68	0.8510 ± 0.0016
ALD 3/1	15.20	0.57	26.55	0.9414 ± 0.0016
ALD 5/1	10.62	4.02	2.61	0.7403 ± 0.0013
ALD 6/1	11.05	3.36	3.25	0.7427 ± 0.0013

standard deviation of the least squares fit. The decay constant used in calculating the age is the latest value adopted, 1.42 x $10^{-11}Yr^{-1}$ (Steiger and Jager, 1977). The Y-intercept of the isochron indicates an initial $^{87}Sr/^{86}Sr$ ratio of about 0.7171 ± 0.0022 (Santosh et al. 1985).

3.2 K-Ar Geochronology

Monomineralic fraction of biotite separated from the granite by crushing, grinding and sieving followed by a combination of heavy liquid and isodynamic separation techniques was used for K-Ar dating. The final purity of the sample was ascertained by hand-picking under a binocular microscope. K-Ar dating was done in the laboratory of IGEM, Academy of Sciences, USSR (Nair et al., 1985). Content of radiogeneic argon was determined in a mass spectrometer MI-1301 (90° sector, magnetic deflection type) using more than 98% pure ^{38}Ar mixed with CO_2 as tracer. The analytical techniques are the same as those given in Soman et al. (1982). The results are as follows:

Mineral	K(%)	Vol. Radiogenic Argon (nl/gm)	$\frac{Ar^{40}Rad}{Ar^{40}General}$	Age
Biotite	4.48 ± 0.04	204 ± 6	78:83	560±30

3.3. Discussion

The Rb/Sr whole rock age agrees within experimental error with

the K/Ar age of 560± 30Ma measured on biotite separate from the Ambalavayal granite. Since the blocking temperature of biotite is about 300°C (Hanson and Gast, 1967), the region around the Ambalavayal granite has not experienced any significant thermal event since the emplacement of the granite about 600 Ma ago. The Rb/Sr age of the Ambalavayal granite thus marks a Late Precambrian-Early Paleozoic magmatism in this part of the south-western Indian shield. This confirms the earlier assumption and available ages pertaining to this episode (Nair and Vidyadharan, 1982; Soman et al., 1982; Holmes, 1955; Sarkar, 1980). This age is also in accord with the ca.500 Ma tectonothermal event recognised in south India (Aswathanarayana, 1964; Crawford, 1969).

Plutons of similar ages and petrochemical characters occur in other shield areas of Africa also where they have been convincingly related to anorogenic magmatism (eg. Anderson et al, 1980; Harris, 1982). In the present case, the intrusives are spatially related to regional fault-lineaments. It is probable that the generation and emplacement of the granite is related to the pre-rift tectonics of the Indian continent and signify an event of taphrogenic magmatism. This aspect is considered in detail on the section on taphrogenic affiliation.

Though the initial Sr isotopic composition of the Ambalavayal granite is not precise by modern standards, it is very different from the upper mantle composition about 600 Ma ago. The

evolved value is suggestive of a crustal source. However, the geochemical features of the granite do not substantiate this view, as discussed later. It is probable that the high initial Sr isotope values indicate significant crustal contamination.

CHAPTER - 4

MINERAL CHEMISTRY

4.1. Feldspars

Monofractions of alkali feldspar were separated from fresh, coarse grained samples of the granite adopting the procedure outlined by Collerson (1976). From the plagioclase-quartz assemblage of the left over fraction, coexisting plagioclase grains were hand picked. Coarse K-feldspar grains were separated in a similar manner from pegmatite samples. All the fractions were subjected to final separation by hand picking under a stereo microscope to obtain 99% purity for analyses. As the analyses have been carried out on bulk separates, it is assumed that contamination by exsolved or mobilised Or and Ab components is negligible (cf. Collerson, 1976).

Major element data for seventeen feldspar fractions are presented in Table 4. The analyses include seven alkali feldspar-plagioclase pairs from the granite and three alkali feldspars from the pegmatites.

Table 4 Major element analyses of coexisting alkali fledspar (Al/1/AF to AL/7/AF) and plagioclase (AL/1/PL to AL/7/PL) from Ambalavayal granite and alkali feldspars (AL/P1/AF to AL/P3/AF) from pegmatites.

Oxide	AL/1/AF	AL/2/AF	AL/3/AF	AL/4/AF
SiO_2	72.55	65.0	64.17	64.32
Al_2O_3	12.75	17.34	17.33	17.84
Fe_2O_3	0.06	0.36	0.15	0.51
FeO	0.45	0.11	0.12	0.19
Mg	0.40	0.08	0.01	0.01
CaO	0.56	0.62	0.90	1.12
Na_2O	4.12	4.72	4.83	5.04
K_2O	8.71	10.58	12.00	10.34

Cont

Table : 4 (contd.)

Oxide	AL/5/AF	AL/6/AF	AL/7/AF	AL/P1/AF	AL/P_2/AF	AL/P_3/AF
SiO_2	63.60	65.26	63.35	63.72	63.28	64.20
Al_2O_3	17.33	17.84	18.35	17.82	18.10	18.55
Fe_2O_3	0.34	0.28	0.16	0.12	0.02	0.36
FeO	0.23	0.14	0.14	0.14	0.20	0.12
MgO	0.01	0.01	0.01	0.07	0.16	0.12
CaO	1.68	0.90	1.46	0.88	0.97	0.71
Na_2O	4.61	4.58	4.72	3.84	3.32	2.53
K_2O	11.0	10.56	10.88	12.47	12.80	12.62

contd.

Table : 4 (Contd.)

Oxide	AL/1/PL	AL/2/PL	AL/3/PL	AL/4/PL	AL/5/PL	AL/6/PL	AL/7/PL
SiO_2	66.03	65.68	65.35	64.41	65.08	65.50	64.58
Al_2O_3	18.35	18.47	19.88	19.88	20.39	20.39	20.39
Fe_2O_3	0.12	0.24	0.24	0.34	0.42	0.22	0.28
FeO	0.40	0.32	0.22	0.27	0.16	0.23	0.22
MgO	0.48	0.42	0.01	0.01	0.01	0.01	0.01
CaO	2.12	1.98	2.24	2.46	2.69	2.24	2.35
Na_2O	10.37	10.04	9.52	10.95	9.30	9.50	10.51
K_2O	1.72	2.24	1.54	1.21	1.12	1.18	1.16

The structural formulae of the feldspars, calculated on 32 (O) basis, together with the mol per cent feldspar end members are listed in Table 5. The structural formulae fit well with the standard structural formulae of alkali feldspars and plagioclase. The X values range from 3.487 to 4.768 in the case of alkali feldspars and 4.007 to 4.607 in the case of plagioclase. Z values show a range of 15.546 to 15.889 in alkali feldspars and 15.546 to 16.530 in plagioclase. Mol per cent feldspar end members range from $Or_{54.73}Ab_{22.51}An_{2.83}$ to $Or_{74.00}Ab_{40.52}An_{7.38}$ in alkali feldspars and $Or_{5.76}Ab_{79.57}An_{8.70}$ to $Or_{11.73}Ab_{83.87}An_{12.84}$ in the case of plagioclase.

When the data are recalculated to Or + Ab = 100% for alkali feldspar from the granite, the range is $Or_{57.58}Ab_{37.94}$ to $Or_{62.06}Ab_{42.42}$ For plagioclase, when recalculated to Ab + An = 100%, the range is from $Ab_{86.30}An_{9.85}$ to $Ab_{90.15}An_{13.70}$.

In order to check the structural state of the alkali feldspars, two samples, one from the granite and the other from the pegmatite were selected for X-ray studies. X-ray analyses were conducted using a Philips X-ray Diffractometer with V-filtered Cr K_{α} radiation. The 2 θ values were then converted to those for Cu K_{α} radiation. The compositionally inhomogeneous nature of the feldspars is characterised by the presence of peaks at 2θ values of 30.49 and 41.94, which correspond to 022 and 223 reflections of albite.

Table :5 Structural formulae of feldspars from Ambalavayal

	AL/1/AF	AL/2/AF	AL/3/AF	AL/4/AF	AL/5/AF
	STRUCTURAL FORMULAE (BASED ON 32 OXYGEN ATOMS)				
Si	12.935	11.771	11.900	11.856	11.859
Al	2.679	3.700	3.788	3.878	3.809
Fe^{3+}	0.009	0.075	0.022	0.066	0.045
Fe^{2+}	0.067	0.016	0.022	0.033	0.034
Ca	0.107	0.121	0.178	1.222	0.336
Na	1.424	1.655	1.738	1.794	1.658
K	1.983	2.493	2.830	1.438	2.622
Z	15.623	15.546	15.710	15.800	15.713
X	3.581	4.285	4.768	3.487	4.650
Or	56.43	58.40	59.70	54.73	56.83
Ab	40.52	38.77	36.50	40.32	35.79
An	3.05	2.83	3.80	4.95	7.38

Table : 5 (contd.)

	AL/6/AF	AL/7/AF	AL/P1/AF	AL/P2/AF	AL/P3/AF	AL/1/PL
			STRUCTURAL FORMULAE (BASED ON 32 OXYGEN ATOMS)			
Si	11.955	11.643	11.805	11.853	11.815	11.758
Al	3.853	3.977	3.890	3.921	4.023	3.848
Fe^{3+}	0.044	0.022	0.018	-	0.051	0.017
Fe^{2+}	0.022	0.022	0.022	0.032	0.019	0.060
Ca	0.176	0.287	0.175	0.195	0.140	0.404
Na	1.528	1.678	1.368	1.206	0.902	3.578
K	2.464	2.540	2.949	3.060	2.965	0.391
Z	15.852	15.642	15.713	15.774	15.889	15.623
X	4.290	4.527	4.514	4.493	4.026	4.433
			MOL PER CENT FELDSPAR END MEMBERS			
Or	57.75	56.45	65.65	68.59	74.00	9.24
Ab	38.03	37.11	30.45	27.04	22.51	81.82
An	4.22	6.44	3.90	4.37	3.49	8.94

Table 5 (Contd.)

	AL/2/PL	AL/3/PL	AL/4/PL	AL/5/PL	AL/6/PL	AL/7/PL
Si	11.771	12.089	11.539	11.602	11.658	11.531
Al	3.700	4.333	4.198	4.285	4.278	4.291
Fe^{3+}	0.075	0.045	0.043	0.643	0.021	0.043
Fe^{2+}	0.016	0.033	0.043	0.021	0.032	0.032
Ca	0.121	0.444	0.474	0.514	0.428	0.452
Na	1.655	3.422	3.810	3.214	3.272	3.648
K	2.493	0.356	0.280	0.258	0.278	0.258
Z	15.546	16.467	15.780	16.530	15.957	15.865
X	4.285	4.255	4.507	4.007	4.010	4.390
			MOL PER CENT FELDSPAR END MEMBERS			
Or	11.73	8.31	6.14	6.30	6.80	5.76
Ab	79.57	81.24	83.55	80.86	82.37	83.87
An	8.70	10.45	10.31	12.84	10.83	10.37

AL/1/AF to AL/7/AF are alkali feldspars that coexist with plagioclase AL/1/PL to AL/7/PL in granite. AL/P1/AF to AL/P3/AF are alkali feldspars from pegmatites.

It is possible to arrive at the degree of ordering of the feldspars based on diffractometer data. Goldsmith and Laves (1954) defined the measure of triclinicity, Δ of alkali feldspars based on the d-spacings of 131 and $1\bar{3}1$ reflections. According to their procedure, $\Delta = 12.5\ (d\ 131 - d\ 1\bar{3}1)$. The 131 and $1\bar{3}1$ doublet gives differences in d-spacings of 0.0214 and 0.0527 which correspond to Δ values of 0.2675 and 0.6588. The effect of Ab content on Δ is negligible as long as Ab-component is below 20% (Laves and Viswanathan, 1967). Smith (1974) proposed a correction of 0.007 for each 1% ab, based on the data of Orville (1967). Thus, the corrected Δ values in the present case are 0.2955 for alkali feldspar of the granite and 0.6742 for that of the pegmatite. As 0.25 is the value to be taken as the dividing line between orthoclase or sanidine and microcline (Dietrich, 1962; Smith, 1974), the present values seem to correspond to a triclinic symmetry with varying degrees of triclinicity, the higher degree of ordering being attained in the alkali feldspar sample from the pegmatite (Santosh, 1985b).

Ternary Ab-Or-An plots of the analysed feldspars from the granite are shown in Fig.15. The tie lines are dominantly parallel and non-intersecting, suggesting equilibrium conditions of crystallization of the two feldspars. From the figure, the following relations are evident. The alkali feldspars lie towards the K-rich side of the ternary critical solution curve and the tie lines joining feldspar pairs from the granite are sub-

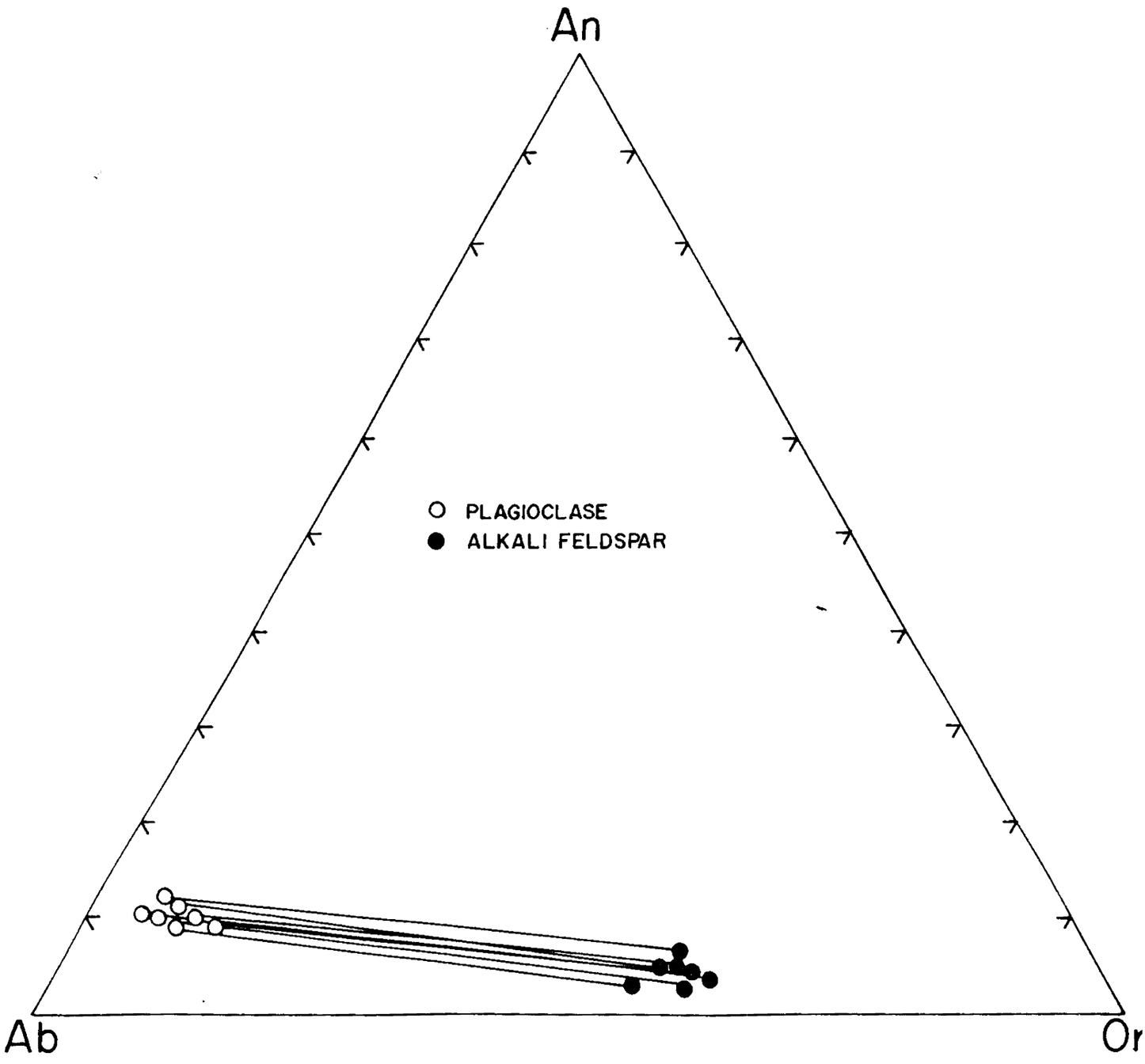

Fig. 15 Ternary Ab-Or-An plots of coexisting feldspars from Ambalavayal, connected by tie-lines.

parallel to the tie lines experimentally determined by Seck (1971). The modified two-feldspar geothermometer of Brown and Parsons (1981) can hence be used for a precise estimate of temperature based on the data of exchange of albite component between coexisting plagioclase and alkali feldspar. This thermometer is more practical than those of Stormer (1975) and Whitney and Stormer (1977), as evident from the discussions given by Brown and Parsons (1981). Plots of coexisting feldspars from the Ambalavayal granite fall close to the 700°C isotherm in Whitney and Stormer's diagram. In Brown and Parsons' (1981) diagram, calibrated for 1 Kb pressure, the feldspars plot near the 650°C isotherm (Fig.16). Whitney and Stormer's calibration is independent of pressure whereas Brown and Parsons estimate a systematic increase of 18°C/Kb for feldspar pairs formed at higher pressure. Assuming pressures of 4 to 5 Kb at the time of feldspar equilibration (see section on fluid inclusions) and applying pressure correction for the thermometric data, a temperature range of 722-740°C is obtained (Santosh, 1985b).

The molecular percentages of Or in the three alkali feldspar samples from the pegmatites are plotted in the strain free solvus of the Or-Ab system (Fig.17); after Yund, 1975 in Ribbe, 1975). The plots indicate feldspar equilibration temperatures between 525 and 580°C. This temperature range is supported by the experimental deductions of Jahns and Burnham (1969) and studies of Fersman (1960) and Sheshulin (1963) who reported a

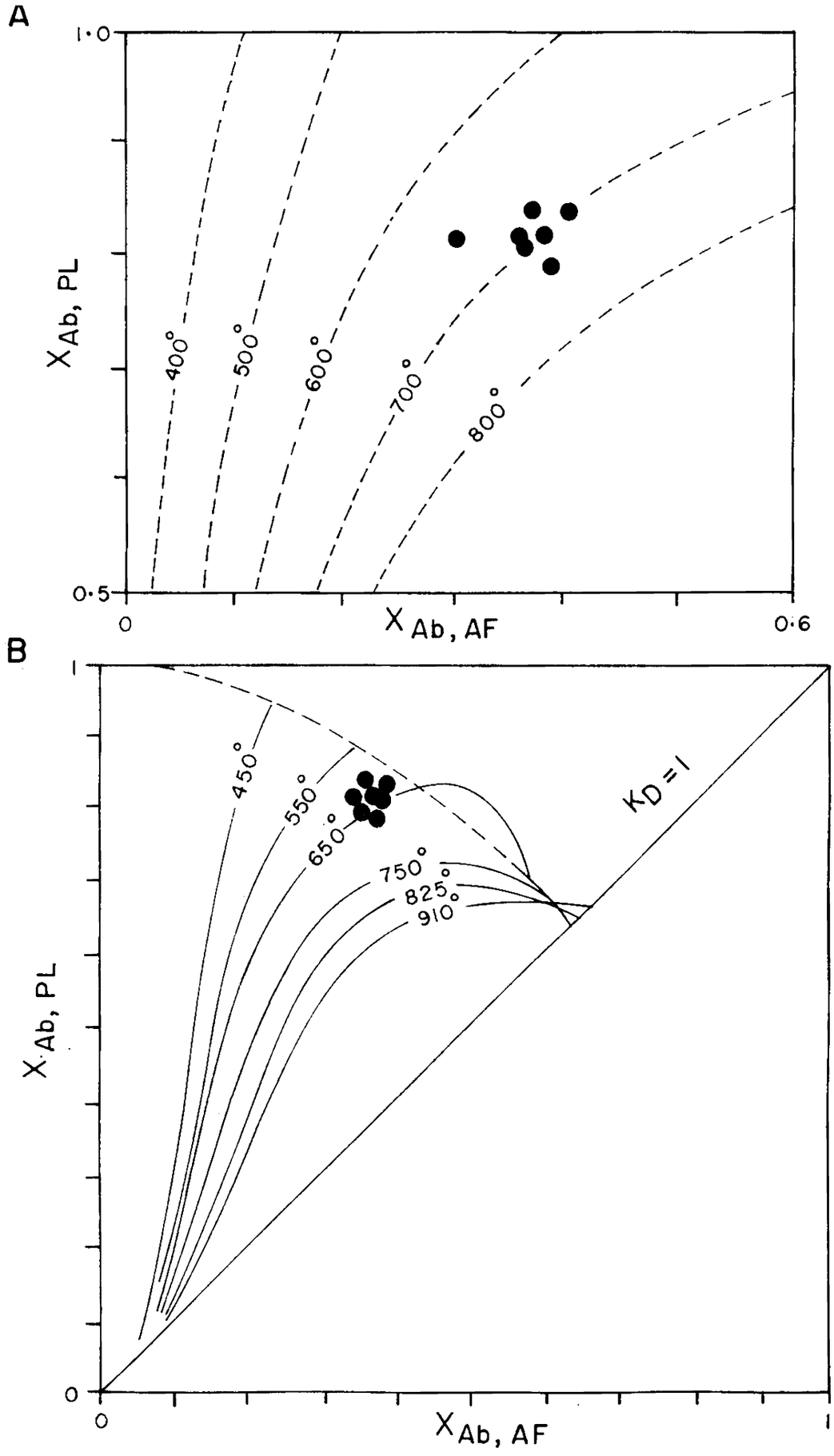

Fig. 16 Plots of albite content in coexisting alkali feldspar and plagioclase pairs from the Ambalavayal granite in Whitney and Stormer's (1977) diagram (A) and Brown and

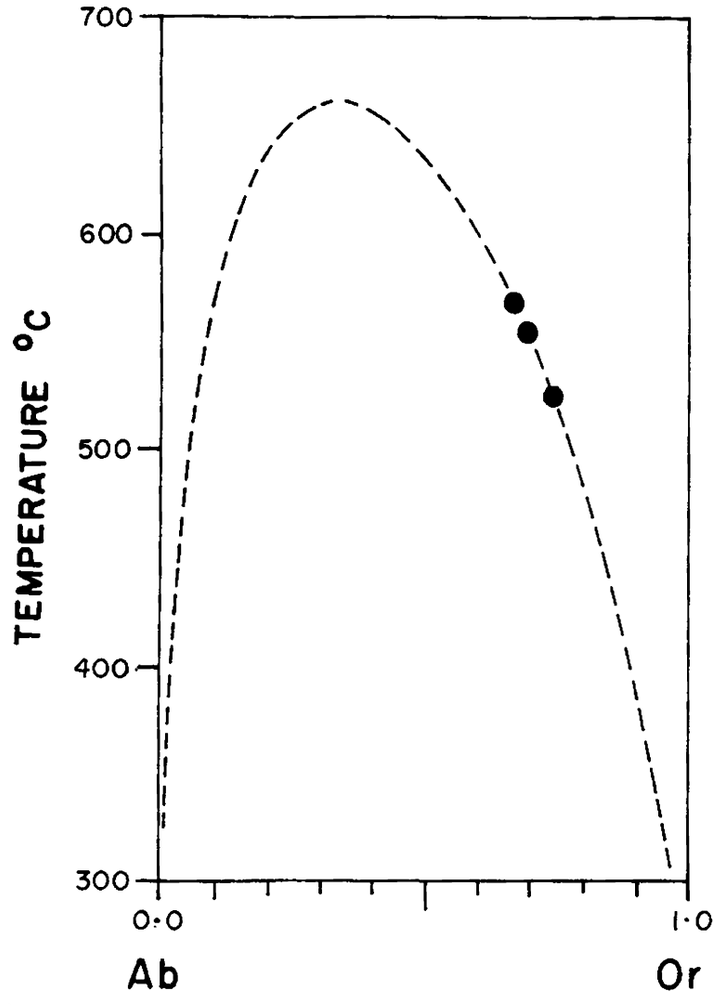

Fig. 17 Plots of alkali feldspars from pegmatites of Ambalavayal in the strain-free solvus of the Or-Ab system (after Ribbe, 1975).

temperature regime of 550-650°C for unmixing and formation of perthitic feldspar in pegmatites.

4.2. Hornblende and Biotite

Biotite and hornblende fractions were separated by a combination of repeated heavy liquid and electromagnetic techniques. The final purity of the samples was checked by hand picking under stereo-microscope (Santosh, 1985C).

The major elements were analysed by conventional wet chemical techniques and trace elements by Atomic Absorption Spectrophotometer (see Appendix).

4.2.1. Geochemistry of biotite

The chemical analyses of biotite from Ambalavayal and their structural formulae (based on 22 atoms, anhydrous) are presented in Table 6. Si cations range from 5.57 to 5.92 per formula unit compared to 6.00 for ideal phlogopite-annite series. There is sufficient Al in the sample to fill the tetrahedral sites not occupied by Si. The octahedral sites are occupied by 4.91 to 5.25 Y group cations compared with 6.00 in the trioctahedral mica,. The sum of the inter-layer X group cations (K, Na, Ca) ranges from 2.01 to 2.24, compared with the ideal 2.00 cations per formula unit. Plots of Fe/Fe+Mg ratios of biotite against Al atoms/22 oxygens define a field close to the phlogopite-annite join (Fig.18), with Al atoms indicating composition close to that of annite (2.2-2.8).

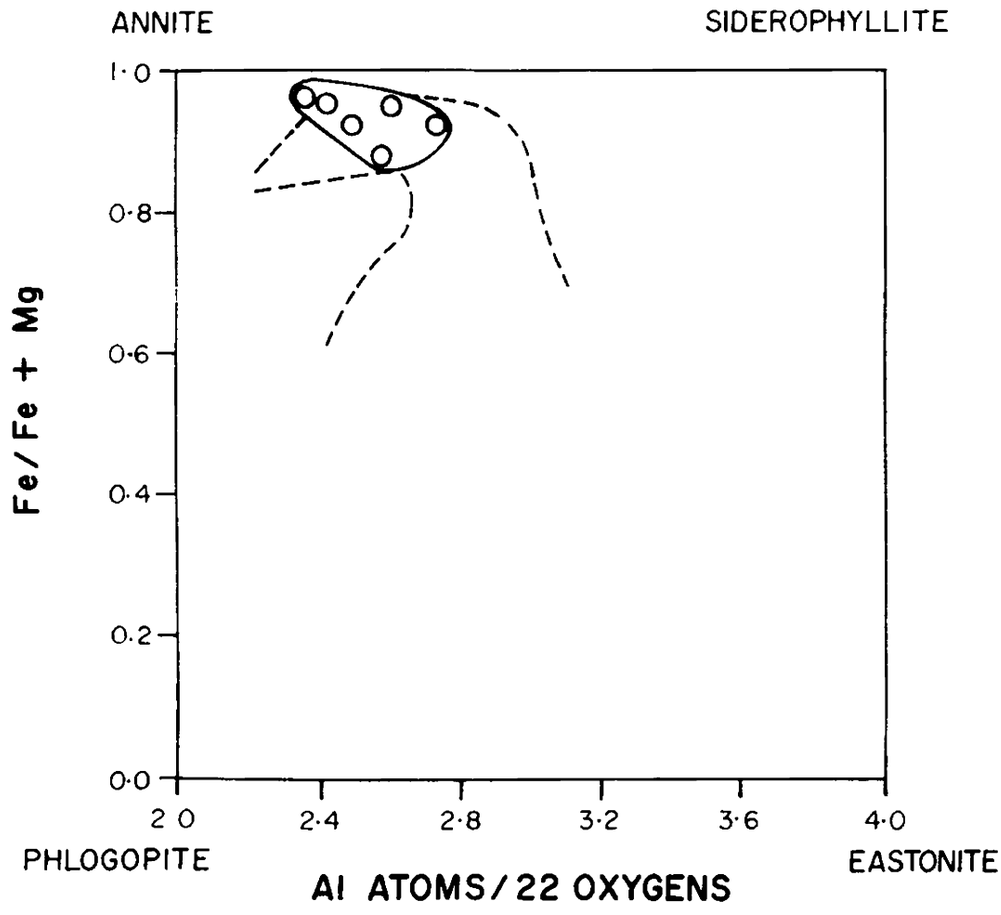

Fig. 18 Composition of Ambalavayal biotites in terms of Fe/Fe+Mg vs. Al atoms/22 oxygens. The broken line represent the field of biotites as given by Anderson (1980).

Table : 6 Chemical analysis and structural formulae of biotite from Ambalavayal

	A/BT/1	A/BT/2	A/BT3	A/BT/4	A/BT/5	A/BT/6
SiO_2	35.01	36.10	36.28	37.10	38.18	37.51
Al_2O_3	13.77	13.26	14.62	12.75	14.07	12.82
TiO_2	2.80	2.88	2.23	2.60	1.96	2.14
Fe_2O_3	5.02	5.44	5.21	8.39	1.46	6.47
FeO	29.21	28.10	26.28	26.05	21.37	25.86
MnO	0.33	0.42	0.46	0.18	0.53	0.34
MgO	0.96	1.12	1.42	0.65	2.02	0.84
CaO	1.57	1.84	1.13	1.12	1.48	1.12
Na_2O	0.80	0.76	0.74	0.65	0.58	0.63
K_2O	8.51	7.89	9.12	8.10	8.98	8.42

(Contd.)

Table : 6 Structural formulae (based on 22 oxygens per formula unit)

Si	5.570	5.697	5.732	5.830	5.923	5.955
Al^{iv}	2.430	2.303	2.268	2.170	2.077	2.045
Al^{vi}	0.153	0.164	0.455	0.192	0.496	0.356
Ti	0.336	0.343	0.265	0.307	0.229	0.256
Fe^{3+}	0.601	0.647	0.619	0.991	0.871	0.773
Fe^{2+}	3.886	3.709	3.472	3.423	2.772	3.434
Mn	0.045	0.056	0.062	0.024	0.070	0.046
Mg	0.228	0.264	0.334	0.150	0.467	0.198
Ca	0.268	0.311	0.191	0.189	0.246	0.191
Na	0.246	0.234	0.036	0.198	0.176	0.194
K	1.726	1.592	0.919	1.624	1.776	1.706
Sum Y	5.249	5.183	5.207	5.087	4.905	5.063
Sum X	2.240	2.137	2.065	2.011	2.198	2.091
$Mg/Mg+Fe^{2+}$	0.055	0.067	0.088	0.042	0.209	0.055

The most striking feature of the biotites is the very low magnesium content of the octahedral layers (0.15-0.47). Fig. 19a depicts a comparison of the composition of these biotites with those delineated for biotites from elsewhere. The Ambalavayal biotites lie outside Foster's (1960) field, away from the Mg apex and are comparable with similar low Mg biotites reported by Day et al. (1980). The biotites show low sodium content in the alkali site varying from 0.04 to 0.25. These characters are comparable with those for biotites from alkaline rocks (cf. Czamanske et al. 1977).

Experimental work by Buddington and Lindsley (1964) show that Ti and Fe^{3+} contents of biotites are important in understanding their genetic processes. The Al^{vi}-Ti-Fe^{3+} diagram reflects various conditions during the crystallization of the magma such as temperature, pressure, fH_2O and FO_2 (Albuquerque 1973). Ti and Fe^{3+} are mostly temperature and FO_2 dependent, whereas Al^{vi} is a variable that is controlled by the alumina activity as compared to the silica acitvity. The biotites occupy a well-defined area in the diagram (Fig.19b), and are characterised by slightly lower Ti and moderate Al and Fe^{3+}. The plots indicate an overall slight increase in Ti with a corresponding increase in Al^{vi}. Such a distribution is explained by the influence of silica and alumina activities which increase towards the more felsic end. Higher temperature favours the entry of Ti in the biotite structure but does not favour Al^{iv}.

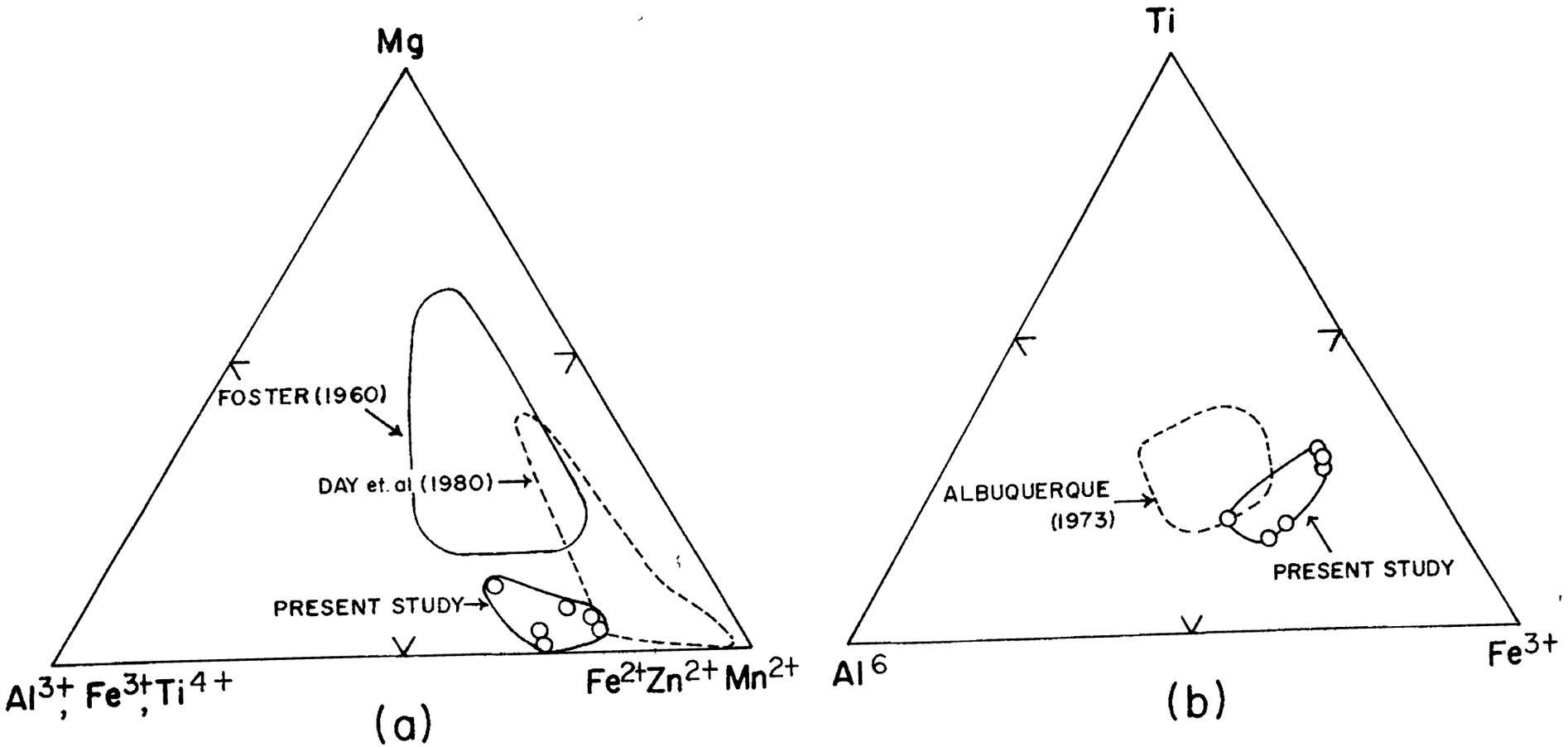

Fig. 19 Composition of Ambalavayal biotites compared with those from elsewhere. Note the low Mg-content (a) and lower Ti with moderate Al and Fe^{3+} (b).

Al^{iv} is higher in biotites formed at lower temperature to balance the substitution of Al^{vi} for Mg^{2+} and Fe^{2+} (Albuquerque 1975). It is likely that both Si and Al activities increase towards the felsic end, the latter being more predominant. (Santosh, 1985c).

4.2.2. Geochemistry of hornblende

Chemical analyses and structural formulae (based on 23 oxygen atoms, anhydrous) of hornblende separates from Ambalavayal are presented in Table 7. The analyses and structural formulae overall satisfy the requirements for 'superior analyses' listed by Leake (1968) and indicate an edenitic composition (Fig.20). Si cations range from 6.306 to 6.920 per formula unit with sufficient Al in all the samples to fill the tetrahedral sites not occupied by Si. The total number of Y group cations range from 4.891 to 5.205 per formula unit compared with 5.0 in the ideal hornblende formula.

A notable aspect is the high Al-content of the hornblende (Al_2O_3 = 9.69-11.89), which is comparable with the characteristic high Al_2O_3 values of hornblendes from anorogenic granites (9-11 wt.%) and contrast with the low Al values for hornblendes from calc-alkaline plutons associated with orogenic belts (Anderson 1980). In all samples except one, the sum of W and X group cations (Ca, Na, K) exceeds the theoretical maximum of 2.00 cation per formula unit in the M_4 site and suggests

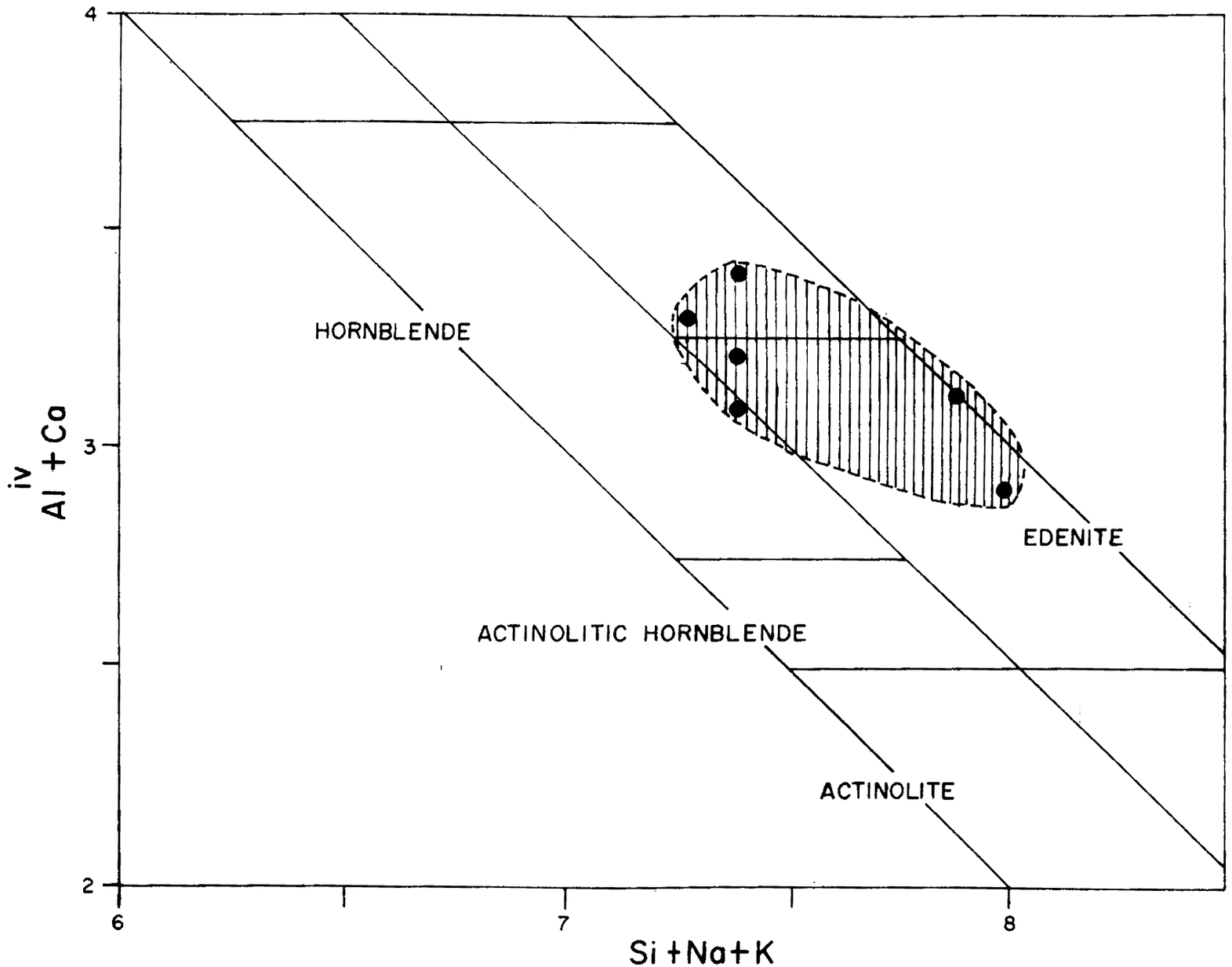

Fig. 20 Composition of hornblendes from Ambalavayal in terms of Si + Na + K vs. Al^{iv} + Ca relations

Table : 7 Chemical analyses and structural formulae of hornblende from Ambalaveyal

	A/HB/1	A/HB/2	A/HB/3	A/HB/4	A/HB/5	A/HB/6
SiO_2	39.83	40.23	39.45	39.83	41.21	39.78
Al_2O_3	10.20	10.67	11.89	10.71	10.71	9.69
TiO_2	1.42	1.41	1.35	1.53	1.58	1.53
Fe_2O_3	5.58	5.11	4.96	6.80	6.56	6.68
FeO	20.20	20.42	20.61	22.85	19.80	23.40
MnO	0.53	0.64	0.61	0.55	0.42	0.56
MgO	2.72	4.01	3.86	2.56	2.56	2.56
CaO	10.53	9.22	8.78	9.41	7.51	10.30
Na_2O	1.87	1.79	1.94	2.15	2.01	2.13
K_2O	2.41	1.98	2.21	1.78	2.48	1.78

(Contd.)

Table : 7 Structural formulae (based on 23 oxygens per formula unit)

Si	6.947	6.443	6.337	6.306	6.716	6.371
Al^{iv}	1.053	1.557	1.663	1.694	1.784	1.629
Al^{vi}	0.894	0.442	0.526	0.306	0.774	0.154
Ti	0.175	0.170	0.163	0.182	0.191	0.135
Fe^{3+}	0.673	0.616	0.601	0.811	0.805	0.809
Fe^{2+}	2.734	2.735	2.769	3.025	2.700	3.137
Mn	0.073	0.086	0.083	0.074	0.058	0.077
Mg	0.656	0.957	0.924	0.604	0.622	0.606
Ca	1.826	1.582	1.512	1.596	1.322	1.771
K	0.588	0.556	0.604	0.660	0.634	0.654
Na	0.498	0.404	0.454	0.360	0.514	0.366
Sum Y	5.205	5.019	5.066	5.002	5.150	4.918
Sum W + X	2.912	2.542	2.570	2.616	2.472	2.791
$Mg/Mg+Fe^{2+}$	0.194	0.259	0.250	0.166	0.187	0.162

partial occupation of the A sites. Na generally exceeds K in these hornblendes. The $Mg/Mg + Fe^{2+}$ values are fairly uniform, ranging between 0.162 and 0.259.

4.2.3. Distribution of major and trace elements

For coexisting minerals α and β the distribution coefficient of element A is defined as:

$$K_{D(A)}^{\alpha-\beta} = \frac{X_A^{\alpha}}{1-X_A^{\alpha}} \qquad \frac{1-X_A^{\beta}}{X_A^{\beta}}$$

Where X_A is the atomic ratio of element A to the sum of major elements occupying the same site or sites in phases α and β. If the elements considered behave as ideal mixtures and reach chemical equilibrium under uniform P-T conditions, then the distribution coefficient, $K_{D(A)}$ is constant (cf. Kretz 1959, 1960, Stephenson 1977). The distribution coefficients, $K_{D(Fe^{2+}-Mg)}^{B-H}$ and $K_{(Fe^{2+}-Mg)}^{H-B}$ were calculated using the atomic ratio, $Fe^{2+}/(Fe^{2+}+Mg)$. $K_{D\ (Al^{iv})}^{B-H}$ and $K_{D\ (Al^{vi})}^{H-B}$ were calculated using the atomic ratio, $Al^{iv}/Al^{iv} + Si$. For the remaining distribution coefficients, the atomic ratio of the element considered is based on the total number of octahedral cations, eg; for $K_{D\ (Ca)}^{B-H}$, $X_{Ca} = Ca/\Sigma$ octahedral cations. The calculated atomic ratios of elements to the sum of major elements occupying the respective sites in coexisting hornblendes and biotites from Ambalavayal are given in Table 8 and the distribution coefficients are given in Table 9. The variations in

Table 8 Atomic ratio of elements to the sum of major elements occupying the respective sites in horrblende and biotite from Ambalavayal.

	$X^{H}_{Al^{iv}}$	$X^{H}_{Al^{vi}}$	X^{H}_{Ti}	$X^{H}_{Fe^{3+}}$	$X^{H}_{Fe^{2+}}$	X^{H}_{Mn}	X^{H}_{Mg}	X^{H}_{Ca}
HORNBLENDE								
A/HB/1	0.132	0.172	0.034	0.129	0.525	0.014	0.126	0.670
A/HB/2	0.195	0.088	0.034	0.123	0.545	0.017	0.191	0.622
A/HB/3	0.209	0.104	0.032	0.119	0.547	0.017	0.182	0.588
A/HB/4	0.212	0.061	0.036	0.162	0.605	0.015	0.121	0.610
A/HB/5	0.223	0.150	0.037	0.156	0.524	0.011	0.121	0.535
A/HB/6	0.204	0.031	0.028	0.165	0.638	0.016	0.123	0.635
	$X^{B}_{Al^{iv}}$	$X^{B}_{Al^{vi}}$	X^{B}_{Ti}	$X^{B}_{Fe^{3+}}$	$X^{B}_{Fe^{2+}}$	X^{B}_{Mn}	X^{B}_{Mg}	X^{B}_{Ca}
BIOTITE								
A/BT/1	0.304	0.029	0.114	0.115	0.740	0.009	0.043	0.120
A/BT/2	0.288	0.032	0.066	0.125	0.716	0.011	0.051	0.146
A/BT/3	0.284	0.087	0.051	0.119	0.667	0.012	0.064	0.093
A/BT/4	0.271	0.038	0.060	0.195	0.673	0.005	0.030	0.094
A/BT/5	0.260	0.101	0.047	0.178	0.565	0.014	0.095	0.112
A/BT/6	0.256	0.070	0.051	0.153	0.524	0.009	0.039	0.091

Table 9 Distribution coefficients for coexisting hornblende and biotites from Ambalavayal.

K^{B-H}	$D(Al^{iv})$	$D(Al^{vi})$	$D(Fe^{3+})$	$D(Fe^{2+})$	D(Ti)	D(Mn)	D(Mg)	D(Ca)
1	2.303	0.169	0.891	1.410	3.353	1.614	0.341	0.179
2	1.477	0.364	1.016	1.314	1.941	0.647	0.267	0.235
3	1.359	0.837	1.000	1.219	1.594	0.727	0.352	0.158
4	1.278	0.623	1.203	1.112	1.607	0.313	0.248	0.154
5	1.666	0.673	1.141	1.078	1.270	1.273	0.785	0.209
6	1.255	2.258	0.927	1.063	1.821	0.130	0.317	0.143
Mean	1.468	0.821	1.030	1.199	1.931	0.784	0.385	0.180

K_D values of each element are shown in Fig. 21 where, the linear to curvilinear trends depict near-chemical equilibrium conditions of crystallization of the two minerals.

Among the tetrahedrally co-ordinated cations, Al and Si show variable distribution with $K_D^{B-H}{}_{(Al^{iv})}$ ranging from 1.17 to 2.30 The distribution of Al^{iv} and Si between coexisting hornblende and biotite is shown to be non-ideal with their K_D values systematically related to the Al^{iv} contents of hornblende (Gorbatschev 1969). The linear distribution pattern of $X_{Al}^{H}iv$ and the curvilinear trend of $X_{Al}^{B}iv$ demonstrate this aspect

The correlation between $X_{Al}^{H}iv$ and $K_D^{B-H}{}_{(Al^{iv})}$ depicts that the Al-Si distribution coefficient is related to compositional variables (Stephenson 1977). A check on the trend defined by Al^{iv} and Si between the coexisting minerals as per the equation of Gorbatschev (1970) indicate near-chemical equilibrium conditions.

Among the octahedral cations, the distribution of Fe^{2+} and Mg is fairly uniform (Table 4) with $K_D^{B-H}{}_{(Fe^{2+})}$ ranging from 1.063 to 1.410 and $K_D^{B-H}{}_{(Mg)}$ ranging from 0.248 to 0.785. $K_D^{B-H}{}_{(Fe^{2}\pm Mg)}$ relationship was also checked and found to be uniform, consistent with the observations of other workers (cf. Saxena 1966; Leelanandam 1970).

The higher charged octahedral cations like Fe^{3+}, Al^{vi} and Ti show overall uniform distribution. The increase in $K_D^{B-H}{}_{(Mn)}$

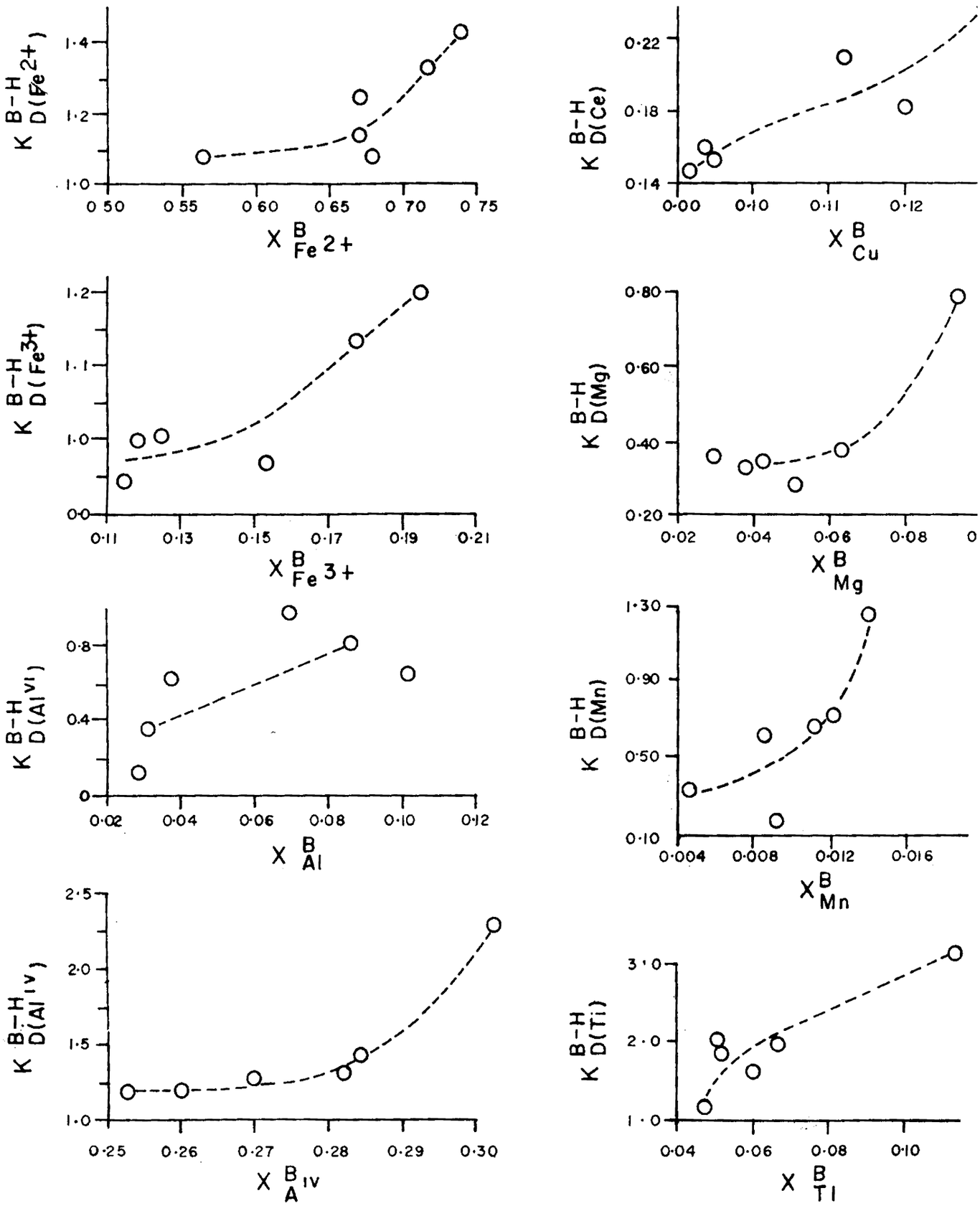

Fig. 21 Variations of K_D values of major elements between coexisting biotite and hornblende from Ambelavayal.

values against increasing Mn content in biotite and their negative correlation in hornblende are consistent with similar observations of Saxena (1966) and Kretz (1959). The non-ideal distribution of Ti and Al^{vi} between hornblende and biotite also correlates with their observations with the feature attributed to be a result of variation in Al^{iv}, Al^{Vi}, Fe^{3+} and alkalies in hornblende (Kretz 1960). Fe^{2+} and Ca in biotite show good fit against their respective K_d values, whereas in hornblende, the Ca distribution is not strictly regular.

The trace element geochemistry of hornblendes and biotites from Ambalavayal is presented in Table 10 and the distribution coefficients are given in Table 11. The pattern of distribution of elements between the coexisting minerals are shown in Fig.22 where the K_D values are plotted against the respective K_D^{B-H} (Mg-Fe) value. Systematic relationship is observed in the distribution of Ba, Cu, Mo and Co, whereas Sr, Li, Zn, Cr, Ni and Rb show an overall correlation, suggesting near-chemical equilibrium conditions during the crystallization of the minerals. The increase in Li and the decrease in other trace elements like Cu, Ni, Co, Zn, Sr and Cr with decreasing Mg/Fe values correspond with the crystal-chemical characters.

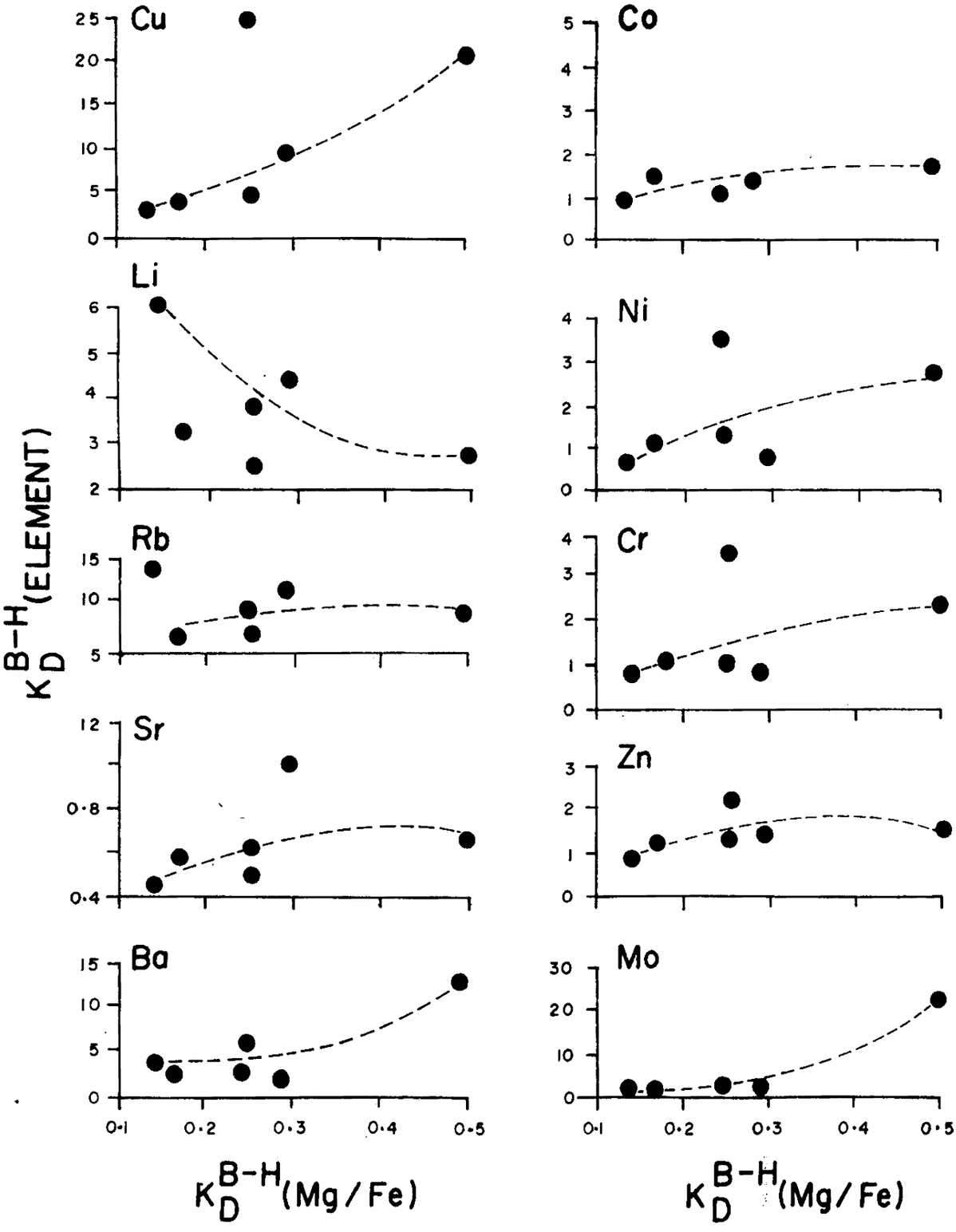

Fig. 22 Variations of trace element K_D values between coexisting hornblende and biotite from Ambalavayal.

Table:10 Trace element analyses of hornblendes and biotites from Ambalavayal.

	Ba	Bi	Co	Cr	Cu	Li	Mo	Ni	Pb	Rb	Sr	V	Zn	Zr
HORNBLENDE														
A/HB/1	72	50	136	122	2	89	24	86	40	62	54	120	1272	180
A/HB/2	64	58	128	128	4	88	22	98	34	56	66	130	1310	170
A/HB/3	76	48	132	116	6	92	38	80	48	72	48	110	1344	280
A/HB/4	22	74	148	128	4	42	24	104	60	24	27	100	1210	260
A/HB/5	30	60	146	116	2	72	2	122	46	50	39	140	1360	160
A/HB/6	60	78	153	124	4	48	14	102	38	30	15	100	1284	460
Mean	54	61	141	122	4	72	21	99	44	49	42	117	1297	252
BIOTITE														
A/BT/1	426	170	529	426	50	350	44	310	108	582	33	60	2600	300
A/BT/2	176	78	175	152	18	284	16	105	50	315	38	10	1530	100
A/BT/3	224	141	144	118	32	216	28	98	84	462	24	52	1840	220
A/BT/4	88	64	154	98	14	260	24	84	38	342	12	20	1142	400
A/BT/5	418	86	235	268	42	204	46	320	96	468	26	24	1860	280
A/BT/6	84	152	220	86	39	212	26	78	34	320	16	58	1780	360
Mean	236	115	243	191	33	254	31	166	68	415	25	37	1792	277

Table 11 Distribution coefficients of elements between coexisting biotite and hornblende from Ambalavayal.

K_D^{B-H}	Mg/Fe	Ba	Bi	Co	Cr	Cu	Li	Mo	Ni	Pb	Rb	Sr	V	Zn
(1)	0.25	5.9	3.4	3.9	3.5	25	3.9	1.8	3.6	2.7	9.4	0.6	0.5	2.1
(2)	0.17	2.3	1.3	1.4	1.2	4.5	3.2	0.7	1.1	1.5	3.2	0.6	0.1	1.2
(3)	0.25	2.9	2.9	1.1	1.0	5.4	2.4	0.7	1.2	1.8	2.4	0.5	0.5	1.4
(4)	0.14	4.0	0.9	1.0	0.8	3.5	6.2	1	0.8	0.6	6.2	0.4	0.2	0.9
(5)	0.50	13.9	1.4	1.6	2.3	21	2.8	23	2.6	2.1	2.8	0.7	0.2	1.4
(6)	0.29	1.4	2.0	1.4	0.7	9.8	4.4	1.9	0.8	0.9	4.4	1.1	0.6	1.4
Mean	0.32	5.2	2.0	1.7	1.6	11.5	3.8	4.9	1.7	1.6	4.7	0.7	0.4	1.4

4.2.4. Intensive parameters

As shown by Wones and Eugster (1965), the dominant factors that influence the conditions of crystallization of biotite are temperature and fO_2. Calculations based on the composition of biotite will hence give the minimum values of fO_2. The most important elements to be considered are Fe^{2+} and Mg as the variations of these elements are largely temperature dependent. Also, Fe^{3+} and Fe^{2+} give an indication of the degree of oxidation. Composition of the Ambalavayal biotite when related to Wones and Eugster's (1965) experimental system suggests that oxygen fugacities during biotite crystallization were slightly higher than that defined by the Ni-NiO buffer and that the granite magma was buffered with respect to oxygen by oxides existing within the magma (Dodge et al., 1969; Dodge and Ross, 1971). If buffering continued during the crystallization of both biotite and hornblende, the tie lines between coexisting biotite and hornblende tend to be parallel to Wones and Eugster's estimated trends of buffered biotites. This is the case with Ambalavayal, where tie lines between coexisting biotites and hornblendes lie almost parallel to the trends of buffered biotite in the compositional triangle, Fe^{3+}-Fe^{2+}-Mg (Fig.23). Eventhough ferric iron plays different structural roles in the micas and amphiboles, the parallelism of the biotite-hornblende tie lines with those of the buffered biotite indicates that the effect of oxygen pressure with respect to ferrous-

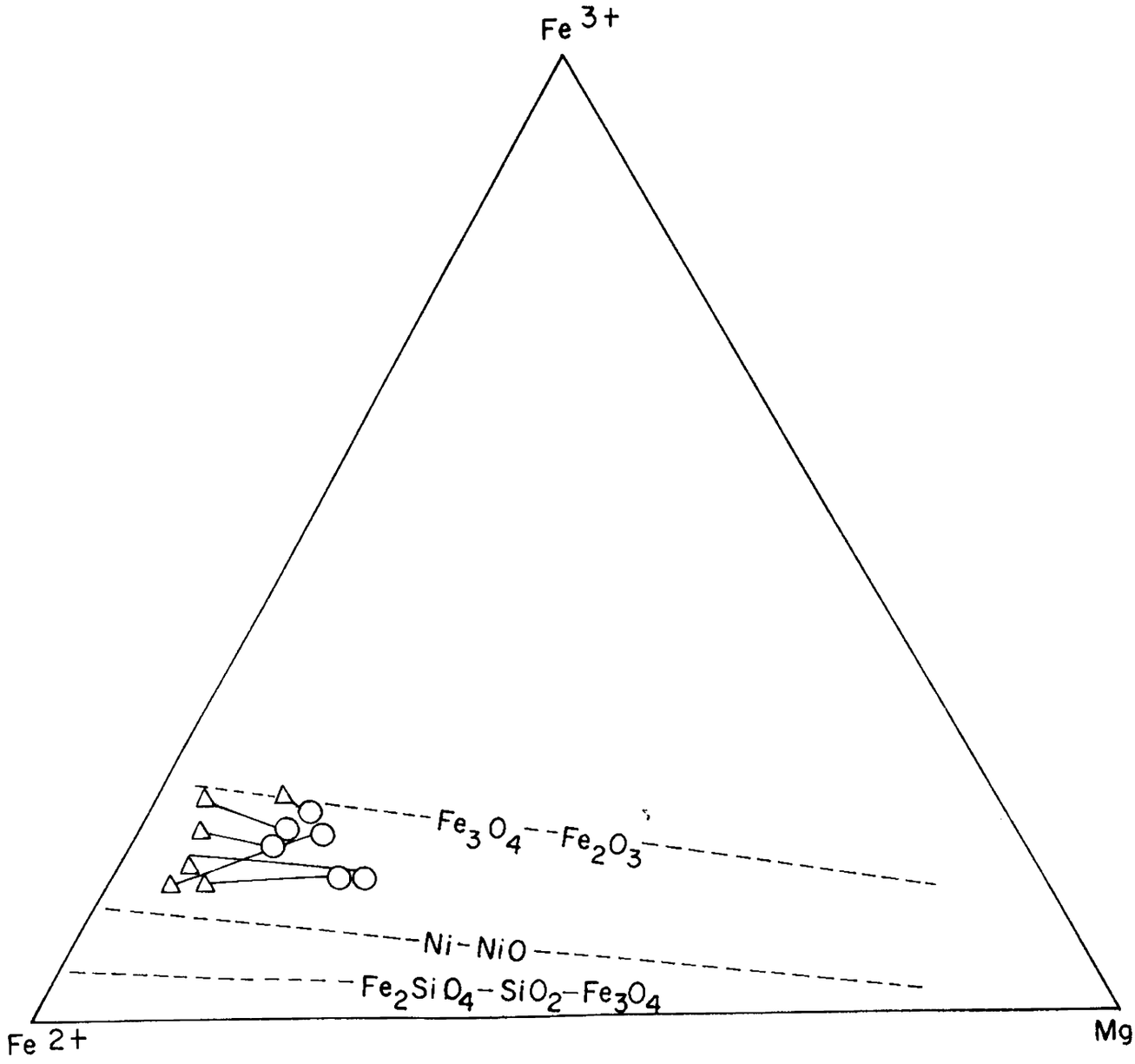

Fig. 23 Fe^{3+}- Fe^{2+}- Mg plots of coexisting biotite (circles) and hornblendes (triangles) from Ambalavayal. The buffer limits are after Wones and Eugster (1965).

ferric iron distribution is almost the same for biotite and hornblende. This is consistent with the observation that hornblende and biotite of plutonic rocks commonly form in an environment closed to oxygen with oxygen fugacities determined by buffer reactions (Dodge et al., 1969).

Qualitative aspects of intensive variables such as T, P, fH_2O and fO_2 can be deduced from the sequence of crystallization of constituent minerals. The sequence of crystallization at T-fO_2 constrained to the Ni-NiO buffer for a rock of adamellitic composition was determined by Maaloe and Wyllie (1975). Their data show that hydrous minerals like biotite crystallize early under wet conditions and late under dry conditions. Hornblende and biotite are texturally late crystallized minerals in the Ambalavayal granite, and the early crystallization regime of the granite, as inferred from fluid inclusion studies, was under $P_{CO_2} > P_{H_2O}$. This, together with the presence of pegmatites and aplites in the granite suggest an increase in fH_2O to a probable saturation towards the final stages of crystallization (Santosh, 1985c).

Ishihara (1977) noted that Fe-Ti oxides indicate the relative levels of oxygen fugacity. His 'magnetite-series' refers to granites with high total Fe-Ti oxides with higher proportion of magnetite to ilmenite. The high Fe^{3+}/Fe^{2+} ratios of coexisting biotites and hornblendes indicate higher oxygen fugacities during their crystallization (fO_2>Ni-NiO). An estimate

of fO_2 is depicted in Fig.24 with the aid of an independent geothermometer obtained from coexisting feldspar pairs. Crystallization temperature for the coexisting alkali feldspar-plagioclase pairs from Ambalavayal has been estimated to be in the range of 722-740°C based on the mol % Ab content (Santosh, 1985b). For granitic plutons, the lower limit of temperature is their wet solidus. As each stability field has pressure contours, the solidus for granitic melts in equilibrium with biotite can be plotted. Thus, the stability fields depicted in Fig.24 is derived from the two-feldspar geothermometer, which define a window in P-T-fO_2 space, denoting high fO_2 conditions of crystallization of about 10^{-15}bars. The result is consistent with the qualitative estimate that the magnetite series granites crystallize at higher levels of fO_2, well above the Ni-NiO buffer.

4.3. Molybdenite

Five molybdenite samples, which were ascertained to be pure under the microscope, were subjected to X-ray diffraction using a PHILLIPS X-ray diffractometer at the Department of Geology, University of Delhi.

X-ray diffraction by crystals results from a scattering process in which the X-rays are scattered by electrons without change in wavelength. However, a diffracted beam is produced only when the equation, $n\lambda = 2d \sin\theta$, is satisfied where n is an integer, λ the wave length of X-rays used, d the distance bet-

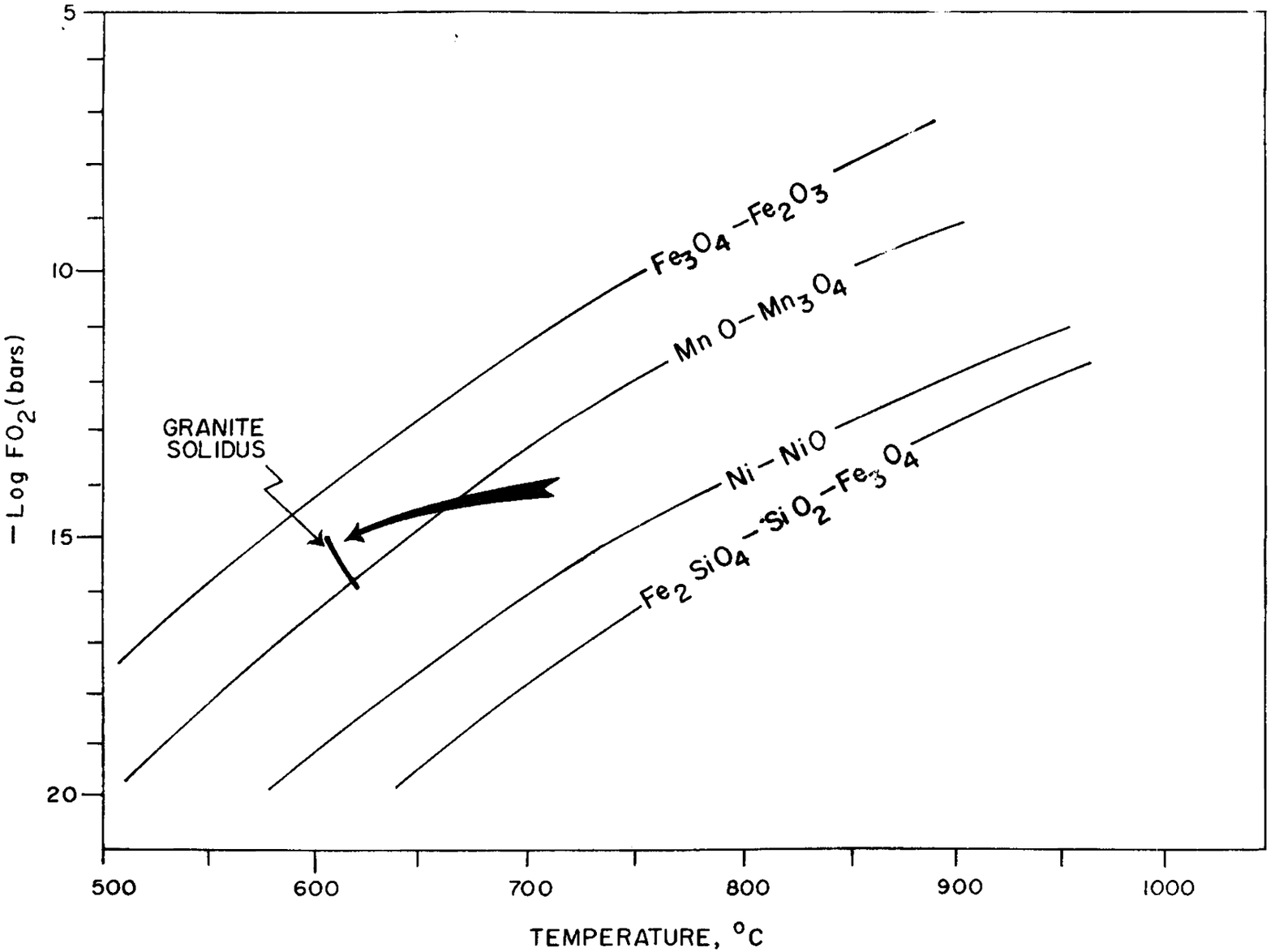

Fig. 24 Log FO_2 vs. temperature diagram with buffer limits after Wones and Eugster (1965), showing the stability field of biotites from Ambalavayal. The solidus temperature has been estimated from the feldspar geothermometer.

ween the successive parallel planes in the crystals (inter-planar spacing) and θ, the angle of incidence and reflection of the X-ray beam for a given atomic plane. For a given d - spacing and a given wavelength, reflection can take place only at those angles of θ which satisfy the above equation, known as the Bragg equation. The resulting diffraction pattern of a crystal, comprising both the position and intensities of the diffraction effects, is a fundamental physical property of the mineral. This property serves in the perfect identification of the crystal and for complete elucidation of its structure.

Required quantity of the powdered sample of molybdenite was mounted on a sample slide. The instrumental specifications used are: G.M. Speed-½° per minute; Chart Speed-0.5 cm/minute, Signal: 1Khz. Target-Chromium, Filter-Nickel and Scanning Range-5-40°.

2θ values were read from the diffractograms thus obtained. d-values were calculated using the equation, $\lambda = 2d \sin\theta$ (where $\lambda = 1.5418$). The results obtained are given in Table 12, where the values obtained for molybdenite samples from Kondappalli (Rao, A.T. 1978) are also shown for comparison.

The X ray data show prominent peaks at 2θ values of ca. 14.5 29.3, 39.6 and 44.4 in majority of the samples, corresponding to d-spacings of 6.15, 3.05, 2.28 and 2.04 respectively. The peaks at 14.5 and 44.4 are common in all the samples, compar-

Table : 12 2θ and d values of molybdenites from Ambalavayal compared with that from Kondappalli.

	2θ	d		2θ	d
ALM-1	14.4	6.15	ALM-15		
	29.2	3.06			
	32.8	2.73		14.5	6.11
	39.6	3.02		44.4	2.04
	44.2	2.05	Kondappalli		
	49.9	1.33		14.4	6.15
	56.1	1.97		28.0	3.08
ALM-2	14.4	6.15		32.7	2.74
	29.3	3.05		35.9	2.50
	39.6	2.28		44.2	2.05
	44.4	2.04		49.8	1.83
				56.1	1.64
ALM-3	14.5	6.11			
	29.4	3.04			
	44.4	2.04			
ALM-4	14.6	6.07			
	29.4	3.04			
	39.8	2.27			
	44.4	2.04			

Analysis of Kondappalli molybdenite from A.T. Rao, 1978.

able with the peaks at 14.4 and 44.2 in the Kondappalli molybdenite.

Molybdenite has two structural modifications, hexagonal ($2H_1$) and rhombohedral (3R) (Takeuchi and Nowacki, 1964). The rhombohedral type is mainly seen as an accessory of high temperature assemblages, like carbonatites, quartz-feldspar prophyries and wolframite-cassiterite ores. In contract, the 3R type in quartz-molybdenite veins, porphyry copper deposits and pegmatites, is comparatively rare and the hexagonal modification is more common. Morimotto and Kullerud (1962) showed that at temperatures below 600°C (500 $\pm$ 100°C), the rhombohedral form attains an upper stability limit, breaking down to molybdenite $2H_1$ + molybdenum. By analogy with these observations and by comparison with the moderate to strong reflections of $2H_1$ type (Traill, 1963) recorded at d - 2.27 and 1.82 (2.27-2.28 and 1.97 in Ambalavayal), the molybdenite of Ambalavayal is presumed to be of hexagonal $2H_1$ polytype.

Results of chemical analyses of the five molybdenite samples are presented in Table 13, where the molybdenum content is seen to range from 57.83 to 58.99 wt.%. Although compositional differences between hexagonal and rhombohedral polytypes have been noted by several workers, they have not been quantified. However, many observations show that the hexagonal molybdenite has lesser content of Mo compared to that of the rhombohedral polytype. The present data are in agreement with this.

Table : 13 Analyses of molybdenite fractions from Ambalavayal

Sample No.	Mo%	Cr	Fe	Cu	Ni	Ti	Bi	Zn	Pb	Co
ALM-1	57.83	2	877	2069	76	57	166	34	40	28
ALM-2	58.09	4	377	115	72	20	135	48	28	24
ALM-3	58.99	1	196	90	79	20	192	41	39	31
ALM-4	58.32	2	1078	10	68	32	153	37	34	23
ALM-5	58.78	1	588	70	74	72	161	79	31	27
Mean	58.40	2	615	471	74	40	161	48	34	27

Mo - in% ; all the rest in ppm.

The trace elements which show significant abundance in the Ambalavayal molybdenite are: Fe (196-1078ppm), Cu (10-115ppm; one anomalous value shows 2069ppm), Ni (68-79ppm), Ti (20-72 ppm), Bi (135-192ppm), Zn (34-70ppm), Pb (28-40ppm) and Co (23-31ppm). Such high concentrations of 'impurities' are considered to be a common feature of the hexagonal $2H_1$ polytype (Takeuchi and Nowacki, 1964).

CHAPTER - 5

GEOCHEMISTRY OF GRANITE

Major and trace element analyses of twentyfour samples of the granite have been carried out. The analytical procedures are given in Appendix.

5.1. Major elements

The analytical data of major elements in the granite are given in Table 14, together with the range, mean and standard deviation. SiO_2 values show a moderate range from 68.73 to 75.27, whereas Al_2O_3 gives a limited range, from 11.73 to 14.27. Fe_2O_3 ranges from 0.30 to 2.86 and FeO has a range between 0.50 and 3.20. The Fe_2O_3 / FeO ratio exhibits considerable variation, from 0.33 to 3.93. Among the alkalies, K_2O shows high levels (upto 7.24) with K_2O/Na_2O ratio consistently greater than unity, which is a common feature among most of the alkaline plutons of the region (Santosh and Nair, 1983b; Nair and Santosh, 1984). The low CaO (0.46-2.69) and MgO (0.32-0.64) values are also comparable and are noted to be a

Table:14 Major element analyses of Ambalavayal granite

Oxide, wt.%	AG 001	AG 002	AG 003	AG 006	AG 010	AG 011	AG 013	AG 014	AG 015
SiO_2	72.46	73.88	73.17	73.53	73.38	72.95	74.10	72.87	74.57
TiO_2	0.24	0.13	0.16	0.07	0.09	0.28	0.13	0.17	0.12
Al_2O_3	12.24	12.24	13.26	11.73	13.26	13.26	12.24	12.75	13.26
Fe_2O_3	2.48	1.87	2.86	0.75	0.98	0.84	1.23	2.07	1.57
FeO	1.03	1.05	0.83	0.50	1.66	0.80	1.02	1.30	1.16
MnO (ppm)	284	142	186	115	262	246	184	235	112
MgO	0.64	0.32	0.32	0.32	0.48	0.48	0.32	0.32	0.32
CaO	0.74	1.79	1.34	0.55	1.12	1.34	1.79	1.34	1.34
Na_2O	3.17	3.64	3.97	3.58	4.19	4.12	3.87	3.86	3.15
K_2O	6.24	4.56	4.19	7.24	4.53	3.46	4.24	4.69	3.94
P_2O_5	0.08	0.06	0.12	0.04	0.03	0.11	0.09	0.14	0.04
Moisture	0.20	0.08	0.04	0.06	0.14	0.30	0.68	0.17	0.42
L.O.I.	0.16	0.18	0.08	0.04	0.16	1.08	0.42	0.26	0.36
Total	99.68	99.80	100.34	100.41	100.02	100.02	100.13	99.94	100.35

Table 14 (Contd.)

Oxide wt%	AG 023	AG 025	AG 030	AG 035	AG 100	AG 101	AG 102	AG 111
SiO_2	74.02	71.30	71.26	73.86	68.73	72.16	72.54	70.90
TiO_2	0.10	0.26	0.20	0.18	0.29	0.17	0.17	0.20
Al_2O_3	12.24	13.26	12.24	12.75	12.27	12.24	13.25	13.78
Fe_2O_3	1.48	1.21	0.76	0.54	1.23	1.05	2.24	1.71
FeO	0.61	1.54	1.74	1.41	3.20	1.71	0.57	2.05
MnO (ppm)	148	240	232	325	410	254	155	407
MgO	0.32	0.48	0.48	0.64	0.48	0.48	0.32	0.32
CaO	0.61	2.02	2.69	2.24	1.65	1.09	0.46	0.86
Na_2O	4.04	3.61	3.59	3.57	2.05	4.76	4.24	3.77
K_2O	5.78	3.74	4.93	3.64	7.56	4.85	5.62	5.67
P_2O_5	0.06	0.06	0.08	0.13	0.22	0.11	0.09	0.10
Moisture	0.36	0.27	0.62	0.26	0.19	0.20	0.14	0.20
L.O.I.	0.34	1.41	0.47	0.41	1.52	0.19	0.11	0.08
Total	99.96	99.16	99.06	99.63	99.39	99.01	99.75	99.64

Table 14 (Contd.)

Oxide, wt%	AG 112	AG 113	AG 118	AG 123	AG 126	AG 127	AG 130
SiO_2	71.04	72.16	72.58	72.72	74.99	74.10	75.27
TiO_2	0.21	0.18	0.14	0.23	0.06	0.05	0.11
Al_2O_3	13.78	14.27	13.10	13.24	13.25	13.25	11.73
Fe_2O_3	1.89	1.27	1.18	1.24	0.30	0.80	0.38
FeO	1.96	1.94	2.10	1.90	0.90	1.15	1.89
$MnO_{(ppm)}$	356	304	225	268	80	156	241
MgO	0.48	0.48	0.64	0.64	0.64	0.48	0.64
CaO	0.78	1.12	0.99	0.66	0.90	1.34	1.12
Na_2O	3.79	2.74	3.96	3.79	3.82	3.03	3.23
K_2O	5.75	5.19	4.92	5.70	4.24	5.24	4.07
P_2O_5	0.11	0.08	0.04	0.08	0.05	0.02	0.04
Moisture	0.17	0.25	0.09	0.07	0.08	0.10	0.07
L.O.I.	0.07	0.13	0.26	0.25	0.23	0.13	0.09
Total	100.03	99.81	100.00	99.52	99.46	99.69	99.44

Table 14 (Contd.)

Oxide	Range	Mean	Standard Deviation
SiO_2	68.73-75.27	72.86	1.50
TiO_2	0.05-0.29	0.16	0.07
Al_2O_3	11.73-14.27	12.83	0.58
Fe_2O_3	0.30-2.86	1.33	0.57
FeO	0.50-3.20	1.42	0.53
MnO_{ppm}	80 - 410	232	88.4
MgO	0.32-0.64	0.46	0.13
CaO	0.46-2.69	1.25	0.56
Na_2O	2.05-5.58	3.73	0.68
K_2O	3.64-7.24	5.07	0.99
P_2O_5	0.02-0.22	0.08	0.04
Moisture	0.04-0.68	0.22	0.17
L.O.I.	0.07-1.52	0.35	0.40
Total	99.16-100.41	99.76	0.39

characteristic feature of alkali granites in general (Greenberg, 1981).

The CIPW normative composition of the granite is given in Table 15. All analyses are quartz normative. However, the presence of normative diopside in most of the cases (upto 6.56) depicts the alkaline character and corresponding alumina deficiency of the rock. In some cases, normative acmite is present, and in one analysis (AG 003), even normative sodium silicate is present, clearly indicating an alkaline nature.

Variations in major elements with respect to SiO_2 are shown in Fig 25, where trend lines have been drawn in from visual best fit. Al_2O_3 and Na_2O show a moderate enrichment towards higher values of silica whereas all other oxides show a progressive decreasing trend. The depletion in CaO, MgO, FeO, TiO_2 and P_2O_5 may be correlated with the early crystallization of mafic minerals and accessory phases. $Na_2O + K_2O$ (A) - FeO^t (F) - MgO (M) and K-Na-Ca variations of the granite are shown in Fig.26. The A-F-M plots fall close to the A-F tie line and almost parallel to it, indicating an alkali-enrichment trend. Among the alkalies, an enrichment in K relative to Na and Ca is observed.

A number of classification schemes have been proposed by various workers based on geochemistry, among which that of Harpum (1963) is widely used. His scheme takes into account the

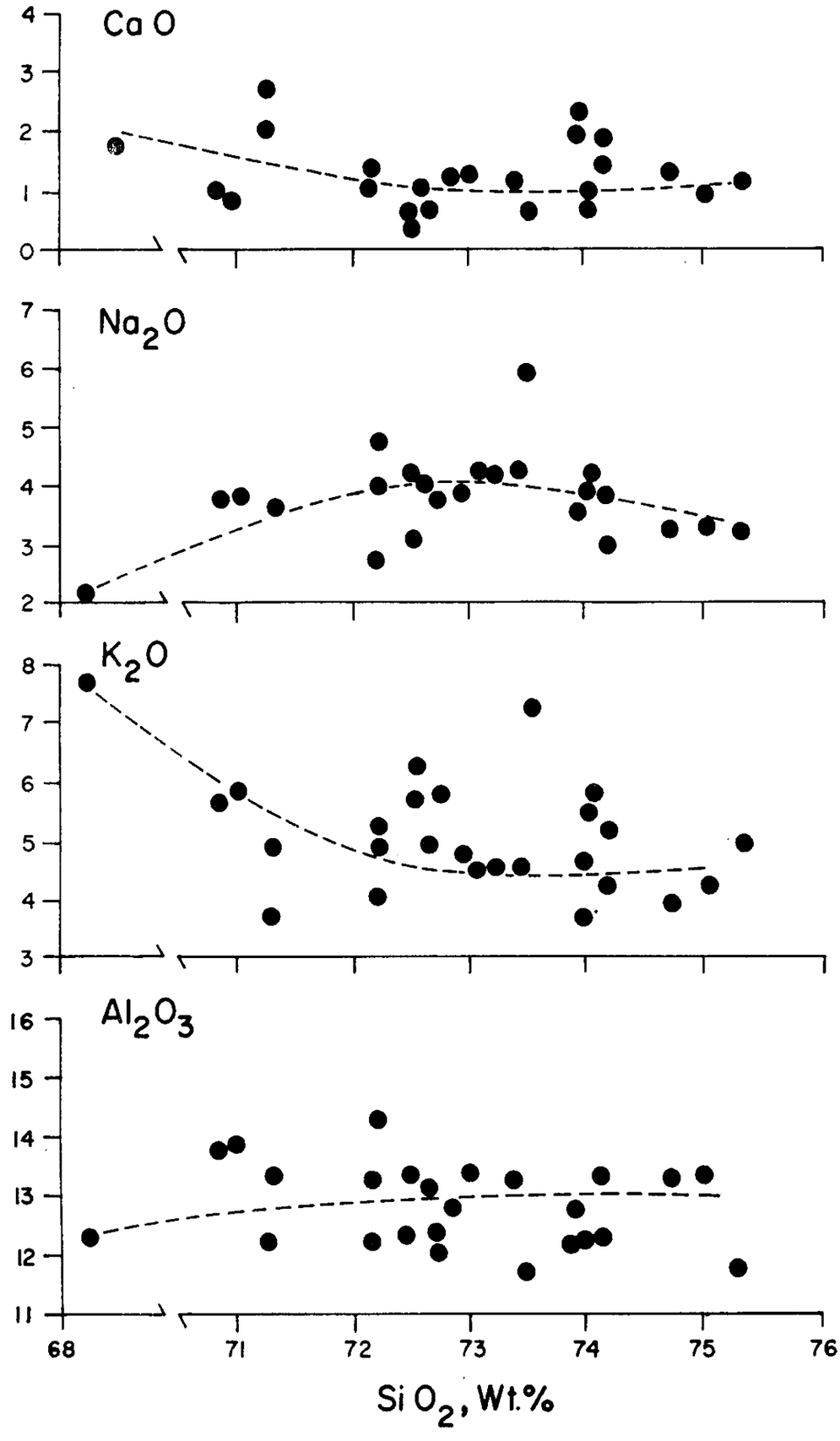

Fig. 25 Variations of major element oxides in the Ambalavayal granite with respect to SiO_2.

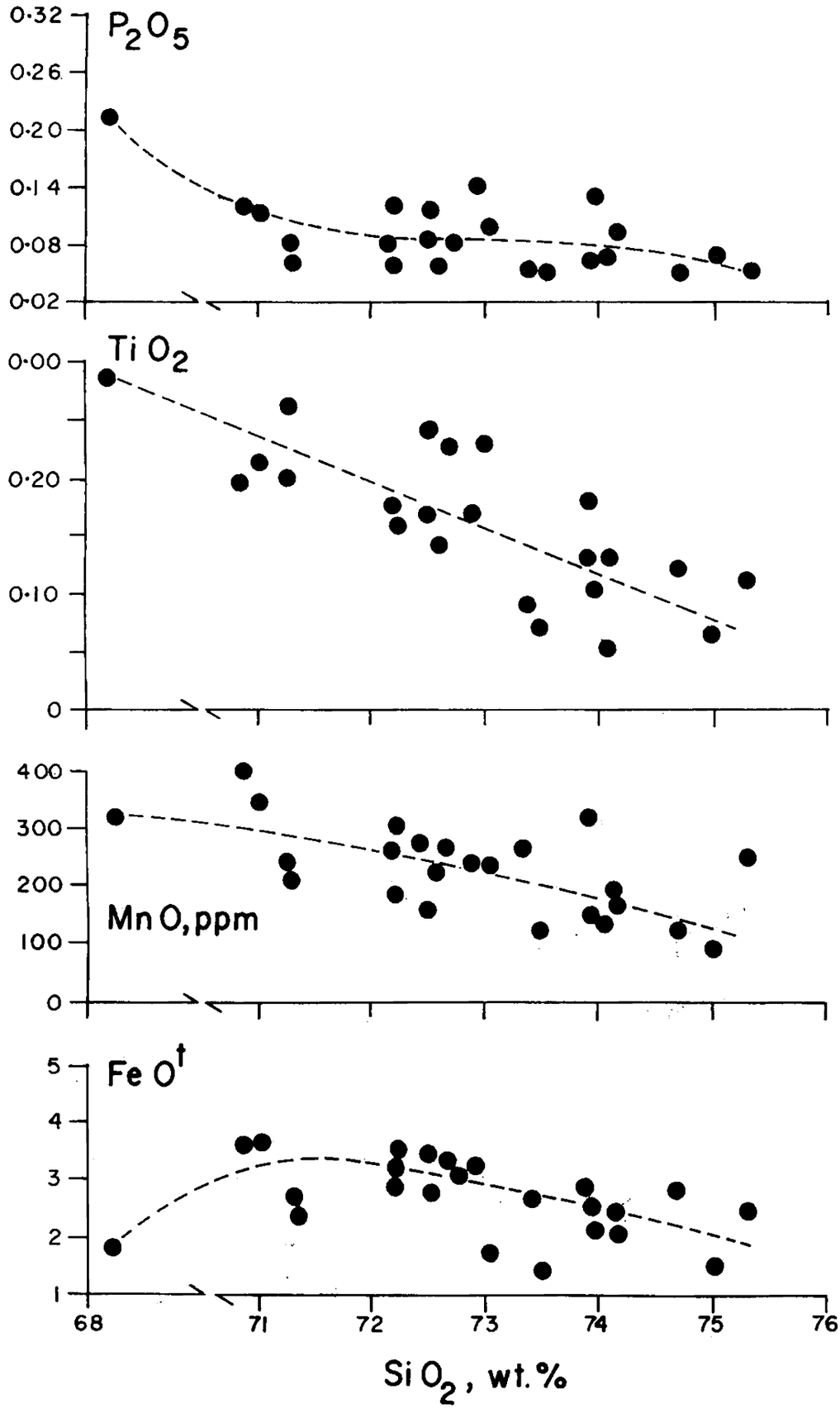
0·32
0·26
0·20
0·14
0·08
0·02
P_2O_5
0·00
0·20
0·10
0
TiO_2
400
300
200
100
0
MnO, ppm
5
4
3
2
1
FeO^t
68
71
72
73
74
75
76
SiO_2, wt.%

Fig. 25 cont.

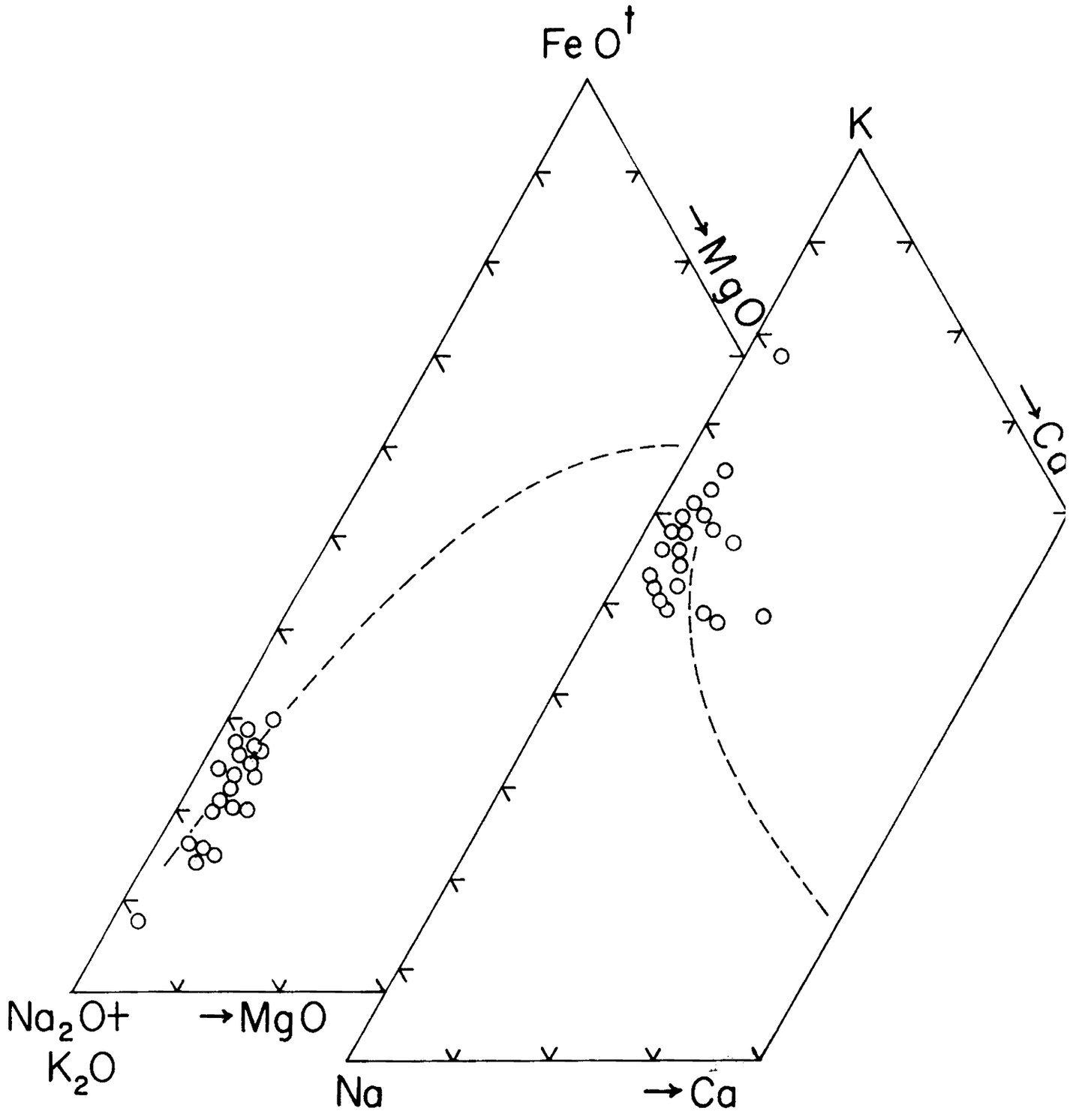

Fig. 26 A-F-M and A-Na-Ca triangular variation diagrams of the Ambalavayal granite.

Table 15 Normative composition of Ambalavayal granite

	AG 001	AG 002	AG 003	AG 006	AG 010	AG 011	AG 013	AG 014
Q	28.44	31.12	30.66	26.64	27.90	28.98	32.34	29.88
Or	36.70	27.24	25.58	42.21	26.69	26.13	25.02	27.80
Ab	26.72	30.92	33.54	19.91	35.77	34.58	32.49	32.49
An	0.68	3.34	5.56	-	3.89	4.73	3.61	3.61
C	-	-	-	-	-	-	-	-
Ac	-	-	-	2.31	-	-	-	-
Ns	-	-	-	5.73	-	-	-	-
Di	1.51	3.38	0.22	2.32	1.43	1.54	2.19	1.79
Wo	-	1.39	-	-	-	-	0.46	-
Hy	0.90	-	0.70	0.56	2.58	0.73	-	0.33
Mt	2.55	2.78	2.32	-	1.39	1.16	1.86	3.02
He	0.80	-	1.28	-	-	-	-	-
Il	0.46	0.30	0.30	0.15	0.15	0.61	0.30	0.30
Ap	0.34	-	0.34	-	-	0.34	0.34	0.34

Table : 15 (contd.)

	AG 015	AG 023	AG 025	AG 030	AG 035	AG 100	AG 101
Q	37.62	27.54	30.60	26.10	33.54	23.64	23.88
Or	23.35	33.92	23.24	28.91	21.68	44.48	28.91
Ab	26.72	30.92	30.39	30.51	30.39	17.29	35.63
An	6.67	-	8.90	2.78	7.78	1.95	-
C	1.33	-	-	-	-	-	-
Ac	-	3.23	-	-	-	-	3.23
Ns	-		-	-	-	-	0.24
Di	-	2.57	0.92	6.56	2.07	4.14	4.52
Wo	-	-	-	1.97	-	-	-
Hy	1.33	0.56	1.06	-	1.76	3.44	2.05
Mt	2.32	-	1.86	1.16	0.70	1.86	-
He	-	0.32	-	-	-	-	-
Il	0.30	0.15	0.46	0.46	0.30	0.61	0.30
Ap	-	-	-	0.34	0.34	0.67	0.34

Table : 15 (Contd.)

	AG 102	AG 111	AG 112	AG 113	AG 118	AG 123	AG 126
Q	26.16	24.00	24.36	32.76	27.00	26.16	33.00
Or	33.36	33.36	33.92	30.58	28.91	33.92	25.02
Ab	35.63	31.96	31.96	23.14	33.66	30.92	32.49
An	0.56	3.34	3.06	4.73	3.34	0.92	4.45
C	-	0.20	0.20	2.45	-	-	0.71
Ac	-	-	-	-	-	-	-
Ns	-	-	-	-	-	-	-
Di	0.65	-	-	-	1.43	2.81	-
Wo	-	-	-	-	-	-	-
Hy	0.50	2.65	2.78	3.44	3.31	2.82	2.92
Mt	1.62	2.55	2.78	1.86	1.62	1.39	0.46
He	1.12	-	-	-	-	-	-
Il	0.15	0.46	0.46	0.30	0.30	0.46	-
Ap	0.34	0.34	0.34	0.34	-	0.34	-

Table 15 (Contd.)

	AG 127	AG 130	Mean	Range
Q	32.10	33.66	29.09	23.64 - 37.62
Or	25.02	28.91	29.79	23.24 - 44.48
Ab	32.49	27.25	30.41	17.29 - 35.63
An	4.45	3.06	3.24	0 - 8.90
C	0.71	-	0.93	0.20 - 2.45
Ac	-	-	2.77	0 - 3.23
Ns	-	-	2.98	0 - 5.73
Di	-	2.10	2.34	0 - 6.56
Wo	-	-	1.21	0 - 1.97
Hy	2.92	3.58	1.95	0 - 3.44
Mt	0.46	0.46	1.72	0.46 - 3.02
He	-	-	0.88	0 - 1.28
Il	0.15	0.15	0.32	0.15 - 0.61
Ap	-	-	0.36	0 - 0.67

relative proportion of Na_2O and K_2O. Plots of the granite in this diagram (Fig.27) mainly fall in the field of adamellite, which correlate well with the subequal amounts of K-feldspar and albitic plagioclase in the granite, as shown by modal data. Rogers and Greenberg (1981) differentiated calc-alkalic batholiths and alkali granites based on the proportions of SiO_2 and $Log_{10}K_2O/MgO$ values. Plots of the Ambalavayal granite in this diagram fall dominantly in the field delineated for alkali granites (Fig.28).

5.2. Trace elements

Trace element contents of the granite are presented in Table 16. and their variations with respect to SiO_2 levels are plotted in Fig.29. Behaviour of individual trace element is discussed below:

Barium: Barium has an ionic radius similar to that of potassium and hence it is partitioned in K-bearing minerals like potash feldspar and biotite. The Ba values in the granite are low (av. 112.3ppm), ranging from 9 to 309 ppm. Ba shows an overall decrease with increasing SiO_2, sympathetic with the trend of K_2O and consistent with the general trend expected during magmatic differentiation.

Bismuth: Bi^{3+} substitutes Ca^{2+} in apatite. In the present case, Bi shows a range of 10-126 ppm, with a decrease towards higher SiO_2 values, correlatable with the trend of CaO.

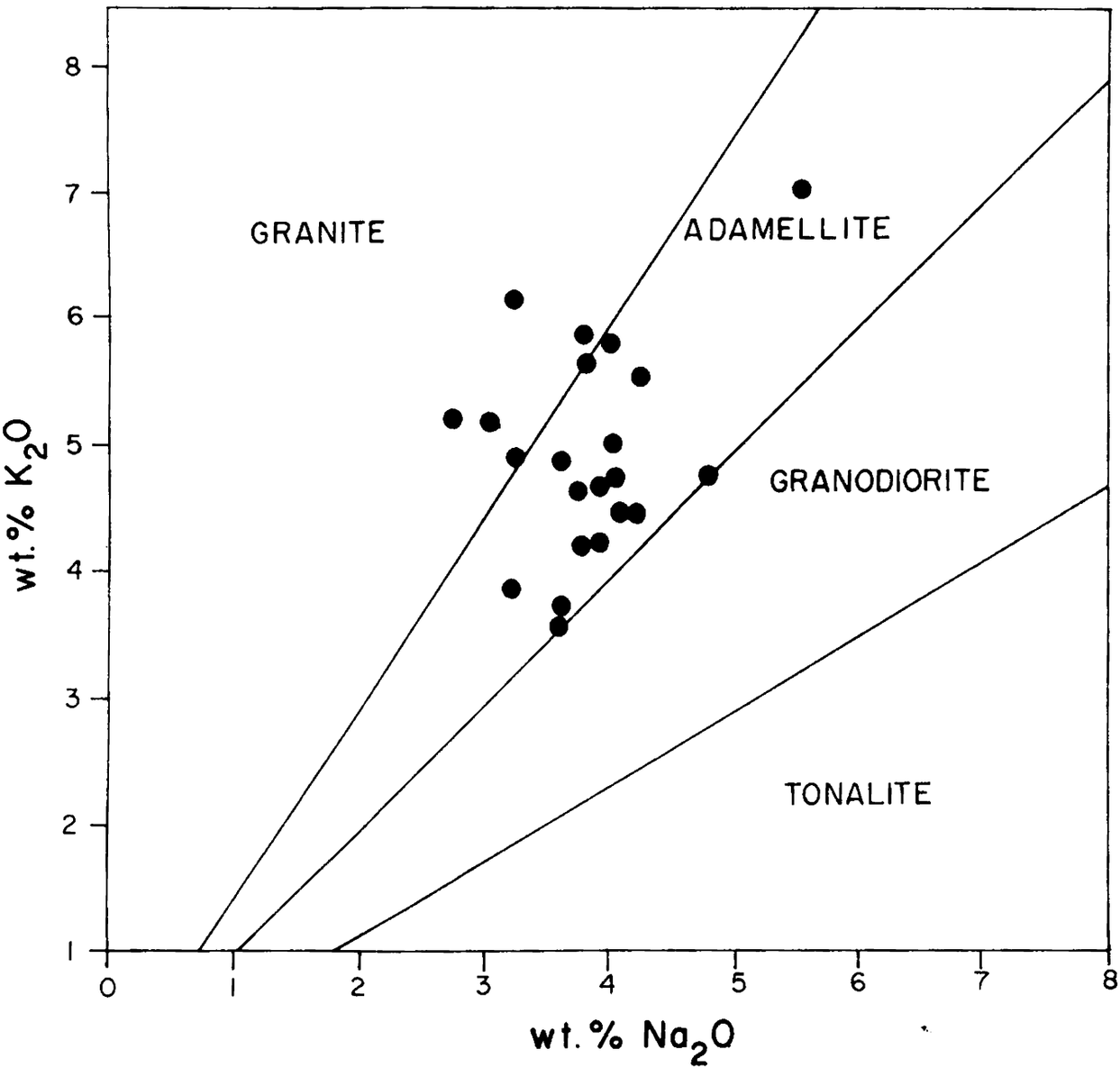

Fig. 27 Na_2O vs. K_2O plots of the Ambalavayal granite. The field boundaries are after Harpum (1963).

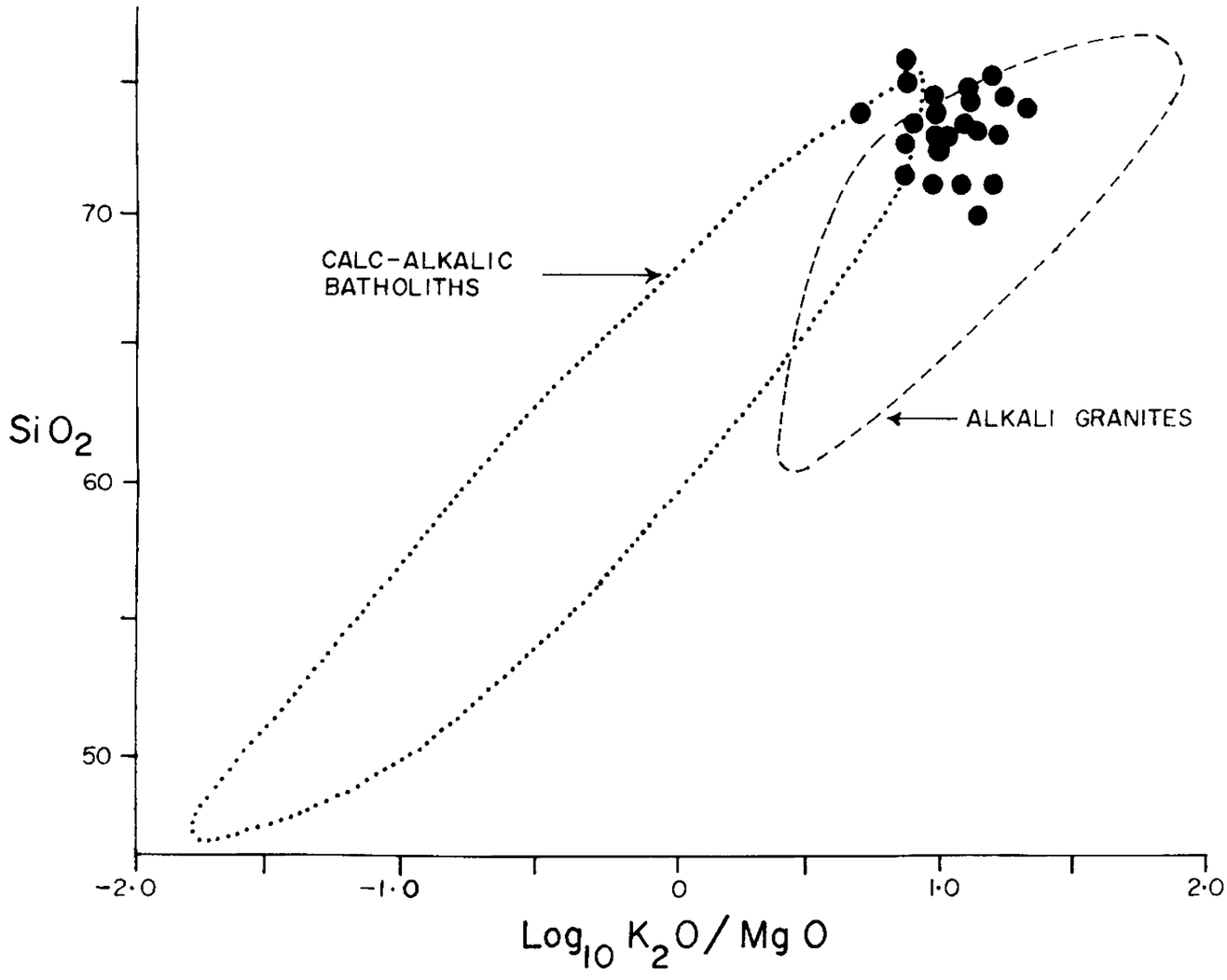

Fig. 28 SiO_2 vs. $Log_{10} K_2O/MgO$ plots of the granite. The fields of calc-alkalic batholiths and alkali granites are after Rogers and Greenberg (1981).

Table: 16 Trace element analyses of Ambalavayal granite

Element, ppm	AG 001	AG 002	AG 003	AG 006	AG 010	AG 011	AG 013	AG 014	AG 015	AG 023
Ba	72	9	230	309	29	32	48	36	137	220
Bi	64	126	98	46	52	61	87	67	75	46
Ce	315	-	-	54	-	-	-	-	290	-
Co	11	24	11	12	21	18	22	8	12	9
Cr	52	134	74	42	92	86	62	82	81	
Cu	34	14	22	16	18	12	8	28	32	20
La	156	-	-	24	-	-	-	-	143	-
Li	46	12	18	8	21	14	6	14	28	32
Mo	28	13	17	12	18	11	12	16	18	21
Nb	38	-	-	11	-	-	-	-	37	-

Table : 16 (Contd.)

	AG 001	AG 002	AG 003	AG 006	AG 010	AG 011	AG 013	AG 014	AG 015	AG 023
Ni.	32	114	68	21	54	28	16	68	38	74
Pb	18	17	12	18	16	14	18	19	18	21
Rb	65	64	63	69	67	62	56	72	61	75
Sr	13	15	42	38	11	18	26	8	24	5
Th	19	11	16	5	33	41	-	21	13	36
U	2	8	8	2	24	6	-	7	2	15
Y	60	-	-	15	-	-	-	-	57	-
Zn	91	114	80	25	100	112	88	85	68	43
Zr	309	120	160	199	224	138	164	314	328	227

Table : 16 (Contd.)

Element ppm	AG 025	AG 030	AG 035	AG 100	AG 101*	AG 102*	AG 111*	AG 112*	AG 113	AG 118*
Ba	147	104	16	216	159	57	142	145	104	23
Bi	84	112	82	80	46	58	76	10	70	14
Ce	-	-	-	540	334	125	331	315	-	118
Co	11	9	13	16	14	16	20	12	12	12
Cr	77	108	51	145	117	170	102	56	36	179
Cu	6	10	8	15	7	8	1	24	20	35
La	-	-	-	253	176	46	161	156	-	44
Li	15	12	6	64	4	5	6	6	16	22
Mo	11	17	10	27	14	17	12	19	21	22
Nb	-	-	-	54	26	173	37	37	-	165

. Table : 16 (Contd.)

Element ppm	AG025	AG030	AG035	AG100*	AG101*	AG102*	AG*****	AG112*	AG113	AG118*
Ni	42	84	33	132	107	113	43	40	40	139
Pb	8	51	12	20	16	20	19	17	28	29
Rb	54	60	43	101	47	87	62	61	54	131
Sr	49	11	5	62	31	51	22	26	10	16
Th	40	-	-	30	13	18	19	7	-	22
U	23	-	-	3	n.f.	4	3	3	-	9
Y	-	-	-	102	38	170	55	54	-	215
Zn	123	184	110	254	172	190	160	248	182	246
Zr	189	246	118	528	279	118	374	327	280	124

Table : 16 (Contd.)

Element ppm	AG 123	AG 126	AG 127	AG 130	Range	Mean	S.D.
Ba	146	148	9	156	9-309	112.3	31.3
Bi	28	34	52	38	10-126	62.0	20.5
Ce	426	-	94	-	54-540	267.5	150.
Co	12	12	16	12	9-22	14	4.3
Cr	132	131	169	113	36-184	104.7	47.3
Cu	40	4	6	7	4-40	16.5	11
La	223	-	33		24-253	128.6	79.7
Li	9	20	6	7	5-64	16.3	14.3
Mo	22	6	28	12	6-28	16.8	6.9
Pb	42	-	146	-	11 146	70.5	51.5

Table : 16 (Contd.)

Element ppm	AG 123*	AG 126	AG 127*	AG 130	Range	Mean	S.D.
Ni	152	106	139	100	16-152	76.6	41.8
Pb	18	40	19	26	8-51	20.5	9.1
Rb	65	122	96	80	43-131	71.5	21.8
Sr	27	3	6	4	3-62	21.8	16.5
Th	15	-	16	-	5-40	20.3	10.8
U	3	-	3		2-24	5.9	5.9
Y	66	-	164	-	15-215	90.5	64.1
Zn	184	220	192	220	48-254	145.7	66.9
Zr	348	140	115	260	115-528	234.5	104.6

Asterix(*) indicates analyses of Ba,Ce,La,Nb,Pb,Rb,Sr,Th,U &Zr by XRF.
Dash(-) denotes not analysed.
n.f. not found, below detection limit.
S.D. standard deviation.

Cerium: The Ce levels range from 54 to 540 ppm with an average of 267.5ppm. The high level of light rare earth elements (LREE) (La and Ce) is a unique feature of the Ambalavayal granite. Considering the role of LREE in the fractionation of accessory phases like sphene and apatite in acid and alkaline magmas (Miller and Mittlefehldt, 1982; Fleischer and Altschuler, 1969) it is to be presumed that these elements are concentrated in the accessory sphene, which is ubiquitously present in the Ambalavayal granite. Ce shows a decreasing trend towards higher SiO_2 levels indicating the early crystallization of accessory minerals.

Cobalt: Co has an ionic radius intermediate between Mg^{2+} and Fe^{2+}. Since Mg follows Ca in granitic rocks, higher Ca-granites have higher Co. In the present case, the Co values are low (9-22ppm), consistent with the low calcic nature of the granite. Co shows an overall decrease with progressive fractionation.

Chromium: Cr follows Fe^{2+} and Mg and hence low Mg-granites have usually low Cr content. The average Cr content of the Ambalavayal granite is 102.7ppm, which is higher than the values reported for adamellites from other regions. The possibilities of contamination during sample preparation has been checked and the relatively high Cr contents in the granite are presumably correct. Moreover, they correlate well with the general Cr-enriched nature of the alkali granites of the region

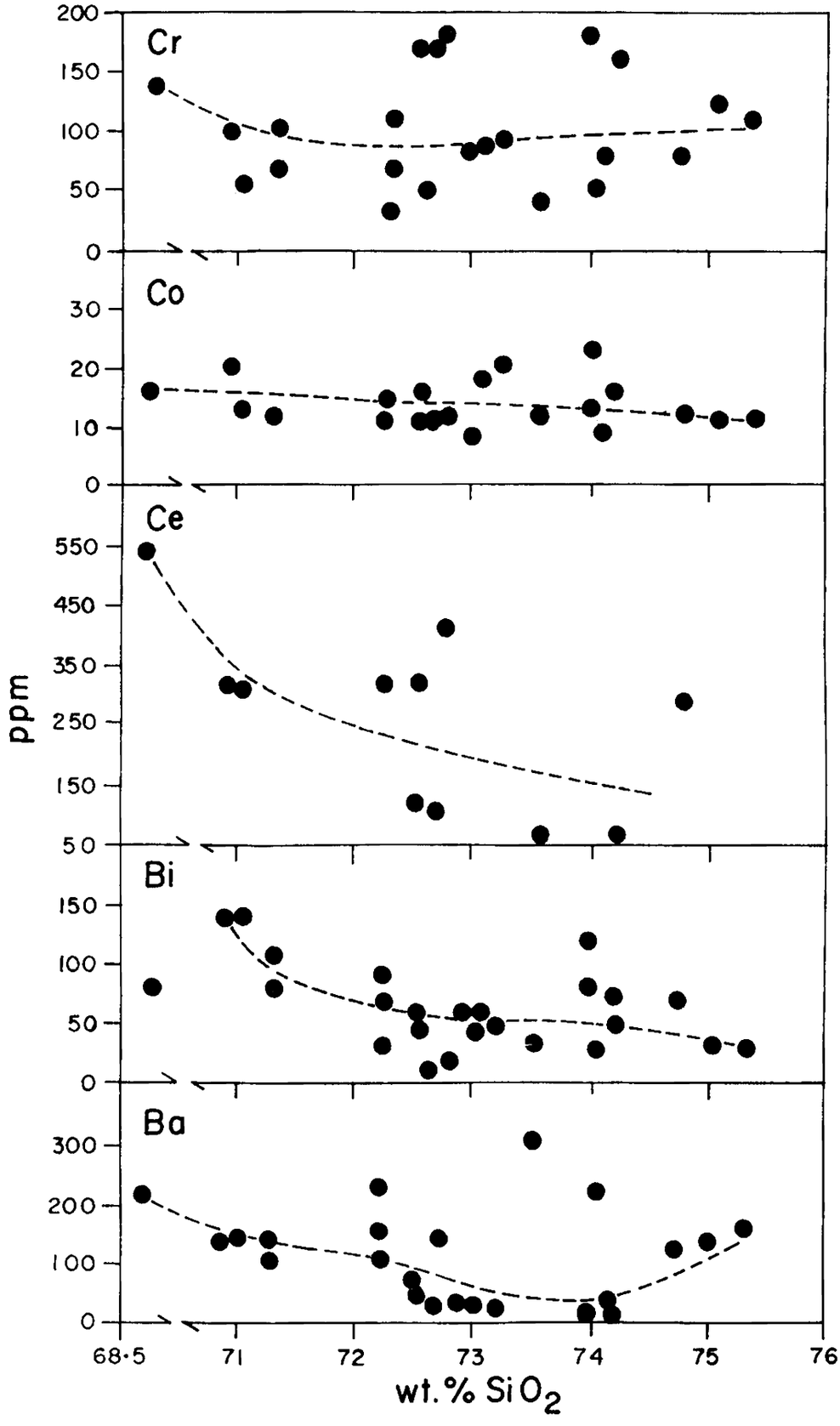

Fig. 29 Trace element variations in the Ambalavayal granite.

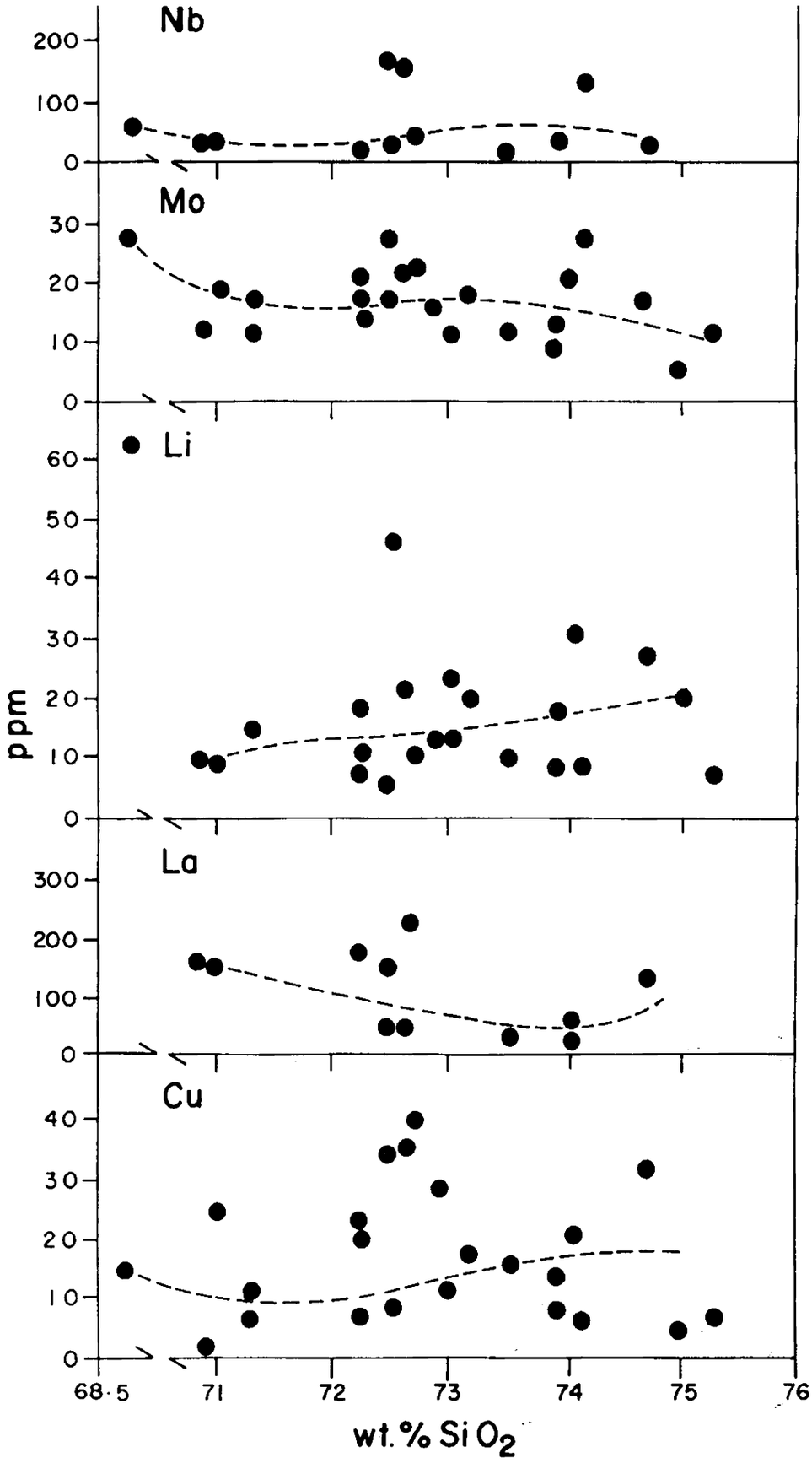
Nb
200
100
0
Mo
30
20
10
0
Li
60
50
40
30
20
10
0
ppm
La
300
200
100
0
Cu
40
30
20
10
0
68·5
71
72
73
74
75
76
wt.% Si O2

Fig. 29 cont.

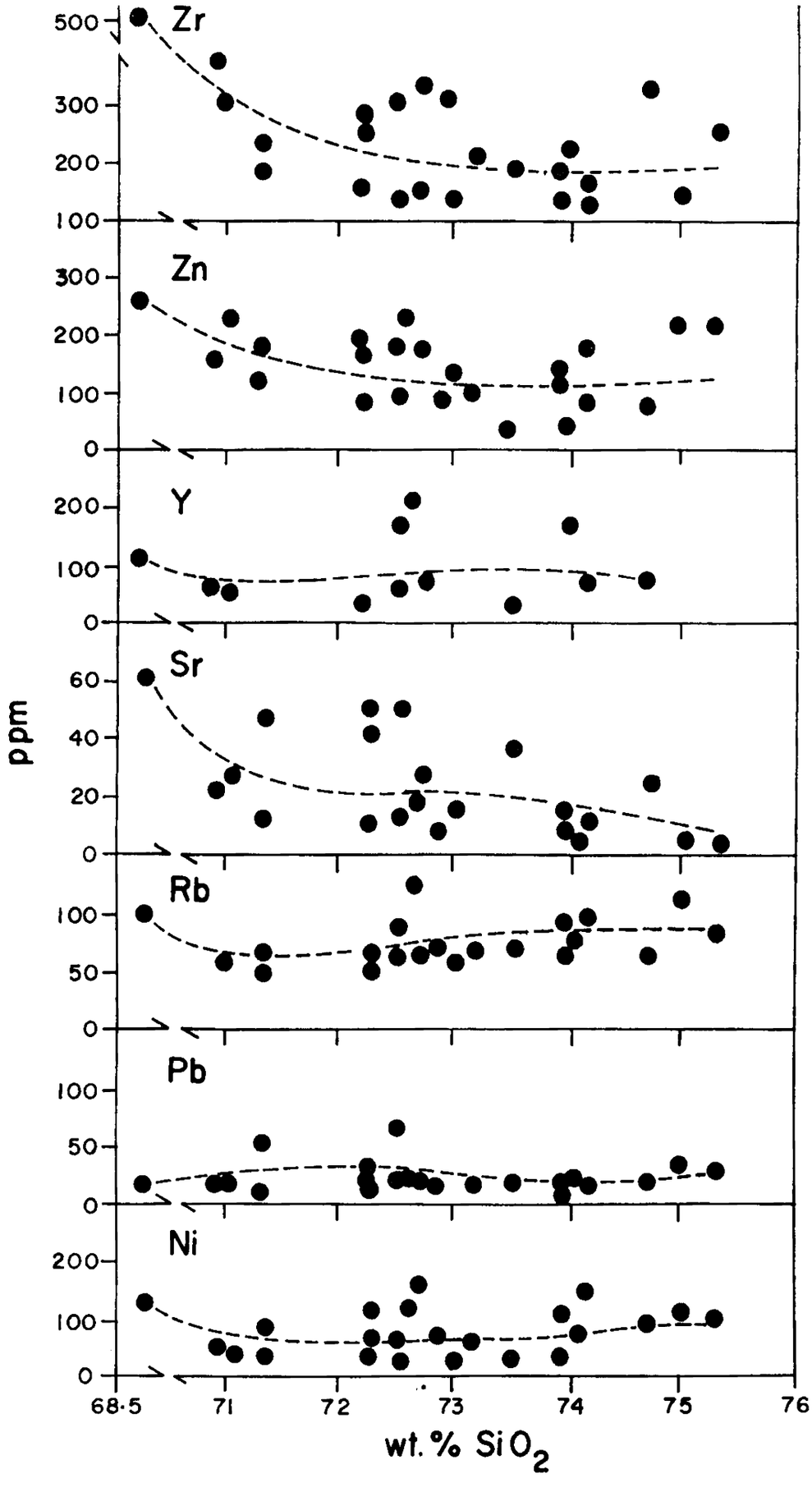
Zr
500
300
200
100
Zn
300
200
100
0
Y
200
100
0
Sr
60
40
20
0
Rb
100
50
0
Pb
100
50
0
Ni
200
100
0
ppm
68·5
71
72
73
74
75
76
wt. % SiO2

Fig. 29 contd.

(Nair et al., 1983a). Cr shows a scattered distribution against SiO_2, precluding any significant role of iron-rich minerals like magnetite in the fractionation process of the granite.

Copper: Similar to Cr and Co, Cu is partitioned in Fe and Mg minerals. The Cu values of the granite range from 4 to 40ppm, with a mean at 16.5. Cu shows scattered distribution.

Lanthanum: Like Ce, La also shows anomalously high values in the granite, ranging from 24 to 253 ppm. La decreases with higher silica content.

Lithium: Li follows Mg since the ionic sizes are similar. It is however, partitioned into volatiles and may concentrate in the residual liquid during differentiation of felsic melts. In the present case, eventhough Li values are very low (av. 16.3ppm), it tends to concentrate towards the felsic end.

Molybdenum: Diadochic replacement takes place between Mo and Fe^{2+} or Mg^{2+}. However, since Mo is also partitioned into volatile phase, it sometimes concentrates in residual liquids. The Mo content shows depletion towards higher SiO_2 levels. This is because of the partitioning and removal of molybdenum into a vapour phase which evolved towards the residual stage, as would be discussed later.

Niobium: Niobium values are fairly high (upto 146ppm) consistent with the general high Nb-content of alkali granites. Nb does not show any systematic variation against SiO_2.

Nickel: Ni has similar ionic radius and charge as that of Mg. Usually, high Ca and high Mg bearing granites have higher Ni content. Nickel content ranges from 16 to 152 ppm in the Ambalavayal granite and is slightly high as compared to that of the granites of other regions. However, higher Ni values, like high Cr-content, are noted to be a general geochemical feature of the granites in the region. Nickel values show an overall decrease with fractionation, consistent with entrance in early crystallizing ferromagnesium minerals.

Lead: Lead is partitioned into K-bearing minerals as Pb^{2+} has a similar ionic radius as that of K^{+}. Pb content of Ambalavayal granite shows an average of 20.5ppm, which is very close to the average Pb content for granites in general (20ppm). Lead does not show much variation against the silica values.

Rubidium: Like Ba, Rb is also partitioned in K-bearing minerals. The Rb-enrichment trend and its negative correlation with Sr, as noted for the granite, is in agreement with the ideal conditions of magmatic crystallization. The Rb-values of Ambalavayal granite are low, ranging from 43 to 131ppm (av.71.5), correlating with the general low Rb-content of other alkaline plutons of the Kerala region.

Strontium: Sr shows diadochy with Ca and is dominantly partitioned in calcic plagioclase, but also in apatite or other Ca-bearing phases like pyroxene or amphibole. The Sr levels are very low in the present case (av.21.8ppm), correlating with

the low Ca-content of the granite. Sr values show an overall depletion towards higher SiO_2 levels, sympathetic with the behaviour of CaO.

Yttrium: The Ambalavayal granite shows relatively high Y-content (upto 215 ppm). The Y values show a slight decrease towards the higher SiO_2 levels, consistent with the fractionation of Ca-bearing minerals like sphene, apatite and hornblende.

Zinc: The granite shows fairly high Zn values (av. 145.7ppm). High Zn values are typical of alkali granites (Collerson 1982) Zn is partitioned in ferromagnesium minerals in felsic rocks, mainly biotite. With increase in SiO_2, Zn shows a decreasing trend.

Zirconium: The Zr values of the granite are considerably high, ranging from 115 to 528ppm (av. 234.5). High Zr levels are noted to be an index for alkali granites (Bowden and Turner, 1974). Zr contents show decrease upto a SiO_2 level of about 72 wt. % and subsequently a variable distribution towards higher silica levels.

Uranium and Thorium: The uranium levels in the granite range from 2 to 24ppm (av. 6.9) whereas thorium shows high values, ranging upto 40ppm (av.20.8). Plots against K show that both the radioelements initially increase but then gradually decrease towards higher K values. The Th/U ratio shows a pronounced positive correlation with K. Th vs.U plots also show an overall positive correlation (Fig.30).

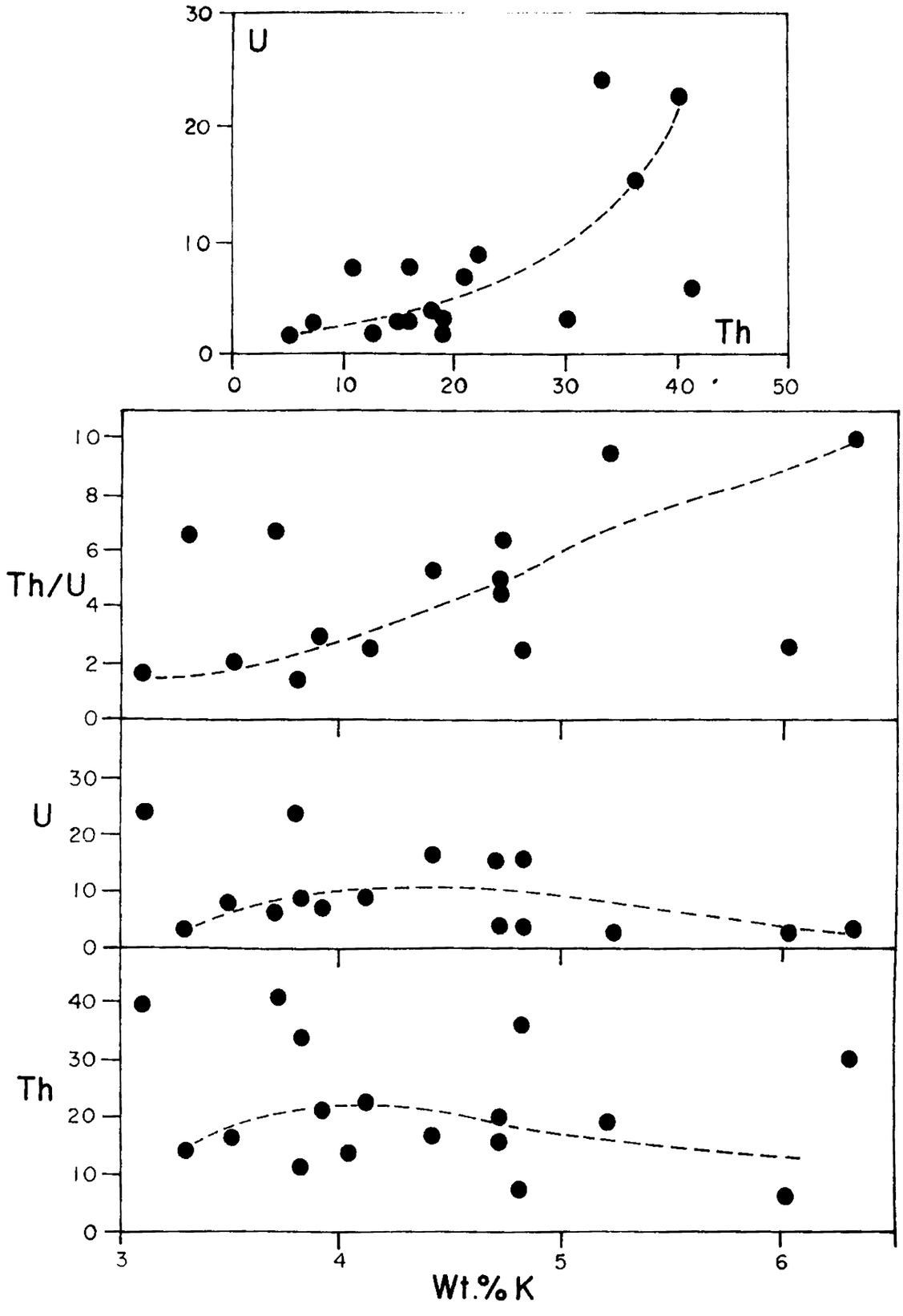

Fig. 30 Radioelement variations in the Ambalavayal granite.

5.3. Discussion

The K_2O:Na_2O ratios indicate the granite to be of adamellite variety. Considering the albitic composition of the plagioclase, the modal mineral content indicates the rock to be alkali-feldspar granite. The high SiO_2 levels with respect to higher Log_{10} K_2O/MgO values, characterise its alkaline nature, substantiated by the normative and modal mineral data. Some of the notable features of major and trace element abundances in alkali granites from different regions are summarised in Table 17, alongwith that of Ambalavayal granite for comparisons The relatively higher SiO_2, K_2O and Na_2O values among major elements, together with low abundance of Ba, Rb and Sr and the enrichment of Nb and Zr are common features.

Many schemes of classification of granites have been proposed from time to time by various workers. More recently, Chappell and White (1974) proposed a classification of granites into I-type and S-type which has attracted considerable attention. According to this scheme, the salient features of I-type granites include (1) linear trend lines in variation diagrams, (2) wide silica range, (3) relatively high Na_2O content, (4) presence of CIPW normative corundum, (5) mol. % A/CNK ($Al_2O_3/Na_2O + K_2O + CaO$) values exceeding 1.5, (6) minor mineral assemblage characterised by biotite + hornblende $\pm$ sphene $\pm$ magnetite and (7) low intial Sr-isotope levels

TABLE 17 : COMPARISON OF SELECTED MAJOR AND TRACE ELEMENTS IN AMBALAVAYAL GRANITE WITH THOSE OF OTHER ALKALI GRANITES.

	1	2	3	4	5	6	7
Wt%							
SiO_2	72.86	75.50	74.04	74.0	72.4	73.20	71.08
K_2O	5.07	4.74	4.54	5.00	4.93	3.98	4.21
Na_2O	3.73	4.15	4.11	3.97	4.49	5.03	4.92
ppm							
Ba	112	138	237	495	333	-	
Rb	72	149	111	161	204	311	
Sr	17	21	24	46	26	9	
Nb	71	55	63	44	81	50	
Zr	235	104	823	210	1013	-	

1. Ambalavayal granite
2. Egyptian Younger granites (Greenberg, 1981).
3. Late Precambrian alkali granites of Arabian Shield (Jackson et al., 1984)
4. Early Paleozoic alkali granite of Llanbedrog, N. Wales (Croudace, 1982)
5. Peralkaline granite of Labrador (Analysis 34 R/B, Collerson, 1982)
6. Riebeckite granite of Bokan Mountain, Alaska (Thompson et al., 1982)
7. Average peralkaline granite (Nockolds and Allen, 1954)

(0.704-0.706). On the other hand, the S-type granites are characterised by (1) variation diagrams yielding irregular trends, (2) restricted to high silica range, (3) low Na-content, (4) presence of CIPW normative corundum exceeding 1%, (5) A/CNK values exceeding 1.1, (5) presence of biotite + muscovite ± cordierite ± garnet ± ilmenite and (6) high initial Sr-isotope ratios (0.708). The Ambalavayal granite shows the presence of biotite, hornblende, sphene and magnetite with absence of aluminous minerals like muscovite, garnet or cordierite, typical of I-type granites. The overall linear patterns of variation diagrams, the high abundance of normative diopside and low A/CNK values are also characteristics, which attribute I-type affinity. However, with regard to high initial Sr-isotope ratio, the granite has more correlation with S type. Recently, Loiselle and Wones (1979) proposed another category, called the A-type. The A-type granites with low Ca content, are marginally peralkaline or metaluminous and characterised by lower Ba, Rb and Sr with higher La, Nb, Y, Zn and Zr, like the late Precambrian granites of the Arabian shield (Jackson et al, 1984). Considering the mineralogical and geochemical features, a transition between I and A-types is to be invoked for the Ambalavayal granite. The high initial Sr-isotope ratio, much higher than that for S-type granites which is not clearly explained, may be assumed to be a result of crustal contamination.

The granite shows higher transition element contents (Cr, Ni) comparable with similar values obtained for the alkaline plutons of the Kerala region. The variation of these elements is however, limited, precluding any significant role for them in the fractionation processes.

The behaviour of large ion lithophile (LIL) elements is significant in delineating the fractionation trends in granitic melts, because of their general partitioning in typical granite minerals like feldspars, biotite and amphiboles (Hanson, 1978). In particular, Ba, Sr and Rb are used to evaluate fractionation processes (McCarthy, 1976). Barium is concentrated in K-feldspar, biotite and muscovite relative to melt by factors of 3-13, Sr is concentrated in the feldspars by 1-2. During fractional crystallization of granitic magma, in which biotite and muscovite are less than 20%, plagioclase is more than 20% and K-feldspars comprise most of the remainder in the crystallizing assemblage, as in the present case, the bulk distribution coefficient for Ba and Sr will be greater than 1 and for Rb less than 1. Hence, fractional crystallization will result in decreasing Ba and Sr and increasing Rb. This is the trend observed for the Ambalavayal granite. The distribution of Sr, Ba and Rb between alkali feldspar and granitic liquids is strongly influenced by composition and temperature. It has been observed that the partitition coefficients for Ba and Sr between K-feldspar and peraluminous liquids are much greater

than for liquids of peralkaline composition. The lower Ba, Rb and Sr levels of the granite imply probable crystallization from alkali-enriched melt. The interelement relations do not show any pronounced trends of variations observed. Nevertheless, a weak positive correlation of Ba-Rb, K-Rb and K-Ba with a negative correlation of Rb-Sr is discernible. The granite shows extremely high K/Rb values, indicative of Rb-depleted source for the magma. Moderate to high K/Ba values are also observed. The K/Rb ratio, when plotted against fractionation indices (figures not presented) show an initial increase in the ratio, denoting hornblende fractionation. Towards later stages, the plots define a decreasing trend, denoting feldspar fractionation. Ba/Sr ratio in a melt is increased by crystallization of plagioclase, reduced slightly by K-feldspar and is further reduced by biotite (Hanson, 1978). This ratio shows a progressive decrease towards the felsic end, depicting fractionation of K-feldspar and biotite. It has, however, to be cautioned that the LIL elements are highly mobile and easily influenced by later processes, resulting in redistribution and causing error in interpretations based on their abundance levels. But around Ambalavayal region, there is no evidence of later teconomagmatic events which could possibly alter the original constitution and hence the interpretations made above hold good.

The abundance of high field strength (HFS) elements namely, Nb, Zr and Y, on the other hand, is not usually altered by secondary processes and hence is highly significant. Their high concentrations in the present case conclusively indicate an alkaline affinity of the pluton. The dependence of HFS elements on minor mineral phases in felsic rocks was noted by Saunders et al. (1980). The high concentrations of LREE (La and Ce) are also a unique feature of the granite. Recent investigations (Miller and Mittlefehldt, 1982) show that LREE and HFS-elements are mainly partitioned in accessory phases of granitic rocks. Plots of La, Ce and Zr against P_2O_5 (Fig.31) and TiO_2 (Fig.32) show discernible positive correlations. A depletion in these elements have also been observed towards higher SiO_2 values. The LREE partition coefficients for the major mineral phases are likely to be less than unity, based on measured phenocryst-matrix coefficients (Nagaswa and Schnetzler, 1971). The biotite/K-feldspar data of Condie and Lo (1971) argue that LREE partition coefficients for micas are less than unity. This rules out the possibility that major and/or minor mineral species were responsible for the depletion of LREE during fractionation. As no major phase which is abundant in felsic rocks has LREE partition coefficients greater than one, the crystallization of typical minerals like quartz, feldspar and micas should result in enrichment of LREE in the liquid (Simmons and Hedge, 1978). Sufficient quantities of some LREE-rich accessory minerals would raise the bulk

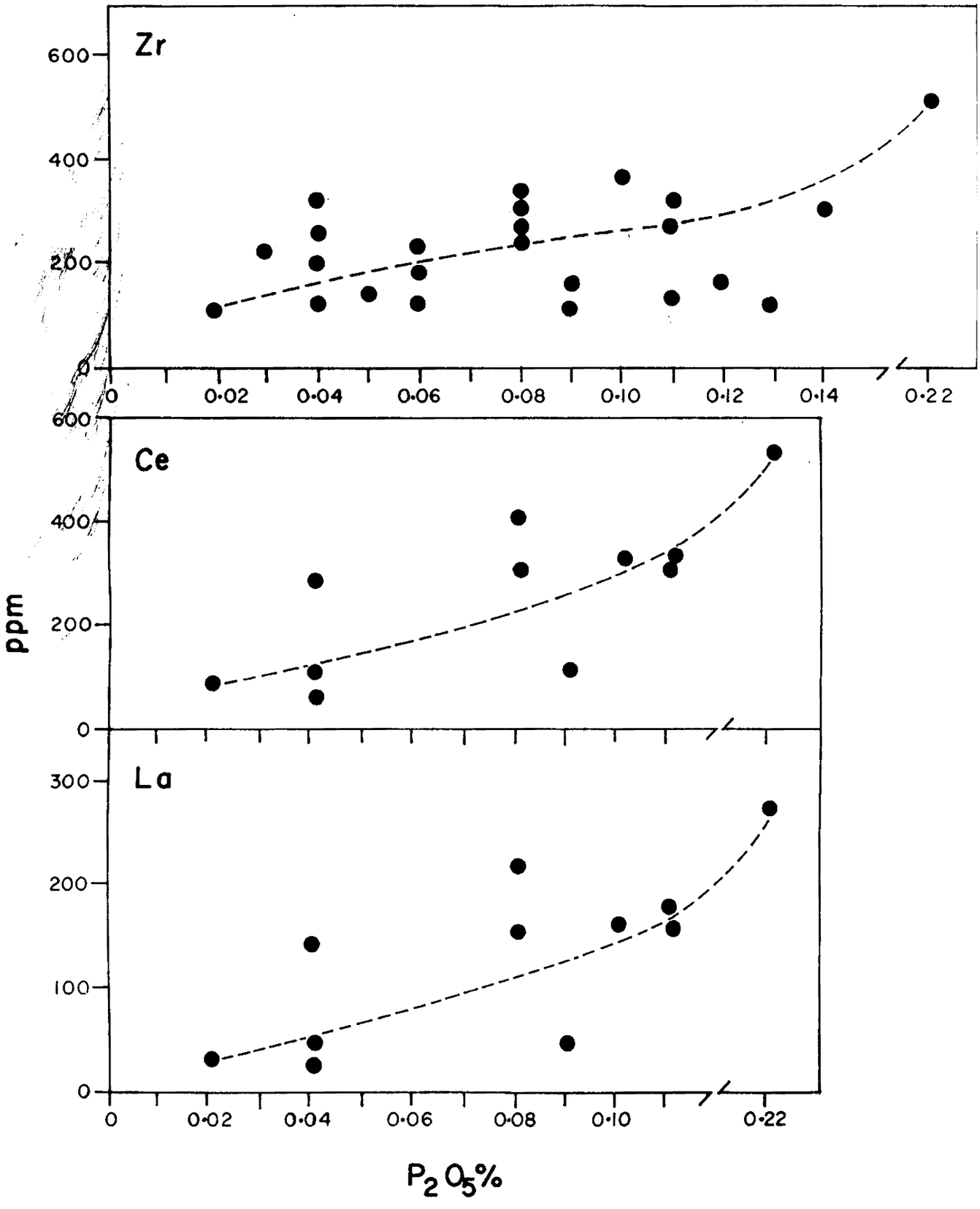

Fig. 31 Variations of La, Ce and Zr against P_2O_5 in the granite.

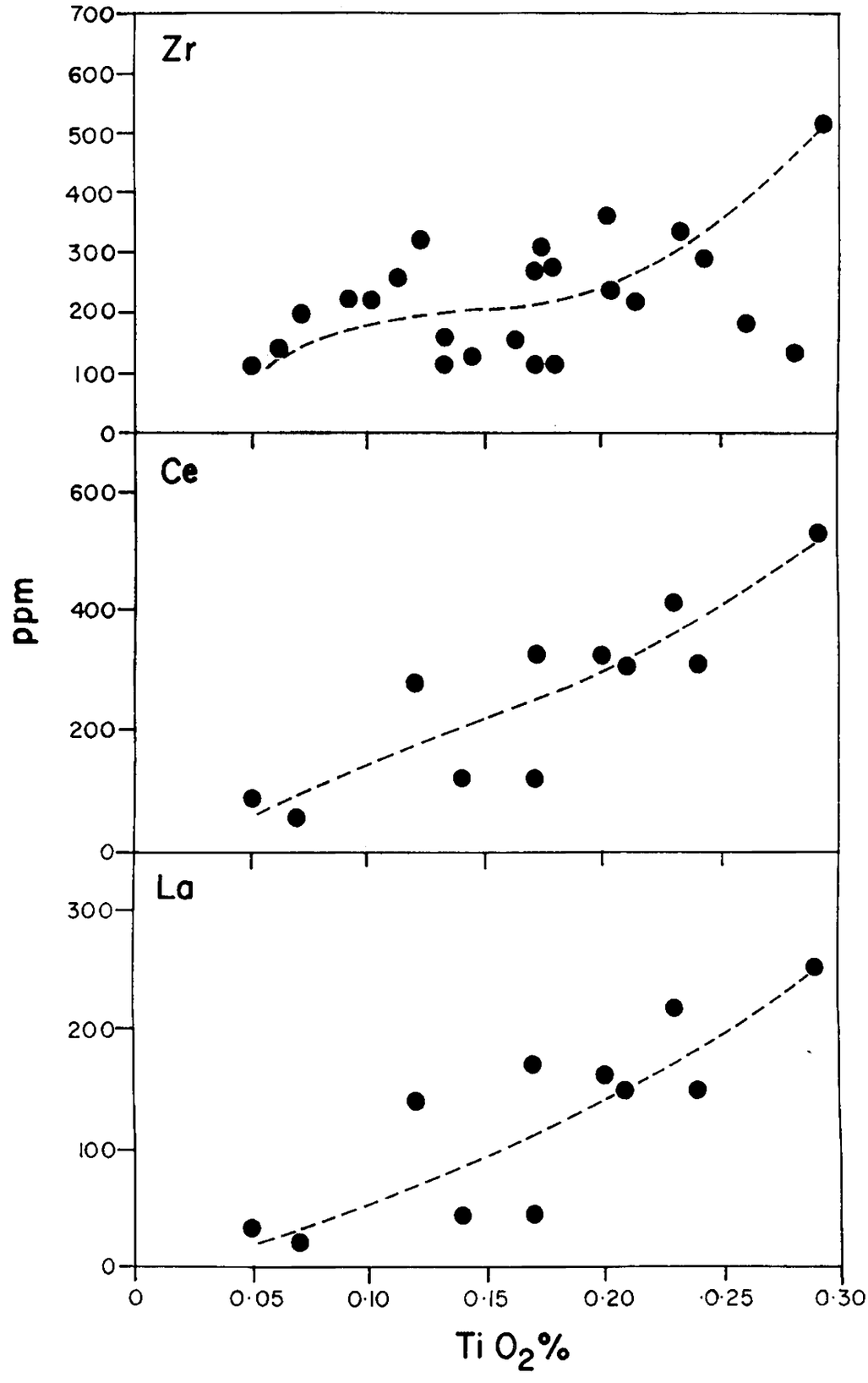

Fig. 32 Variations of La, Ce and Zr against TiO_2 in the granite.

distribution coefficient for LREE of the crystallizing assemblage above unity, and thus result in depletion of the liquid. Such minerals include accessories like sphene, apatite, allanite and monazite, some of which are ubiquitously present in the Ambalavayal granite. Wendlandt and Hanson (1979) showed that REE, particularly LREE, partition very strongly into CO_2 vapor. Pure CO_2 has a high partition coefficient of LREE (about 50) and thus it could effectively scavenge the LREE from a magma. This is very important in the case of Ambalavayal granite, where the presence of a CO_2 rich phase is commonly noted in fluid inclusions, as will be discussed later. The depletion of LREE towards the felsic end correlates with the separation of CO_2 rich vapor phase. In the absence of analytical data on all the HREE, the La/Y ratio can be taken as an indicator of LREE/HREE proportion as Y behaves similar to HREE (Tarney, 1976). The average ratio of 2.34 for the granite falls within the range of 1.3 to 4.5 recorded for alkaline granites of Nigeria (Bowden and Turner, 1974). La/Y and Ce/Y ratios show pronounced decrease against Y (Fig.33).

The chemical changes observed in the granite pluton thus suggest limited fractional crystallization. The sequence of crystallization with aplites and pegmatites formed at the late stage is consistent with this. However, the absence of cumulate rocks indicate that fractionation did not occur largely by continuous and efficient removal of crystals from liquid,

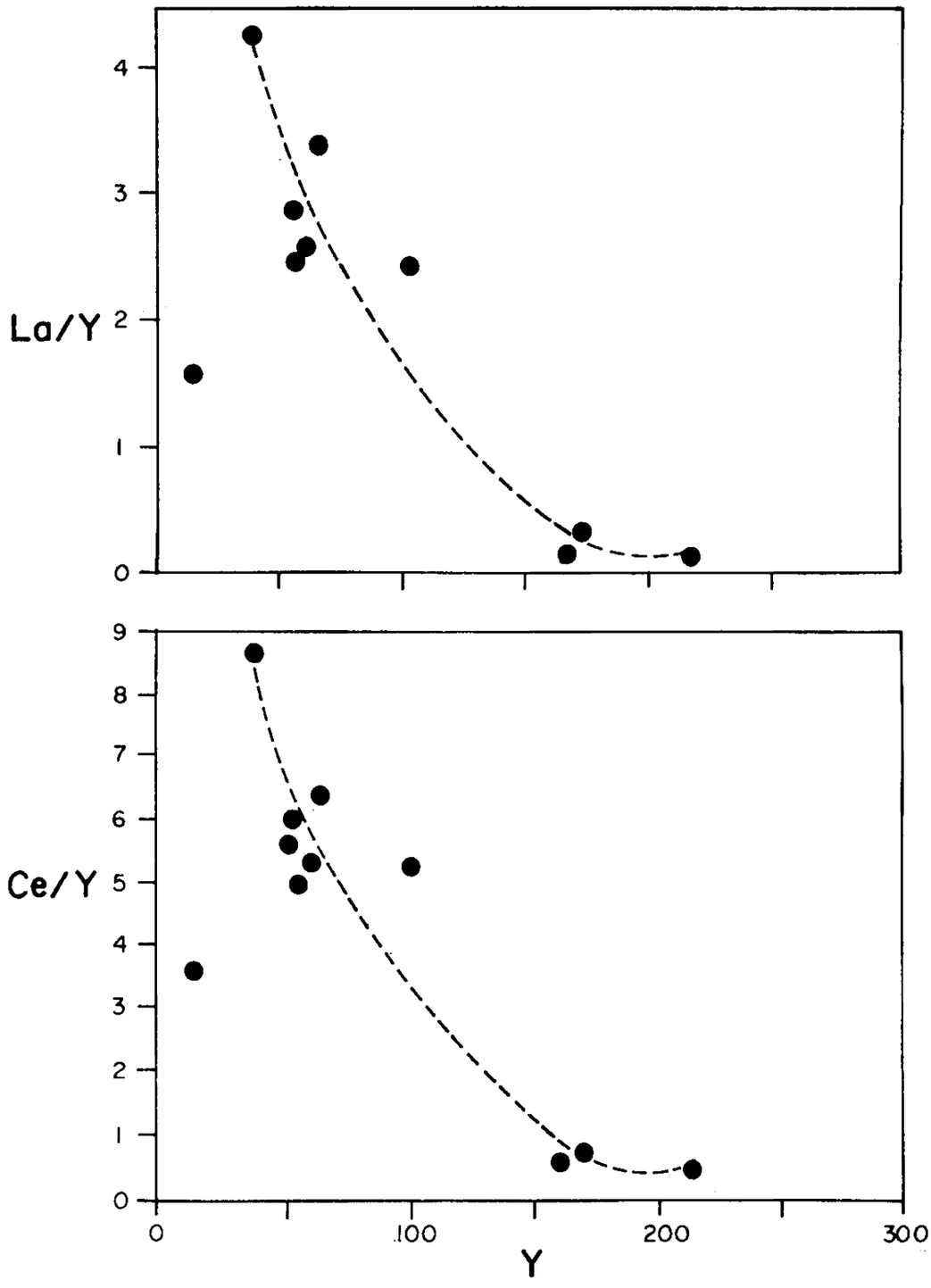

Fig. 33 La/Y and Ce/Y vs. Y plots of the granite.

as this would have produced a highly zoned pluton (Michael, 1984). It is suggested that the granite magma underwent in situ fractionation with late stage separation of the residual phase which crystallized as pegmatites and aplites.

5.4. Petrogenesis

The petrogenesis of granitic rocks has ever been a topic of debate through the decades. It is not intended to summarise the classical theories of granite genesis here. More systematic and realistic approaches have been adopted by recent workers based on geochemical data from which petrogenetic models can be evolved. Only those works pertaining to the present study have been treated here.

In order to elucidate the petrogenetic history of the Ambalavayal granite, the main aspects to be considered are (1) composition of source material, (2) mode of melting and (3) evolution of the magma. The possibility that the younger granite magmas are ultimately differentiates of calc-alkaline magma series seems remote, in the absence of other associated differentiates. Except for the high initial Sr-isotope ratio, the probable cause of which will be discussed later, partial melting of high-level crustal material is also not probable as indicated by the geochemical characters. The alternate suggestion would be partial fusion and subsequent fractionation of lower crustal or upper mantle material as envisaged for other alkaline plutons of the region as well for similar alkali

granites in various other regions. Anatexis near the base of the crust with sufficient SiO_2 content to produce highly siliceous magmas and : comparatively low abundances of most LIL elements is a possible mechamism (Greenberg, 1981). Experimental studies show that as a consequence of the incongruent melting of orthopyroxene, silica-saturated magmas can be generated from olivine-rich parent rocks. Investigations indicate that at higher pressures, the mineral stabilities change, resulting in the change of position of the thermal divide in the forsterite-silica-nepheline-diopside system, leading to the formation of alkaline magmas directly by fusion and indirectly by fractionation from hypersthene-normative liquids. These observations imply that silica-saturated alkaline melts can also be generated from the upper mantle.

In a tensional tectonic environment, bodies of juvenile basic magma could be emplaced into the lower and intermediate crust. As these magmas fractionate, latent heat of crystallization liberated by the formation of cumulate rocks would partially melt the country rocks and mixing between the different bodies of melt would be expected to follow. Barker et al. (1975, 1976) proposed a reaction melting model, which envisages a basic magma of mantle derivation emplaced into the lower crust where it undergoes fractional crystallization. As a result of the formation of cumulates, latent heat of crystallization is liberated which causes partial melting in the lower crust. Conta-

mination occurs during this process and some of the magma differentiate producing a peralkaline trend. The energy budget here is principally the heat liberated during the cumulate formation.

The formation of granites in tensional tectonic environments may occur by (1) fractional crystallization of a basic melt, (2) partial melting of short or long-lived crustal precursor or (3) interaction between preexisting crust and melts derived by either the first or the second mechanism. However, models for the generation of anorogenic granites are equivocal (Collerson, 1982).

Of particular interest is the mechanism by which peralkaline trends can evolve. Bailey (1974) demonstrated that peralkaline liquids can evolve by partial melting or by low pressure fractionation of anhydrous phases from alkaline or slightly basic magmas. A number of intrusions in the Gardar Province of Greenland exhibit oversaturated alkaline differentiation trends as a result of this process (Parsons, 1972; Blaxland and Parsons, 1975).

Many peralkaline granites are volumetrically much larger than potential source compositions. Consequently their formation by differentiation processes is unlikely. In view of the high concentration in these granites of HFS-elements, Harris and Marriner (1980) suggested that slightly peralkaline magmas

may be generated by partial melting of lower crust under a high flux of mantle-derived volatiles. This model seems to be best applicable in the present case. In order to produce melting in the mantle, a geotherm is required to intersect the appropriate melting curve. The general processes of heating within the earth, radioactivity, thermal radiation and thermal conduction would be too diffused to cause heat focussing (Bailey, 1977). Other modes for the energy budget, that is, raising the temperature, would be frictional heating, or heating of the overlying rocks by a body of rising magma. The most probable mechanism of melting in stable plate interiors, as in the present case, is mantle upwarping due to extensional tectonics, producing rapid decompression melting, resulting in anorogenic magmatism. Crustal distension can cause large-scale mantle degassing leading to the addition of volatiles to the overlying rocks, causing localised melting (Bailey , 1974; Harris and Marriner, 1980; Nair et al., 1983a; Santosh and Thara, 1985). At higher temperatures, gas fluxing can cause heat focussing which functions as a doubly effective mechanism of melting. The intrinsic association of CO_2-rich fluid inclusions in the granite is significant. It is presumed that the fault-lineaments of the region acted as conduits for considerable volatile influx, triggering generation of magma of the alkaline plutons. The extremely high K/Rb values of the granite imply a K-enriched, but Rb-depleted deep-crustal or

upper mantle source. The enrichment of LREE and HFS-element serves as additional proof for the involvement of CO_2 rich volatiles which effectively scavenged these elements.

The high initial Sr-isotope levels exhibited by the granite may be interpreted to be the result of crustal contamination, as similar feature is observed in the case of the anorogenic alkali granites of several regions, like that of Labrador (Collerson, 1982). McCarthy and Cawthorn (1980) showed that rapid growth of ^{87}Sr occurs during the fractionation of peralkaline magmas, leading to anomalously high initial Sr-isotope levels. Selective enrichment of ^{87}Sr through volatiles could also occur (Blaxland, 1976). Bulk assimilation of locally derived partial melt via a reaction-melting-type mechanism similar to that proposed by Barker et al. (1975) is another probability.

Plots of the granite in normative Q-Ab-Or ternary diagram show a spread ranging from more than 3Kb to 5Kb. A precise estimate of the pressure regime is given in the section on fluid inclusions. The plots generally fall in the field of 'magmatic granites' as defined by Tuttle and Bowen (1958). The points on the E_5-E_3P cotectic surface of the system, Q-Ab-Or-An-H_2O at 5Kb (Winkler, 1976) has been radially projected from the Q-apex on to the An-Ab-Or side and shown in Fig. 34, where the plots of the granite tend to fall in the space bounded by 685

Fig. 34 Projection of cotectic lines and isotherms on cutectics surface of the system Q-Ab-Or-An at pH_2O =5 Kb (after Winkler, 1976) showing the plots of Ambalavayal granite.

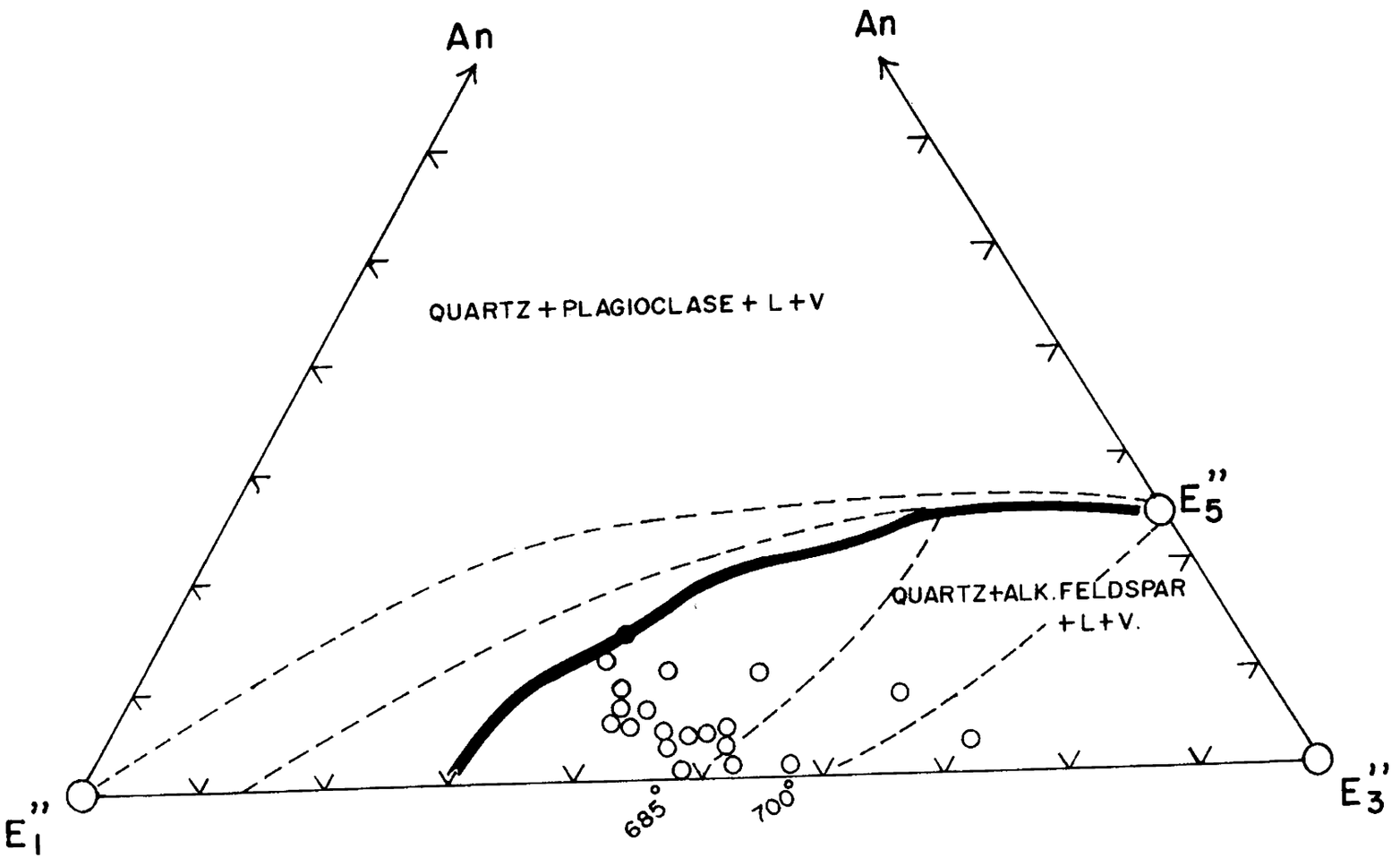

and 700°C isotherms. Regarding the depth of formation, Log Rb vs. Log Sr plots (Fig. 35) fall mostly within the region of 20-30 Km as defined by Condie (1973). In the system relevant to alkaline rocks, namely, SiO_2-Al_2O_3-Na_2O+K_2O, the plots of the granite fall close to the peralkaline-peraluminous divide. Some of the plots fall in the comendite field (Fig. 36). The plots are close to the quartz-feldspar cotectics projected on to this plane. Bailey and Scharier (1966) showed that liquids evolving in a plane close to the peralkaline-peraluminous divide will eventually reach the quartz-feldspar cotectic curve, tending to attain a natural eutectic anologous to the oversaturated eutectic (q+ab+ac+Na-silicate) determined in the system Na_2O-Al_2O_3-Fe_2O_3-SiO_2.

After the evolution of the melt, there is little evidence to show that any extensive crystal fractionation occurred during ascent and emplacement. The restricted range of silica values and other major element oxides, absence of porphyritic textures or zoning effects and the general high values of K/Rb ratios imply limited crystal-liquid fractionation (Jackson et al., 1984). Fractionation involving hornblende and feldspars to a moderate extent is indicated by the trace element data. Fractionation of feldspars ultimately leads to the development of a peralkaline residuum in any suite, especially when there is a deficiency of alumina with respect to the total alkalies (Bailey and Macdonald, 1969). Supplemented by the normative

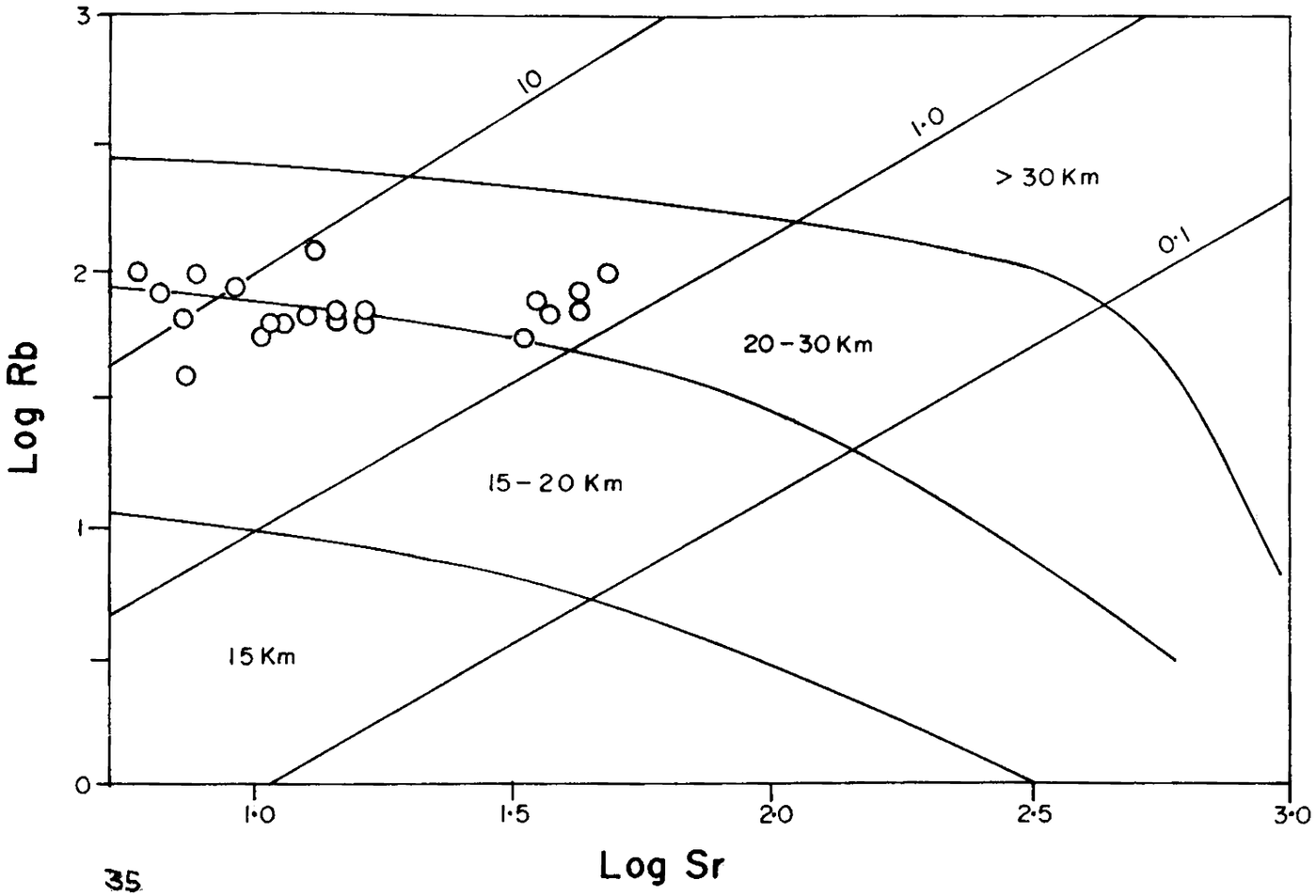

Fig. 3 Log Rb vs. Log Sr plots of the granite. The boundary lines are from Condie (1973).

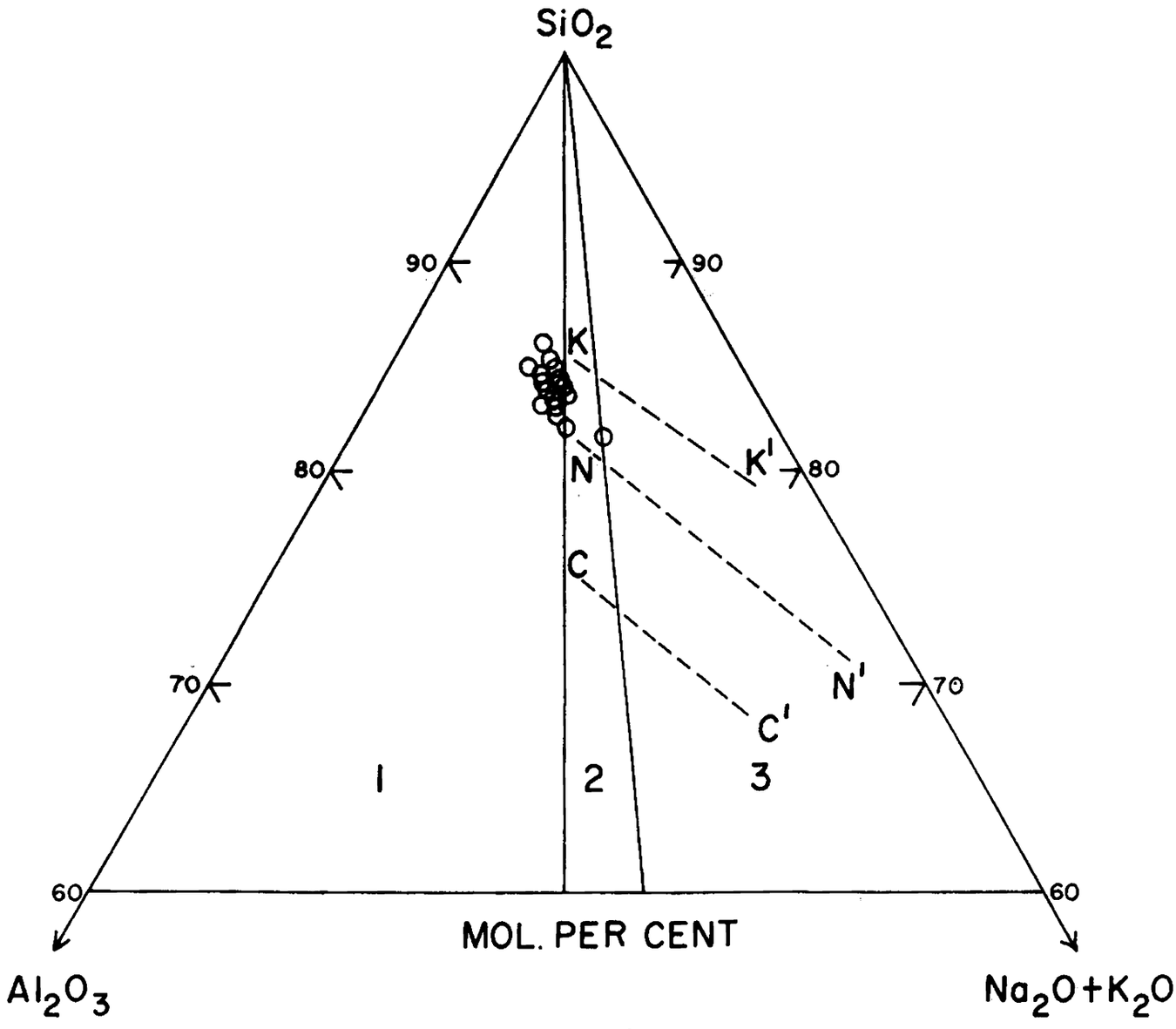

1. CALC-ALKALINE FIELD.	K_K'	QUARTZ-FELDSPAR
2. COMENDITE FIELD.	N_N'	COTECTICS.
3. PANTELLERITE FIELD.	C_C'	ALBITE-NEPHELINE COTECTIC.

Fig. 36 ~~39~~ SiO_2-Al_2O_3 - Na_2O + K_2O (mol.%) ternary plots of the Ambalavayal granite. The classification boundaries are as compiled by Greenberg (1981).

abundance of diopside and the modal abundance of alkali minerals like riebeckite, an alkaline nature of the melt is thus conceivable. Accessory phases, mainly sphene, apatite and monazite played a dominant role in the fractionation process as implied by the behaviour of LREE and HFS-elements.

5.5. Geochemical signatures of ore potential

The geochemical characters applicable to granitic host rocks for molybdenite mineralization include higher SiO_2, K_2O and Na_2O levels (Mutschler et al., 1981), which are characteristic of the Ambalavayal granite also. The Mol.% Al_2O_3/Na_2O+K_2O values are generally close to or greater than unity and their plots fall dominantly in the peraluminious-metaluminous field, close to the divide with peralkaline field (Fig. 37). Westra and Keith (1981) proposed a classification scheme of molybdenite deposits based on their host rock geochemistry. They plotted the data of various molybdenite associations in Al_2O_3 vs. $Na_2O + K_2O$ diagram and differentiated the fields of calc-alkaline, alkalic and Climax-type molybdenum deposits. However, all the three fields overlap considerably in their diagram. Plots of the Ambalavayal granite also fall over a wide region, encompassing parts of all the three fields. However, other geochemical characters proposed by Westra and Keith (1981) like the high $K_{57.5}$ values (ie. K_2O at 57.5% SiO_2) indicate an alkalic affinity. Mutschler et al (1981) noted that the normative $Q \geq 20\%$, $Ab \geq 20\%$ and $Or \geq 20\%$ is a finger-print for

Fig. 34 Mol % $Na_2O + K_2O$ vs. Al_2O_3 plots of the granite. The field boundaries are after Westra and Keith (1981).

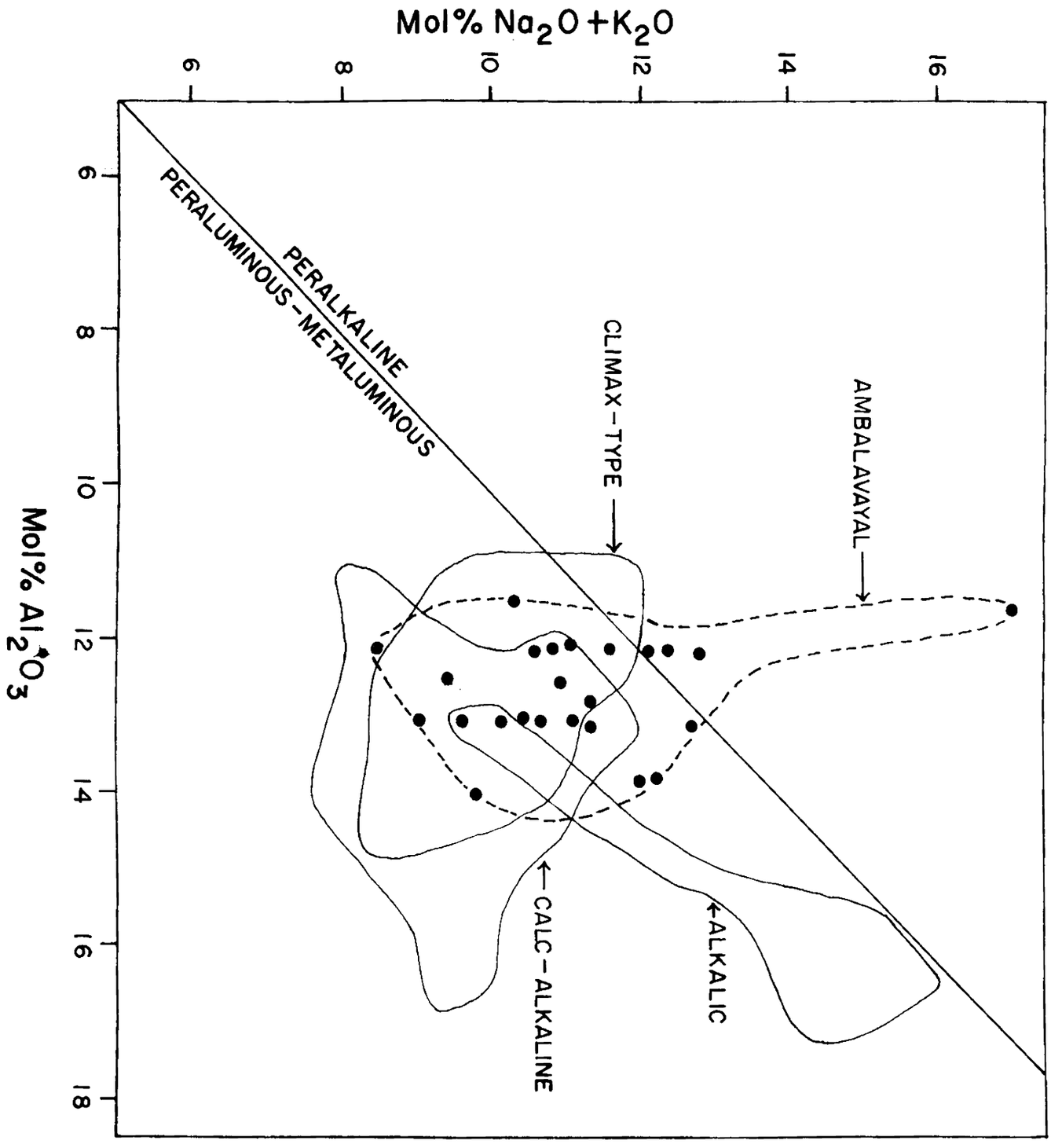

granite-molybdenite systems, which is consistent in the present case. Normative Q-Ab-Or plots of the granitic host rocks for molybdenite are noted to fall within the field of magmatic granites as defined by Tuttle and Bowen (1958) and lie within the compositional spectrum of unaltered source rocks for molybdenite. The Q+Ab+Or values of the granite range from 87.8 to 95.4, which are in good agreement with the estimated value of greater than 80% for granite-molybdenite systems.

Hudson et al (1979) also noted that high silica values (74.4 to 77.7 wt. %) and limited range in the abundance of other oxides are characteristic of granitic intrusives associated with molybdenite mineralization. The strong negative correlation of CaO, positive correlation of Na_2O and the depletion of femic oxides (FeO and MgO) against SiO_2 are also typical, comparable with the present data. In his studies, as in the present case, Hudson et al (1979) noted the conspicous absence of any significant concentration of volatile fugitive elements such as Pb and Li. Based on studies on the Adanac molybdenum deposit in British Columbia, White et al (1976) noted that high K_2O/Na_2O ratios (1.4), low CaO and MgO and low concentrations of lithophile elements are characteristic. These features are noted in the Ambalavayal granite also. Among radioelements, Hudson et al (1979) reported 12 to 35 ppm Th and 4 to 13 ppm U, with Th/U ranging between 1.8 and 3.3, comparable with the present case.

The whole-rock molybdenum levels in Ambalavayal range from 6 to 28 ppm (av. 16.8), being much higher than the 0.4-0.7 ppm range recognised in granitic host rocks associated with molybdenum deposits (Pokalov, 1977). The Mo-values have been plotted and contoured in Fig. 38, where an anomalous zone, trending approximately NW-SE with high concentration at two adjacent regions is discernible. These regions are the Ayiram-kolli and Ambalavayal-hospital quarries. The trend of the anomaly coincides with the general trend of the ore zone. Westra and Keith (1981) observe that the $K_2O/K_2O + Na_2O$ ratio of host rocks is a potential indicator of mineralization. This ratio shows high values in Ambalavayal and has been shown in a contour map in Fig. 39. It is seen that the outcrop pattern of the granite itself roughly concides with an intermediate anomaly. The highly anomalous zone along a NW-SE region is compatible with the whole-rock Mo anomaly.

5.6 Taphrogenic Affiliation

The generation of peralkaline magmas within non-orogenic zones of major crustal fractures has been observed by various workers (Murthy and Venkataraman, 1964; Le Bas, 1971; Bowden, 1974). Peralkaline plutonism is an essential part of pre-rift tectonics and is especially important in the early stages of tensional tectonics. Abnormal enrichment of alkalies is considered to be the key-note of rift-mechanism. Crustal fractures

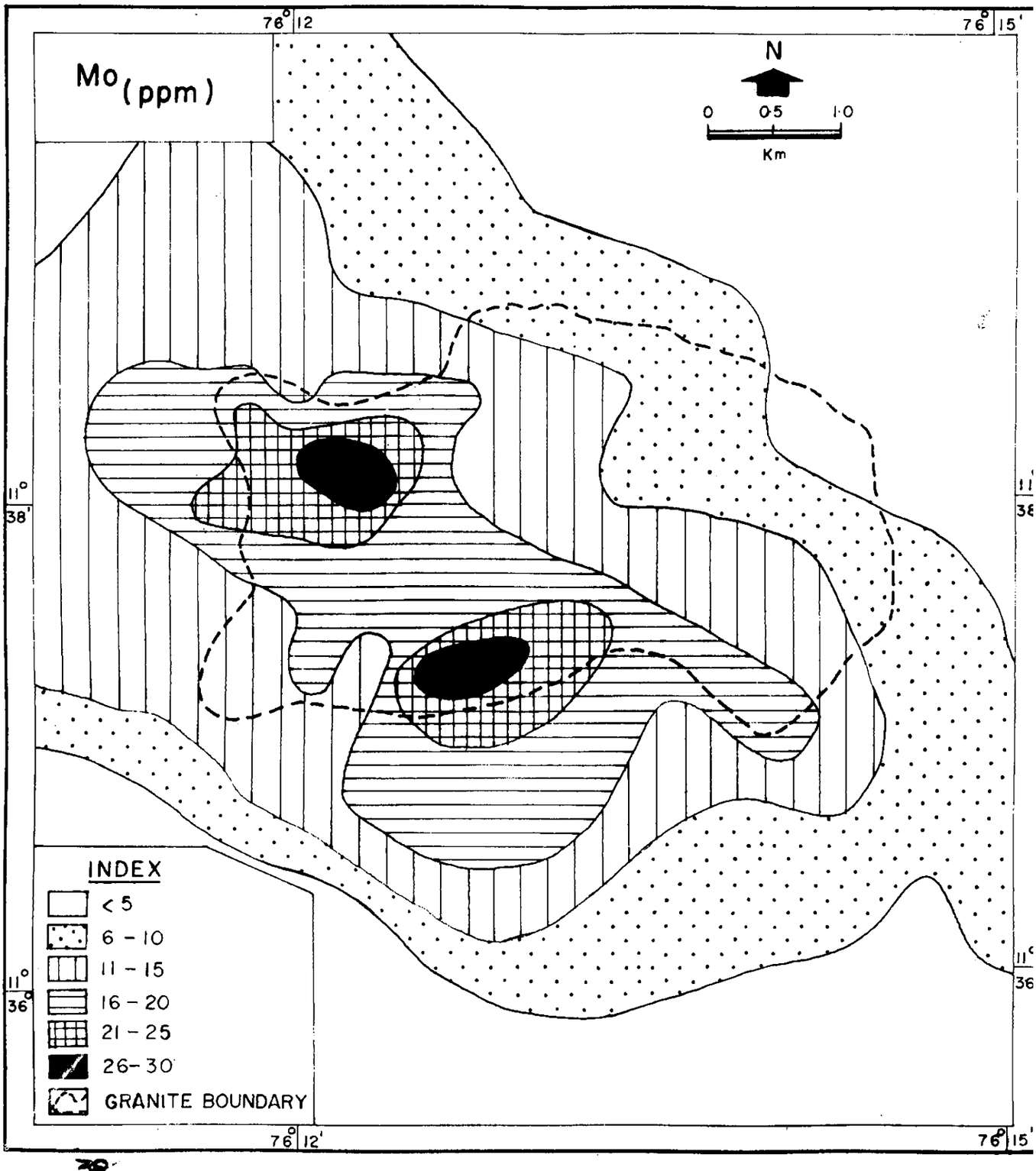

Fig. 38 Contour diagram of whole rock molybdenum levels in the Ambalavayal granite, showing the anomalous zones.

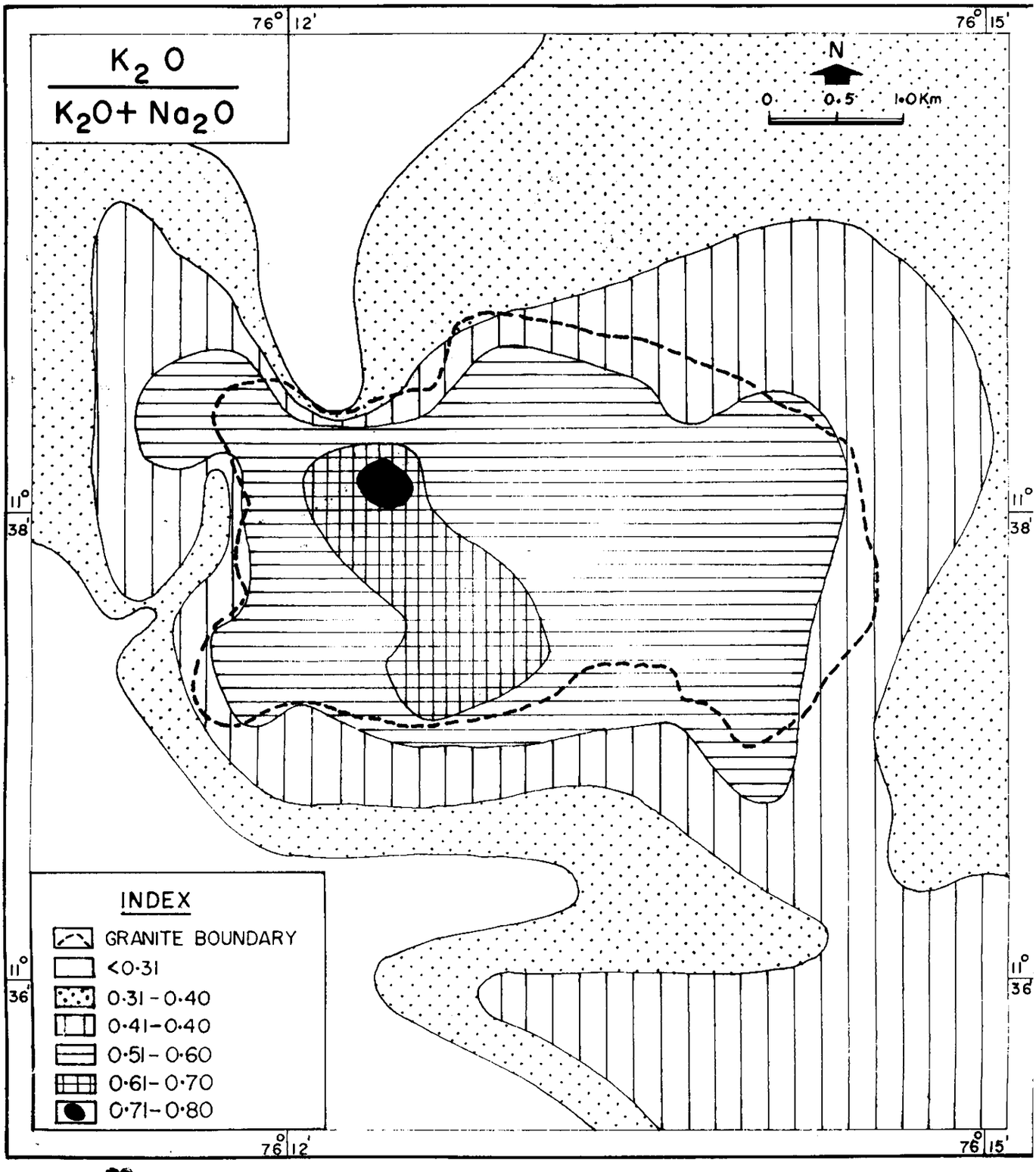

Fig. 39 Contour diagram of whole rock $K_2O/K_2O + Na_2O$ levels in the granite, showing the anomalous zones.

act as conduits for heat and volatile transfer from the underlying mantle. The volatile influx brings with it mobile elements, especially alkalies.

The spatial relationship of granite and syenite intrusives in Kerala, including the Ambalavayal pluton, to regional lineaments is significant. Many of these lineaments are taphrogenic (rift-related) in nature (Katz, 1978). This suggests that the magmatism has probable affiliation with the taphrogenesis of the continental margin (Nair and Santosh, 1984; Santosh and Nair, 1983b). Relationship of granite-molybdenite systems with rift-tectonics is noted elsewhere also (Westra and Keith, 1981). In mobile belts, tensional faulting is known to trigger taphrogenic mineralization (Gableman, 1971). The taphrogenic faults supply juvenile mineralization through the release of metals and volatiles from the lower crust or mantle. Thus the mineralization associated with the granite and pegmatitic phases in the Kerala region suggests an episode of Late Precambrian-Early Paleozoic taphrogenic metallogeny.

Molybdenite occurrences in diverse rock types are reported from the adjacent terranes of Tamil Nadu, Andhra Pradesh and Sri Lanka (Subramonian, 1979). The regional distribution of molybdenite is in favour of the concept of a molybdenum province in the southern part of the Indian shield (Santosh and Nair, 1983b). Spatial relationship of individual molybdenite occurrences and their host rocks with seismically active deep

faults, margins of shear belts or major fault-lineaments were pointed out by Santosh and Nair (1983b), which further suggest a regional metallogenic episode related to the taphrogenesis of the continental margin.

The Late Precambrian-Early Paleozoic ages obtained from the intrusives of the region are correlatable with a Pan-African magmatic regime, recognised in other shield areas also. The mineralogic and geochemical features are also comparable. The magmatism, essentially of anorogenic nature, is characterised by geochemical and tectonic imprints suggestive of crustal distension leading to sudden pressure relief, as a result of which, there had been considerable influx of volatiles from the mantle. This mechanism is envisaged to have triggered localised melting in the lower crust, generating small pockets of alkaline magmas, which were subsequently emplaced as a number of minor intrusive plutons. The magma generation and emplacement were controlled by the taphrogenic lineaments.

CHAPTER 6

GEOCHEMISTRY OF BASEMENT ROCKS

The major element geochemistry of twenty four representative samples of the gneisses, two samples of enclaves and two of fuchsite quartzites from the study area, together with their range, mean and standard deviation, are presented in Table18.

Table:18 Major element analyses of gneisses, 'restites' and fuchsite quartzite from Ambalavayal

Oxide, Wt%	AS 005	AS 009	AS 016	AS 018	AS 019	AS 022	AS 024	AS 026	AS 028
SiO_2	72.54	72.67	73.92	67.77	73.75	73.21	75.17	74.50	73.38
TiO_2	0.18	0.07	0.17	0.26	0.01	0.02	0.07	0.03	0.02
Al_2O_3	12.75	13.24	13.77	15.29	14.27	13.75	12.94	13.76	14.24
Fe_2O_3	1.98	0.84	1.06	2.20	0.88	0.92	0.78	0.84	1.02
FeO	0.58	0.36	0.70	1.79	0.56	0.82	0.66	0.62	0.90
MnO (ppm)	94	139	68	220	76	54	82	88	102
MgO	0.64	0.80	0.32	0.97	0.32	0.16	0.32	0.48	0.48
CaO	1.79	2.24	0.90	2.69	0.67	0.90	0.90	0.90	2.24
Na_2O	6.42	4.70	5.31	6.60	5.72	5.69	5.09	4.86	4.39
K_2O	2.57	3.61	2.34	0.88	3.41	3.02	3.11	3.32	2.93
P_2O_5	0.10	0.09	0.11	0.16	0.02	0.02	0.04	0.04	0.05
Moisture	0.24	0.32	0.28	0.16	0.21	0.46	0.06	0.44	0.06
L.O.I	0.18	0.14	0.42	0.88	0.15	0.62	0.82	0.08	0.14
Total	99.97	99.08	99.30	99.65	99.97	99.59	99.96	99.87	100.85

Table : 18 (Contd.)

Oxide, Wt.%	AS 034	AS 036	AS 104	AS 106	AS 109	AS 115	AS 116	AS 117	AS 119
SiO_2	73.96	75.03	73.60	74.11	72.36	73.04	67.82	70.70	74.19
TiO_2	0.16	0.09	0.02	0.02	0.06	0.10	0.82	0.31	0.02
Al_2O_3	13.77	13.54	13.78	13.25	14.78	14.04	14.04	15.44	13.57
Fe_2O_3	1.88	1.02	1.23	1.04	1.98	1.48	2.32	1.36	0.85
FeO	0.84	0.58	0.48	0.50	0.16	0.83	3.45	1.72	0.75
MnO (ppm)	74	110	155	111	22	87	391	181	185
MgO	0.32	0.64	0.48	0.32	0.32	0.32	1.44	0.96	0.80
CaO	1.79	1.34	1.12	1.34	0.90	0.12	3.58	2.46	1.12
Na_2O	4.31	4.43	4.43	4.79	4.71	3.88	3.29	4.64	4.17
K_2O	2.98	2.31	3.89	3.51	3.95	4.49	1.78	1.56	3.75
P_2O_5	0.11	0.05	0.06	0.05	0.03	0.04	0.23	0.08	0.06
Moisture	0.11	0.48	0.17	0.20	0.52	0.09	0.26	0.12	0.18
L.O.I	0.12	0.22	0.14	0.10	0.03	0.11	0.72	0.46	0.11
Total	100.35	99.68	99.40	99.23	99.80	99.54	99.75	99.81	99.57

Table 18 (Contd.)

Oxide, wt.%	AS 120	AS 121	AS 122	AS 124	AS 125	AS 134	Range	Mean	S.D.
SiO_2	75.53	71.15	70.61	71.86	71.67	74.45	67.77-75.73	72.96	2.07
TiO_2	0.09	0.08	0.19	0.08	0.08	0.13	0.01- 0.82	0.13	0.17
Al_2O_3	12.17	12.17	14.04	14.04	14.51	15.29	12.17-15.29	13.85	0.92
Fe_2O_3	1.80	1.12	1.71	1.76	1.39	0.63	0.63- 2.32	1.34	0.50
FeO	0.63	1.15	2.34	0.72	1.19	0.66	0.16- 3.45	0.96	0.72
MnO (ppm)	70	75	318	68	128	125	22-391	128	85.41
MgO	0.48	0.64	0.96	0.48	0.48	0.32	0.16- 1.44	0.56	0.30
CaO	0.90	0.90	1.12	1.34	1.12	0.90	0.67- 3.58	1.43	0.73
Na_2O	3.82	4.58	3.85	3.78	4.69	3.91	3.29- 6.42	4.67	0.82
K_2O	3.37	2.96	3.70	3.76	3.91	3.28	1.56-4.49	3.10	0.85
P_2O_5	0.05	0.02	0.08	0.06	0.05	0.04	0.02-0.23	0.07	0.05
Moisture	0.11	0.16	0.46	0.08	0.07	0.04	0.04-0.52	0.22	0.15
L.O.I.	0.28	0.33	0.19	0.07	0.48	0.24	0.03-0.88	0.29	0.25
Total	99.28	99.26	99.25	98.03	99.64	99.89	99.08-100.85	99.65	0.52

Table: 18 (Contd.)

Element, wt%	AR 107	AR 131	AR 132	Mean	AFQ 136	AFQ 137	Mean
SiO_2	50.77	65.48	55.62	57.29	81.71	86.88	84.30
TiO_2	1.59	0.40	0.44	0.81	0.44	0.20	0.32
Al_2O_3	16.31	15.29	11.73	14.44	10.75	8.67	6.47
Fe_2O_3	2.20	2.42	4.92	3.18	0.24	0.24	0.24
FeO	6.86	2.86	6.14	5.29	0.29	0.36	0.33
MnO (ppm)	765	493	1713	990	18	14	16
MgO	2.08	1.76	4.80	2.88	0.32	0.32	0.32
CaO	8.74	4.70	8.96	7.47	0.90	0.90	0.90
Na_2O	4.60	4.36	2.53	3.83	0.40	0.26	0.33
K_2O	3.89	1.20	1.77	2.29	2.46	0.92	1.69
$P_2$5	1.22	0.88	1.16	1.09	0.02	0.01	0.02
Moisture	0.43	0.15	0.09	0.22	0.20	0.07	0.14
L.O.I.	0.52	0.32	1.88	0.91	1.82	0.83	1.33
Total	99.21	99.82	100.04	99.69	99.55	99.66	99.61

AS 005 to AS 134 - Gneiss ; AR 107; 131 & 132 - Restite ; AFQ-136 & 137 - Fuchsite quartzite. S.D.- Standard deviation

Their trace element abundances are given in Table 19. The CIPW normative compositions of the gneisses are given in Table 20.

6.1. Major Elements

Among major elements, SiO_2 values show a range of 67.67-75.53. Al_2O_3 varies from 12.17 to 15.29 (av. 13.85). The heterogeneity in the alumina: alkali distribution is displayed by the occurrences of normative corundum in many of the analyses and normative diopside in others. Na_2O values are characteristically high (upto 6.42) whereas K_2O values are low (av. 3.10) with Na_2O/K_2O ratio consistently greater than 1. Low MgO values (upto 1.44) and high CaO contents (upto 3.58) are also noted. Major element geochemistry of the gneisses is compared with other Precambrian gneisses of the Karnataka region and other terrains in Table 21, where they show a close correlation. The high SiO_2 levels, moderate Al_2O_3 and CaO, high Na_2O and low MgO of the gneisses are comparable with the mean composition of Archaean low alumina trondhjemites (Condie, 1981). This is further brought out by plots on a normative An-Ab-Or diagram (Fig. 40). O'Conner (1965) proposed classification boundaries based on the normative feldspar proportions. Plots of the gneisses dominantly fall in the trondhjemite field. They also fall in the trondhjemite field as delineated by Barker (1979).

Harker variation diagrams of major elements are shown in Fig. 41, wherein discernible trends of magmatic crystalliza-

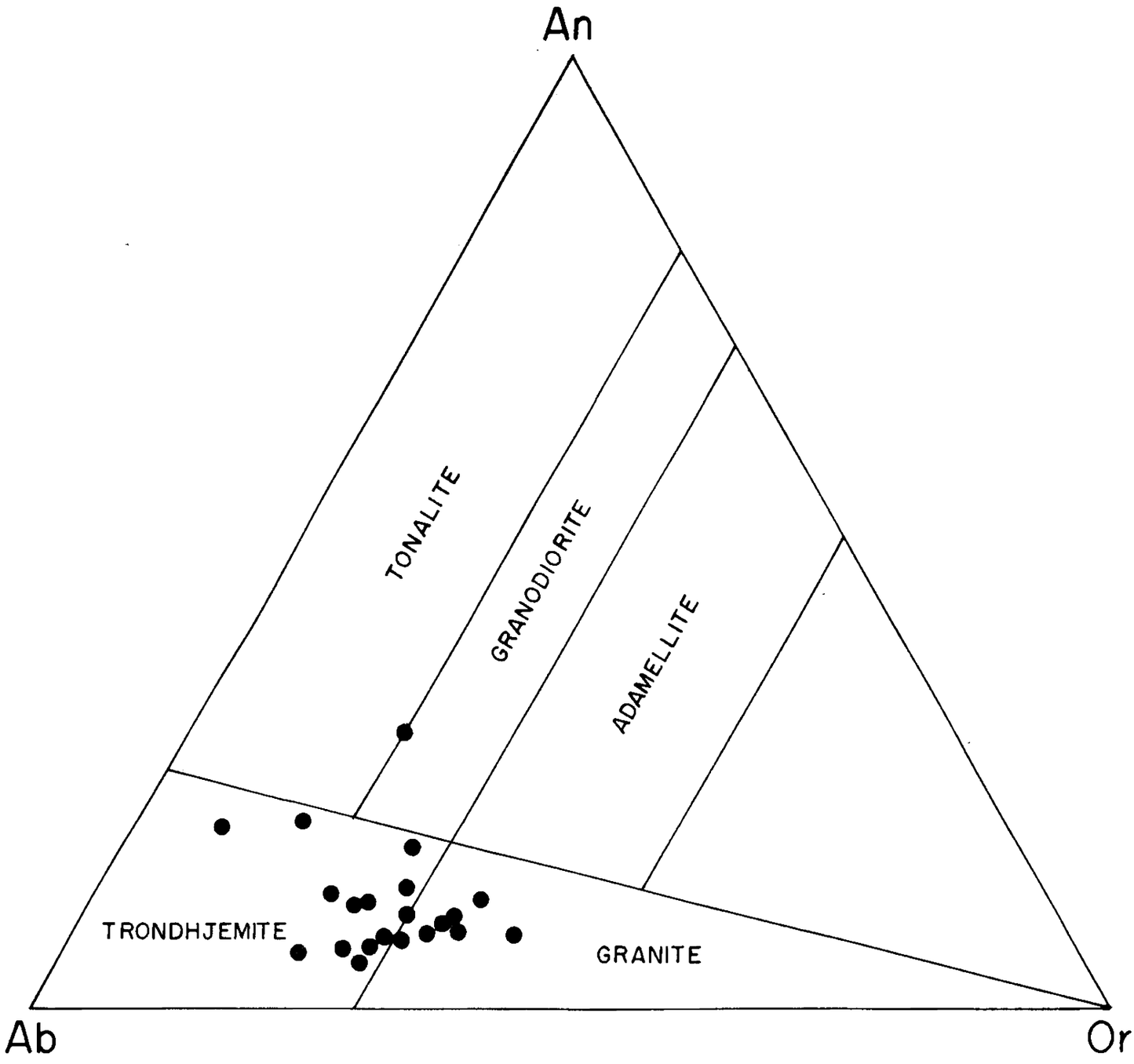

Fig. 40 Normative An–Ab–Or plots of gneisses from the Ambalavayal area. The classification boundaries are after O' Conner (1965).

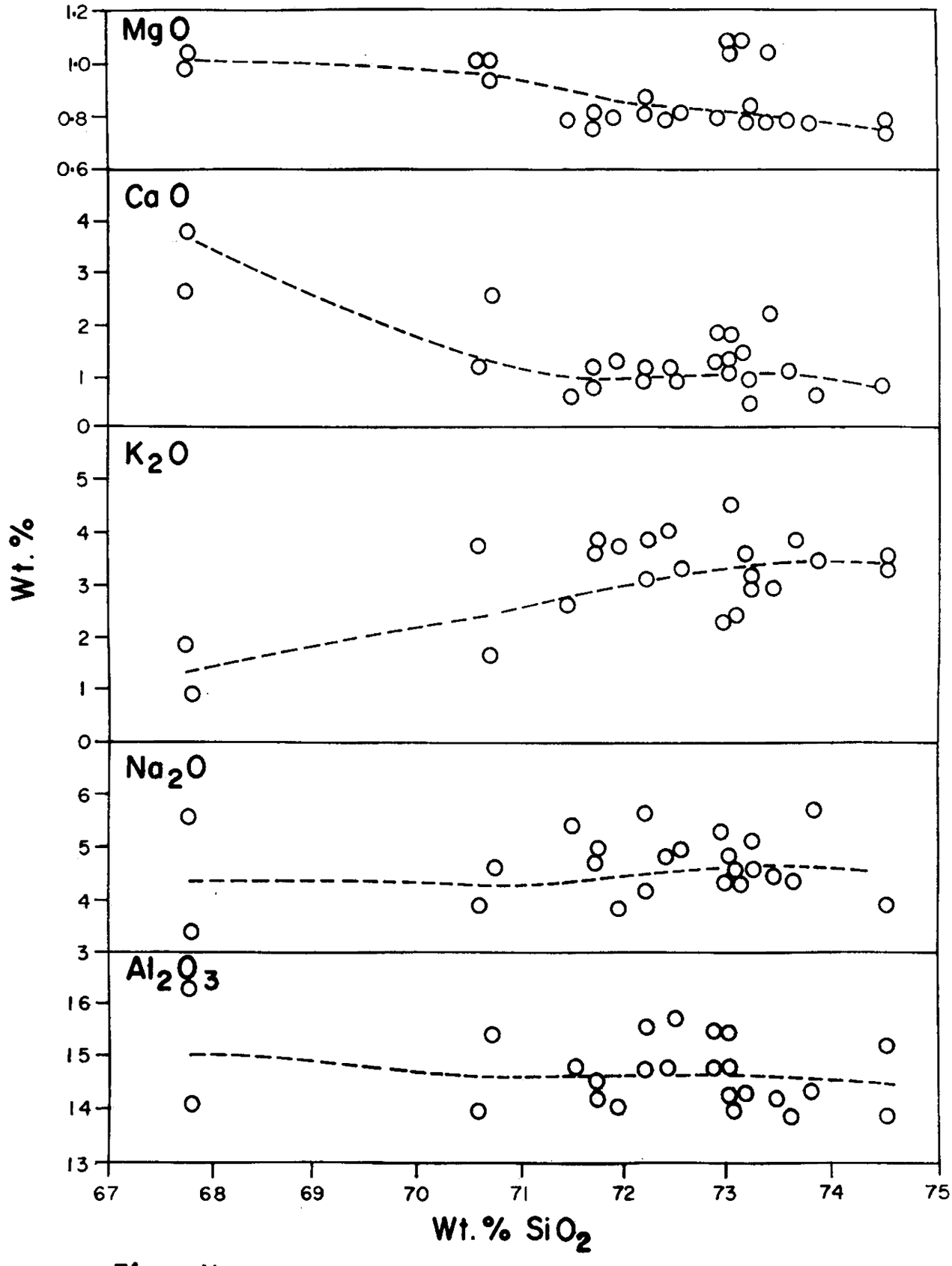

Fig. 41 Harker variation diagrams of major elements in the gneisses.

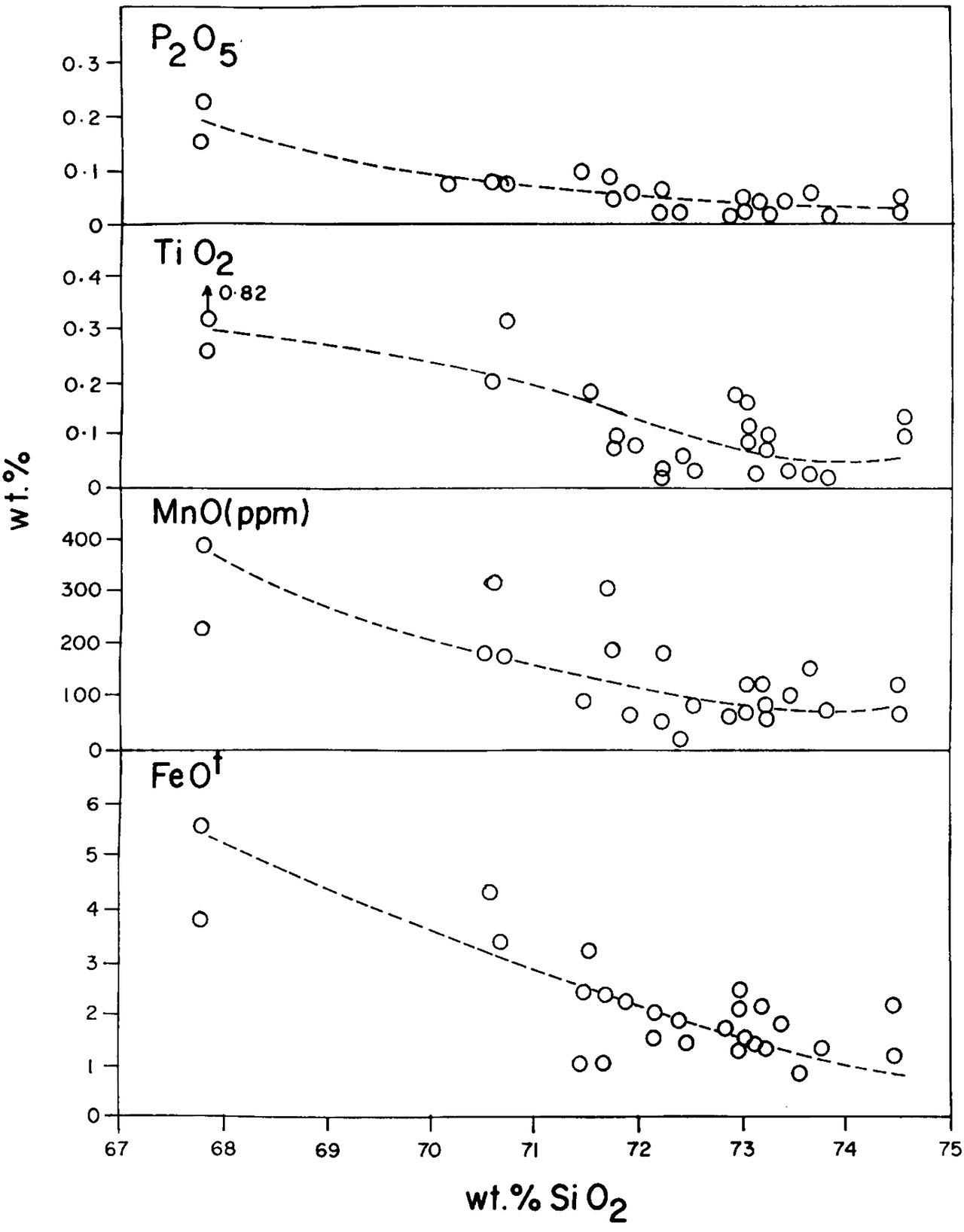
P2O5
TiO2
0·82
MnO(ppm)
FeOt
wt.%
wt.% SiO2
0·3
0·2
0·1
0
0·4
400
300
200
100
6
5
4
3
2
1
67
68
69
70
71
72
73
74
75

fig. 41 contd.

Table: 19 Trace element analyses of gneisses restites and fuchsite quartzite from Ambalavayal.

Element ppm	AS 005	AS 009	AS 016	AS 018	AS 019*	AS 022	AS024	AS 026	AS028
Ba	433	4	46	84	9	130	148	112	14
Bi	24	60	18	28	18	19	50	82	60
Ce	-	..	-	-	94	-	-	-	-
Co	14	8	12	9	7	8	9	11	9
Cr	110	177	139	167	195	227	244	179	154
Cu	4	2	14	5	3	3	5	20	20
La	-	-	-	-	34	-	-	-	-
Li	6	42	38	32	48	36	18	8	6
Mo	4	21	14	16	24	16	14	8	8
Nb	-	-	-	-	25	-	-	-	-

Table 16 (Contd.)

Element ppm	AS 005	AS 009	AS 016	AS 018	AS 019*	AS 022	AS 024	AS 026	AS 028
Ni	168	48	123	184	88	96	74	63	108
Pb	6	25	19	16	24	12	12	8	15
Rb	168	269	124	112	334	248	280	186	146
Sr	178	4	12	24	17	44	29	52	15
Th	-	-	-	-	1	-	-	-	-
U	-	-	-	-	n.f	-	-	-	-
Y	-	-	-	-	256	-	-	-	-
Zn	42	137	85	67	43	128	123	140	196
Zr	116	248	98	120	183	220	238	180	123

Table 19 (Contd.)

Element, ppm	AS 034	AS036	AS104*	AS106*	AS109	AS115*	AS116*	AS117	AS119
Ba	45	94	28	18	48	9	469	144	16
Bi	12	12	32	84	86	28	38	96	n.f.
Ce	-	-	42	37	-	44	140	-	-
Co	7	12	14	14	14	14	16	14	14
Cr	187	213	127	17	n.f.	203	213	204	125
Cu	23	11	6	n.f.	2	33	29	33	18
La	-	-	14	9	-	13	100	-	-
Li	14	9	48	30	1	11	46	6	82
Mo	12	8	8	3	4	18	14	16	3
Nb	-	-	75	62	-	207	29	-	-

Table 19 (Contd.)

Element ppm	AS034	AS036	AS104*	AS106*	AS109	AS115*	AS116*	As117	AS119
Ni	116	74	120	21	33	160	156	145	104
Pb	16	20	49	40	32	27	13	28	60
Rb	302	138	314	295	96	153	98	24	290
Sr	15	28	1	7	23	5	323	70	n.f.
Th	-	-	16	11	-	26	22	-	-
U	-	-	4	2	-	7	3	-	-
Y	-	-	166	165	-	215	80	-	-
Zn	44	49	326	244	96	220	156	118	286
Zr	196	86	139	96	140	197	500	60	n.f.

Table 19 (Contd.)

Element ppm	AS120	AS121*	AS122	AS124	AS125*	AS134*	Range	mean	S.D.
Ba	106	8	113	24	9	150	8-469	94.2	121.2
Bi	4	44	20	24	40	66	4-96	39.4	27.7
Ce	-	41	54	-	22	74	22-140	60.9	36.6
Co	12	8	14	12	18	14	7-16	11.8	3.0
Cr	156	167	165	150	99	118	17-244	155.7	59.0
Cu	29	34	31	36	6	12	2-36	15.8	12.5
La	-	15	18	-	8	26	9-100	26.3	28.8
Li	18	8	28	5	24	40	1-82	25.2	19.7
Mo	8	6	18	16	12	2	2-21	11.4	6.2
Nb	-	185	97	-	168	31	25-207	97.7	71.4

Table 19 (Contd.)

Element ppm	AS120	AS121*	AS122	AS124	AS125*	AS134*	Range	Mean	S.D.
Ni	118	93	106	117	93	85	21-184	103.9	41
Pb	22	22	19	90	23	29	6-90	26.1	18.4
Rb	66	133	119	100	136	335	24-335	186	94.3
Sr	16	3	61	5	9	5	1-323	39.4	71
Th	-	14	13	-	10	16	10-26	15.3	5.5
U	-	5	3	-	6	n.f.	2-7	3.3	2.4
Y	-	193	99	-	155	288	80-288	179.7	67.5
Zn	142	238	268	176	230	326	42-326	161.7	89.2
Zr	120	75	154	160	48	115	48-500	150.5	96.2

Table 19 (Contd.)

Element ppm	AR107*	AR131	AR132	Range	Mean	AFQ136	AFQ137	Mean
Ba	536	280	342	280-536	386	502	436	469
Bi	76	52	62	52-76	63.3	72	74	73
Ce	89	-	-	-	-	-	-	-
Co	48	22	56	22-56	42	16	8	12
Cr	117	148	483	117-483	249.3	545	548	546.5
Cu	9	70	52	9-70	43.7	6	23	14.5
La	51	-	-	-	-	-	-	-
Li	236	22	32	22-236	96.7	n.f.	n.f.	-
Mo	13	16	6	6-16	11.7	4	8	6
Nb	60		-	-		-	-	-

Table 19 (Contd.)

Element ppm	AR107*	AR131	AR132	Range	Mean	AFQ136	AFQ137	Mean
Ni	174	128	374	128-374	225.3	95	108	101.5
Pb	33	32	38	32-38	34.3	n.f.	18	-
Rb	398	44	68	44-398	170	54	18	36
Sr	432	96	52	52-432	193.3	10	11	10.5
Th	18	-	-	-	-	-	-	-
U	3	-	-	-	-	-	-	-
Y	88	-	-	-	-	-	-	-
Zn	240	162	240	162-240	214	126	96	111
Zr	160	100	220	100-220	160	240	260	250

AS005 to AS134 - Gneisses; AR107,131 & 132 - Restites; AFQ 136 & 137 - Fuchsite Quartzite.

Asterix* indicates determination of Ba,Ce,La,Pb,Rb,Sr,Th,U & Zr by XRF.

Dash ( ) denotes not analysed. n.f. not found; below detection limit.

S.D. standard deviation.

Table : 20 Normative composition of trondhjemitic gneisses around Ambalavayal

	AS 005	AS 009	AS 016	AS 018	AS 019	AS 022	AS 024
Q	26.04	25.96	30.84	28.84	25.62	25.14	29.22
Or	15.01	21.13	13.90	5.04	20.02	17.79	18.35
Ab	45.59	39.36	45.06	47.16	48.21	48.21	42.97
An	8.06	7.51	3.61	12.51	3.34	4.45	4.45
C	0.20	-	2.14	1.63	-	0.51	1.53
Di	-	2.16	-	-	-	-	-
Wo	-	-	-	-	-	-	-
Hy	1.60	1.0	0.93	3.46	1.06	1.06	1.20
Mt	1.39	0.93	1.62	3.25	1.39	1.39	1.16
He	0.96	0.16	-	-	-	-	-
Il	0.30	0.15	0.30	0.46	-	-	0.15
Ap	0.34	0.34	0.34	0.34	-	-	-

Table : 20 (Contd.)

	AS 026	AS 028	AS 034	AS 036	AS 104	AS 106	AS 109
Q	28.92	31.08	32.28	34.56	30.18	28.74	27.48
Or	19.46	17.24	17.79	13.90	22.80	20.57	23.35
Ab	40.87	36.68	36.68	37.20	37.20	40.35	39.82
An	4.45	11.12	8.06	6.67	5.56	6.67	4.45
C	2.65	-	1.43	3.26	0.31	0.20	1.12
Di	-	-	-	-	-	-	-
Wo	-	-	-	-	-	-	-
Hy	1.73	2.12	0.80	1.73	1.20	0.80	0.80
Mt	1.16	1.39	2.32	1.39	1.62	-	0.23
He	-	-	0.32	-	0.16	1.62	1.76
Il	-	-	0.30	0.15	-	-	0.15
Ap	-	-	0.34	-	-	-	-

Table : 20 (Contd.)

	AS 115	AS 116	AS 117	AS 119	AS 120	AS 121
Q	30.42	31.38	30.24	29.76	36.60	31.98
Or	26.69	10.56	9.45	22.24	20.02	17.24
Ab	32.49	27.77	39.30	35.11	32.49	38.78
An	5.56	16.12	11.40	5-56	4.45	4.45
C	0.82	0.82	1.84	2.65	1.53	1.84
Di	-	-	-	-	-	-
Wo	-	-	-	-	-	-
Hy	1.06	6.61	3.85	2.66	1.20	2.66
Mt	2.09	3.48	2.09	1.16	1.86	1.62
He	-	-	-	-	0.48	-
Il	0.15	1.52	0.61	-	0.15	0.15
Ap	-	0.68	0.34	-	-	-

Table : 20 (Contd.)

	AS 122	AS 124	AS 125	AS 134	Mean
Q	29.58	31.92	25.68	36.30	29.95
Or	21.68	22.24	23.35	19.46	18.30
Ab	32.49	31.96	39.82	33.01	39.00
An	4.73	6.67	5.56	4.45	6.66
C	2.04	1.33	0.41	3.67	1.52
Di	-	-	-	-	-
Wo	-	-	-	-	-
Hy	5.04	1.20	2.12	1.20	1.96
Mt	2.55	2.09	2.09	0.93	1.70
He	-	0.16	-	-	1.42
Il	0.30	0.15	0.15	0.30	0.32
Ap	0.34	-	-	-	0.38

-tion are observed. Al_2O_3 shows a scattered plot whereas Na_2O slightly increases towards higher SiO_2 values. K_2O shows a pronounced decrease. CaO, FeO^t, MgO, TiO_2 and P_2O_5 show a sharp decrease towards the silicic end, denoting early crystallization of ferromagnesium minerals.

6.2 Trace Elements

Among trace elements, Ba (4-469ppm), Rb (24-335ppm) and Sr (1-323ppm) show a wide range. Cr (upto 244ppm), Ni (upto 184 ppm) and Zn (upto 326ppm) show high values. The abundance of La (8-100ppm), Ce (22-140ppm), Nb (25-207ppm), Y (80-288ppm) and Zr (42-326ppm) is highly variable. Co and Pb show moderate levels. Molybdenum ranges from 2 to 24ppm. Low uranium (2-7 ppm) and high thorium (3-26ppm) contents are also noted.

Trace element variations with respect to SiO_2 are shown in Fig. 42. Bi, Co, Cu and Li do not show any significant variation trends. Ba and Sr show smooth decrease towards higher silica levels, whereas Rb shows overall increase, consistent with ideal fractionation process (McCarthy, 1976) involving feldspar. The late stage increase in Pb is also indicative of the same. The concentration of Zn towards the felsic end marks the fractionation of ferromagnesium minerals, mainly amphibole and biotite. La, Ce and Zr show depletion whereas Y and Nb concentration increases with progressive fractionation.

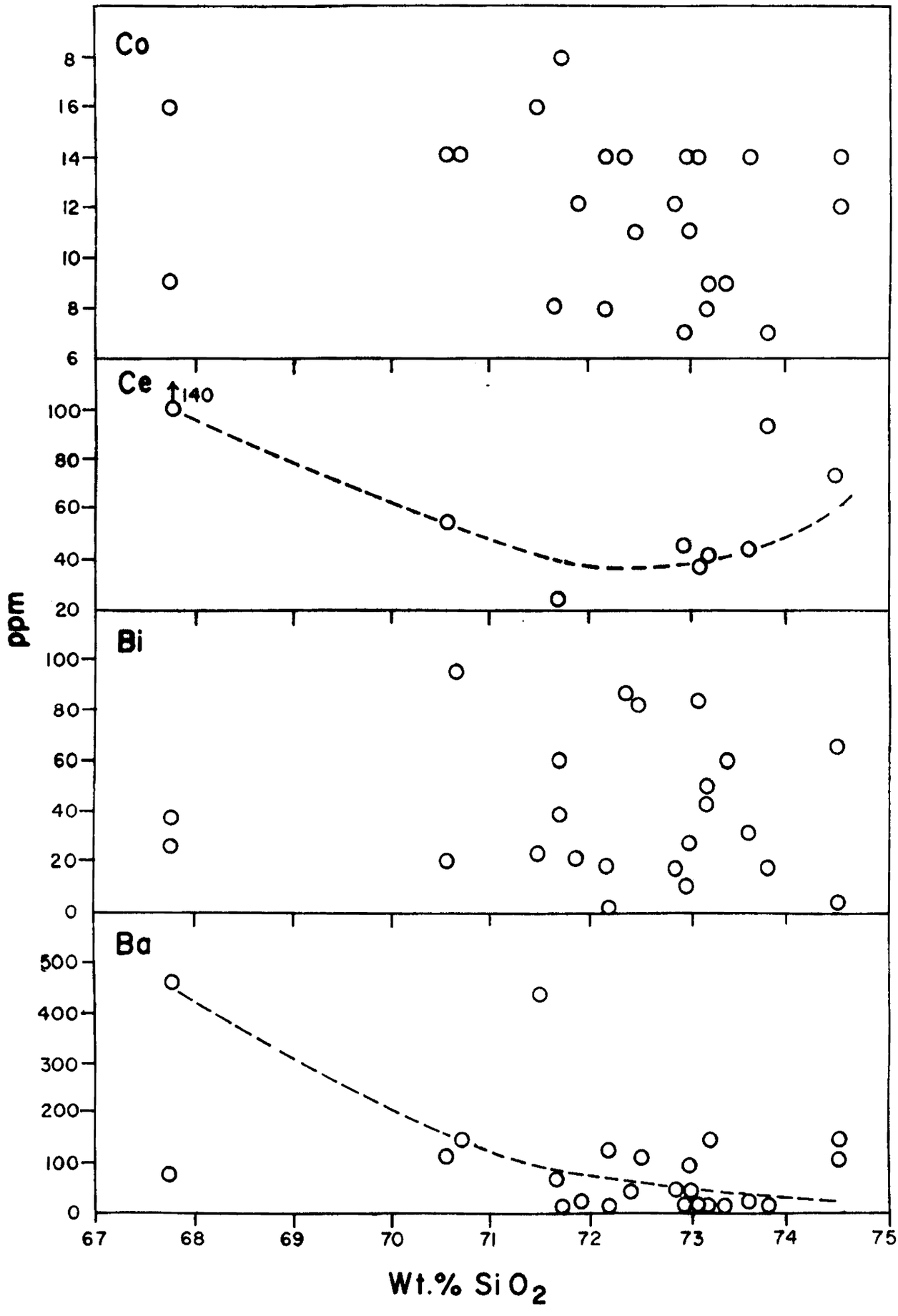

Fig. 42 Trace element variations in the gneisses against

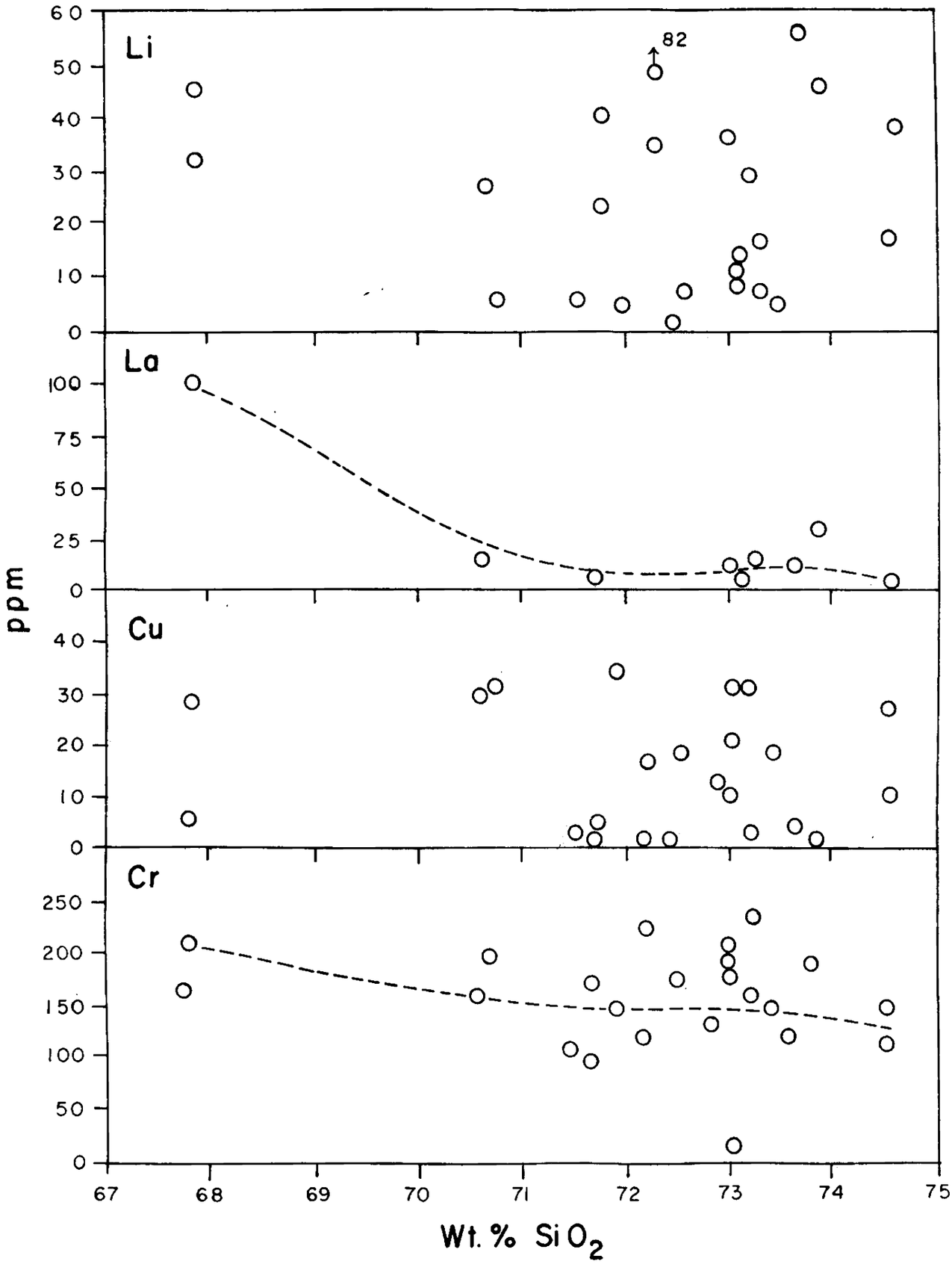
Li
82
La
Cu
Cr
ppm
Wt. % SiO2
60
50
40
30
20
10
0
100
75
50
25
0
40
30
20
10
0
250
200
150
100
50
0
67
68
69
70
71
72
73
74
75

Fig. 42 contd.

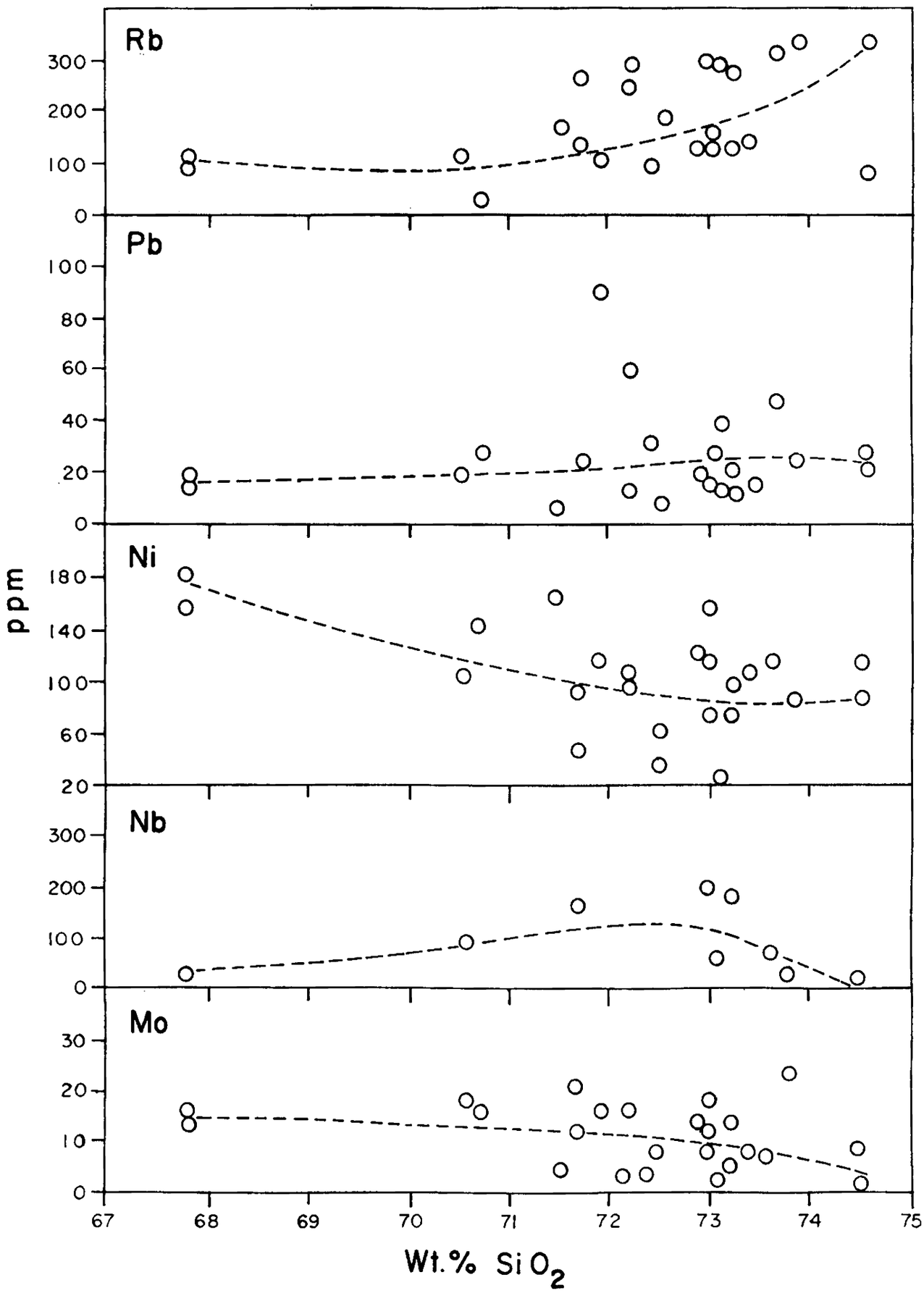

Fig. 42 contd.

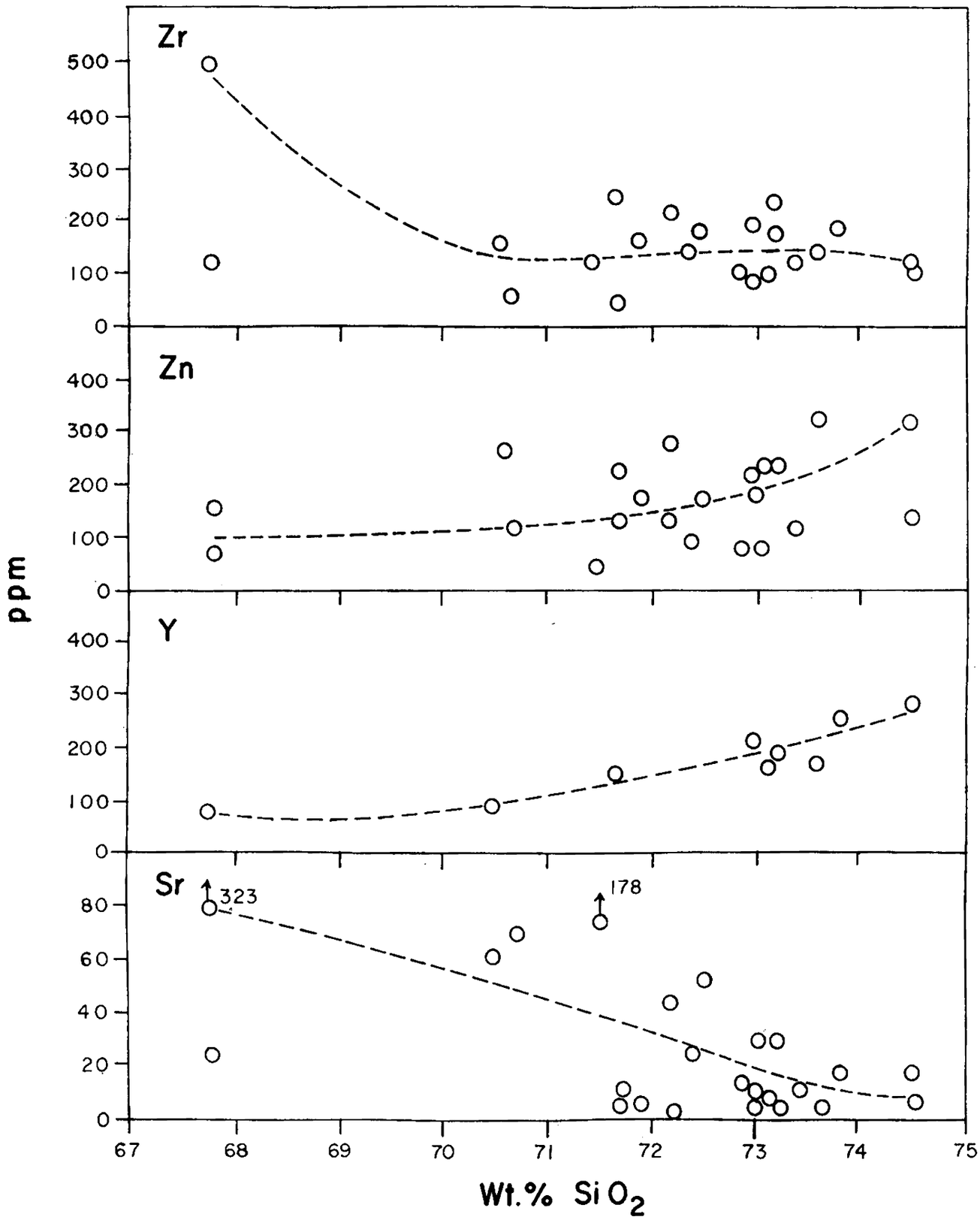
Zr
Zn
Y
Sr
323
178
ppm
Wt.% Si O2
0
100
200
300
400
500
20
40
60
80
67
68
69
70
71
72
73
74
75

Fig. 42 contd.

The interelement variations are shown in Fig.43. Ba and Sr exhibit a pronounced positive correlation whereas Rb and Sr yield a negative trend. Rb correlates positively with K. All these observations are characteristic of magmatic crystallization and crystal fractionation.

The variations in element ratios with increasing SiO_2 are shown in Fig.44, where K/Ba, K/Rb, Ba/Sr and Rb/Sr show increase towards the felsic end. The increase in K/Ba, Ba/Sr and Rb/Sr ratios conclusively indicate feldspar fractionation (Hanson, 1978). The concentration of K/Rb towards later stages is indicative of fractionation involving amphibole.

The major and trace element characters of the enclaves are characteristic of their being refractory residual fractions of partial melting.

The fuchsite quartizites show enrichment in Mg, Al, K, Ni, Cr and Zn with depletion in Si, Ca, Rb and Sr, correlating with similar features noted for fuchsite quartzites of the region (Sinha Roy and Ravindrakumar, 1984). They belong to the Wynad schist belt and probably represent chemical sediments indicating the presence of ultramafics in the source region (Narayana et al., 1983).

6.3. Petrogenesis

It is now widely accepted that Archaean gneissic complexes

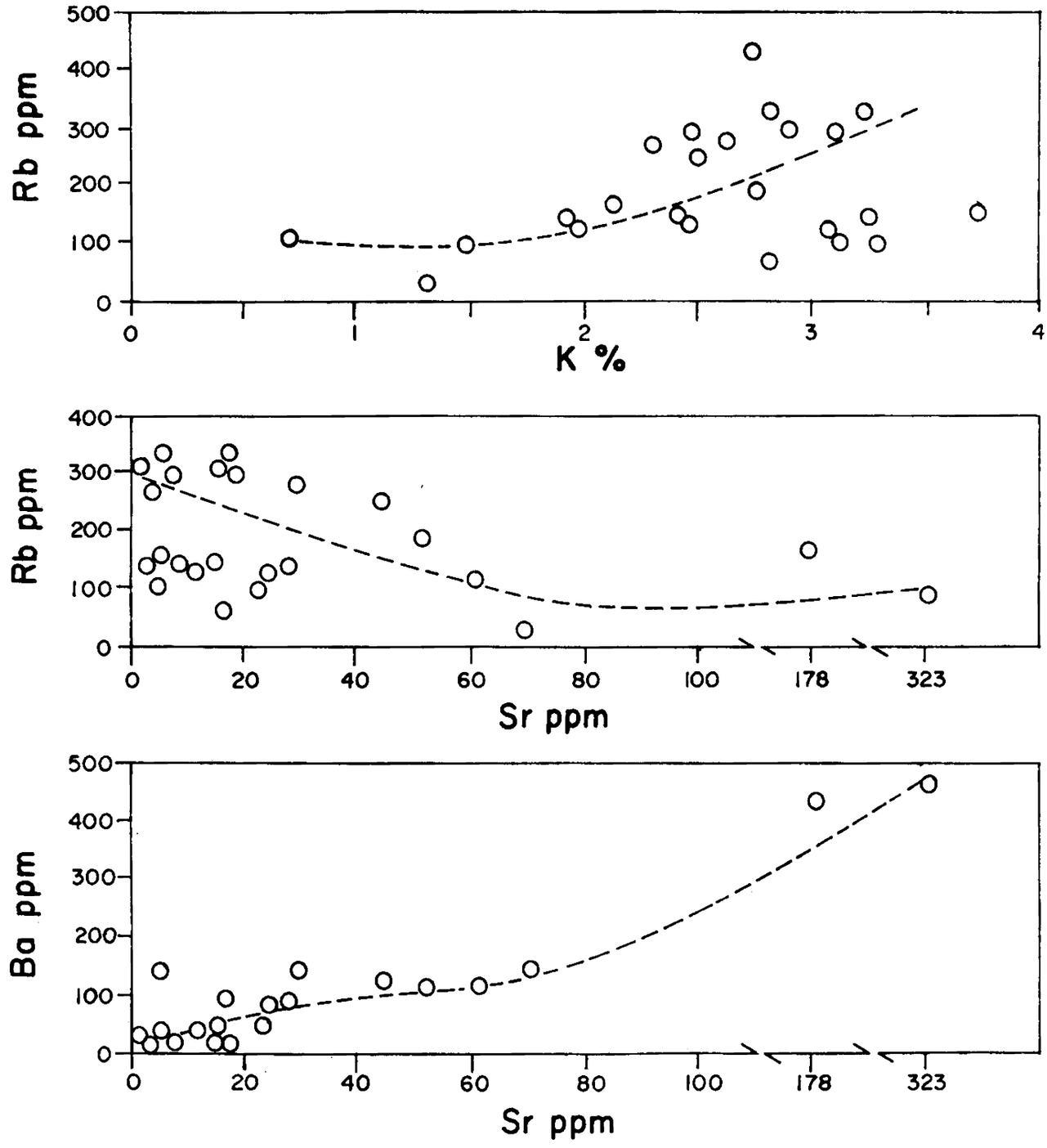

Fig. 43 Inter-element variations in the gneisses.

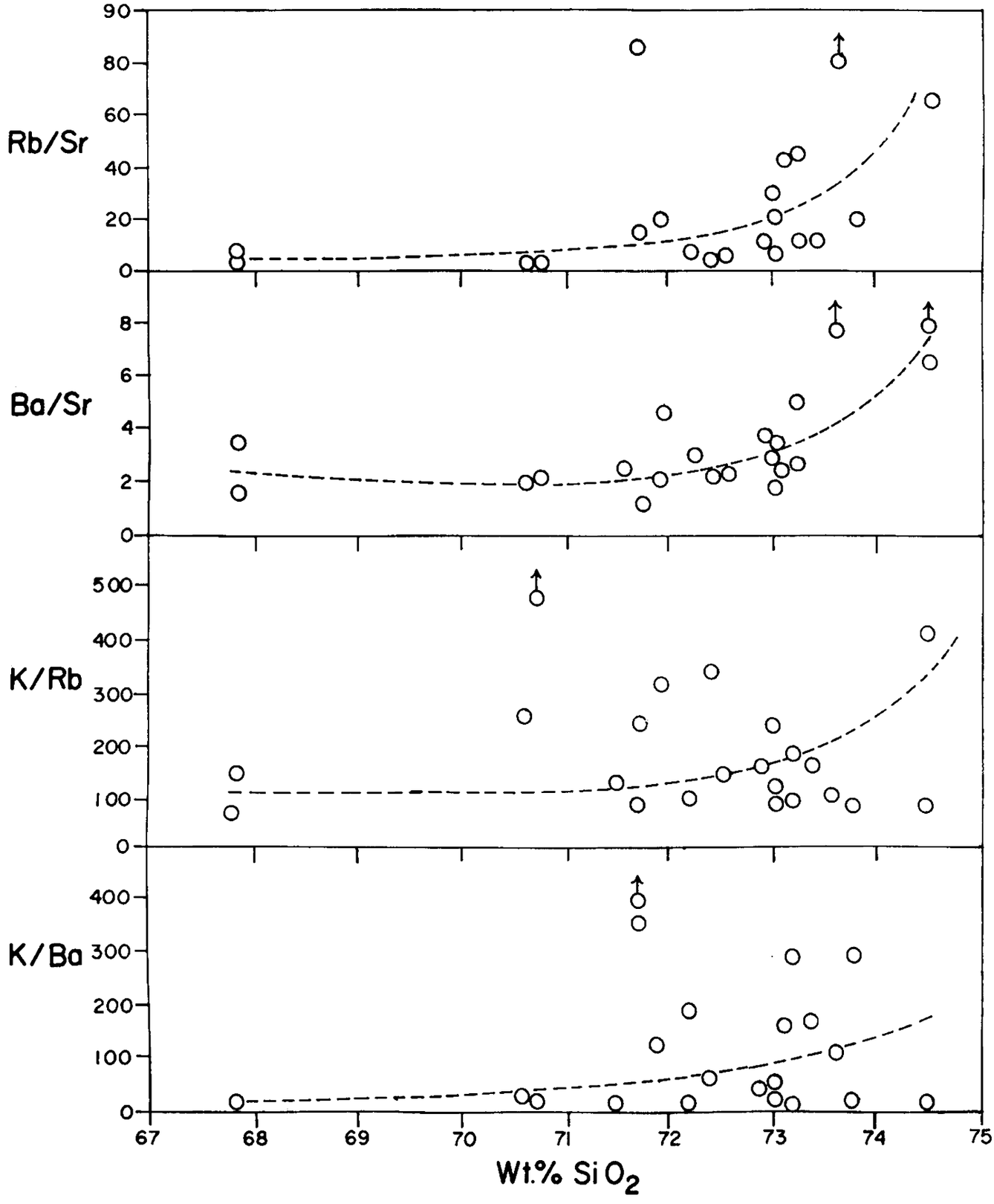

Fig. 44 Variations of element ratios in the gneisses.

TABLE 21 : MAJOR ELEMENT DATA OF AMBALAVAYAL GNEISSES COMPARED WITH OTHER GNEISSES

	1	2	3	4	5	6	7
SiO_2	72.96	67.80	67.20	65.40	70.05	74.50	72.02
TiO_2	0.13	0.51	0.76	0.50	1.14	0.39	0.11
Al_2O_3	13.85	15.70	13.46	16.00	11.41	14.20	16.78
Fe_2O_3	1.34	2.20	5.99	4.90	2.64	0.36	0.86
FeO	0.96	1.58			2.46	1.92	
MgO	0.56	0.93	0.99	2.10	2.64	0.43	0.24
CaO	1.43	2.44	2.71	3.40	3.57	2.49	1.60
Na_2O	4.67	3.53	3.80	3.90	2.68	4.08	5.65
K_2O	3.10	4.64	4.07	2.80	1.18	1.95	2.51

1. Ambalavayal gneiss
2. Diatexites of central Kerala (Rajan et al., 1984)
3. Potash-rich Uivak gneiss (Bridgwater and Collerson, 1976)
4. Banded gneiss and migmatites (Eade and Fahrig, 1971)
5. Biotite-hornblende gneiss (Janardhan et al., 1978)
6. Mean Archaean low alumina trondhjemites (Condie, 1981)
7. Halekote trondhjemite of Dharwar craton (Stroch et al., 1983).

had an igneous origin and the igneous precursor for them may be either a volcanic succession dominated by dacitic rocks or intrusive plutons (Condie, 1981, Naqvi, 1979; Naqvi et al., 1978). Anatexis, migmatisation and K-metasomatism in such terranes are significantly younger than the igneous event (Bridgwater and Collerson, 1976). Tonalites and trondhjemites are modelled to be the products of fractional crystallization of magmas produced by about 20% partial melting of Archaean tholeiitic basalt metamorphosed to amphibolite or eclogite (Arth and Hanson, 1972; Arth and Barker, 1976). The quartz monzonites and granodiorites of Barberton region, South Africa, are conceived to have formed by 70-80% fractional crystallization of a granodioritic magma, derived by the partial melting of acid and intermediate granulites. Similarly, geochemical modelling of the Louis Lake batholith, Wyoming show that the Precambrian granodioritic and quartz monzonitic rocks were derived from a parent granodioritic magma involving hydrous partial melting of quartz eclogite in the upper mantle (Condie and Lo, 1971). Collerson and Bridgwater (1979) recognised the potassic members of Uivak gneissic suite, Saglek area, Labrador, to be products of partial melting of tonalites and trondhjemites under granulite facies conditions.

The mineral assemblage of the gneisses could be explained in terms of a simple model involving partial melting of greywackes (Winkler, 1976), with a probable mixing of greywackes

with pelites or psammopelites. Plots of the gneisses, however, do not cluster around the minimum-melt point, but show a wide scatter in the Q-Ab-Or diagram (Fig.45). Moreover, the geochemical characters of the gneisses, as discussed previously, indicate a magmatic crystallization involving crystal-liquid fractionation.

Under the influence of high Archaean geothermal gradients, partial melting of eclogites or amphibolites would take place, since granulite facies assemblages would exist under the P-T conditions where melting could occur (Collerson and Bridgwater, 1979). With mafic granulites as the starting material, a small degree of hydrous partial melting at intermediate depths will yield trondhjemitic magmas (Wyllie, 1977), in contrast to the granodioritic magma from quartz eclogites (Condie and Lo, 1971). The melting of mafic granulites was probably achieved under the high Archaean geothermal gradients of more than 100°C/Km. The melt derived was fractionated with respect to feldspars and amphibole as evidenced from the trace element behaviour. The enclaves of restite represent the refractory residue, which is commonly associated in Archaean gneissic terranes (eg. Collerson and Bridgwater, 1979; Mehnert, 1968).

Plots of the gneisses in A-F-M and K-Na-Ca diagrams (Fig.46) indicate an intermediate position between calc-alkaline and gabbro-trondhjemitic differentiation trends (Barker and Arth 1976). This is also evident from their position in Q-Ab-Or

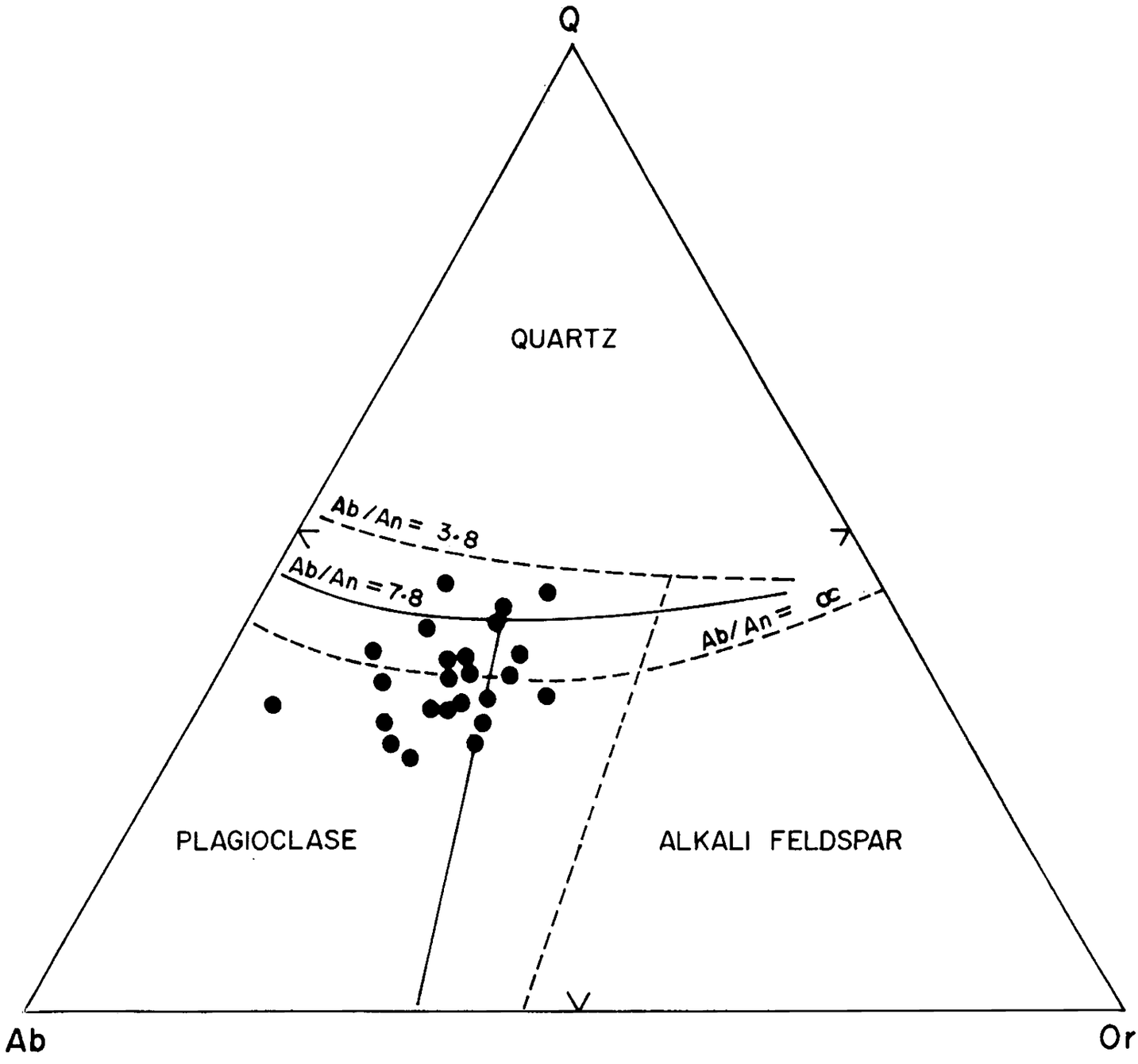

Fig. 45 Normative Q-Ab-Or plots of the gneisses (after Winkler, 1976).

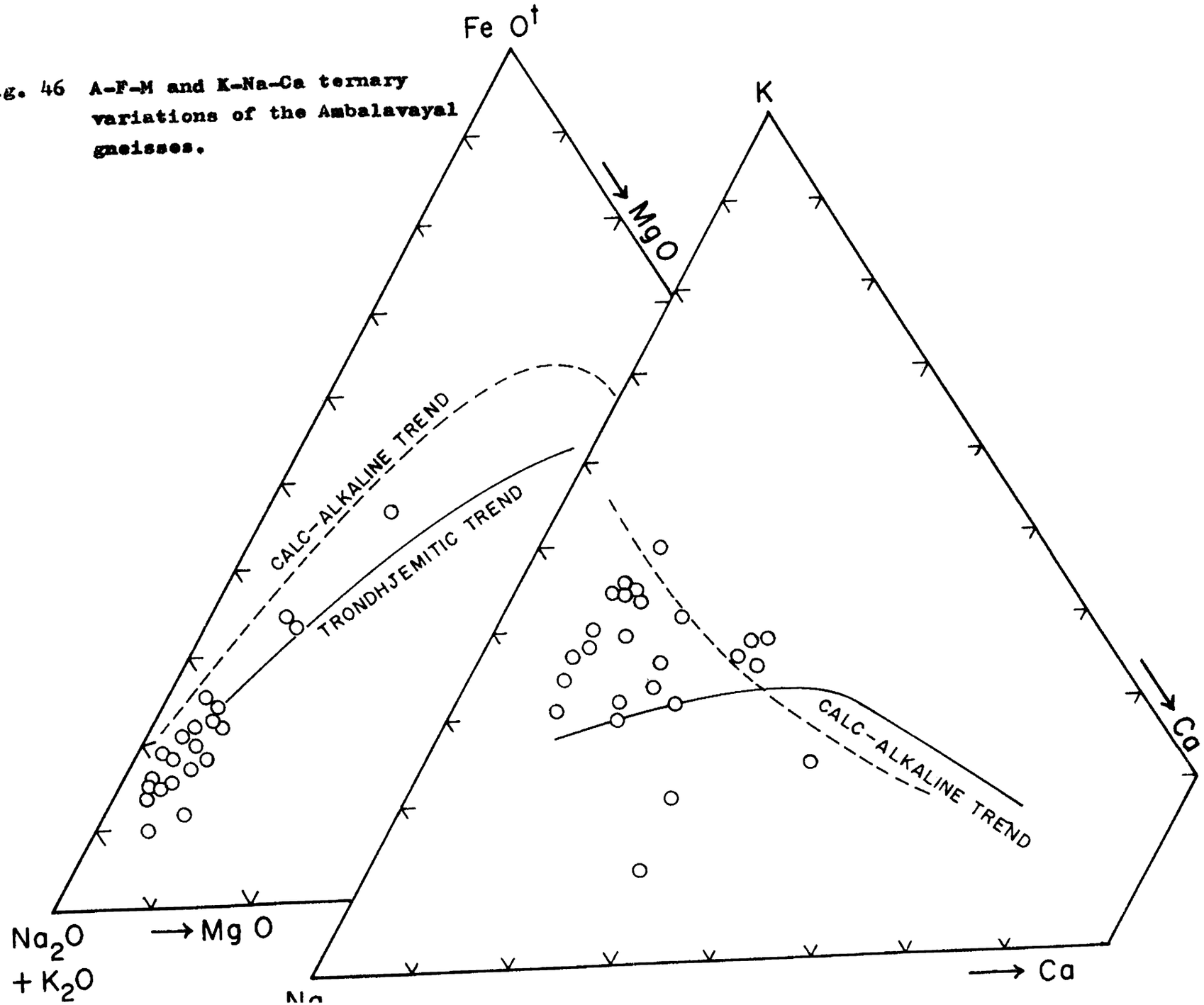

Fig. 46 A-F-M and K-Na-Ca ternary variations of the Ambalavayal gneisses.

normative diagram (Fig.47), where the plots of the gneisses fall close to the field of Uivak gneisses of Labrador.

In summary, the geochemical characters of the gneisses attribute them to be low alumina trondhjemites. Mass balance relationships between the compositions of similar trondhjemites from adjacent terranes with that of primitive Archaean upper mantle proposed by Sun and Nesbitt (1977) indicate that a mixture of 5% trondhjemite and 95% of solid mantle residue could yield the proposed primitive upper mantle composition (Stroh et al., 1983). An analogy with this would indicate that a lithophile-rich trondjemite magma was extracted from the mantle which underwent subsequent crystal fractionation. This magmatism may be correlated with the type of regional magmatism contemporaneous with the stabilisation of the craton during the Archaean times.

CHAPTER - 7

FLUID INCLUSION STUDIES

The thermodynamically isolated microgeochemical systems entrapped in various minerals during their growth are popularly known as fluid inclusions. Since they preserve the 'fossil fluids', their study is an important clue in understanding the complex geologic processes. Each inclusion, hermetized in a mineral, records the state of the mineral-forming medium at the

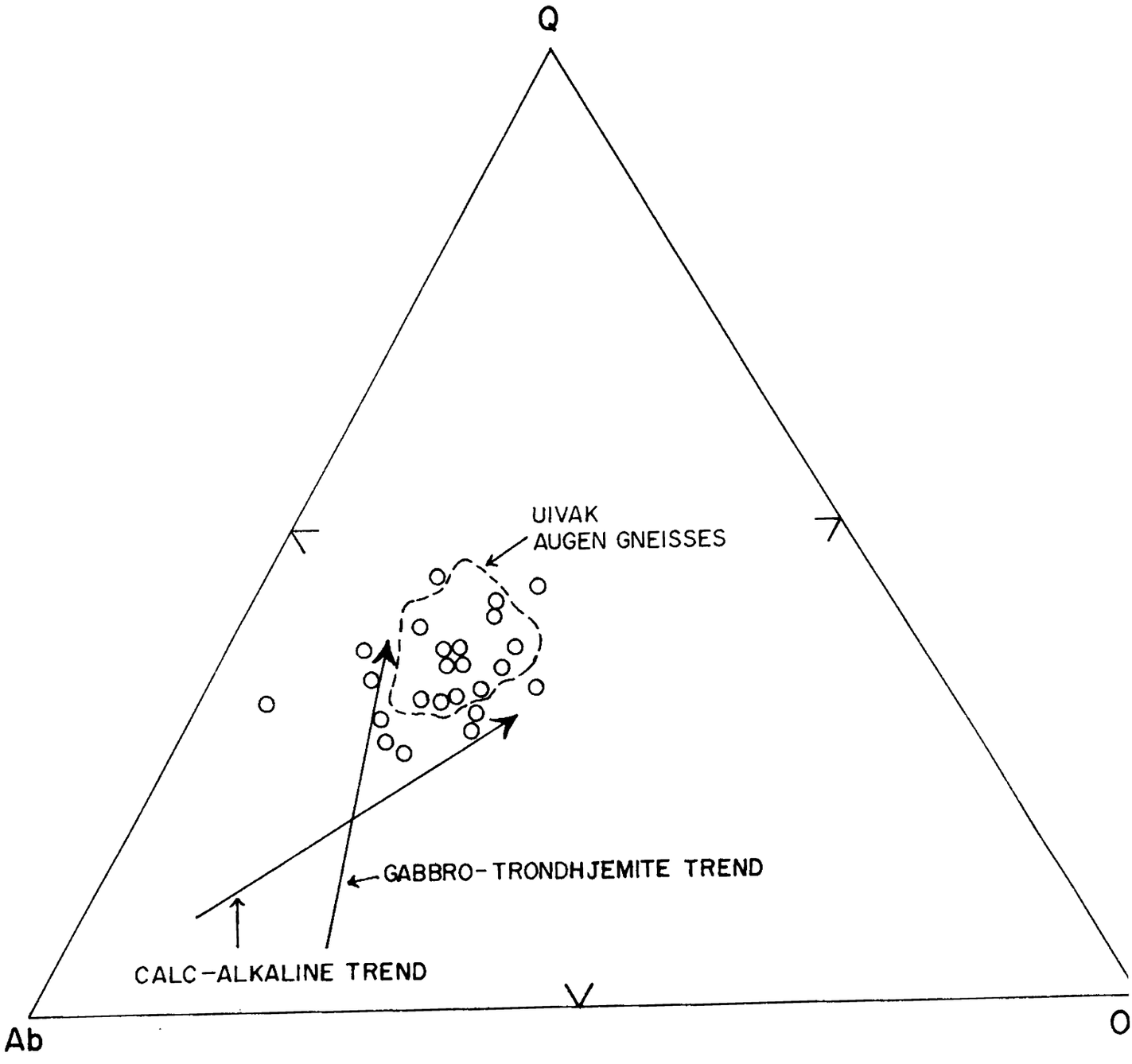

Fig. 47 Q-Ab-Or plots of the gneisses. The field of Uivak gneisses is after Collerson and Bridgwater (1979) and the trend lines are after Barker and Arth (1976).

moment of its entrapment. They are used for understanding the P-T-X parameters of fluids associated with mineralization, magmatism and metamorphism. Comprehensive discussions on the principles and applications of fluid inclusion studies with related references are given in Roedder (1979, 1984), and Hollister and Crawford (1981) [illegible]. In India, fluid inclusion studies are yet in a pioneer stage. Related researches include those of Sahu and Panchapakesan (1982), Jaireth et al (1982) and Santosh (1981, 1984a, 1985a, d).

7.1. Sample preparation

Samples of quartz from the quartz-feldspar association of the granite, from pegmatite and from quartz veins associated with molybdenite mineralization were selected for fluid inclusion studies. A number of thin slices were cut and one side ground and polished well before mounting on glass plate. The other side was then ground for optimum thickness and then polished. The grinding and polishing were done slowly and in wet media in order to prevent temperature raise due to friction. The doubly polished plates thus prepared are taken out of the glass slides by dissolving the mounting glue and cleaned well. The thickness of the plates prepared varies from 0,03 to 0.8mm, depending on the transparency of the quartz sample.

7.2. Fluid inclusion petrography

The doubly polished quartz plates were carefully studied under a Leitz Ortholux petrographic microscope. Fluid inclusions are commonly present in the quartz associated with the granite. However, their density of distribution increases in pegmatitic quartz and reaches maximum in vein quartz. Similarly there is a gradation in the size of the inclusions also. Those found in the granite are relatively small in size (5-30 microns) whereas those associated with the pegmatites generally range in size from 10 to 50 microns. A few inclusions in the quartz show cavities upto 100 microns length. With respect to the shape of inclusions, the monophase type in the granite usually shows diamond-shaped cavities whereas the bi-phase types are polygonal. In pegmatites, the monophase type is diamond-shaped. Among bi-phase inclusions, some are rhombododecahedral (negative-crystal) or diamond-shaped whereas the others show polygonal, elongate or irregular cavities. In the quartz veins, most of the inclusions are ovoidal, elongate or polygonal.

A distinct pattern of distribution of inclusions, corresponding to various genetic categories is observed in the quartz types (Fig.48). In granite quartz, inclusions of scattered type corresponding to the 'primary' category show complete filling of the cavity with a dense dark fluid phase at room temperature. Their composition shows that they are monophase carbonic in-

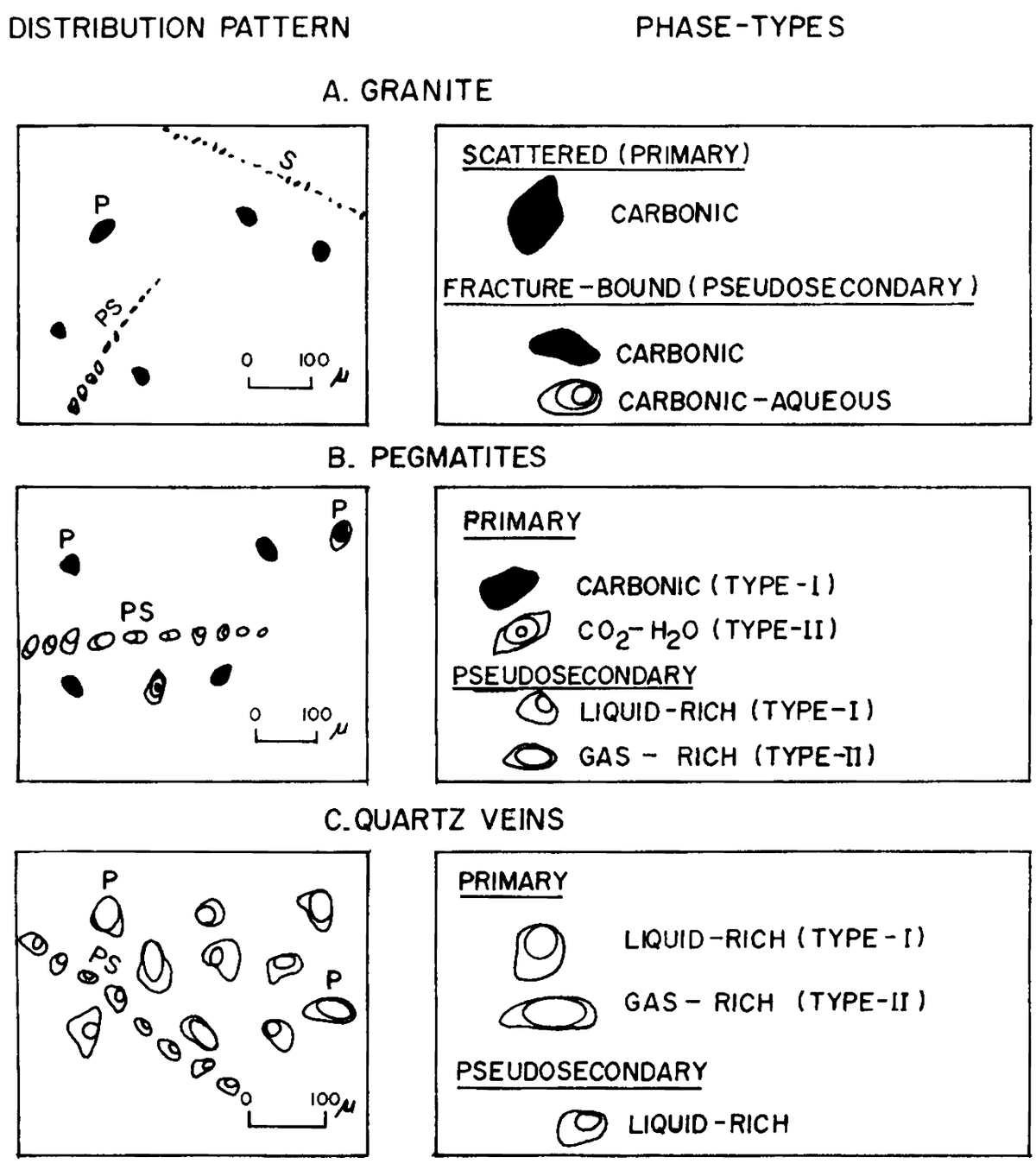

Fig. 48 Pattern of distribution and various phase-types of fluid inclusions in quarts from the granite, pegmatites and quarts veins of the Ambalavayal area.

clusions. Such monophase inclusions also occur along arrays that start at a grain boundary and peter out in the middle and are hence 'pseudosecondary' in nature. Secondary inclusions of bi-phase type with or without a CO_2 phase are also observed.

The relative distribution of the various phase-types of inclusions in the granite-quartz is shown in Fig.49. Interestingly there is a positive correlation between the percentage of carbonic inclusions and the major mafic mineral content. Thus, in localities where the density of distribution of carbonic inclusions is relatively small, biotite is the dominant mafic constituent. Towards the eastern part of the pluton, where the hornblende/biotite ratio is generally greater than 1, carbonic inclusions are more abundant. Such a correlation was noted by Konnerup-Madsen (1977), where a progressive increase in abundance of CO_2 inclusions was observed while passing from biotite rich through hornblende rich to the pyroxene rich zone.

In the pegmatite quartz, primary inclusions are represented by two categories. Type I contains a dense dark fluid phase at room temperature which completely fills the cavity. Type II inclusions are bi-phase at room temperature, but develop a third phase on cooling, consistent with the composition, CO_2 (liquid) CO_2 (gas) + H_2O (liquid), a category commonly found in pegmatitic quartz (Santosh, 1984a). Pseudosecondary inclusions comprise a liquid-rich type (Type I) with vapor phase occupying 10-30%

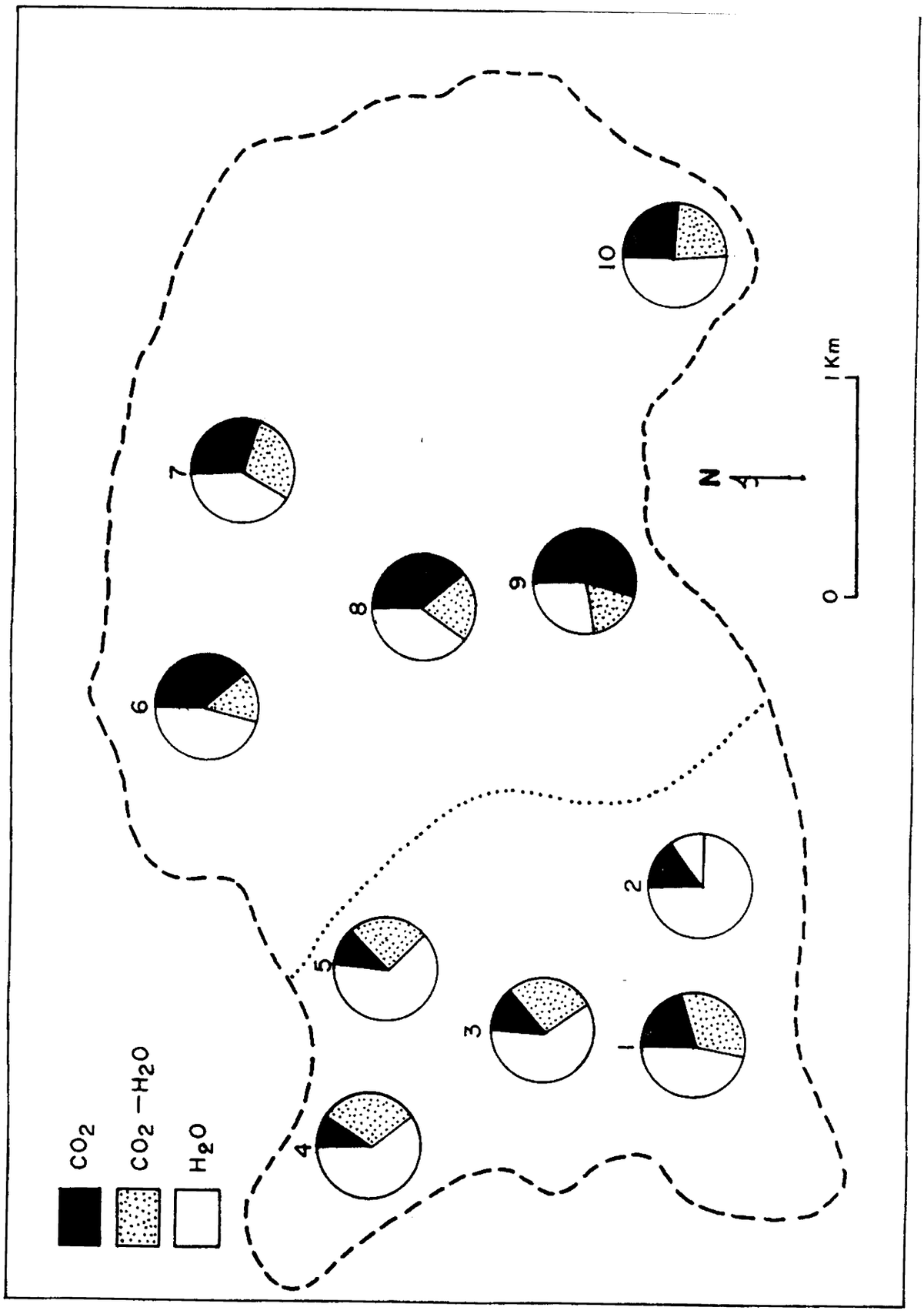

Fig. 49 Percentage of fluid inclusion phase-types in various localities in the granite pluton. The dotted line separates the biotite-rich zone (west) from the hornblende-rich zone (east).

volume of the cavity and a vapor-rich type (Type II) with a gas bubble that fills 80-90% volume of the inclusion cavity.

In the quartz veins, large primary inclusions which are generally bi-phase occur. They show varying vapor: liquid ratios. Thus, liquid rich inclusions with small gas-bubble (Type I) are seen coexisting with gas-rich inclusions with less liquid phase (Type II). The co-existence of inclusions with ... varying degrees of filling signify entrapment of 'boiling' fluids (Roedder, 1971; Roedder and Bodhar, 1980). Aqueous liquid rich inclusions with a small gas bubble constitute secondary inclusions in vein quartz.

Photomicrographs of fluid inclusions in the three different quartz varieties are shown in Fig.50. From the distribution pattern of various phase types of inclusions, it is inferred that the scattered carbonic inclusions were entrapped during the initial crystallization regime of the quartz-feldspar assemblage in the granite. The primary carbonic inclusions, in turn, represent the fluids present during pegmatite crystallization. Primary inclusions with varying vapor: liquid proportions in vein quartz are contemporaneous with molybdenite precipitation. It is seen that inclusions of primary nature constitute pseudosecondary in pegmatite quartz and form secondary in granite quartz, which are consistent with the crystallization history of the three quartz types. This chain-relation

Fig. 50 Photomicrographs of various types of fluid inclusions in quartz from the Ambalavayal area. Bar scales represent 50 milli microns.

(a) Arrays of carbonic inclusions in granite-quartz

(b), (c) & (d) Scattered monophase carbonic inclusions in granite-quartz.

(e) Coexisting carbonic and CO_2-H_2O inclusions in pegmatite quartz.

(f) CO_2-H_2O inclusion in pegmatite quartz showing three fluid phases on slight cooling.

(g) Liquid-rich inclusion in pegmatite quartz

(h) Vapor-rich inclusion in pegmatite quartz.

(i) & (j) Coexisting liquid-rich and vapor-rich inclusions in vein quartz

(k) Vapor-rich inclusions in vein-quartz

(l) Pseudosecondary aqueous inclusions in vein quartz.

is further substantiated by the similarity of fluid composition, density and P-T parameters of entrapment conditions as discussed in the following sections.

7.3. Heating freezing techniques

Only inclusions of primary nature in the granite quartz and pegmatite quartz were selected for heating freezing studies. However, from the vein quartz, the pseudosecondary inclusions were also studied in addition to primary inclusions. Heating studies were done using a Leitz-1350. Heating stage was calibrated with a precision of ± 5° at 400°C. Freezing runs were made on a CHAIX-MECA heating-freezing stage calibrated at -56.6°C with the melting point of pure CO_2 in natural standards and the precision was within ± 0.5°C. The fluid inclusion heating-freezing data, together with the P-T estimates and fluid compositions recorded from each quartz type are discussed below.

7.4. Fluid inclusions in granite

The primary carbonic inclusions in granite quartz were supercooled. Most of them solidified at about -70 to -90°C. On slow warming, first melting occurred at temperatures ranging from -55.2 to -59.6°C, with the peak melting between -56.4 and -57.2°C (Fig.51a). This range is close to the triple point for pure CO_2 (-56.6°C); Takenouchi and Kennedy, 1964). The melting point depression in some inclusions shown by the lower range of first melting temperatures imply that eventhough CO_2

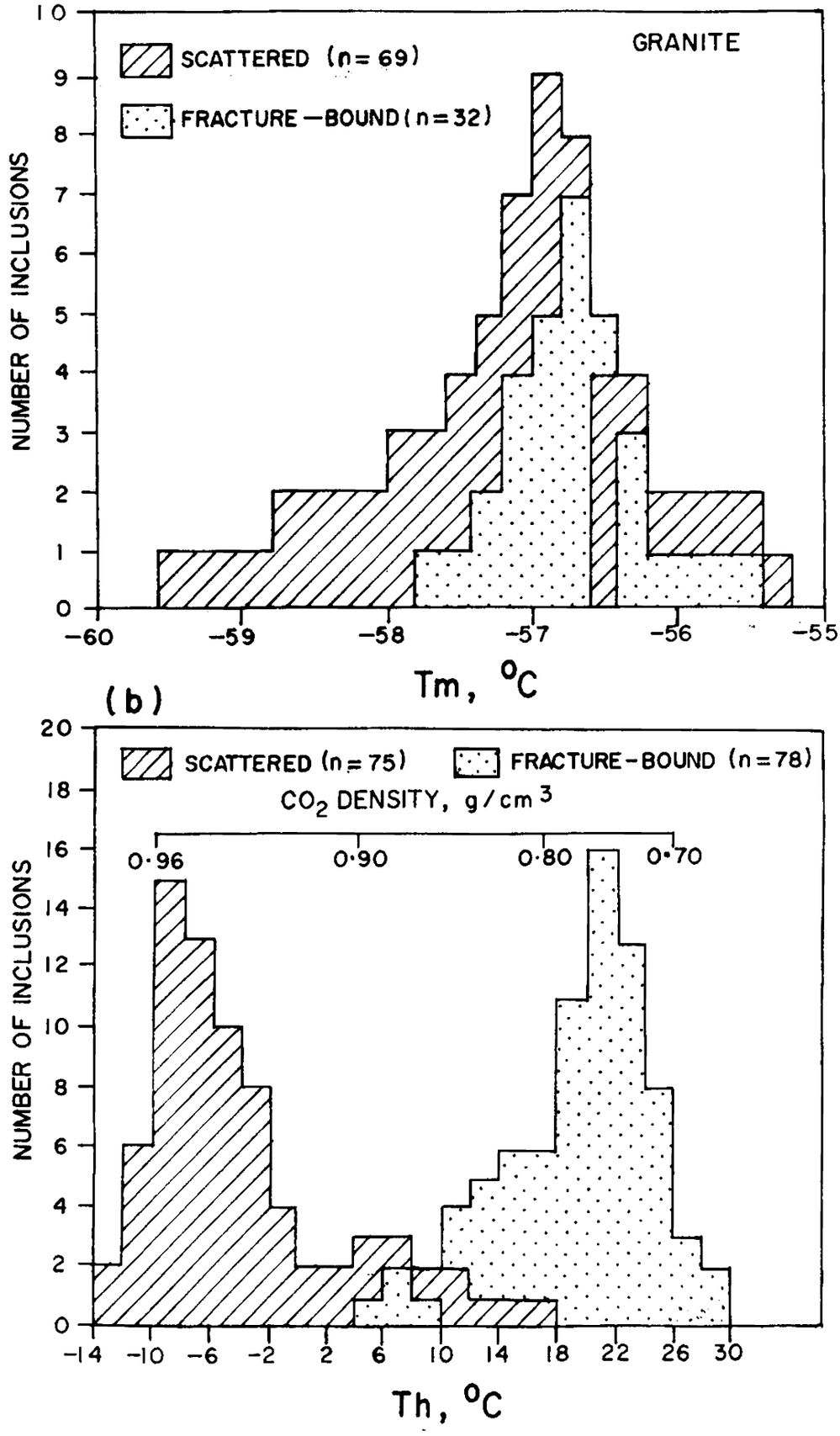

Fig. 51 Temperatures of melting (A) and CO_2 homogenisation (B) of monophase inclusions in quarts from the Ambalavayal granite.

is the dominant phase, traces of additional phases like CH_4 and or N_2 may also be present in some inclusions, as these phases are known to depress the melting temperature of the unary system, CO_2 (Swarenberg, 1979). The occurence of CH_4 and N_2 with CO_2 in fluid inclusions associated with alkaline rocks is commonly noted (Konnerup-Madsen and Rose-Hansen, 1982; Santosh 1985d).

The fracture-bound inclusions show melting temperatures of -55.4 to -57.8°C with peak melting between -56.4 and -57°C, corresponding to a near-pure CO_2 composition. Such evolution of fluids from mixed CO_2-CH_4 to almost pure CO_2 is recorded in the Puttetti syenite of adjacent Tamil Nadu region (Santosh, 1985d).

On continued heating, the scattered carbonic inclusions homogenize into a liquid phase at temperatures between -14 and + 18°C the peak homogenization being in the range, -6 to 10°C (Fig.51b). The homogenization temperatures indicate CO_2 densities ranging from 0.90 to 0.95 g/cm^3. The pseudosecondary inclusions homogenize into liquid between 10 and 30°C with a peak between 18-26°C, corresponding to CO_2 densities of 0.80-0.70 g/cm^3.

Data on the equilibria in the CO_2-CH_4 system was first applied quantitatively to fluid inclusion observations by Hollister and Burruss (1976). The significant features of the CO_2-CH_4 system are the shift of the univariant, solid-liquid-vapor equilibrium and the critical curve to lower temperature with increasing

pressure (Fig.52A). Based on investigations on fluid compositions in the C-O-H-S system, Holloway (1981) constructed the generalised fluid composition [illegible] regimes. His calculations demonstrate that for a given value of fO2 and P, decreasing T below the maximum value causes a fluid coexisting with graphite to become depleted in CO_2 and enriched in CH_4, H_2 and H_2S. In the case of graphite bearing sillimanite gneisses (khondalites) and graphite-bearing cordierite-sillimanite gneisses of the region, the present author has observed pseudosecondary CO_2-CH_4 inclusions, where the primary inclusions are almost pure CO_2 (data under publication). In the present case, pure CO_2 inclusions are subsequent to CO_2-CH_4 type, which is the reverse case because here the system is 'closed to graphite'. Holloway (1981) further showed that as temperature falls, the bulk composition moves along the graphite boundary (Fig.52b). The bulk composition of a CO_2-CH_4 system is a function of the relative volumes of the two phases. Swanenberg (1979) used an estimate of the relative abundance of liquid and vapor phase, at the melting temperature to calculate mol per cent CH_4. Eventhough his technique is limited to CH_4 contents of less than or equal to 30 mol per cent, it is possible to apply this prodedure in the present case as shown in Figs.52c & d. The degree of filling at the first melting temperature of CO_2-CH_4 inclusions in the granite quartz varies from 0.8 to almost 1.0 thus denoting a range of 2 to 10 mol per cent CH_4 contents.

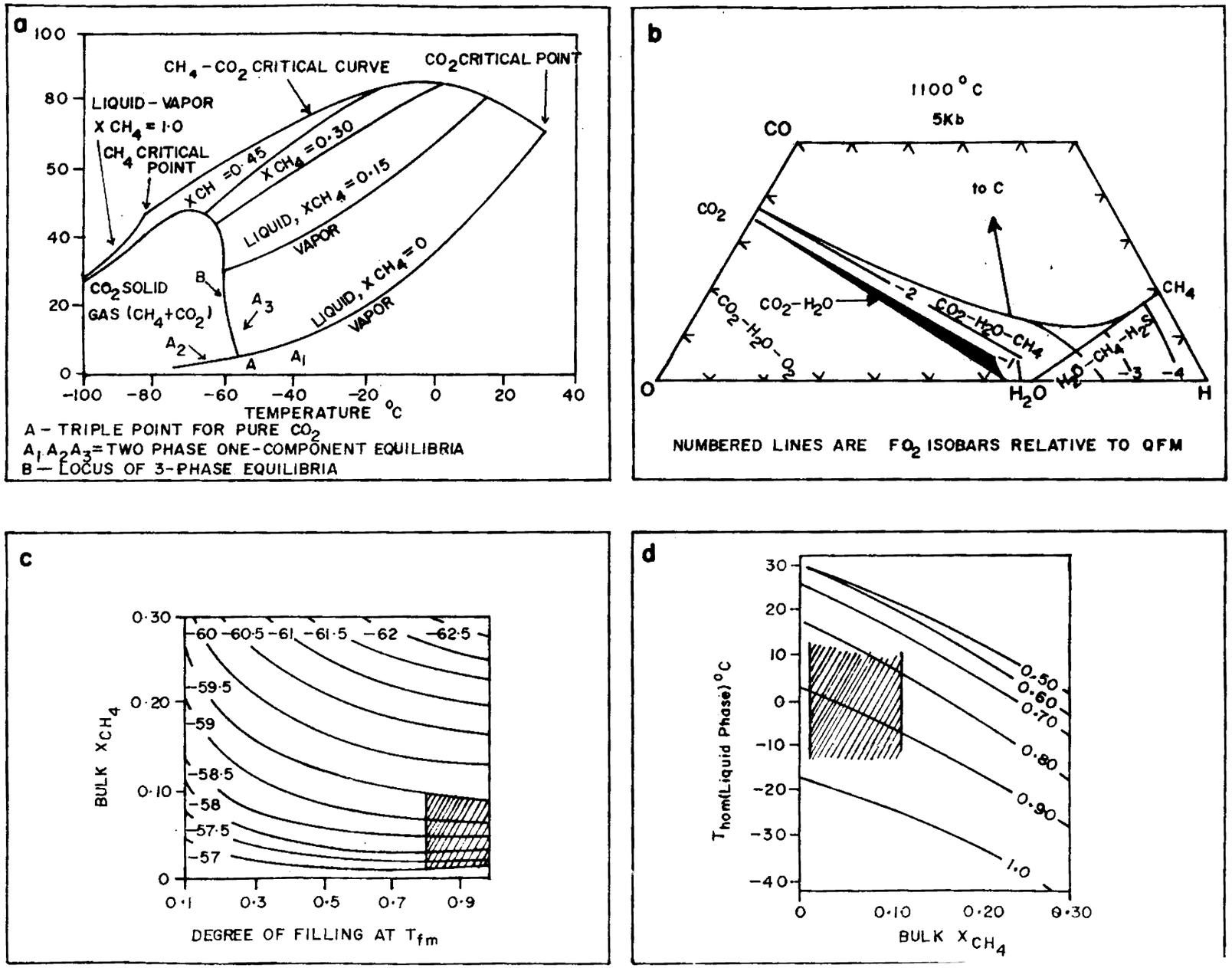

Fig. 52 Thermodynamics of CO_2-CH_4 (a) and C-O-H-S systems (b) with plots of Ambalavayal data (shaded region in c and d). See text for details.

CO_2 and CH_4 have similar excluded volumes and eventhough CH_4 lacks a quadrupole moment, the quadrupole moment of CO_2 is relatively small because of which the volumetric properties of CO_2 and CH_4 are similar. Thus, it is possible to express the density of CO_2-CH_4 mixtures in terms of equivalent CO_2. Based on homogenization temperatures the highest equivalent CO_2 density obtained for CO_2-CH_4 inclusions is 0.95 g/cm^3 (Fig.52d), comparable to that for pure CO_2 inclusions.

7.5. Fluid inclusions in pegmatites

The Type I scattered carbonic inclusions in the pegmatite quartz show melting temperatures close to that for pure CO_2. They homogenize into a liquid phase at temperatures between 13 and 27°C, with a peak in the range, 16-22°C, corresponding to CO_2 densities of 0.80-0.74 g/cm^3(Fig.53a). These fluids correlate with the carbonic fluids having CO_2 densities in the range of 0.80-0.70 g/cm^3 entrapped as pseudosecondary inclusions in granite quartz. The coexisting Type II bi-phase inclusions that develop a third phase on cooling (CO_2-H_2O type) show homogenization of the CO_2 phase into liquid at temperatures between 18 and 31°C with a peak in the range, 22-25°C (Fig.53b). The aqueous bi-phase inclusions that occur along secondary arrays homogenize by complete filling with liquid at temperatures between 310 and 410°C with a peak at 350-380°C (Fig.53c).

The coexisting Type I (CO_2) and Type II (CO_2-H_2O) inclusions

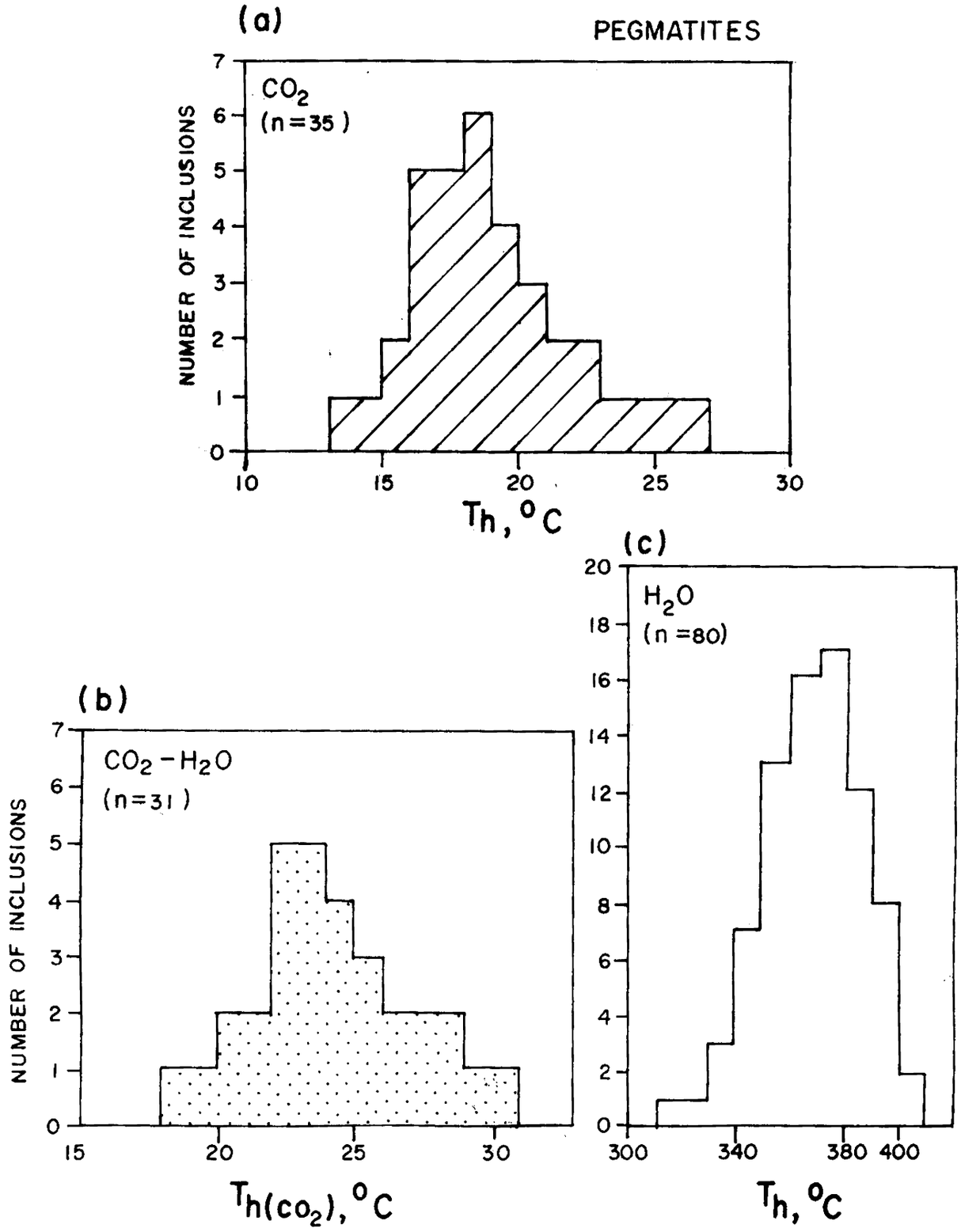

Fig. 53 Thermometric data of inclusions in pegmatitic quarts.
(a) CO_2 homogenisation temperatures in monophase inclusions;
(b) CO_2 homogenisation temperatures in CO_2-H_2O inclusions;
(c) homogenisation temperatures of aqueous bi-phase

signify simultaneous entrapment. Hence their combined P-V-T data can be used to estimate the P-T parameters of entrapment. The isochore obtained for monophase inclusion is shown in Fig. 54. The combined CO_2-H_2O isochore computed by adding the partial pressures of CO_2 and H_2O in the CO_2-H_2O inclusion according to Dalton's Law (cf. Konnerup-Madsen, 1979; Santosh, 1984a) is also shown. The CO_2 isochore for 0.80 g/cm intersects the combined CO_2-H_2O isochore at 2.2 Kb and 500°C. This estimate probably marks the P-T conditions of simultaneous entrapment of CO_2 and CO_2-H_2O fluids and corresponds to the P-T parameters of crystallization of the pegmatites. Although the solvus crest is only at 275°C at 1Kb for pure CO_2 and H_2O mixtures (Todheide and Franck, 1963), the presence of electrolytes greatly expands this solvus (Takenouchi and Kennedy, 1965) as a result of the strong partitioning of salts into the aqueous phase relative to the CO_2 phase (inset in Fig.54). Gehrig et al. (1979) showed that for a salt content of 6 wt. % in the aqueous phase, the solvus crest is at about 420°C at 1.5 Kb. The melting of CO_2-clathrate observed in the CO_2-H_2O inclusions range from 6-8°C, as against 10°C in the case of pure CO_2-H_2O mixtures, indicative of moderate salinity. Thus, the estimate of 2.2 Kb and 500°C corresponds with the increased P-T conditions in CO_2-H_2O immiscibility with increasing salt content.

The H_2O isochore for the aqueous inclusions intersect the CO_2-H_2O isochore at 310°C and 0.5 Kb pressure. This marks the

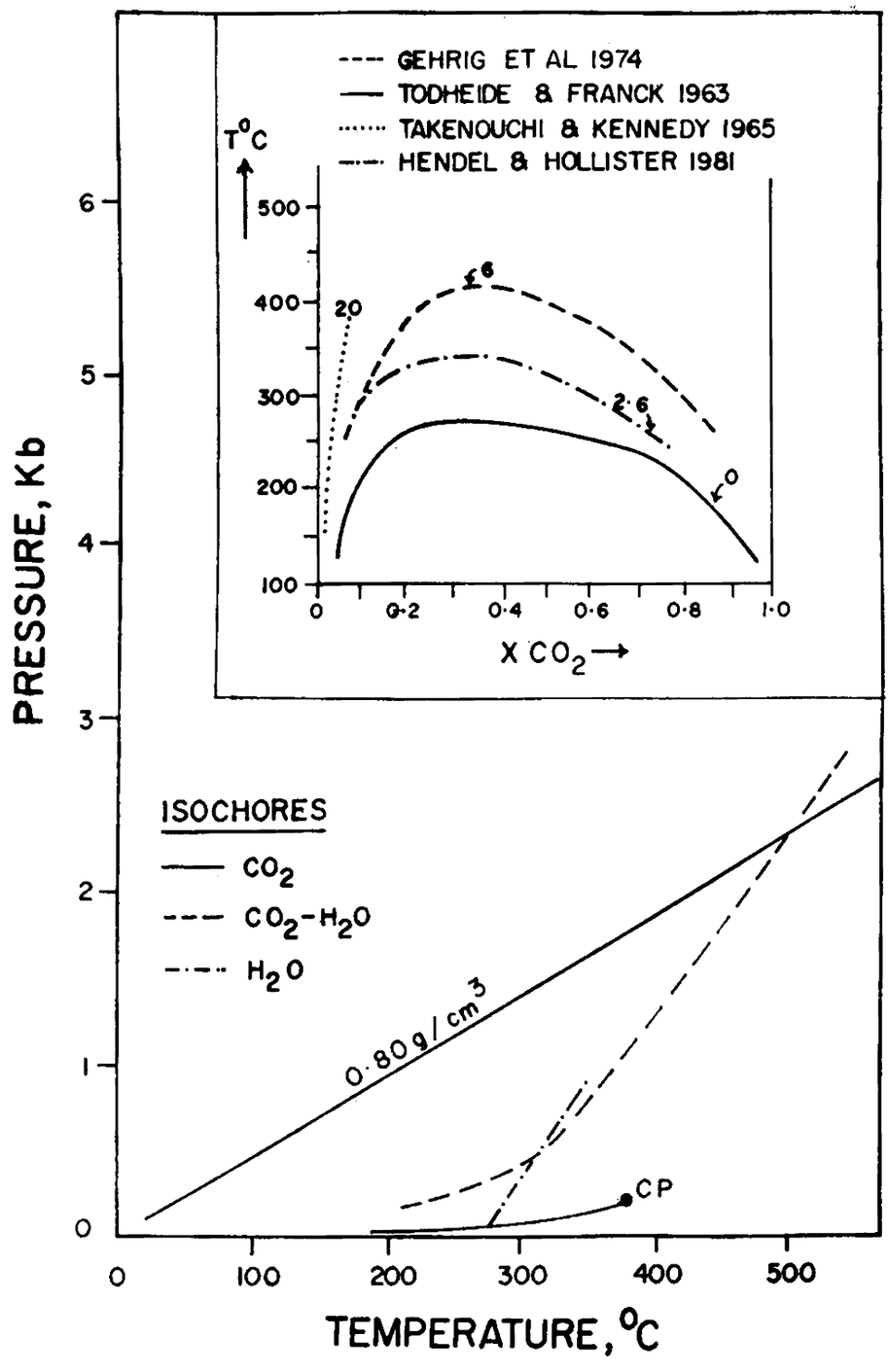

Fig. 54 P-T data from coexisting CO_2 and CO_2-H_2O inclusions in pegmatitic quartz. The inset shows immiscibility data on the CO_2-H_2O system. See text for discussion.

probable lower limit of fluid immiscibility in the Ambalavayal pegmatites.

7.6 Fluid inclusions in quartz veins

Type I liquid rich inclusions in the vein quartz homogenize by complete filling with liquid at temperatures between 280 and 420°C with a peak at 340-360° (Fig.55a). The coexisting vapor rich inclusions (Type II) homogenize by increase in the volume of vapor bubble and complete filling with vapor at temperature between 290 and 380°C with a peak at 340-360°. Such coexisting inclusions with different vapor: liquid ratios, homogenizing into different phases at the same temperature interval conclusively indicate heterogeneous entrapment of 'boiling' solutions (Roedder, 1971; Roedder and Bodnar, 1980; Santosh, 1984a). As discussed in a previous section, boiling or coexistence of vapor and liquid denote trapping of fluids close to the boiling curve. Hence no pressure correction is needed in the homogenization temperatures and the filling temperatures obtained can be taken as the true temperature of mineral formation.

On freezing, the type I inclusions show first melting temperatures close to the eutectic of NaCl-H_2O system (-21.1°C). On warming, the ice melts in the range, -10 to -6°C, denoting moderate equivalent salinites (Sourirajan and Kennedy, 1962) of about 8 to 15 wt. % NaCl (Fig.55b). The above P-T estimate and fluid composition from the primary inclusions in the quartz

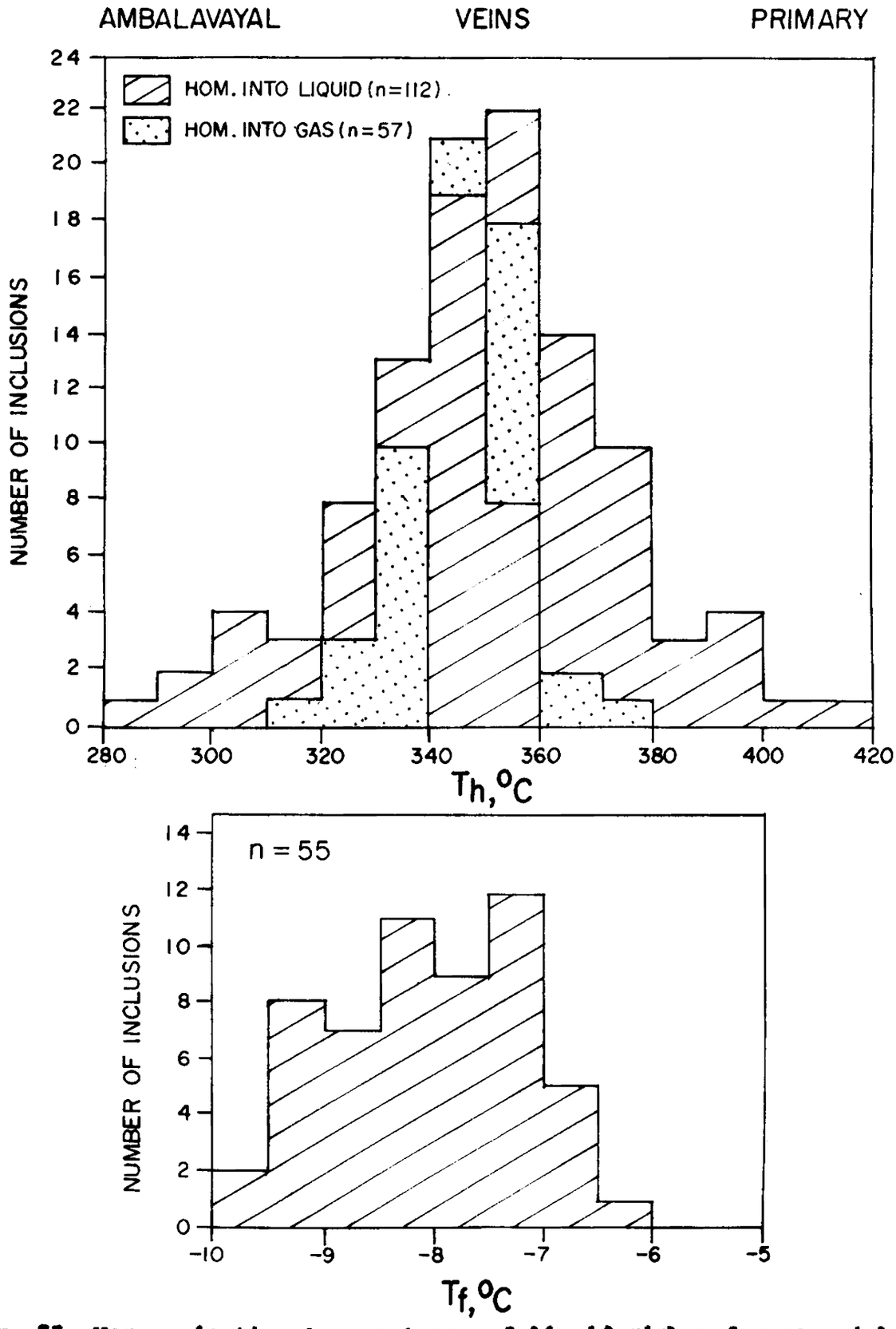

Fig. 35 Homogenisation temperatures of liquid-rich and vapor-rich inclusions (top) and ice melting temperatures of liquid -rich inclusions (bottom) in quarts from themineralised veins.

veins mark the deposition conditions and fluid parameters related to molybdenite mineralization in Ambalavayal. Similar temperature range, evidence of boiling and moderate salinity for the fluids have been recorded from molybdenite deposits elsewhere also (Bloom, 1981).

The combined temperature salinity data are plotted in the boiling point curves of NaCl-H_2O system as delineated by Haas (1971) in Fig.56. The data yield minimum fluid pressures ranging from 110-150 bars at the time of molybdenite precipitation. The depths estimated are from 1300-2000m.

Pseudosecondary aqueous inclusions in vein quartz homogenize into liquid between 170 and 280°C with a peak in the range, 200-230°C. The melting temperature of ice formed on freezing range from -7 to -3°C (Fig.57).

7.7. Cooling history of Ambalavayal granite

The isochores for carbonic inclusions associated with the granite quartz and pegmatite quartz are shown in a P-T space in Fig.58. The geothermometric estimate obtained from feldspar geochemistry can be used as independent controls of temperature. These have been superimposed in the figure, for a precise estimate of the actual pressure regimes. The intersection of the two-feldspar geothermometer with the CO_2 isochores for high density fluids yield pressures of 4.5-5.2 Kb for the granite crystallization. Feldspar thermometer of the pegmatites inter-

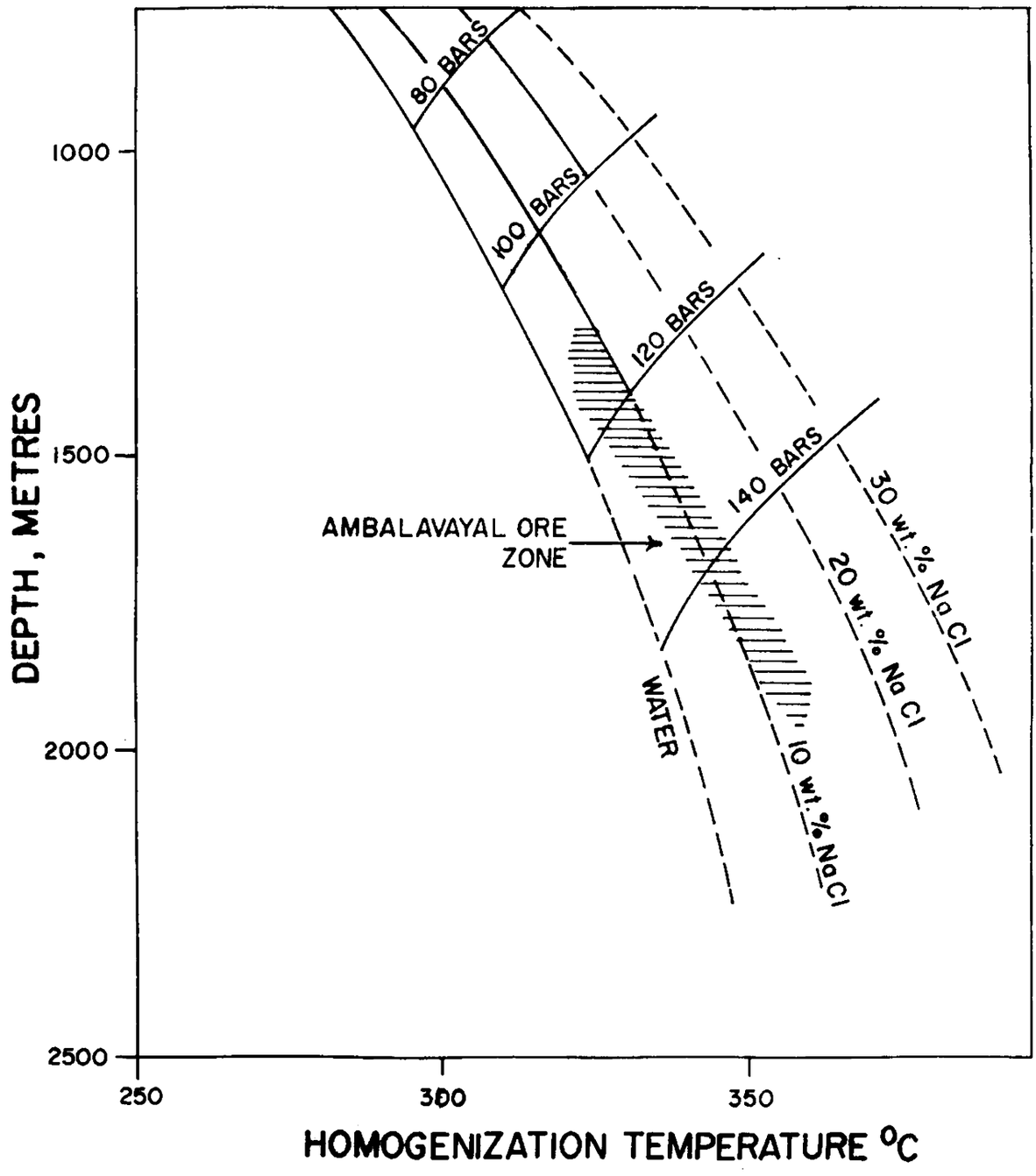

Fig. 36 Boiling point curves for various Na Cl-H_2O fluids (after Haas, 1971) showing the region of fluid inclusion data from Ambalavayal.

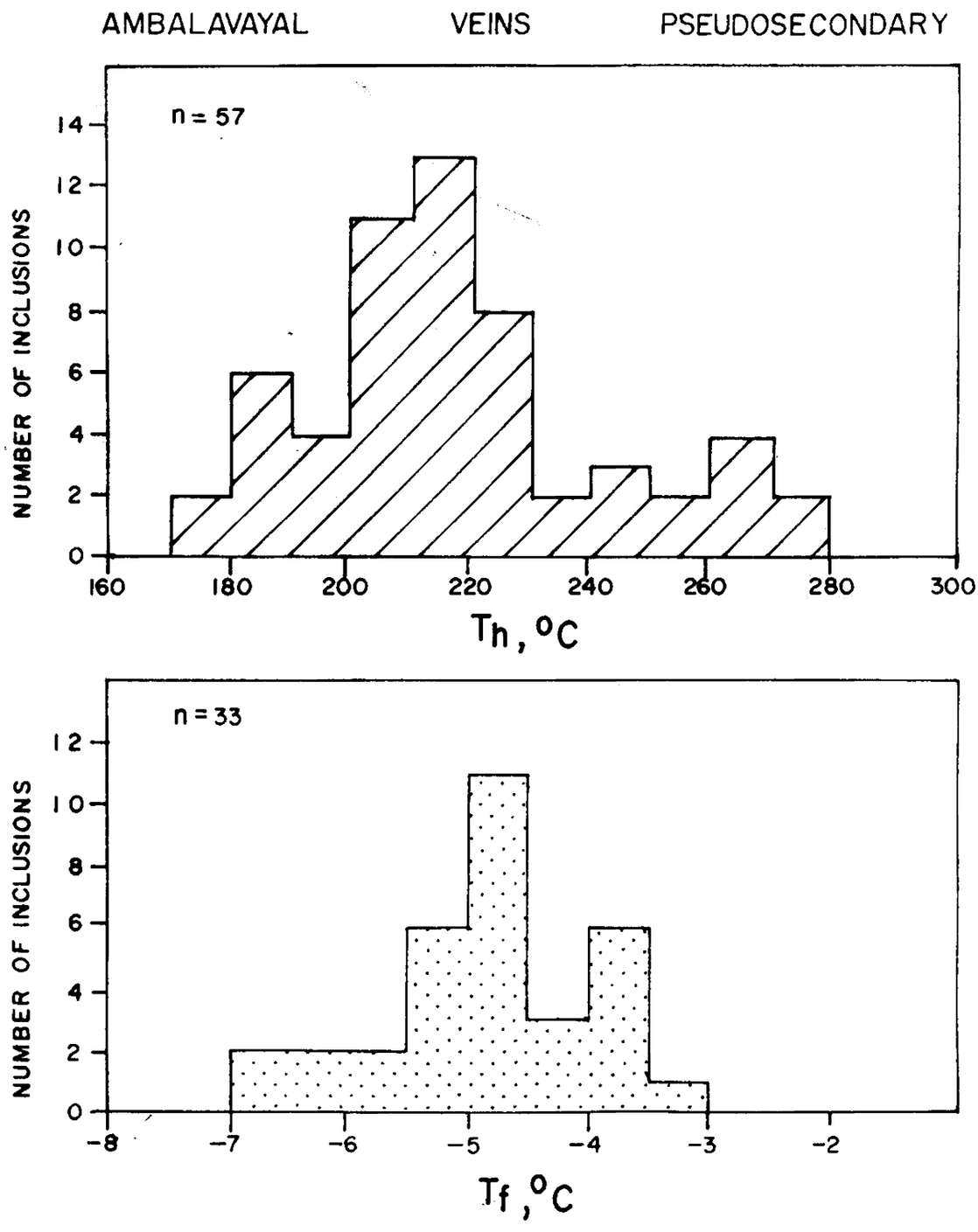

Fig. 57 Homogenisation (a) and ice-melting (b) temperatures of pseudosecondary liquid-rich inclusions in vein-quartz.

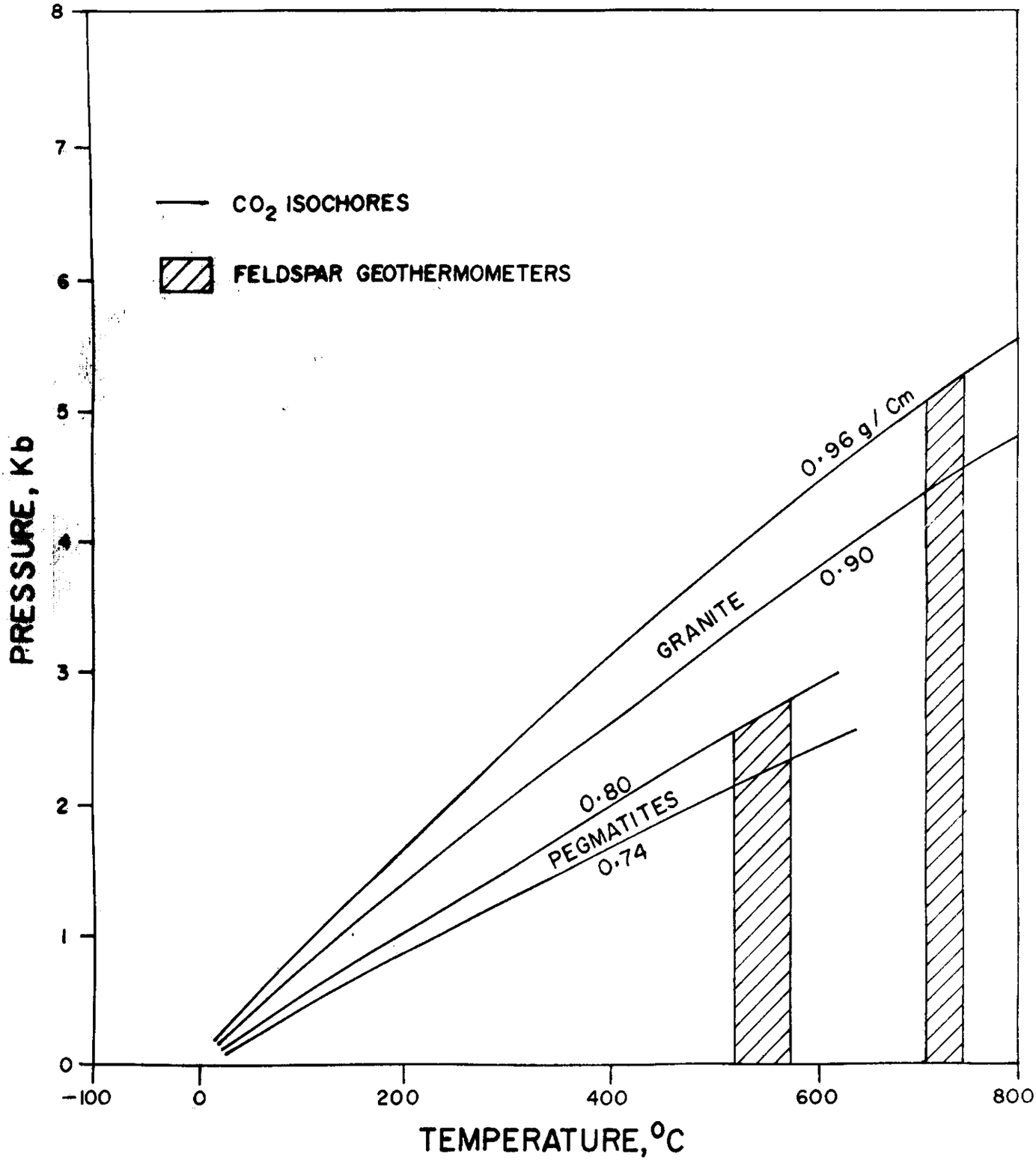

Fig. 58 Combined P-T diagram showing the isochores for carbonic inclusions in granite and pegmatites. The temperature estimates obtained from feldspar thermometry are superimpo

sect the moderate density CO_2 inclusions at 2.2 to 2.8 Kb. This value closely compares with the pressure estimate of 2.2 Kb obtained from the intersection of the CO_2-H_2O and CO_2 isochores of coexisting inclusions.

Combining the data from various isochores and thermometers, an evolution path of the fluids can be traced in a P-T space (Fig.59). This path or array would correspond to the cooling curve of the granite. The array obtained originates at the temperature region beyond that for the granite solidus. The trend followed is sub-parallel with the adiabatic gradient computed for a cooling granite pluton. The characteristic features of the array is its convexity towards the temperature axis, indicating that the rate of upward movement of the magma exceeded the rate of heat transfer. This is possible in the case of isothermal upward movement brought by extensional tectonics (Harris and Holland, 1984). As the Ambalavayal granite is emplaced near the intersection of two major fault-lineaments, it is envisaged that crustal distension resulting in decompression effected rapid upward movement under near-isothermal conditions. The convexity of the array is more pronounced in the temperature range of 350-500°C, correlatable with the values obtained for the region of CO_2-H_2O unmixing due to decompression. However, the absence of granophyric textures and the higher pressure-depth estimates obtained indicate that even-though extensional tectonics aided in magma generation and

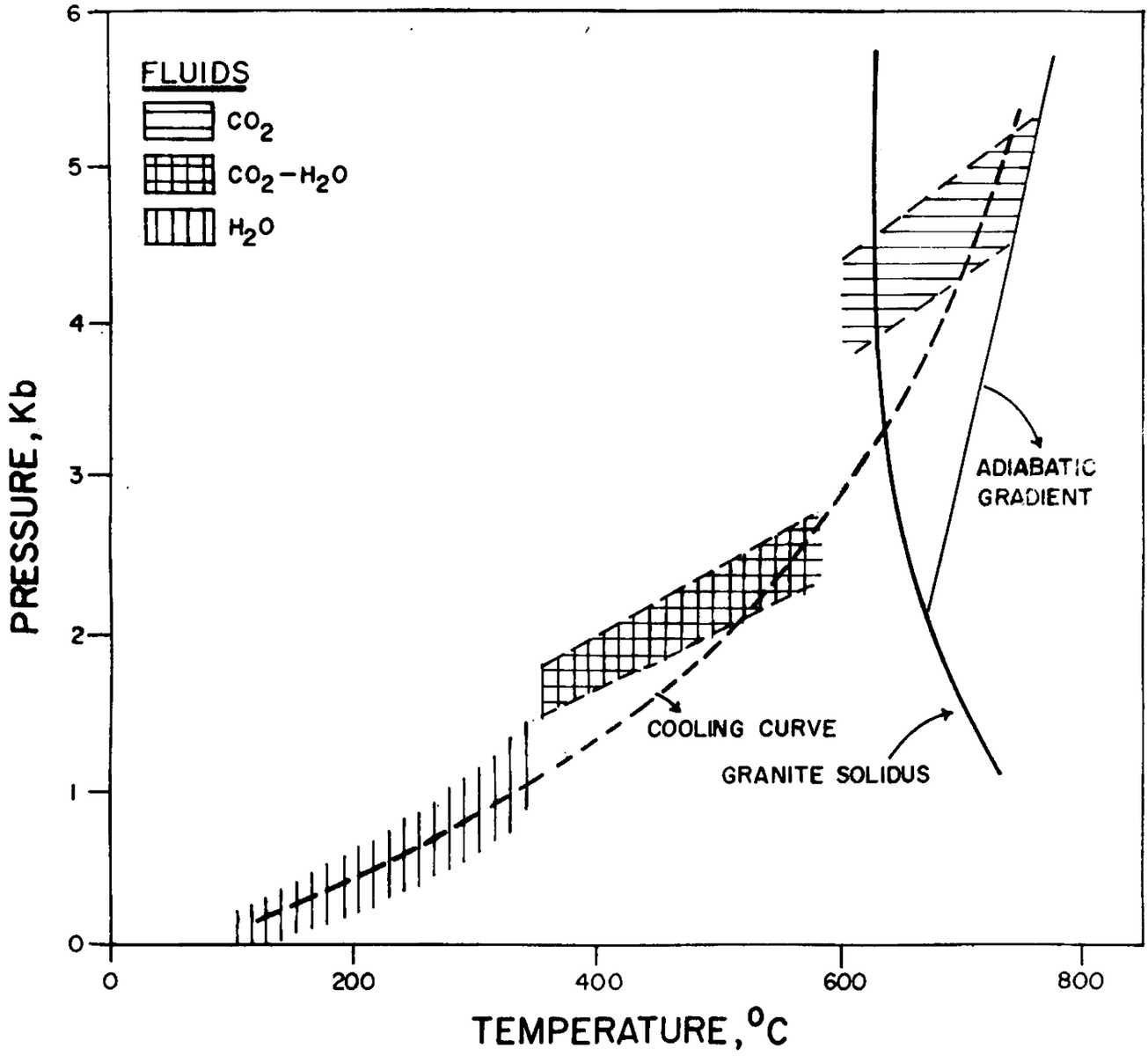

Fig. 59 Cooling curve of the granite computed from fluid inclusion data. The region of various fluids are also shown.

emplacement, the pluton was not emplaced near-surface. This is substantiated by the lower temperature region of the array, where it defines a rather steep dp/dT path.

7.8. Fluid evolution characteristics

The combined fluid inclusion data from the three quartz types show that the fluids evolved from early high density carbonic (0.95 g/cm^3) with traces of CH_4 (upto 10 mol. %) in the granite. The evolution proceeded through moderate density carbonic (0.80 g/cm^3) and mixed carbonic aqueous in the pegmatites where the fluids exsolved due to decreasing P-T conditions and increasing salinity. It is noted that traces of H_2O usually occur in carbonic inclusions entrapped at high P-T conditions. This aqueous phase occurs as a thin film wetting the inner surface of the inclusion cavity (Touret, 1981). With decrease in P-T regime, this H_2O phase and the one subsequently introduced during the crystallization of the granite together contributed to the unmixing of CO_2 and H_2O. Towards the late stage, the internal vapor pressure exceeded the external hydrostatic pressure resulting in adiabatic decompression and boiling of fluids. It is known that boiling of moderate salinity fluids can generate a large volume of vapor (Bloom, 1981). Boiling will also result in an enhancement of salinity (Roedder and Bodnar, 1980). Both these features are applicable in the area. The sudden pressure release and effervescence of vapor triggered the precipitation of molybdenite.

The computed fluid evolution path for Ambalavayal in terms of temperature, salinity and density is presented in Fig.60. Initially P_{CO_2} was dominant and P_{H_2O} subordinate. Subsequently, with the onset of hydrostatic regime, P_{CO_2} subsided, marked by the presence of H_2O rich fluids of density ranging from 0.50-0.75 g/cm^3. Fluids with moderate to high H_2O density (0.75-0.85 g/cm^3) and salinity mark the main ore stage in Ambalavayal. In the waning stage, the salinity again dropped with simultaneous increase in H_2O density (upto 0.95 g/cm^3) indicating that the late fluids were dominantly water-rich.

7.9. Transport and Deposition of molybdenum

Molybdenum is one of the trace elements which tend to be enriched in residual liquids during magmatic differentiation. While much work has been done on the distribution of a variety of trace elements, very little published data are available on the behaviour of molybdenum in silicic melts. The recent studies of Isuk (1983), Isuk and Carman (1981), Candella and Holland (1981) and Tingle and Fenn (1984) are the pioneer works in this regard.

Isuk and Carman (1981) suggest that the association of Mo with alkalic-silicic rocks indicates Mo-silicate and/or Mo-hydroxylated silicate complexes, based on the enhanced solubility of molybdenite in hydrous sodium and potassium disilicate melts. Isuk (1983) examined the effect of excess SiO_2 and

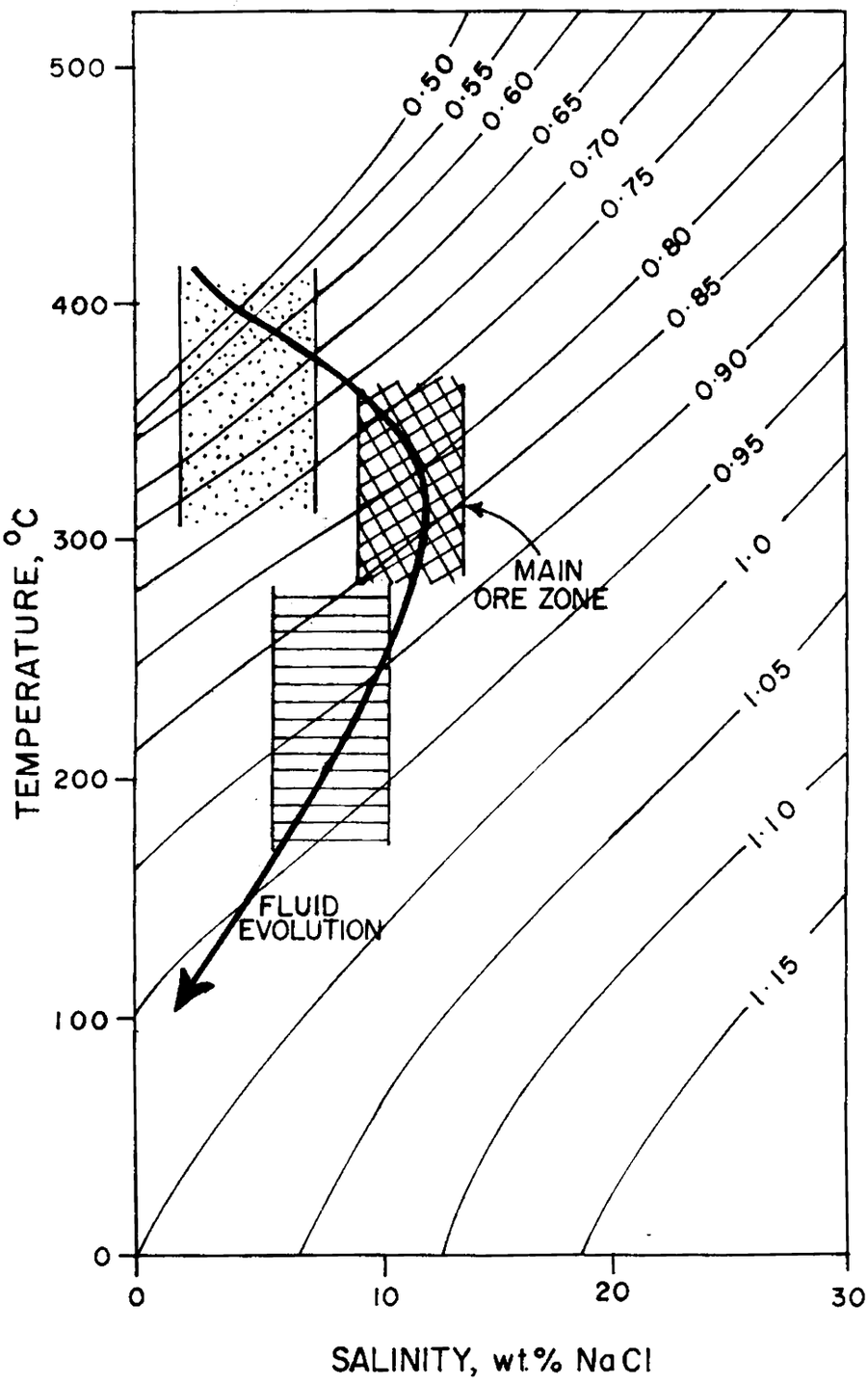

Fig. 60 Evolutionary path of ore fluids in Ambalavayal as computed from fluid inclusion data. The thin lines denote H_2O densities.

and CO_2 on the behaviour of molybdenite in vapor-saturated sodium silicate liquids, which is of importance in the present study. His experimental results show that molybdenite solubility in the vapor-saturated liquid decreases with increasing SiO_2 content. At SiO_2 + MoS_2 saturation, the hydrous sodium disilicate liquid contains approximately 2.5 wt. % molybdenite, representing 75% decrease relative to the value determined in the $Na_2Si_2O_5$ - H_2O system. With respect to the effect of CO_2 on the behaviour of molybdenum, it is found that CO_2 not only decreases the water content of the silicate liquid but also the molybdenite solubility. In the experimental study of Isuk (1983), a decrease of upto 64% in molybdenite solubility under CO_2-rich conditions relative to the value obtained in CO_2 deficient system is noted. The experimentally determined effect of CO_2 on the solubility of molybdenite can also be readily appreciated through a consideration of the solubility mechanism of CO_2 in silicate liquids and the concomitant effect on melt structure. CO_2 dissolves in silicate liquids principally as CO_3^{-2} complexes. Because of the affinity of CO_3^{-2} for Na^+ the degree of polymerization of the melt is further increased by the removal of Na^+ ions from their network-modifying role to form Na_2CO_3. The cumulative effect of these interactions is thus to substantially diminish Mo solubility in the silicate melt with increasing P_{CO_2}, consistent with the experimental data.

Regarding the effect of sulfur, it is found that sulfur lowers the Mo solubility further. Experimental results demonstrate that solubilities of alkali silicate melts decrease sympathetically with increasing polymerization. At sulfur saturation, molybdenum combines with any excess sulfur to form MoS_2, because of its strong chalcophile affinities, rather than dissolve inthe silicate melt.

Tingle and Fenn (1984) investigated the effects of fluorine and sulfur on the transport and concentration of molybdenum in granite-molybdenite deposits. Their studies indicate that fluorine is not important for the transport and concentration of molybdenum; the same magmatic processes that concentrate Mo must also concentrate fluorine. Candella and Holland (1984) also arrived at a similar conclusion. This implies that granitic melts that do not contain high fluorine content can also produce molybdenum mineralization.

The major aspect of Tingle and Fenn's (1984) study is their observation that molybdenum is preferentially partitioned into the vapor phase. The evolution of the vapor phase from the magma is a critical factor which controls the transport and deposition of molybdenum. They found that the initial water content of the magma, which controls the timing of theevolution of the vapor phase, and the presence of sulfur are major controls on Mo-ore deposition. The timing of the evolution of vapor phase may explain why many granites bear no economic

mineralization. When the vapor phase evolves at a later stage in the crystallization history of a magma, the volume of vapor available for ore deposition is small. This will cause deposition as small veinlets or crystallization as interstitial grains leading to disseminated-type deposits.

The presence of CO_2-rich fluid inclusions in quartz from the granite indicates that in the initial stages of crystallization CO_2 activity was dominant, which must have acted against the effective extraction of molybdenum from the source and its incorporation in the melt. The increased CO_2 activity also implies less water content, which controlled the timing of vapor evolution. The absence of fluorine-rich minerals in the granite is consistent with the view that F is not an important factor in the transport of molybdenum. With progressive fractionation, the melt became increasingly silicic, which reduced the solubility of molybdenum. This, coupled with the late stage evolution of a vapor phase (boiling) as observed from fluid inclusion data, triggered the precipitation of molybdenum. Combining with available sulfur, it formed disseminated molybdenite flakes. Tingle and Fenn (1984) observe that vapor saturation is most likely triggered by pressure decrease (decompression) during ascent. The granite petrogenesis as well as fluid inclusion data confirm decompression. It is presumed that the high initial CO_2 partial pressures and the late stage evolution of vapor phase adversely affected the effective extraction,

mineralization. When the vapor phase evolves at a later stage in the crystallization history of a magma, the volume of vapor available for ore deposition is small. This will cause deposition as small veinlets or crystallization as interstitial grains leading to disseminated-type deposits.

The presence of CO_2-rich fluid inclusions in quartz from the granite indicates that in the initial stages of crystallization CO_2 activity was dominant, which must have acted against the effective extraction of molybdenum from the source and its incorporation in the melt. The increased CO_2 activity also implies less water content, which controlled the timing of vapor evolution. The absence of fluorine-rich minerals in the granite is consistent with the view that F is not an important factor in the transport of molybdenum. With progressive fractionation, the melt became increasingly silicic, which reduced the solubility of molybdenum. This, coupled with the late stage evolution of a vapor phase (boiling) as observed from fluid inclusion data, triggered the precipitation of molybdenum. Combining with available sulfur, it formed disseminated molybdenite flakes. Tingle and Fenn (1984) observe that vapor saturation is most likely triggered by pressure decrease (decompression) during ascent. The granite petrogenesis as well as fluid inclusion data confirm decompression. It is presumed that the high initial CO_2 partial pressures and the late stage evolution of vapor phase adversely affected the effective extraction,

transportation and deposition of molybdenite in Ambalavayal. However, association of CO_2 seems to have played a positive role in concentrating the light rare earths as indicated by their higher levels in the granite.

Hence the epilogue would be: 'had there been higher initial water content in the magma and had the vapor phase evolved at an earlier stage, an economic mineral deposit of molybdenum would have been present in Ambalavayal'.

CONCLUSIONS

The Ambalavayal granite is an E-W elongated elliptical pluton emplaced within Precambrian trondhjemitic gneisses. The granite is spatially related to the intersection point of two major taphrogenic lineaments, namely, the E-W trending Moyar and the NE-SW trending Calicut lineaments. The rock is pink, medium to coarse grained, composed of interlocking quartz and feldspar, with hornblende as the major mafic constituent. E-W and NE-SW trending pegmatites cut across the granite, mainly towards the western region of the pluton. The pegmatites show a mineral assemblage of quartz, pink K-feldspar and hornblende with subordinate biotite.

Molybdenite occurs as small flakes and flaky aggregates. It is found as disseminations within an 800 m wide zone trending NW-SE in the granite. Disseminated flakes of molybdenite also occur associated with the pegmatites. Molybdenite forms flaky aggregates measuring upto 20 cm in quartz veins. The wall rock alteration is mainly of potassic type, represented by the development of large pink K-feldspar megacrysts.

The granite exhibits a general hypidiomorphic granular texture with quartz, perthitic K-feldspar and plagioclase as the dominant minerals. Modal analyses show the following ranges: quartz: 22.3-37.1; K-feldspar: 24.2-48.3; plagio-

-clase: 22.3-37.5; hornblende: 0.5-3.6; biotite: 0.7-4.1; riebeckite: 0.2-2.5; sphene + monazite: 0.2-3.2; opaques: 0.2-1.5; calcite + apatite: 0.2-1.3 and the rest comprising alteration products like epidote and sericite. Considering the albitic composition of plagioclase, the modal Q-A-P data classify the rock as quartz alkali feldspar granite.

The structural formulae of feldspars calculated from chemical analyses of seventeen feldspar fractions fit well with the standard structural formulae. Mol per cent feldspar end members range from $Or_{54.73}Ab_{22.51}An_{2.83}$ to $Or_{74.0}Ab_{40.52}An_{7.38}$ in alkali feldspars and $Or_{5.76}Ab_{79.57}An_{8.70}$ to $Or_{11.73}Ab_{83.87}An_{12.84}$ in plagioclase. X-ray studies on the structural state of feldspars indicate varying degree of triclinicity, the higher degree of ordering being attained in the alkali feldspars from the pegmatites. Plots of albite content in coexisting alkali feldspar and plagioclase pairs from the granite indicate a temperature of 722-740°C for their equilibration. The alkali feldspars in the pegmatites yield an estimate of 525-580°C.

Geochemistry of hornblende separates from the granite indicates an edenitic composition, while the biotites correspond to annite. The hornblendes typically show high Al_2O_3 contents (9.69-11.89) comparable with those from anorogenic granites. The biotites are characteristically low Mg-type, similar to those reported from alkaline rocks. The variations in the distribution coefficients of elements between coexisting

biotite and hornblende indicate near-chemical equilibrium conditions of crystallization. The biotite-hornblende tie lines in the compositional triangle, Fe^{3+}-Fe^{2+}-Mg lie parallel to those of buffered biotites, indicating crystallization in an environment closed to that of oxygen and well above the Ni-NiO buffer. It is inferred that the fH_2O increased towards the residual stage and fO_2 values were very high.

X-ray studies of molybdenite samples show peaks at 2 θ values of ca. 14.5, 29.3, 39.6 and 44.4. The data indicate that the molybdenite corresponds to hexagonal $2H_1$ polytype. Chemical analyses show molybdenum contents of 57.83 to 58.99 wt. per cent.

The Rb-Sr isochron constructed on the basis of Rb and Sr determinations of seven whole rock samples of the granite yields an age of 595 $\pm$ 20 Ma and an initial Sr-isotope ratio of 0.7171 $\pm$ 0.0022. K-Ar age of biotite from the granite is measured as 560 $\pm$ 30 Ma. The data correspond to a Late Precambrian-Early Palaeozoic magmatism in the region, envisaged to be part of a widespread anorogenic magmatic event in the region, with probable relation to the pre-rift tectonics of the Indian continent. Further geochronologic studies on similar alkaline plutons of the region are recommended.

Major and trace element determinations in twenty four representative samples of the granite indicate close

correspondence with those of other alkali granites of the region and elsewhere. Higher K_2O (upto 7.24) with K_2O/Na_2O ratios consistently greater than unity and low CaO (0.46-2.69) and MgO (0.32-0.64) are characteristic. A-F-M plots show an alkali enrichment trend and K-Na-Ca plots indicate a dominant K-enrichment. In Harker variation diagrams, the oxide weight percentages show overall smooth variation trends against SiO_2. Thus, Al_2O_3 and Na_2O show slight increase whereas all the other elements show depletion towards higher SiO_2 levels. In Na_2O vs. K_2O diagram, the plots of the granite fall in the field of adamellite. In SiO_2 vs. $Log_{10}K_2O/MgO$ diagram, the plots fall dominantly in the field of alkali granite. In the mol per cent SiO_2-Al_2O_3-Na_2O +K_2O diagram, the plots of the granite fall close to the divide between calc-alkalic and comendite fields, being close to the quartz-feldspar cotectics. The mineralogic and geochemical characters of the granite indicate a transition between I and A-type granites.

Among trace elements, the granite shows high transition elements (Cr, Ni) and low contents of large ion lithophile elements (Ba, Rb, Sr). Enrichment of high field strength elements (Nb, Zr, Y) is characteristic. The trace element data indicate that alkali feldspar and hornblende were the dominant fractionating phases. The depletion of LREE and La/Y and Ce/Y ratios is also typical. The chemical changes observed in the granite pluton suggest that the melt under-

-went in situ fractionation with late stage separation of the residual phase which crystallized as pegmatites and aplites.

Petrogenetic considerations show that the generation and emplacement of the magma were controlled by the pre-rift tectonics of the continent. Crustal distension caused large scale mantle degassing, leading to the addition of volatiles to the overlying rocks, resulting in localised melting. The taphrogenic lineaments acted as conduits for the transfer of CO_2-rich volatiles. The extremely high K/Rb values imply a K-enriched, Rb-depleted deep crustal or upper mantle source. The enrichment of LREE and HFS elements serves as additional proof for the involvement of CO_2-rich volatiles which effectively scavenged these elements. The high initial Sr-isotope levels exhibited by the granite is conceived to be the result of either crustal contamination or selective enrichment of ^{87}Sr or both. It is proposed that this hypothesis be further tested through detailed studies on similar alkalic plutons of the region.

The geochemical signatures of ore potential in the granite include higher SiO_2, K_2O and Na_2O levels. The Q+Ab+Or values (normative) of the granite range from 87.8 to 95.4, which are in good agreement with the estimated value of greater than 80% for granite-molybdenite systems. Whole rock molybdenum levels define a NW-SE trending anomaly, which closely corresponds to the anomaly defined by the $K_2O/K_2O + Na_2O$ values in the granite. Spatial relationship of the molybde-

-nite mineralization with the major fault-lineaments of the region suggests an episode of taphrogenic metallogeny.

Geochemistry of the basement gneisses indicates a low alumina trondhjemitic composition. Major and trace element variations denote an igneous derivation, involving feldspar and amphibole fractionation. Petrogenetic evaluation suggests a lithophile-rich trondhjemitic magma was extraced from the mantle, which underwent subsequent crystal fractionation. This magmatism is correlatable with a regional magmatism of the type contemporaneous with the stabilisation of the craton during the Archaean times. It is suggested that future work should involve systematic geochronologic and isotope studies of the gneisses in order to evolve a complete picture on the crustal evolution of the region. Similarly, the petrogenetic features can be further characterised only through REE (both LREE and HREE) studies.

Fluid inclusion studies in quartz associated with the granites, pegmatites and quartz veins show various genetic and phase-types of inclusions, corresponding to different generations of fluids. The quartz from the granite shows a positive correlation between the percentage of carbonic inclusions and the major mafic minerals. Carbonic inclusions are thus more abundant in the hornblende-rich zone. Heating-freezing studies show that the monophase inclusions entrapped nearly pure CO_2, with a density of 0.90-0.95 g/cm^3.

Some of them contain upto 10 mol per cent of CH_4. Data on the coexisting CO_2 and CO_2-H_2O inclusions in pegmatites show their simultaneous entrapment at 2.2 Kb and 500°C. The lower limit of mixed fluids is estimated to be 310°C and 0.5 Kb. The mineralised quartz veins record entrapment of heterogeneous fluids at a temperature range of 340-360°C, denoting 'boiling' of the mineral forming media. The salinities of the solution ranged from 8 to 15 wt. per cent NaCl at the time of mineralization. The minimum fluid pressures estimated range from 110-150 bars at depths of 1300-2000 m at the time of molybdenite precipitation. The cooling curve of the granite constructed from the combined P-V-T data show a T-convex path, indicating that the rate of upward movement of the magma exceeded the rate of heat transfer process. This is possible in the case of near-isothermal upward movement brought by extensional tectonics. The fluid evolution is characterised by high P_{CO_2} and low P_{H_2O} in the early stages. Fluids with moderate to high H_2O densities (0.75-0.85) and salinities mark the main ore stage. On the waning stage, the salinity again dropped, with simultaneous increase in H_2O density (upto 0.95 g/cm^3) indicating a later hydrostatic regime.

It is envisaged that high initial P_{CO_2} acted against the effective extraction of molybdenum from the source, as Mo

is less soluble in CO_2-rich fluids. Subsequently, with progressive fractionation, the melt became increasingly silicic, reducing the solubility of molybdenum in the melt. This, coupled with the late stage evolution of vapor phase (boiling) triggered by adiabatic decompression, resulted in the resurgent precipitation of molybdenum. which combined with the available sulfur. Sulfur isotope studies are recommended to evolve a genetic model of the ore fluids in Ambalavayal.


a


b


c

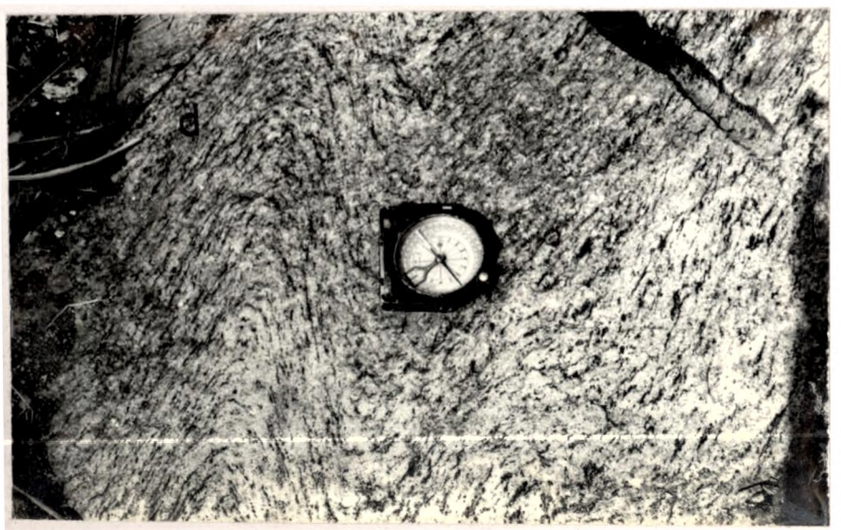
d


a

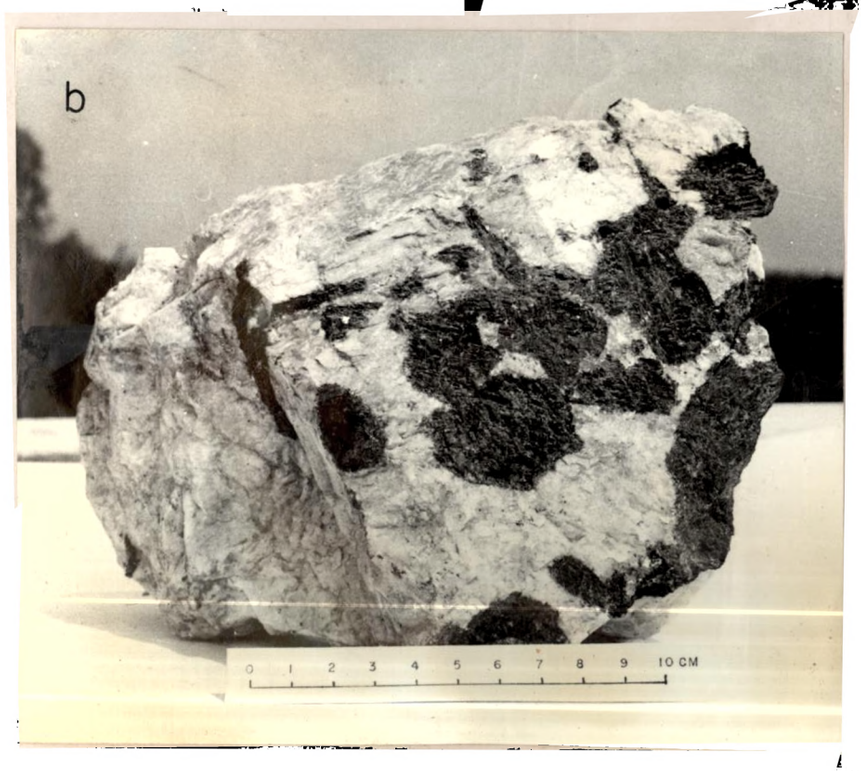
b
0 1 2 3 4 5 6 7 8 9 10 CM

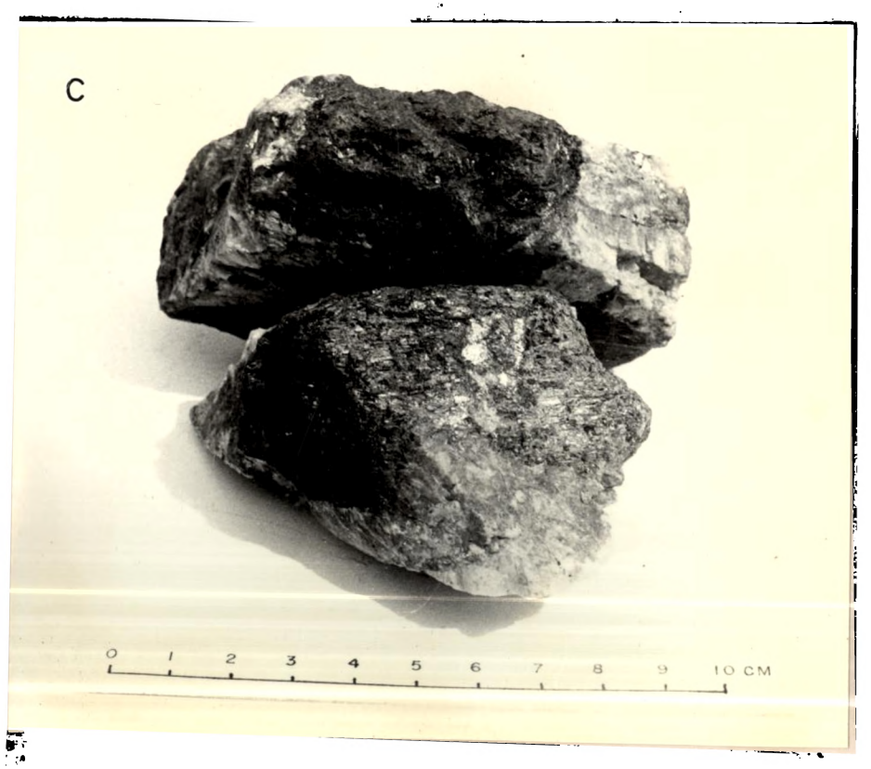
c
0 1 2 3 4 5 6 7 8 9 10 CM

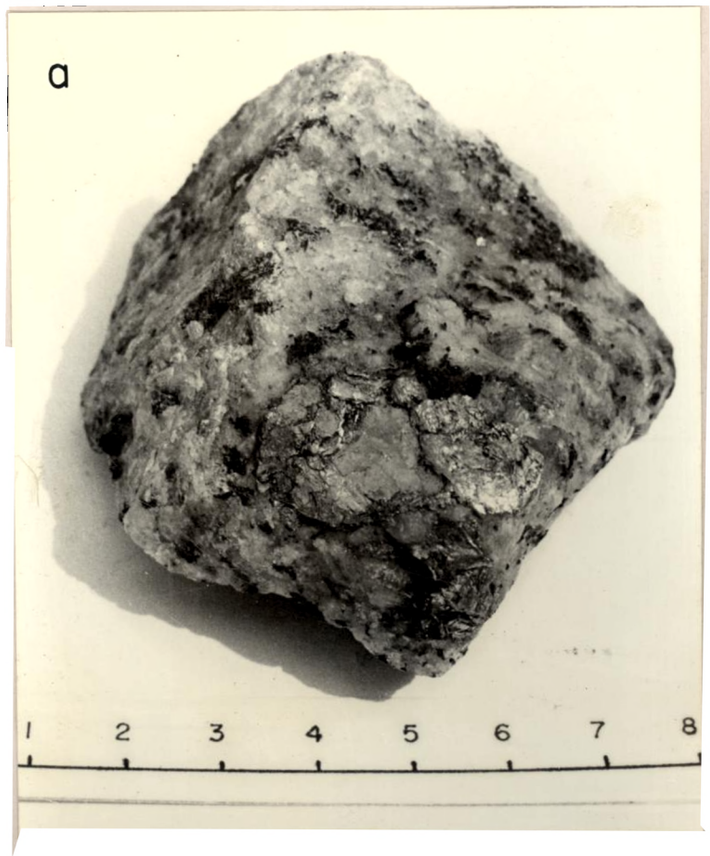
a
1 2 3 4 5 6 7 8


b
1 2 3 4 5 6 7 8 9 10 CM

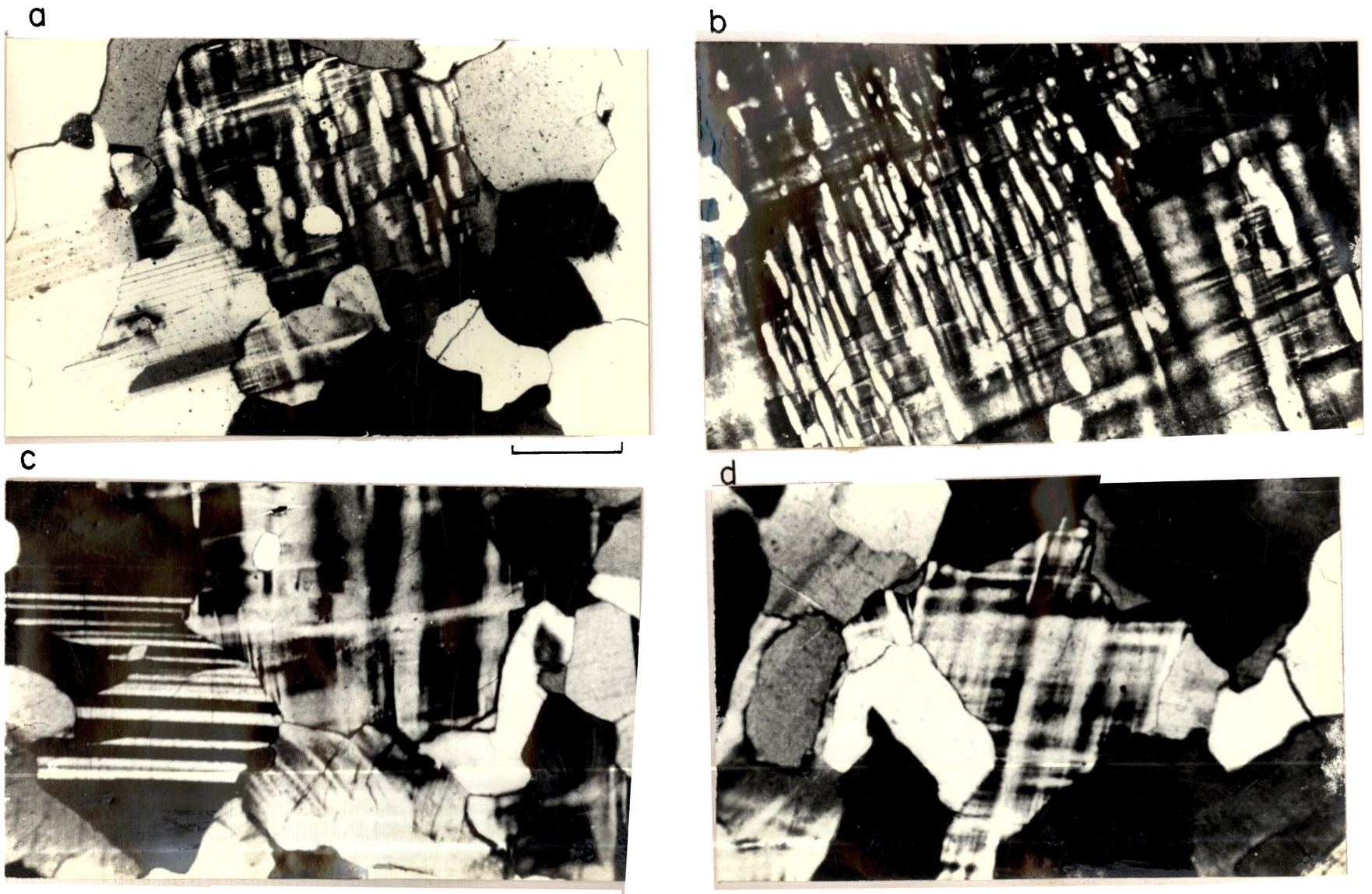
a
b
c
d

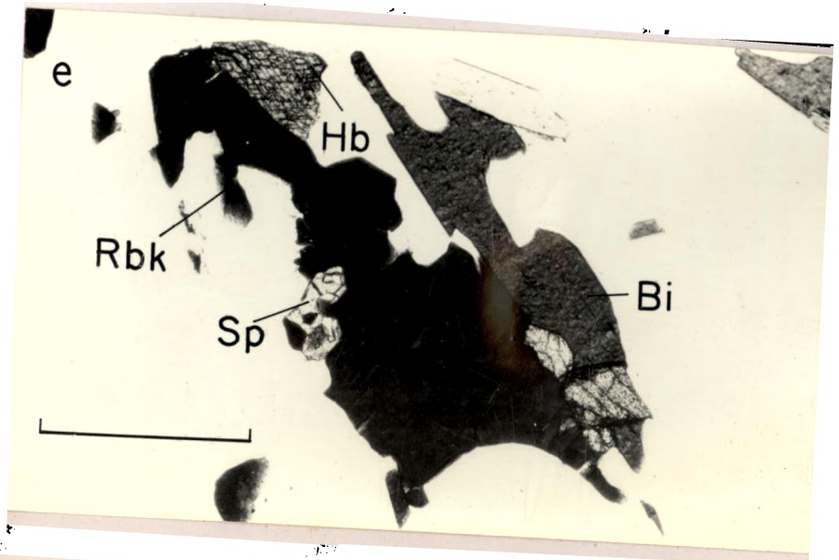
e
Hb
Rbk
Bi
Sp

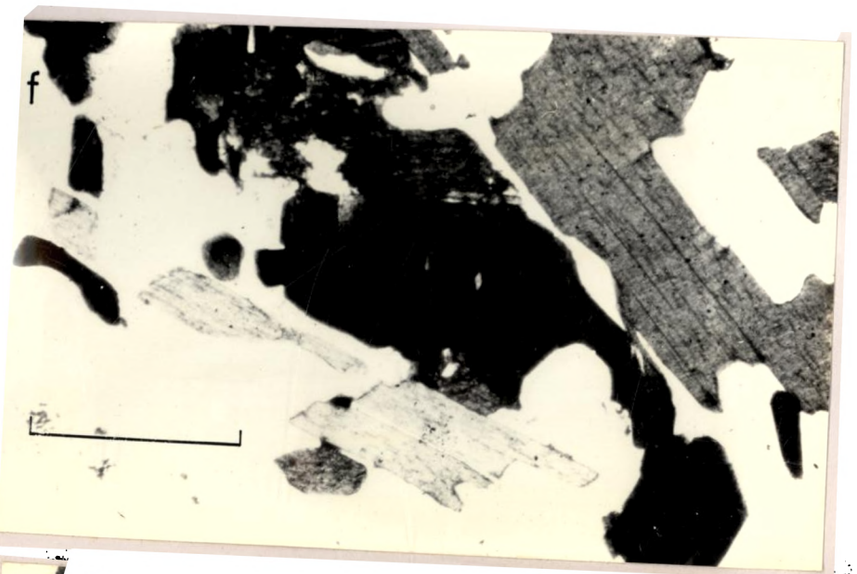
f

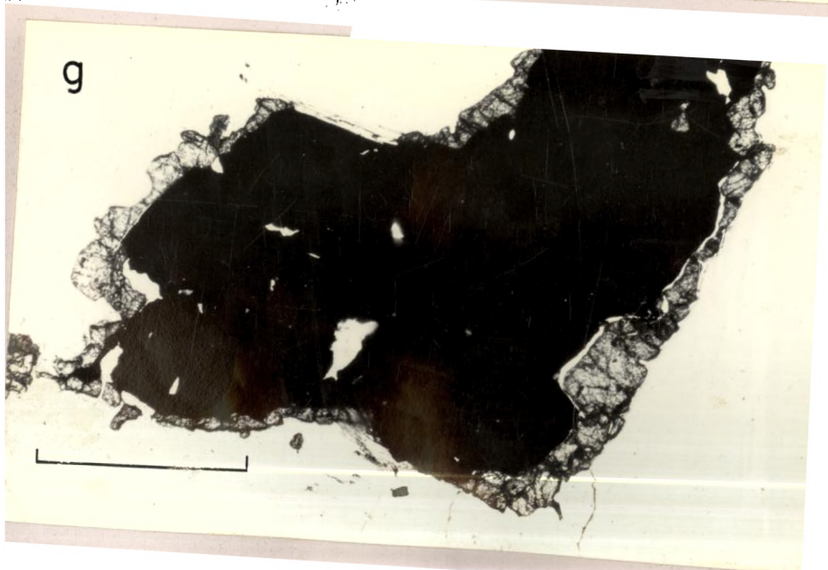
g

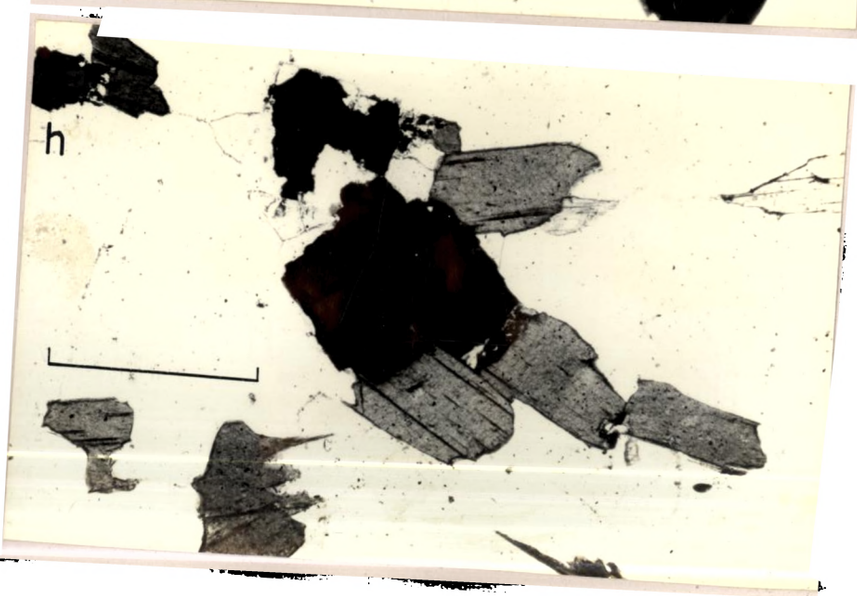
h

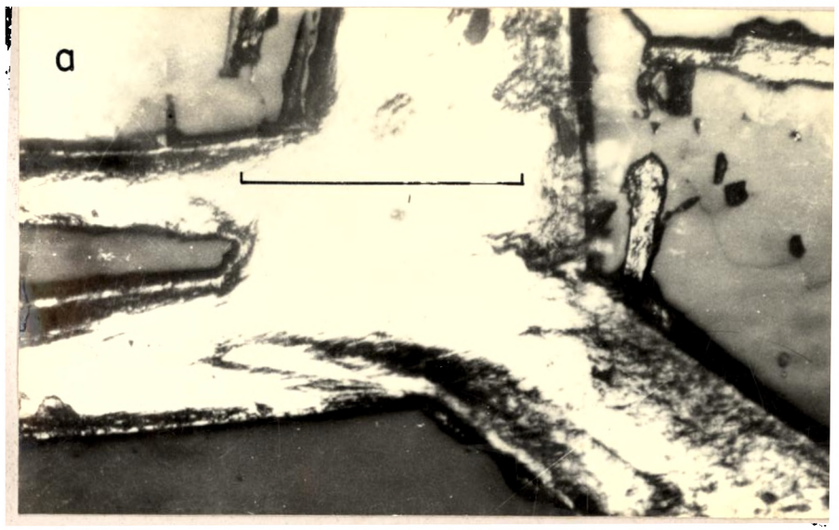
a

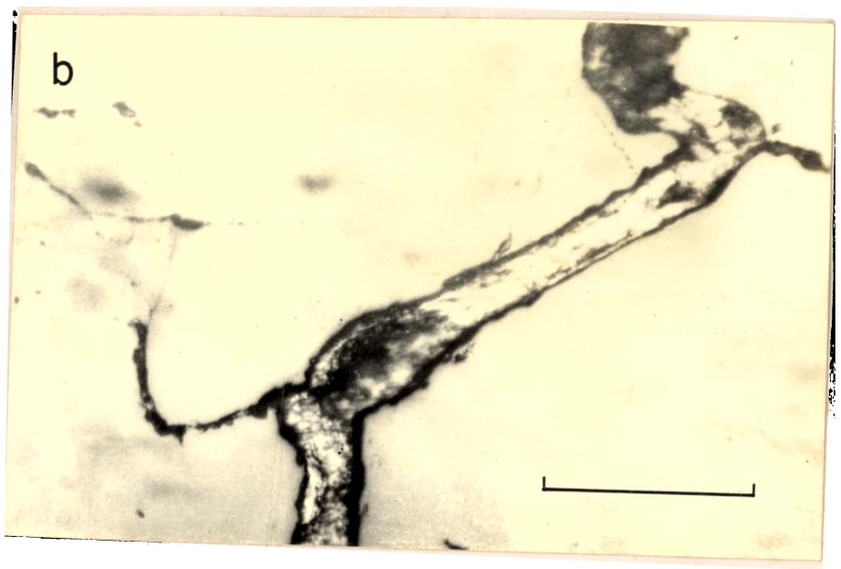
b

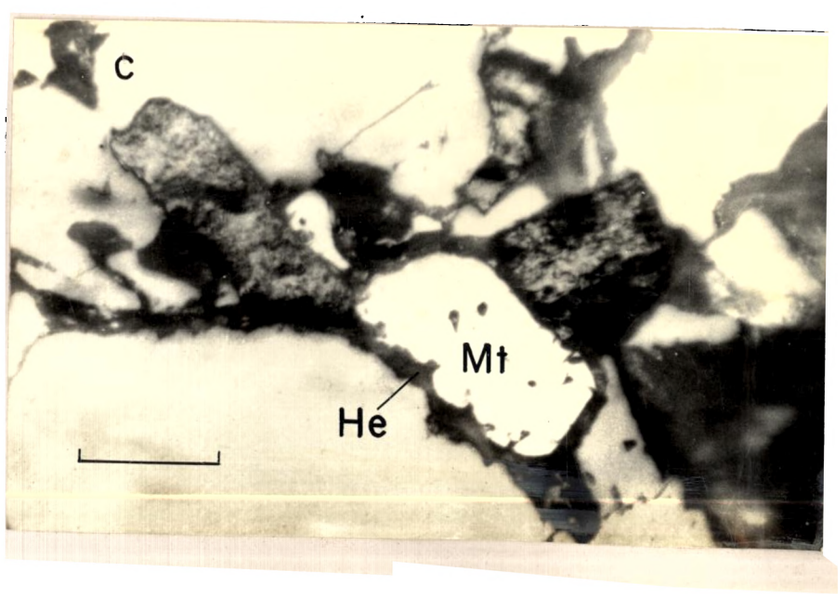
c
Mt
He

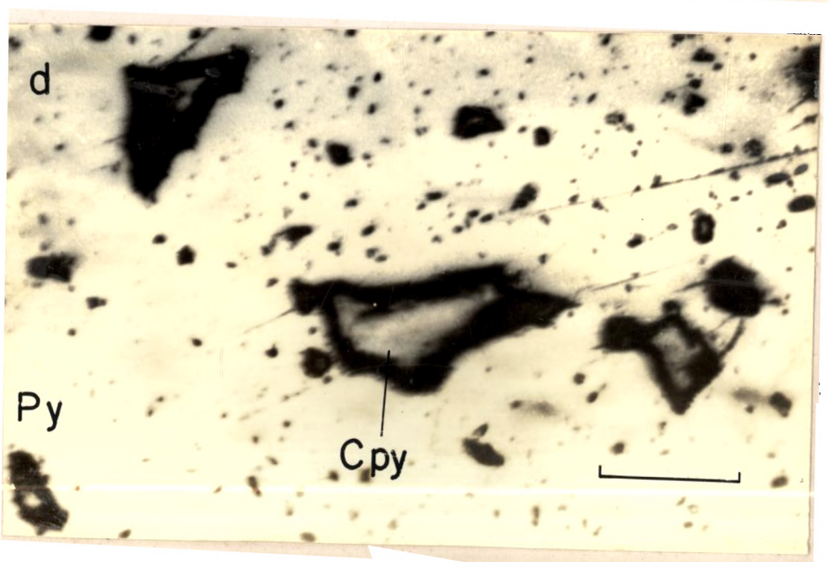
d
Py
Cpy

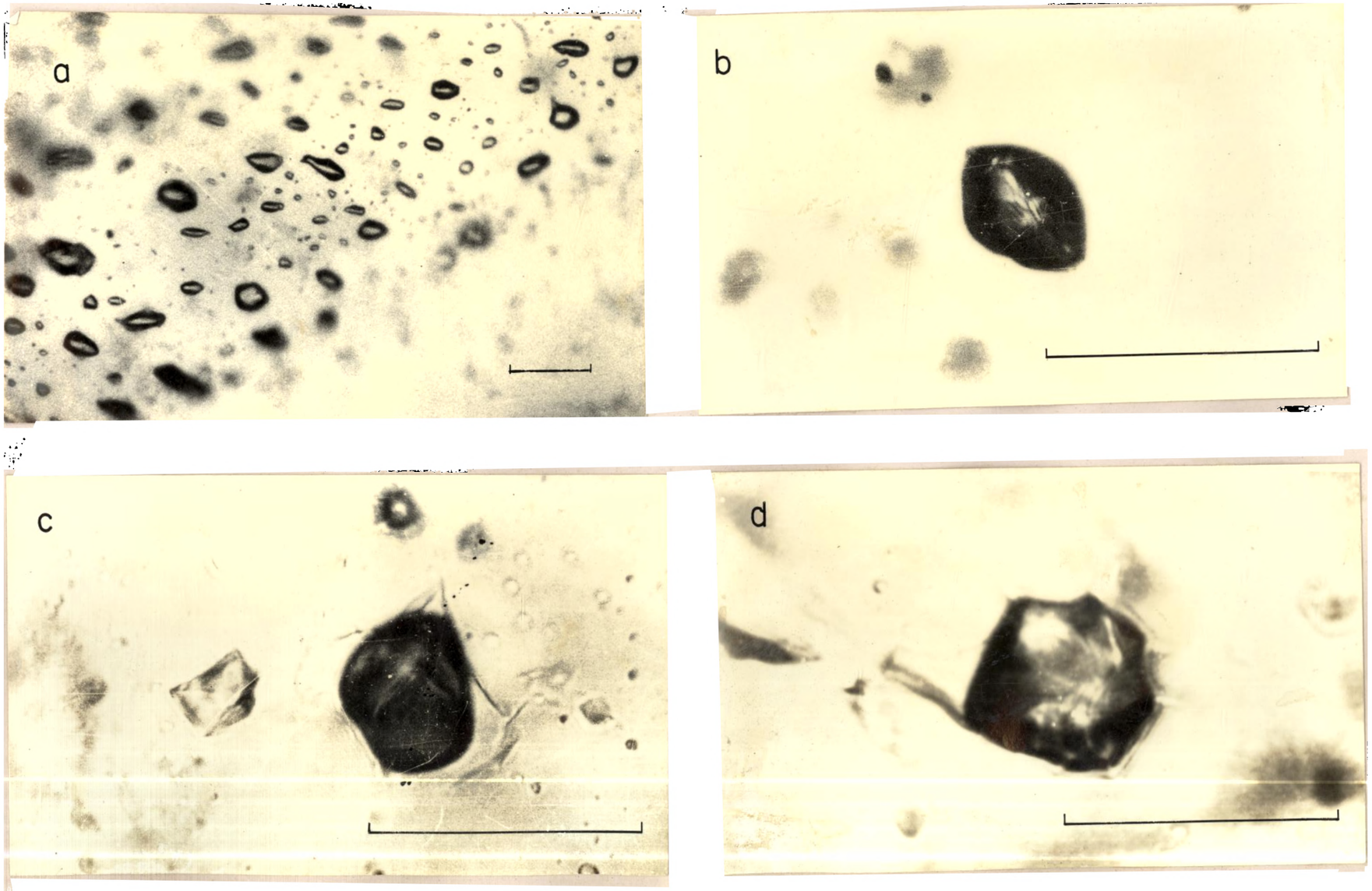
a
b
c
d

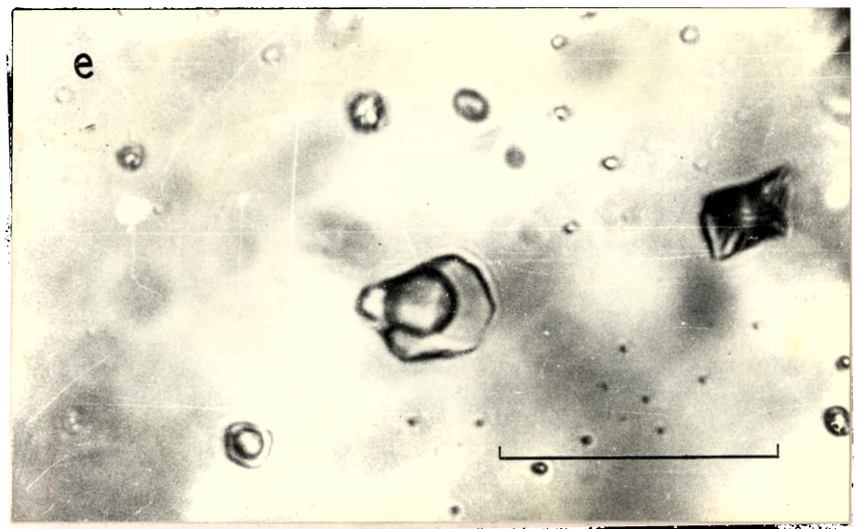
e

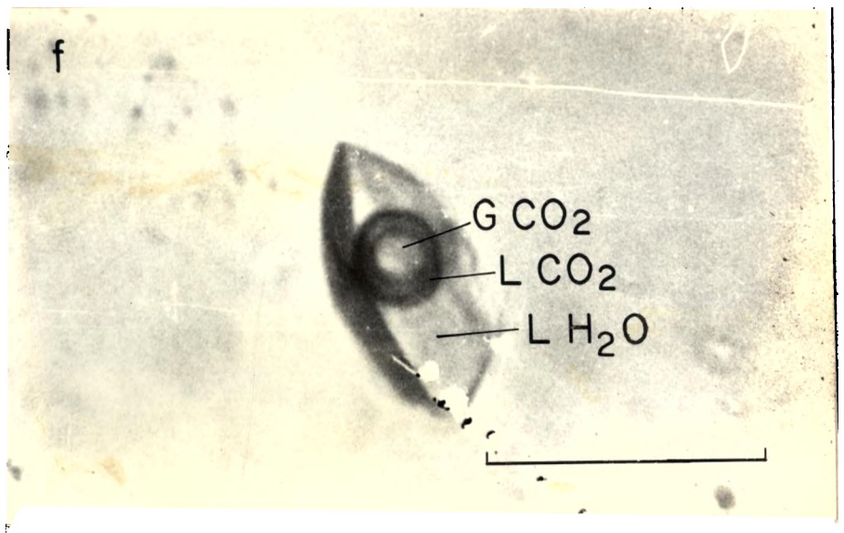
f
G CO_2
L CO_2
L H_2O

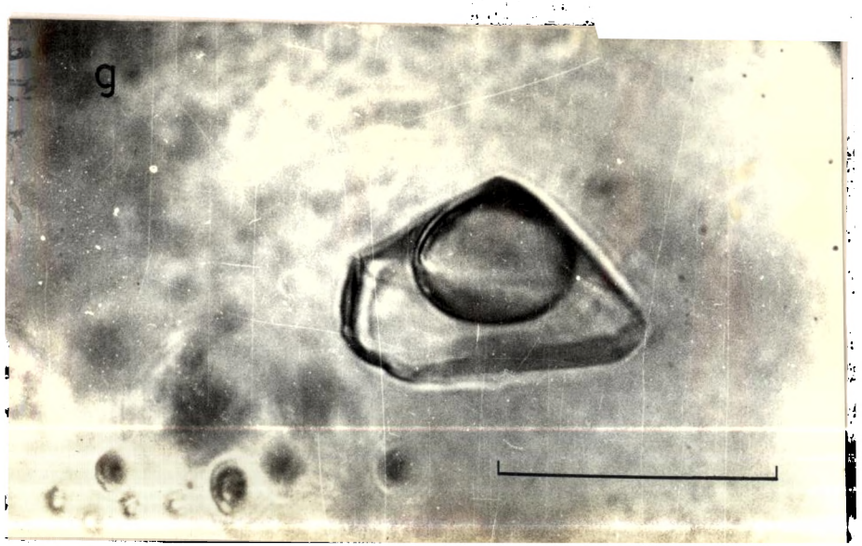
g


h

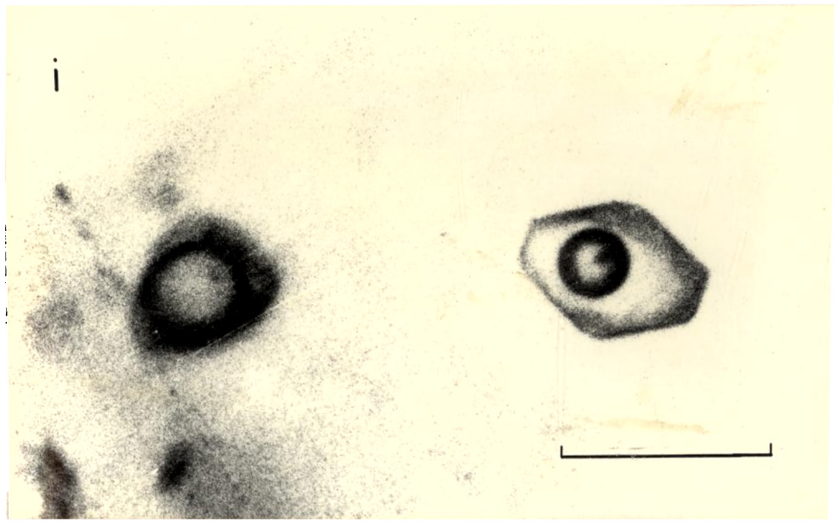
i

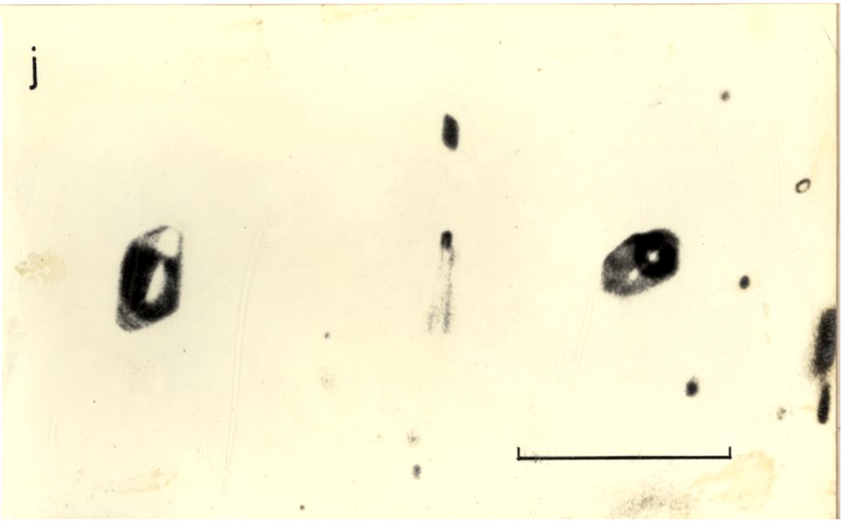
j

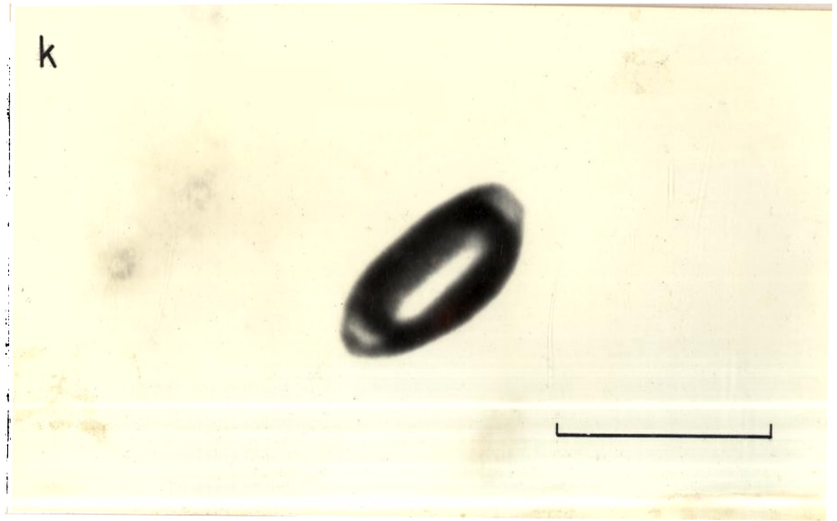
k

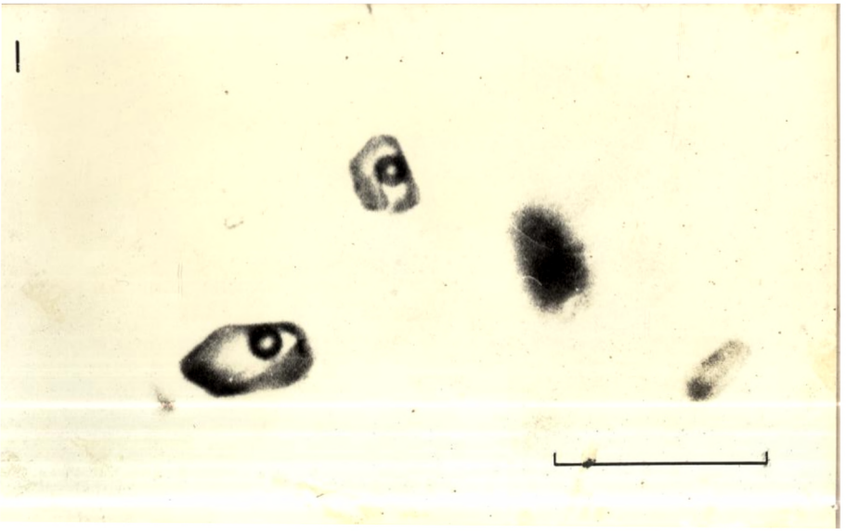
l

REFERENCES

1. Albuquerque, C.A.R., (1973) Geochemistry of biotites from granitic rocks of northern Portugal. Geochim. Cosmochim. Acta, 37, 1779-1802.

2. Albuquerque, C.A.R., (1975) Partition of trace elements in coexisting biotite, muscovite and potassium feldspar of granitic rocks, Northern Portugal. Chem. Geol., 16, 89-108.

3. Anderson, J.L., (1980) Mineral equilibria and crystallization conditions in the late Precambrian Wolf River rapakivi massif, Wisconsin. Am. Jour. Sci., 280, 289-332.

4. Anderson, J.L., Cullers, R.L. and Van Schmus, W.R., (1980) Anorogenic metaluminous and peraluminous granite plutonism in the mid-Proterozoic of Wisconsin, U.S.A. Contrib. Mineral. Petrol., 74 311-328.

5. Arth, J.G. and Barker, F., (1976) Rare earth partitioning between hornblende and dacitic liquid and implications for the genesis of trondhjemitic-tonalitic magmas. Geology, 4, 534-536.

6. Arth, J.G. and Hanson, G.N., (1972) Quartz diorites derived by partial melting of eclogite or amphibolite at mantle depths. Contrib. Mineral. Petrol., 37, 161-174.

7. Aswathanarayana, U., (1965) Isotopic ages from the Eastern Ghats and Cuddapahs of India. Jour. Geophys. Res., 69, 3479-3486.

8. Bailey, D.K., (1974) Experimental petrology relating to oversaturated peralkaline volcanics: a review. Bull. Volcan., 38, 637-652.

9. Bailey, D.K., (1977) Lithosphere control of continental rift magmatism. Jour. Geol. Soc. London, 133, 103-106.

10. Bailey, D.K. and Macdonald, R., (1969) Alkali feldspar fractionation trends and the derivation of peralkaline liquids. Amer. Jour. Sci., 267, 242-248.

11. Bailey, D.K. and Scharier, J.F., (1966) The system Na_2O-Al_2O_3-Fe_2O_3-SiO_2 at 1 atmosphere and the petrogenesis of alkaline rocks. Jour. Petrol., 7, 114-170.

12. Barker, F., (1979) Trondhjemite: definition, environment and hypothesis of origin. in Barker, F., (ed.) Trondhjemites, dacites and related rocks. Elsevier, pp. 1-12.

13. Barker, F. and Arth, J.G., (1976) Generation of trondhjemitic-tonalitic liquids and Archaean bimodal trondhjemite-basalt suites. Geology, 4, 596-600.

14. Barker, F., Arth, J.G., Peterman, Z.E and Friedman, I., (1976) The 1.7-1.8 b.y. old trondhjemites of south-western Colorado and northern New Mexico-geochemistry and depths of genesis. Geol. Soc. Am. Bull., 87, 189-198.

15. Barker, F., Wones, D.R., Sharp, W.N. and Desborough, G.A., (1975) The Pikes Peak Bathalith, Colorado front range, and a model for the origin of the gabbro-anorthosite-syenite-potassic granite suite. Precamb. Res., 2, 97-160.

16. Blaxland, A.B., (1976) Rb-Sr isotopic evidence for the age and origin of the Ivigtut granite and associated cryolite body, south Greenland. Econ. Geol., 71, 864-869.

17. Blaxland, A.B and Parsons, I., (1975) Age and origin of the Klokken gabbro-syenite intrusion, south Greenland: Rb-Sr study. Geol. Soc. Denmark Bull., 24, 27-32.

18. Bloom, M.S., (1981) Chemistry of inclusion fluids: Stockwork molybdenum deposits from Questa, New Mexico, and Hudson Bay Mountain and Endako, British Columbia. Econ. Geol., 76, 1906-1920.

19. Bowden, P., (1974) Oversaturated alkaline rocks, granites, pantellerites and commendites in Sorensen, H., (Ed.). The alkaline rocks. John Wiley, New York, 109-123.

20. Bowden, P. and Turner, D.C., (1974) Peralkaline and associated ring complexes in the Nigeria - Niger province, west Africa. in Sorensen, H., (Ed.) The alkaline rocks. John Wiley, New York, 330-354.

21. Bowen, N.L., (1928) The evolution of the igneous rocks. Princeton University Press, Princeton, N.J., 334 p.

22. Bridgwater, D. and Collerson, K.D., (1976) The major petrological and geochemical characters of the 3600 m.y. Uivak gneisses from Labrador. Contrib. Mineral. Petrol., 54, 43-59.

23. Brown, W.L. and Parsons, I., (1981) Towards a more practical two-feldspar geothermometer. Contrib. Mineral. Petrol., 76, 369-377.

24. Buddington, A.F. and Lindsley, D.H., (1964) Iron titanium oxide minerals and synthetic equivalents. Jour. Petrol., 5, 310-357.

25. Burnham, C.W., (1979) Magmas and hydrothermal fluids. in Barnes, H.L., (Ed.) Geochemistry of hydrothermal ore deposits, John Wiley, New York, Chapter 2, 2nd Ed.

26. Candella, P.A and Holland, H.D., (1981) The partitioning of copper and molybdenum between silicate melts and aqueous fluids. Geochim. Cosmochim. Acta, 48, 373-380.

27. Chappell, B.W and White, A.J.R., (1974) Two contrasting granite types. Pac. Geol., 8, 173-174.

28. Collerson, K.D., (1976) Composition and structural state of alkali feldspars from high-grade metamorphic rocks, central Australia. Amer. Mineral., 61, 200-211.

29. Collerson, K.D., (1982) Geochemistry and Rb-Sr geochronology of associated Proterozoic peralkaline and subalkaline anorogenic granites from Labrador. Contrib. Mineral. Petrol., 81, 126-147.

30. Collerson, K.D. and Bridgwater, D., (1979) Metamorphic development of early Archaean tonalitic and trondhjemitic gneisses: Saglek area, Labrador, in Barker, F., (Ed.) Trondhjemites, dacites and related rocks, Elsevier, Amsterdam, Chapter-7.

31. Condie, K.C., (1973) Archaean magmatism and crustal thickening. Bull. Geol. Soc. Am., 85, 2981-2992.

32. Condie, K.C., (1981) Archaean greenstone belts. Elsevier, Amsterdam, 434 p.

33. Condie, K.C. and Lo, H.H., (1971) Trace element geochemistry of the Louis Lake batholith of early Precambrian age, Wyoming. Geochim. Cosmochim. Acta, 35, 1099-1119.

34. Crawford, A.R., (1969) Reconaissance Rb-Sr dating of the Precambrian rocks of southern Peninsular India. Jour. Geol. Soc. India, 10, 117-166.

35. Croudace, I.J., (1982) The geochemistry and petrogenesis of the lower Paleozoic granitoids of the Lleyn Peninsula, north Wales. Geochim. Cosmochim. Acta, 46, 609-622.

36. Czamanske, G.K., Wones, D.R. and Eichelberger, J.C., (1977) Mineralogy and petrology of the intrusive complex of the Pliny range, New Hampshire. Amer. Jour. Sci., 277, 1073-1123.

37. Day, H.W., Brown, V.M. and Abraham, K., (1980) Precambrian (?) crystallization and Permian (?) metamorphism of hypersolvus granite in the Avalonian terrane of Rhode island. Geol. Soc. Am. Bull., 91, 1669-1741.

38. Dietrich, R.V., (1962) K-feldspar structural states as petrogenetic indicators. Norsk. Geol. Tiddskr., 42, 395-414.

39. Dodge, F.C.W. and Ross, D.C., (1971) Coexisting hornblendes and biotites from granitic rocks near the San Andreas fault, California, Jour. Geol., 79, 158-172.

40. Dodge, F.C.W., Smith, V.C. and Mays, R.E., (1969) Biotites from granitic rocks of the central Sierra Nevada Batholith, California. Jour. Petrol., 10, 250-271.

41. Drury, S.A., Harris, N.B.W., Holt, R.W., Reeves - Smith, J. and Wightman, R.T., (1984) Precambrian tectonics and crustal evolution in south India. Jour. Geol., 92, 3-20.

42. Drury, S.A. and Holt, R.W., (1980) The tectonic framework of the South Indian craton: a reconnaissance involving LANDSAT imagery. Tectonophys., 65,T1-T5.

43. Drysdall, A.R., Jackson, N.J., Ramsay, C.R., Douch, C.J. and Hackett, D., (1984) Rare element mineralization related to Precambrian alkali granites in the Arabian Shield. Econ. Geol., 70, 1366-1377.

44. Eade, R.E. and Fahrig, W.F., (1971) Geochemical evolutionary trends of continental abundances of some trace elements in the Canadian Shield. Geol., Surv. Canada pap., 72-46.

45. Eskola, P., (1932) On the origin of granite magmas.Mineral. Petrog., (N.F.), 42, 455-481.

46. Eugster, H.P., (1985) Granites and hydrothermal ore deposits: a geochemical framework. Mineral. Mag., 49, 7-23.

47. Evans, A.M., (1982) (Ed.) Metallization associated with acid magmatism. John Wiley, 385p.

48. Fersman, A.E., (1960) Collected works of A.E. Fersman. VI. Pegmatites. Acad. Sci. USSR. Moscow, 742 p.

49. Foster, M.D. (1960) Interpretation of the composition of the trioctahedral micas. U.S. Geol. Surv. Prof. Pap., 354-B, 48p.

50. Fleischer, M. and Altschuler, Z.S., (1969) The relationship of the rare-earth composition of minerals to geological environment. Geochim. Cosmochim. Acta, 33, 725-732.

51. Gableman, J.W., (1971) Metallotectonic evidence for continental drift. Rep. Divn. of Production and Management, Washington, 41p.

52. Gehrig, M., Lentz, H. and Franck, E.U., (1979) Thermodynamic properties of water-carbon dioxide-sodium chloride mixtures at high temperatures and pressures. in Timmerhaus, K.D. and Barber, M.S. (Eds) High pressure science and technology, I-properties and material synthesis, Plenum, New York, 539-542.

53. Geological Survey of India (1981) Molybdenite findings in granites in Calicut district, Kerala State G.S.I. News, 2, p. 12.

54. Goldsmith, J.R. and Laves, F., (1954) The microcline - sanidine stability relations. Geochim. Cosmochim. Acta, 5, 1-19.

55. Gorbatschev, R., (1969) Element distribution between biotite and Ca-amphibole in some igneous and pseudoigneous plutonic rocks. Neues Jb. Miner. Abh., 3, 314-342.

56. Gorbatschev. R,, (1970) Distribution of tetrahedral Al and Si in coexisting biotite and Ca-amphibole. Contr. Mineral. Petrol., 28, 251-258.

57. Greenberg, J.K., (1981) Characteristics and origin of Egyptian younger granites. Geol. Soc. Am. Bull., 92, 749-840.

58. Haas, J.I., (1971) The effect of salinity on the maximum thermal gradient of a hydrothermal system at hydrostatic pressure. Econ.Geol., 66, 940-946.

59. Hanson, G.N., (1978) The application of trace elements to the petrogenesis of igneous rocks of granitic composition. Earth planet. Sci. Lett., 38, 26-43.

60. Hanson, G.N. and Gast, P.W., (1967) Kinetic studies in contact metamorphic zones. Geochim. Cosmochim. Acta, 31, 1119-11153.

61. Harpum, J.R., (1963) Rec. Geol. Surv. Tanganyika, 10, 80p.

62. Harris, N.B.W., (1982) The petrogenesis of alkaline intrusives from Arabia and north-east Africa and their implications for within-plate magmatism. Tectonophys., 83, 243-258.

63. Harris, N.B.W. and Holland, T.J.B., (1984) The significance of cordierite-hypersthene assemblages from the Beitbridge region of the central Limpopo Belt., evidence for rapid decompression in the Archaean? Amer. Mineral., 69, 1036-1044.

64. Harris, N.B.W., Holt, R.W. and Drury, S.A., (1982) Geobarometry, geothermometry and late Archaean geotherms from the granulite facies terrain of south India. Jour. Geol., 90, 509-527.

65. Harris, N.B.W., and Marriner, G.R., (1980) Geochemistry and petrogenesis of a peralkaline granite complex from the Median mountains, Saudi Arabia. Lithos, 13, 325-337.

66. Harvey, P.K., Taylor, D.M., Hendry, R.D. and Bancroft, F., (1973) An accurate fusion method for the analysis of rocks and chemically related materials by X-ray fluorescence spectrometry. X-Ray Spectrometry, 2, 33-44.

67. Hollister, L.S. and Burruss, R.C., (1976) Phase equilibria in fluid inclusions from the Khtada Lake metamorphic complex. Geochim. Cosmochim. Acta, 40, 163-175.

68. Holloway, J.R., (1981) Compositions and volumes of supercritical fluids in the earth's crust. in Hollister, L.S. and Crawford, M.L., (eds.) Short course in fluid inclusions: applications to petrology.Mineral. Assoc. Canada, pp.13-28.

69. Holmes, A., (1955) Dating the Precambrians of Peninsular India and Ceylon. Proc. Geol. Assoc. Canada, 7, 81-106.

70. Hudson, T., Smith, J.G. and Elliot, R.L., (1979) Petrology, composition and age of intrusive rocks associated with the Quartz Hill molybdenum deposit, southern Alaska. Can. Jour. Earth. Sci., 16, 1805-1822.

71. Ishihara, S., (1977) The granitoid series and mineralization Econ. Geol., 75, 458-484.

72. Isuk, E.E. and Carman, J.H., (1981) The system $Na_2Si_2O_5$-$K_2Si_2O_5$ -MoS - H_2O with implications for molybdenum transport in silicate melts. Econ. Geol., 76, 2222-2235.

73. Isuk, E.E., (1983) Behaviour of molybdenum in alkali silicate melts: effects of excess SiO_2 and CO_2. Lithos, 16, 17-22.

74. Jackson, N.J., Walsh, J.N. and Pegram, E., (1984) Geology, geochemistry and petrogenesis of late Precambrian granitoids in the central Hijaz region of the Arabian Shield. Contrib. Mineral. Petrol., 87, 205-219.

75. Jahns, R.H. and Burnham, C.W., (1969) Experimental studies of pegmatite genesis: a model for the derivation and crystallization of granitic pegmatites. Econ. Geol., 64, 843-864.

76. Jaireth, S., Santosh, M. and Mohan, P.C., (1982) Fluid inclusion thermobarometry of quartz from Odara pegmatite, Kerala. Proc. Indian Acad. Sci. (Earth Planet. Sci.) 91, 143-152.

77. Janardhan, A.S., Srikantappa, C. and Ramachandra, H.M., (1978) The Sargur schist complex - an Archaean high grade terrain in southern India. in Windley, B.F. and Naqvi, S.M., (Eds.) Archaean geochemistry, Elsevier, Amsterdam, 127-150.

78. Johannsen, A., (1941) Descreptive petrography of the igneous rocks. Chicago Univ. Press, Chicago, III 2, 428 pp.

79. Katz, M.B., (1978) Tectonic evolution of the Archaean granulite facies belt of Sri Lanka and south India. Jour. Geol. Soc. India, 19, 185-205.

80. Konnerup - Madsen, J., (1977) Composition and microthermometry of fluid inclusions in the Klevian granite, south Norway, Am. Jour. Sci., 277, 673-696.

81. Konnerup - Madsen, J. and Rose-Hansen, J., (1982) Volatiles associated with alkaline igneous rift activity: fluid inclusions in the Ilimaussaq intrusion and the Gardar granitic complexes (south Greenland). Chem. Geol., 37, 79-83.

82. Kretz, R., (1959) Chemical study of garnet, biotite and hornblende from gneisses of south-western Quebec, with emphasis on distribution of elements in coexisting minerals. Jour. Geol., 67, 371-402.

83. Kretz, R., (1960) The distribution of certain elements among coexisting calcic pyroxenes, calcic amphiboles and biotites in skarns. Geochim. Cosmochim. Acta, 20, 61-191.

84. Laves, F and Viswanathan, K., (1967) Relations between optic axial angle and triclinicity of potash feldspars and their significance for the definition of 'stable' and 'unstable' states of alkali feldspars. SMPM, 47, 147-162.

85. Leake, B.E., (1968) A catalogue of analysed calciferous and subcalciferous amphiboles together with their nomenclature and associated minerals. Geol. Soc. Am. Spec. Pap. No. 98.

86. Le Bas, M.J., (1971) Peralkaline volcanism, crustal swelling and rifting. Nature, 230, 85-86.

87. Leelanandam, C., (1970) Chemical mineralogy of hornblendes and biotites from the charnockitic rocks of Kondapalli, India. Jour. Petrol., 11, 475-505.

88. Loiselle, M.C. and Wones, D.R., (1979) Characteristics and origin of anorogenic granites. Geol.Soc. Am.Ann. Meeting. Abstr. with Progr., 468 p.

89. Maaloe, S. and Wyllie, P.J., (1975) Water content of a granite magma deduced from the sequence of crystallization determined experimentally with water-under saturated conditions. Contr. Miner. Petrol., 52, 175-191.

90. Marmo, V., (1971) Granite petrology and the granite problem. Elsevier, Amsterdam, 244p.

91. Martin, R.F. and Bonin, B., (1976) Water and magma genesis: The association hypersolvus granite-subsolvus granite. Can. Mineral., 14, 228-237.

92. McCarthy, T.S., (1976) Chemical interrelationships in a low-pressure granulite terrain in Namaqualand, south Africa, and their bearing on granite genesis and the composition of the lower crust. Geochim. Cosmochim. Acta, 40, 1057-1068.

93. McCarthy, T.S. and Cawthorn, R.G., (1980) Changes in initial $^{87}Sr/^{86}Sr$ ratio during protracted fractionation in igneous complexes. Jour. Petrol., 21, 245-264.

94. Mehnert, K.R., (1968) Migmatites and the origin of granitic rocks. Elsevier, Amsterdam, 393p.

95. Michael, P.J., (1984) Chemical differentiation of the Cordillera Paine granite (southern Chile) by in situ fractional crystallization. Contrib. Mineral. Petrol., 84, 179-195.

96. Miller, C.F. and Mittlefehldt, D.W., (1982) Light rare earth element depletion in felsic magmas. Geology, 10, 129-133.

97. Morimotto, N. and Kullerud, G., (1962) The Mo-S system. Ann. Rep. Dir. Geophys. Lab., Carnegie Inst. Wash. Year Book, 1961, 62, 143-144.

98. Murthy, M.V.N. and Venkataraman, P.K., (1964) Petrogenetic significance of certain platform peralkaline granites of the world. in Smith, C.H. and Sorgenfrei, T., (Eds,). The upper mantle symposium, New Delhi, 127-149.

99. Mutschler, F.E., Wright, E.G., Luddington, S. and Abbot, T.J., (1981) Granite-molybdenite systems. Econ. Geol., 76, 874-897.

100. Nagaswa, H. and Schetzler, C.C., (1971) Partitioning of rare earth, alkaline and alkaline-earth elements between phenocrysts and acidic igneous magma. Geochim. Cosmochim. Acta, 35, 953-968.

101. Nair, M.M. and Vidyadharan, K.T., (1982) Rapakivi granite of Ezhimala complex and its significance. Jour. Geol. Soc. India, 23, 46-51.

102. Nair, M.M., Vidyadharan, K.T., Powar, S.A., Sukumaran, P.V. and Murthy, Y.G.K. (1975) The structural and stratigraphic relationship of the schistose and associated rocks of the Tellicherry - Manantoddy area, Cannanore district, Kerala, Ind. Mineralogist., 16, 89-100.

103. Nair, N.G.K. and Santosh, M., (1983) Petrochemistry of the granite and granophyres of the Ezhimala igneous complex, Kerala, India. Proc. Indian Acad. Sci. (Earth Planet. Sci.) 92, 129-140.

104. Nair, N.G.K. and Santosh, M., (1984) Petrochemistry and tectonic significance of the Peralimala alkali granite, Cannanore district, Kerala. Jour. Geol. Soc. India, 25, 35-44.

105. Nair, N.G.K. and Santosh, M., (1985) Geochemistry and petrogenesis of the Puttetti syenite, south India. Neues Jb. Min. Abh., 151, 213-227.

106. Nair, N.G.K., Santosh, M. and Thampi, P.K., (1983a) Geochemistry and petrogenesis of the alkali granite of Munnar, Kerala (India) and its bearing on rift-tectonics. Neues Jb. Miner. Abh., 148, 223-232.

107. Nair, N.G.K., Santosh, M., Thampi, P.K. and Balasubramanian, G., (1982) Petrochemistry of the Ambalavayal granite, Wynad district, Kerala. Jour. Geol. Min. Met. Soc. India, 54, 28-35.

108. Nair, N.G.K., Thampi, P.K., Santosh, M. and Nair, G.S., (1983b) The Kalpatta granite, Wynad district, Kerala (India) and its petrochemistry. Proc. Indian Acad. Sci. (Earth Planet Sci.) 92, 89-97.

109. Nair, N.G.K., Santosh, M. and Thampi, P.K., (1984) The syenite of Sholayar, Trichur district, Kerala. Ind. Jour. Earth Sci., 11, 148-157.

110. Nair, N.G.K., Soman, K., Santosh, M., Arakelyants, M.M. and Golubyev, V.N., (1985) K-Ar ages of three granite plutons from north Kerala. Jour. Geol. Soc. India.,26, 674-676.

111. Naqvi, S.M., (1979) Distribution of trace elements in the crust and mantle during the Archaean: evidence from the Indian shield. Chem. Geol., 24, 1-23.

112. Naqvi, S.M., Divakara Rao, V. and Hari Narain (1978) The primitive crust : evidence from the Indian shield. Precamb. Res., 6, 323-345.

113. Narayana, B.L., Naqvi, S.M., Rama Rao, P., Uday Raj, B. and Ahmad, S.M., (1983) Geology and geochemistry of the Javanahalli schist belt, Karnataka in Naqvi, S.M. and Rogers, J.J.W (Eds.) Precambrian of south India. Geol. Soc. India Mem.4, 143-157.

114. Nockolds, S.R. and Allen, P., (1954) Average chemical composition of some igneous rocks - Geol. Soc. Am. Bull., 65, 1007-1032.

115. O'Conner, J.T., (1965) A classification for quartz rich igneous rocks based on feldspar ratios. U.S. Geol. Surv. Prof. Pap., 525-B.

116. Odom, L.A., (1982) Final report U.N. Case No.81-10084 (Unpub.) 10p.

117. Orville, P.M., (1962) Alkali metasomatism and feldspars. Norsk. Geol. Tiddskr., 42, 283-316.

118. Orville, P.M., (1967) Unit-cell parameters of microcline - low albite and the sanidine - high albite solid solution series. Amer. Mineral., 52, 55-86.

119. Parsons, I., (1972) Petrology of the Puklen syenite, alkali granite complex, Nunarssuit, south Greenland. Medd. Gron., 195, 1-73.

120. Parsons, I., (1978) Feldspars and fluids in cooling plutons. Mineral. Mag., 42, 1-17.

121. Perrin, R. and Roubault, M., (1939) Le granite et les reactions a l'etat solid. Carte Geol. Algerie, Bull, 5e Ser., 4, 1-168.

122. Pokalov, V.T., (1977) in Smirnov, V,I., (Ed.) Ore deposits of the U.S.S.R, Pitman, London, 3, 125p.

123. Qureshy, M.N., Krishna Brahmam, N. and Narayamadhu, P.S., Gravity survey on some granitic bodies of south India. Jour. Ind. Geosc. Assoc., 11, 177-181.

124. Radhakrishna, T., Mitchell, J.G. and Venkatesh, R., (1985) Multiple emplacement of basic dyke swarms in Kerala and crustal evolution of south India. Int. Conf. on mafic dyke swarms, Toronto, (Abstr.).

125. Raha, P.K., Sinha-Roy, S. and Rajendran, C.P., (1983) A new approach to the lithostratigraphy of the Cenozoic sequence of Kerala. Jour. Geol. Soc. India, 24, 325-342.

126. Raith, M., Raase, P., Ackermand, D. and Lal., R.K., (1982) Regional geothermobarometry in the granulite facies terrane of south India. Trans. Roy. Soc. Edinburgh (Earth Sci), 73, 221-244.

127. Rajan, P.K., Santosh, M. and Ramachandran, K.K., (1984) Geochemistry and petrogenetic evolution of the diatexites of central Kerala, India. Proc. Indian Acad, Sci, (Earth Planet. Sci.) 93, 57-70.

128. Ramberg, H., (1944) The thermodynamics of the earth's crust, 1.Preliminary survey of principal forces and reactions in the earth's crust. Norsk. Geol. Tidsskr., 24, 98-111.

129. Rao, A.T., (1978) Molybdenite from charnockites of Kondapalli, Andhra Pradesh. Jour. Geol. Soc. India, 19, 583-584.

130. Rao, P.S., (1978) Some aspects of structure and tectonics of Kerala region, India and related metallogeny in Tectonics and metallogeny of south-east Asia. Geol. Surv. India Misc. Publ., 34, 61-64.

131. Read, H.H., (1948) Granites and granites. In Gilluly, J., (Ed.) Origin of granite. Geol. Soc. Am. Mem., 28, 1-19.

132. Ribbe, P.H., (Ed.) (1975) Feldspar mineralogy. Min. Soc. Amer. Short Course Notes, 2, R-1-Y-54.

133. Roedder, E., (1971) Fluid inclusion studies on the porphyry-type ore deposits at Bingham, Utah, Butte, Montanna and Climax, Colorado. Econ. Geol., 66, 98-120.

134. Roedder, E., (1984) Fluid inclusions. Reviews in Mineralogy vol. 12, Min.Soc. America. 644pp.

135. Roedder, E. and Bodnar, J., (1980) Geologic pressure determinations from fluid inclusion studies. Ann. Rev. Earth. Planet. Sci., 8, 263-301.

136. Rogers, J.J.W. and Greenberg, K., (1981) Trace elements in continental-margin magmatism : III Alkali granites and their relationship to cratonization. Geol.Soc. Am. Bull., 92, 57-93.

137. Rosenbusch, H., (1876) Einige mitteilungen uber zusammensetzung and struktur granitscher gesteine. Z. Deut. Geol. Ges., 28, 369-390.

138. Saha, A.K., (1979) Geochemistry of Archaean granites of the Indian shield. Jour. Geol. Soc. India, 20, 375-390.

139. Sahu, K.C. and Panchapakesan, V (1982) (Eds.) Fluid inclusion studies : Workshop on fluid inclusions, I.I.T. Bombay, March 1982.

140. Santosh, M., (1981) Petrology and fluid inclusion studies of Thiruvalla and Odara pegmatites of Kerala and Bandarchua and Kharonia pegmatites of Bihar. M.Sc. thesis (Unpub.), University of Roorkee, 59 p.

141. Santosh, M., (1984a) Nature of ore fluids in the Odara rare metal pegmatite Kerala, India. Neues Jb. Miner. Mh., H-6, 241-250.

142. Santosh, M., (1984b) Fluid inclusion petrography of charnockites from the granulite facies terrain of Kerala, south-west India. Neues Jb. Miner. Mh., H-8, 337-345.

143. Santosh, M., (1985a) Fluid evolution characteristics and piezothermic array of south Indian charnockites. Geology (Geol.Soc. Am.), 13,361-363.

144. Santosh, M., (1985b) Geochemistry of feldspars from the Ambalavayal molybdenite prospect, Kerala. Jour. Geol. Soc. India (in press).

145. Santosh, M., (1985c) Geochemistry of coexisting hornblende and biotite from the Ambalavayal granite, Kerala. Proc. Indian Acad. Sci. (Earth Planet. Sci.) under publication.

146. Santosh, M., (1985 d) Crystal growth of zircons in Puttetti syenite: nature of fluids and implications on CO_2 activity. Jour. Geol. Soc. India, 26, 695-703

147. Santosh, M. and Nair, N.G.K., (1983a) Petrochemistry of the Chengannoor granite, Alleppey district, Kerala. Jour. Geol. Soc. India, 24, 291-298.

148. Santosh, M. and Nair, N.G.K., (1983b) Granite - molybdenite association in Kerala in relation to taphrogenic metallogeny. Proc. Indian Acad. Sci. (Earth Planet. Sci.), 92, 297-310.

149. Santosh, M. and Nair, N.G.K., (1985) Petrogenesis of the Angadimogar syenite, Kerala and its taphrogenic affiliation, Jour. Geol.Soc. India (in press).

150. Santosh, M., Nair, N.G.K., Pande, K, and Gopalan, K., (1985) Rb-Sr geochronology of the Ambalavayal granite, Kerala. Jour. Geol. Soc. India (in press).

151. Santosh, M., Rajan, P.K. and Nair, N.G.K., (1983) The Pariyaram granite, Trichur district Kerala-its petrochemistry. Bull. Ind. Geol. Assoc., 16, 33-43.

152. Santosh, M. and Thara, K.G., (1985) The Kannapra syenite, central Kerala, India: geochemistry, petrogenesis and bearing on anorogenic magmatism. Proc. Indian Acad. Sci. (Earth Planet. Sci.) 94, 43-56.

153. Sarkar, S.N., (1980) Precambrian stratigraphy and geochronology of Peninsular India: a review. Ind. Jour. Earth Sci., 7, 12-26.

154. Sarkar, S.N., Gopalan, K. and Trivedi, J.R., (1981) New data on the geochronology of the Precambrians of Bhandara-Drug, central India. Ind. Jour. Earth Sci., 8, 131-151.

155. Saunders, A.D., Tarney, J. and Weaver, S.D., (1980) Transverse geochemical variations across the Antartic peninsula: implications for the genesis of calc-alkaline magmas. Earth Plant. Sci. Lett., 46, 344-360.

156. Saxena, S.K., (1966) Distribution of elements between coexisting biotite and hornblende in metamorphic Caledonides, lying to the west and south west of Trondhiem, Norway. Neues Jb. Miner. Mh., 67-80.

157. Schonwandt, H.K. and Peterson, J.S., (1983) Continental rifting and porphyry molybdenum occurrences in the Oslo region, Norway. Tectonophys., 94, 609-631.

158. Seck, H.A., (1971) Koexistierende alkalifedspate Und plagioclase im system Na Al Si_3O_8-KASi_3O_8-$CaAl_2Si_2O_8$-H_2O bei temperaturen von 650°C. Neues Jb. Miner. Abh., 115, 315-345.

159. Scheshulin, G.I., (1963) Composition of gas-liquid inclusions in the minerals of spodumene pegmatites in Ginzburg, A.I. (Ed.) New data on rare element mineralogy. Consultants Bureau, New York, 140p.

160. Sillitoe, R.H., (1972) A plate tectonic model for the origin of porphyry copper deposits. Econ. Geol., 70, 913-927.

161. Simmons, E.C. and Hedge, C.E., (1978) Minor-element and Sr-isotope geochemistry of the Tichka Massif, Morocco, based on rare earth elements. Contrib. Mineral. Petrol., 67, 379-396.

162. Sinha-Roy, S., (1983) Structural evolution of the Precambrian crystalline rocks of south Kerala in Sinha Roy, S., (Ed) Structure and tectonics of Precambrian rocks of India. Hindustan Pub. Corp., Delhi, pp.126-143.

163. Sinha-Roy, S. and Furnes, H., (1982) Petrology and geochemistry of mafic and felsic dykes from passive continental margin of Kerala region, India. Neus Jb. Miner. Abh., 142, 49-70.

164. Sinha-Roy, S., John Mathai and Narayanaswami, (1984) Structure and metamorphic characteristics of cordierite-bearing gneiss of south Kerala. Jour. Geol. Soc. India, 25, 231-244.

165. Sinha-Roy, S. and Ravindra Kumar G.R., (1984) Fuchsite-bearing quartzite in the Sargur equivalent rocks of north Kerala. Jour. Geol. Soc. India, 25, 120-124.

166. Smith, J.V., (1974) Feldspar Mimerals, Springer-Verlag, Berlin.

167. Soman, K. and Nair, N.G.K., (1983) Genesis of chrysoberyl pegmatites of south Kerala, India, and its relation to the tectonic evolution of the region. Trans. Inst. Min. Metall. (Sect.B: Appl. earth Sci.) 92, B-154-B-159.

168. Soman, K., Nair, N.G.K., Golubyev, V.N. and Arkelyan, M.M., (1982) Age data on pegmatites of south Kerala and their tectonic significance. Jour. Geol. Soc. India, 23, 458-462.

169. Soman, K., Santosh, M. and Golubyev, V.N., (1983) Early Palaeozoic I-type granite from central Kerala and its bearing on possible mineralization. Indian Jour. Earth Sci., 10, 137-141.

170. Sorensen, H., (1980) (Ed.) The alkaline rocks. John Wiley - Interscience, New York. 622p.

171. Sourirajan, S. and Kennedy, G.C., (1962) The system H_2O-NaCl at elevated temperatures and pressures. Amer. Jour. Sci., 260, 115-141.

172. Steiger, R.H. and Jager, E., (1977) Subcommission on geochronology: convention on the use of decay constants in geo-and cosmo-chronology. Earth planet. Sci. Lett., 36, 359-362.

173. Stemprock, M., Burnol, L. and Tischendorf, G., (1978) Metallization associated with acid magmatism. UUG, Praha, v.I. (1974), 410p, v.II (1977), 166p, and v. III (1978) 446 p.

174. Stephenson, N.C.N., (1977) Coexisting hornblendes and biotites from Precambrian gneisses of the south coast of Western Australia. Lithos, 10, 9-27.

175. Stormer, J.C., (1975) A practical two-feldspar geothermometer. Am. Mineral., 60, 667-674.

176. Streckeisen, A.L., (1976) To each plutonic rock its proper name. Earth Sci. Rev., 12, 1-33.

177. Stroh, P.T., Monrad, J.R., Fullagar, P.D., Naqvi, S.M., Hussain, S.M. and Rogers, J.J.W., (1983) 3,000 m.y. old Halekote Trondhjemite: A record of stabilization of the Dharwar craton. in Naqvi, S.M. and Rogers, J.J.W (Eds) Precambrian of south India: Geol. Soc. India Mem. 4, 365-376.

178. Strong, D.F., (1981) Granitoid rocks and associated mineral deposits of eartern Canada and western Europe. Geol. Assoc. Canada Spec. Pap. 20, 741-769.

179. Subramanian, K.S., (1979) Molybdenite mineralization associated with acid magmatism in Tamil Nadu, India. Geol. Surv. India Spec. Publ., 13, 155-158.

180. Sun, S.S. and Nesbitt, R.W., (1977) Chemical homogeneity of the Archaean mantle-composition of the earth and mantle evolution. Earth Planet. Sci. Lett., 35, 429-448.

181. Sutherland, I.G. and Brown, A., (1976) Porphyry deposits of the Canadian cordillera. Canad. Inst. Min. Metall. Spec., 15, 510p.

182. Swanenberg, H.E.C., (1979) Phase equilibria in carbonic systems and their application to freezing studies of fluid inclusions. Contrib. Mineral. Petrol., 68, 303-306.

183. Takenouchi S. and Kennedy, G.C., (1964) The binary system H_2O-CO_2 at high temperatures and pressures. Am. Jour. Sci., 263, 445-454.

184. Takenouchi, S, and Kennedy, G.C., (1965) The solubility of carbon dioxide in NaCl solution at high temperatures and pressures. Am. Jour. Sci., 264, 445-454.

185. Takenouchi, Y and Nowacki, J., (1964) Detailed crystal structure of rhombohedral MoS_2 and systematic deduction of possible polytypes of molybdenite. Schweiz. Miner. Petrogr. Mitt., 44, 105-120.

186. Tarney, J., (1976) Geochemistry of Archaean high grade gneisses, with implications as to the origin and evolution of the Precambrian crust. in Windley, B.F. (Ed.). The early history of the earth- Wiley, London, pp.405-417.

187. Taylor, S.R., (1965) The application of trace element data to problems in petrology in Ahrens, L.H., et al., (Eds.) Physics and chemistry of the earth, Pergamon Press, Oxford 6, 133-213.

188. Thompson, T.B., Pierson, J. R and Little, T., (1982) Petrology and petrogenesis of the Bokan granite complex, southern Alaska. Geol. Soc. Am. Bull., 93, 893-908.

189. Tingle, T.N. and Penn, F.M., (1984) Transport and concentration of molybdenum in granite molybdenite systems: effects of fluorine and sulfur. Geology, 12, 156-158.

190. Todheide, K and Franck, E.U., (1963) Das Zweiphasengebiet und die Kristsche Kurve im System Kohlendioxid-Wasser bis zu Drucken von 3500 bar. Z. Phys. Chem. Neuefolge, 37, 388-401.

191. Touret, J., (1981) Fluid inclusions in high grade metamorphic rocks. in Hollister, L.S and Crawford, M.L., (Eds.) Short Course in Fluid Inclusions: Applications to Petrology. Mineral. Assoc. Canada, 182-208.

192. Traill, R.J., (1963) A rhombohedral polytype of molybdenite, Canad. Mineral., 7, 524-526.

193. Tuttle, O.F. and Bowen, N.L., (1958) Origin of granite in the light of experimental studies in the system, Na Al Si_3O_8-K Al Si_3O_8-SiO_2-H_2O. Geol. Soc. Am. Mem. No. 74

194. Wendlandt, R.F. and Harrison, W.J., (1979) Rare earth partitioning between immiscible carbonate and silicate liquids and CO_2 vapor: results and implications for the formation of light rare earth enriched rocks. Contrib. Mineral. Petrol., 69, 409-419.

195. Westra, G. and Keith, S.B., (1981). Classification and genesis of stock work molybdenum deposits. Econ. Geol., 76, 844-873.

196. White, A.J.R. and Chapell, B.W., (1977) Ultrametamorphism and granitoid genesis. Tectonophys., 43, 7-22.

197. White, W.H., Stewart, D. Ganster, M.W., (1976) Adanac (Ruby Creek) in Porphyry deposits of the Canadian Cordillera. Canad. Inst. of Min. and Metall., Spec. Vol., 15, 476-483.

198. Whitney, J.A. and Stormer, J.C., (1977) The distribution of Na Al Si_3O_8 between coexisting microcline and plagioclase and its effect on geothermometric calculations. Amer. Mineral., 62, 687-691.

199. Winkler, H.G.F., (1976) Petrogenesis of metamorphic rocks. 4th Ed., Springer - Verlag, New York.

200. Wones, D.R. and Eugster, H.P., (1965) Stability of biotite: experiment, theory and application. Amer. Mineral., 50, 1228-1272.

201. Wyllie, P.J., (1977) Crustal anatexis: an experimental review. Tectonophys. 43, 41-71.

202. York, D., (1966) Least square fitting of a straight line. Can. Jour. Phys., 44, 1079-1086.

APPENDIX

CHEMICAL ANALYSES: TECHNIQUES AND PRECISION

Fresh, unaltered rock samples were chipped and pulverized in a ball mill, taking extreme precaution at every step to avoid contamination. Pulverzed samples of -230 mesh size were coned and quartered for the analyses.

Major Elements

Major elements were analysed by wet chemical methods at the CESS chemical laboratory. Among trace elements, Ba, Ce, La, Nb, Pb, Rb, Sr, Th, U and Zr were determined by XRF at the University of Nottingham. The precision and accuracy of these analyses are given towards the end of this Appendix. Other trace elements were analysed by Atomic Absorption Spectrophotometer (Perkin-Elmer 4000) at the CESS Chemical Laboratory.

Determination of moisture and loss on ignition

One gram sample is weighed and transferred into a platinum crucible kept in an oven at 100°C for about an hour. It is taken out and weighed again. The loss of weight gave moisture in the sample. The crucible is then kept in a muffle furnace and heated to 950°C for half an hour and again weighed. The difference in weight gave loss on ignition.

Determination of SiO_2

0.5 gm of sample is weighed into a platinum crucible. 5 gm of Na_2CO_3 is added to it and mixed thoroughly. It is fused over

a murker burner at 900°C. The fused mass is dissolved in HCl and transferred into a porcelain dish. It is then dehydrated over a steam bath. The content is diluted with HCl and filtered into a 250 ml standard flask using No. 42 Whatman filter paper. The residue is washed well and then heated with the filter paper to 1100°C in a muffle furnace for half an hour. It is taken out, washed and after adding about 2 to 3 drops of 1:1 H_2SO_4 and 15 ml HF, kept on a hot plate. Treatment with HF is done twice. The residue left is baked on a murker furnace and weighed. The difference in weight gives the weight of silica.

The residue left after HF treatment is fused with a little $K_2Cr_2O_4$ and the fused mass is dissolved in water. This is added to the already collected filtrate and made up to 250 ml in standard flasks. This serves as the stock solution for determination of Fe, Al, Ca and Mg.

Determination of Fe

25 ml of this stock solution is taken in a beaker. 5 ml con. HCl is added to this and boiled for 2 to 3 minutes. $SnCl_2$ is added dropwise till the solution becomes colourless, indicating that all the Fe^{3+} has been reduced to Fe^{2+}. It is then cooled. A few drops of $HgCl_2$ are added to this in order to remove the excess of $SnCl_2$. 5 ml of dilute H_2SO_4 and 2 ml of orthophosporic acid are added to this. The solution is then titrated against standard $K_2Cr_2O_7$ using

barium-diphenyl amino sulfonate as indicator. The end point is indicated when the solution turns violet. Percentage of Fe_2O_3 (total) is estimated from this titration.

Determination of Al_2O_3

25 ml of the stock solution is taken out in a beaker. To this, 5 ml of 20% NaOH is added dropwise. Phenolphthalene is used as indicator which attributes a pink colour. The solution is boiled for 10 minutes. It is filtered and the filtrate is collected in a beaker. The residue is washed well with hot dilute NaOH. The pH of the filtrate is adjusted to be between 6.5 and 7 with HCl. 15 ml of 20% ammonium acetate and 10 ml of standard EDTA are added to this and kept for boiling. A blank solution is also taken. The solution is boiled till all $Al(OH)_3$ has dissolved. It is then cooled and xylene orange indicator and 2-3 drops of acetic acid are added. It is then titrated against standard Zn^{2+} solution. The end point is determined when the solution changes from yellow to orange in colour. From the volume of Zn^{2+} consumed, Al_2O_3% is estimated.

Determination of CaO and MgO

25 ml of the stock solution is taken in a beaker and NH_3 and NH_4Cl are added. It is boiled for five minutes and filtered. The filtrate is used for the determination of Ca and Mg.

25 ml of the filtrate is titrated against standard EDTA using erichrome black-T and NH_3/NH_4Cl buffer. The titre value gives an estimate of Mg. Another 25 ml of the filtrate is titrated against standard EDTA. The titre value gives an estimate of Ca.

Determination of Na_2O and K_2O.

0.2 gm of the sample is weighed into a platinum dish, 3 drops of 1:1 H_2SO_4 and about 15 ml of HF are added. It is kept for fuming over a hot plate. HF treatment is repeated once more. To the baked mass, 5ml of HF are added. It is kept for fuming over a hot plate. HF treatment is repeated once more. To the baked mass, 5 ml of con. HCl and 5 ml of H_2O are added and digested. This is then transferred into a 100 ml standard flask and neutralized with NH_4OH. One gram of solid ammonium carbonate is added to this. After filtering through a Number 41 Whatman filter paper, the filtrate is used for the determination of Na and K using Flame Photometer.

Determination of MnO and TiO_2

0.2 gm of the powdered sample is weighed into a beaker. About 5 ml of each of con. HCl, con. HNO_3 and con. H_2SO_4 are added to this and kept for fuming over a hot plate. After fuming, it is diluted with water and filtered through a quantitative filter paper (Whatman No. 41) and the

filtrate is collected in a 100 ml standard flask. This is used as the stock solution for the estimation of Mn and Ti.

5 ml of the stock solution is taken to which 5 ml of acid mixture is added. It is kept for warming in a water bath for about 30 minutes. A pinch of potassium per-iodate is added to this. It is again kept for warming. Colour comparisons are done in a Spectrophotometer at a wave length of 545 nm.

10 ml of the stock solution is taken in standard flasks, 25 ml of titanium acid is added to this. The colour developed is compared with standard titanium solution in a Spectrophotometer at a wave length of 410 nm. A blank is also done in both the cases. From these, the percentage of MnO and TiO_2 are calculated.

Determination of P_2O_5

0.2 gm of the sample is taken in a test tube and fused with about 1 gm of potassium pyrosulfate. The fused mass is leached with 5 ml and 4 molar HNO_3 in a water bath. It is then made upto 10 ml. One ml of the supernatent clear solution is taken in a measuring cylinder having a stopper. 5 ml of ammonium molybdate and ammonium metavanadate mixture is added to this. This is then made up to 10 ml. The The colour of the phospho-vanado-molybdate extraced with amyl alcohol is compared with standard phosphorous

solutions. A blank determination is also done. P_2O_5 is thus estimated,

Trace Elements

For minor and trace element analyses, solutions are prepared by fusing 0.3 gm of powdered samples with 0.3 gm of $K_2S_2O_7$ in a 25 ml test tube. 5 ml of 4N HNO_3 is added to this. The solution is heated in a water bath for 30 minutes and then the volume is made up to 30 ml with distilled water. This solution is used for A.A.S. analyses.

The molybdenite ore solutions are prepared by fusing 0.1 gm of sample with $K_2S_2O_7$ and digesting in 1:1 HNO_3. The solution is filtered and made up to known volume 3cc of phosphoric acid is added to remove the interference of Fe.

For XRF analyses, the techniques and matrix corrections used are the same as given in Harvey et al (1973). USGS standard rock powders were used as calibration standards and as internal checks. The standards used are GSP-1, AGV-1, NIM-g, G-2, BHVO-1, QLO-1, GA, GH, RGM-1, N-1005, N-1001 and STM-1. Their analytical data re given in Table A-1. The internal precision and accuracy are checked by repeated analyses (Table A-2) and are found to be $\pm$ 2 for Nb, Pb and Rb, $\pm$ 5 for Ba, Ce, U, Y and Zr and $\pm$ 20 for Ba and Sr.

For all major element determinations and trace elements by A.A.S., synthetic multi-elements standards are used. It is

TABLE A-I Trace element data of U.S.G.S. standards analysed along with samples of present study (values in ppm)

Element	GSP-1	AGV-1	NIM-6	G-2	BHVO-1	QlO-1	GA
Ba	1266	1233	119	1833	128	1410	807
Ce	335	73	211	159	52	55	56
La	132	40	108	89	17	29	29
Nb	26	15	54	12	19	12	13
Pb	51	37	35	33	7	22	49
Rb	250	67	319	162	12	73	170
Sr	236	658	11	467	387	332	302
Th	105	7	53	22	--	4	11
U	3	3	15	-	--		
Y	32	19	147	12	26	24	22
Zr	500	233	274	300	174	192	150

TABLE A-I Contd. Trace element data of U.S.G.S standards analysed along with samples of present study (values in ppm).

Element	GH	RGM-1	N-1005	N-1001	STM-1
Ba	28	842	994	195	622
Ce	63	49	62	54	260
La	19	23	31	18	139
Nb	88	11	10	14	253
Pb	45	26	19	29	20
Rb	385	147	54	475	114
Sr	11	102	888	85	714
Th	75	11	6	17	32
U	14	6	4	10	8
Y	89	26	17	21	48
Zr	153	233	180	109	1230

TABLE -A-2 Data of repetitive analyses, mean and standard deviation.

Element	1	2	3	4	5	6	Mean	S.D
Ba	937	969	973	957	984	954	962.3	16.5
Ce	97	97	95	95	95	102	96.8	2.71
La	72	75	75	70	70	70	72	2.45
Nb	59	64	63	62	63	63	62.3	1.75
Pb	46	48	47	45	49	48	47.2	1.47
Rb	89	90	90	89	91	91	90	0.87
Sr	750	803	798	803	797	799	791.7	20.6
Th	30	38	45	44	38	38	38.8	5.38
U	30	37	38	40	38	36	36.5	3.45
Y	67	72	71	72	72	73	71.2	2.14
Zr	174	184	186	186	185	187	183.7	4.84

estimated that for major elements with concentrations greater than 1%, the limit of error is less than 0.6%. For analyses between 1000 ppm and 1%, the error is between 0.6 and 2.5 relative per cent. For trace elements with concentrations less than 1000ppm, the error limit is between 1 and 10 relative per cent.

***

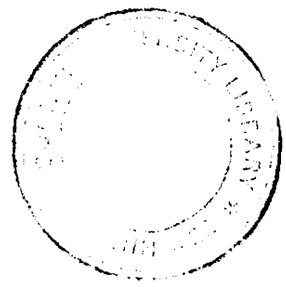

ACKNOWLEDGEMENTS

I am extremely grateful to Dr. N.G.K.Nair, Centre for Earth Science Studies, who introduced me to the challenging aspects of acid magmatism and related metallogeny and initiated my interest in the topic embodied in this thesis. I thank him profoundly for his valuable guidance and constant encouragement.

I express my sincere thanks to Dr. Harsh K. Gupta, Director, CESS, for kindly extending research facilities. I am also grateful to him for his constant encouragement. Prof. C. Karunakaran, founder Director of CESS, is also thanked as the study was taken up at his time. I started the work as a CSIR Research Fellow. I am grateful to the CSIR for extending financial support for one year. I also thank Dr. D. Chandrasekharam, CWRDM, Calicut, for annual assessments of my work.

Dr. K. Gopalan, PRL, Ahmedabad (now in NGRI, Hyderabad) kindly arranged the Rb-Sr dating of the Ambalavayal granite, for which I am grateful to him. Part of the trace element analyses (those by XRF) were kindly arranged by Dr. S.A. Drury, Open University, Milton Keynes, U.K. I also thank Dr. M.L.Griffiths of the Open University and Dr. P.K.Harvey, Nottingham, for the analyses.